Review

Polymer/Silica Nanocomposites: Preparation, Characterization, Properties, and Applications

Hua Zou, Shishan Wu, and Jian Shen

Chem. Rev., **2008**, 108 (9), 3893-3957 • DOI: 10.1021/cr068035q • Publication Date (Web): 23 August 2008

Polymer/Silica Nanocomposites: Preparation, Characterization, Properties, and Applications

Hua Zou,[†] Shishan Wu,*[,†] and Jian Shen*[,†,‡]

School of Chemistry and Chemical Engineering, Nanjing University, Nanjing 210093, P. R. China, and College of Chemistry and Environment Science, Nanjing Normal University, Nanjing 210097, P. R. China

Received August 6, 2007

Contents

* To whom correspondence should be addressed. E-mail addresses: shenj1957@yahoo.com.cn, shishanwu@yahoo.com.cn. Tel: 86-25-8359-4404. Fax: 86-25-8359-4404.
[†] Nanjing University.
[‡] Nanjing Normal University.

1. Introduction

Organic/inorganic composite materials have been extensively studied for a long time. When inorganic phases in organic/inorganic composites become nanosized, they are called nanocomposites. Organic/inorganic nanocomposites are generally organic polymer composites with inorganic nanoscale building blocks. They combine the advantages of the inorganic material (e.g., rigidity, thermal stability) and the organic polymer (e.g., flexibility, dielectric, ductility, and processability). Moreover, they usually also contain special properties of nanofillers leading to materials with improved properties. A defining feature of polymer nanocomposites is that the small size of the fillers leads to a dramatic increase in interfacial area as compared with traditional composites. This interfacial area creates a significant volume fraction of interfacial polymer with properties different from the bulk polymer even at low loadings.[1–5]

Inorganic nanoscale building blocks include nanotubes, layered silicates (e.g., montmorillonite, saponite), nanoparticles of metals (e.g., Au, Ag), metal oxides (e.g., TiO_2,

10.1021/cr068035q CCC: $71.00
Published on Web 08/23/2008

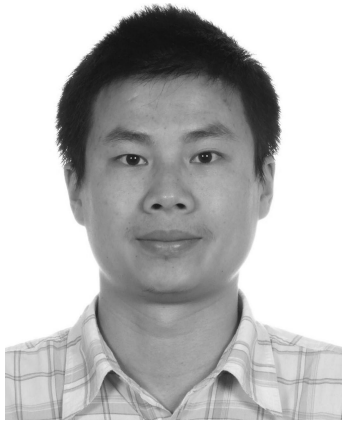

Hua Zou was born in Hubei Province, China, in 1980. He received his B.S. degree in 2002 and his M.S. degree in 2005 in Chemistry at Hubei University. He received an award of excellent master's thesis from Hubei University (2006). Currently, he just obtained his Ph. D. in polymer chemistry and physics from Nanjing University in the group of Prof. Jian Shen, working on polymer/silica colloidal nanocomposites.

Shishan Wu was born in Anhui Province, China, in 1960. He received his B.S. Degree in 1982 from Shangdong Institute of Chemical Technology (now Qingdao University of Science & Technology). He went to work at the Institute of Rubber Industry, Ministry of Chemical Industry, in Shenyang until 1987. He then went to Chengdu University of Science and Technology (now Sichuan University), where he obtained his M.S. degree in Polymer Materials in 1990. After that, he worked in the Department of Polymer, Nanjing Institute of Chemical Technology (now Nanjing University of Technology). Here he was promoted to associate professor and received an award from Ministry of Chemical Industry, China. He earned his Ph.D. degree in Polymer Materials in 2000 at Sichuan University under the supervision of Professor Xi Xu (Academician of Chinese Academy of Sciences). He is currently working as an associate professor in the School of Chemistry and Chemical Engineering, Nanjing University. His primary research interests include polymer nanocomposites.

Jian Shen was born in 1957. He received his B.S. in Chemistry at Nanjing University in 1982. He obtained his M.S. at Nanjing University and Ph.D. at Nanjing University of Science and Technology. Since 1996, he has been a professor of Nanjing University. In 2002, he moved to Nanjing Normal University and served as an adjunct professor of Nanjing University. Now he is the director of Engineering Research Center of Interface Chemistry, Nanjing University and is the Chairman of the Nanjing Chemical and Chemical Industry Society. His primary research interests include surface and interface chemistry, polymer nanocomposites, biomacromolecules, etc. He has contributed to more than 100 international scientific publications.

Al_2O_3), semiconductors (e.g., PbS, CdS), and so forth, among which SiO_2 is viewed as being very important. Therefore, polymer/silica nanocomposites have attracted substantial academic and industrial interest. In fact, among the numerous inorganic/organic nanocomposites, polymer/silica composites are the most commonly reported in the literature. They have received much attention in recent years and have been employed in a variety of applications.

As pointed out by Hajji et al.,[6] nanocomposite systems can be prepared by various synthesis routes, thanks to the ability to combine different ways to introduce each phase. The organic component can be introduced as (i) a precursor, which can be a monomer or an oligomer, (ii) a preformed linear polymer (in molten, solution, or emulsion states), or (iii) a polymer network, physically (e.g., semicrystalline linear polymer) or chemically (e.g., thermosets, elastomers) cross-linked. The mineral part can be introduced as (i) a precursor (e.g., TEOS) or (ii) preformed nanoparticles. Organic or inorganic polymerization generally becomes necessary if at least one of the starting moieties is a precursor. This leads to three general methods for the preparation of polymer/silica nanocomposites according to the starting materials and processing techniques: blending, sol−gel processes, and in situ polymerization (Scheme 1). Blending is generally just mixing of the silica nanoparticles into the polymer; a sol−gel process can be done in situ in the presence of a preformed organic polymer or simultaneously during the polymerization of the monomer(s); the method of in situ polymerization involves the dispersion of nanosilica in the monomer(s) first and then polymerization is carried out. In addition, considerable efforts have been devoted to the design and controlled fabrication of polymer/silica colloidal nanocomposite particles with tailored morphologies in recent years. The colloids represent a relatively new category of nanocomposites.

The preparation, characterization, properties, and applications of polymer/silica nanocomposites have become a quickly expanding field of research. Whereas several books and review articles[4a,7–37] have appeared that are partly devoted to the polymer/silica nanocomposites, this subject has never been reviewed systematically. The aim of this review is to summarize the recent developments in this field based mainly on the literature from 1998 to April 2008. Owing to numerous papers published on polymer/silica nanocomposites, it is impossible to completely describe this field. Therefore, this review will give a general overview of the techniques and strategies used for the preparation of the nanocomposites followed by a brief discussion of their characterization, properties, and applications. Selected examples representative of different routes and systems will be reported. More detailed descriptions on specific themes can be referred from related references.

Perhaps it is necessary to make clear the terms "hybrids" and "nanocomposites" before the discussion of the nanocomposites, since it is somewhat ambiguous to identify

whether materials fall into "nanocomposites" or not. The most wide-ranging definition of a hybrid is a material that includes two moieties blended on the molecular scale. Commonly the term "hybrids" is more often used if the inorganic units are formed in situ by the sol−gel process.[8b] Meanwhile, use of the word "nanocomposites" implies that materials consist of various phases with different compositions, and at least one constituent phase (for polymer/silica nanocomposites, that phase is generally silica) has one dimension less than 100 nm. A gradual transition is implied by the fact that there is no clear borderline between "hybrids" and "nanocomposites".[8b] Expressions of "nanocomposites" seem to be very trendy, and although the size of the silica particles is above 100 nm, the composites are often called "nanocomposites" in some literature. These works are also referred in this review. Polymer/mesoporous silica nanocomposites and polymer/silica/other mineral ternary nanocomposites are excluded from this review.

2. Surface Modification of Silica Nanoparticles

2.1. Preparation and Properties of Silica Nanoparticles

As indicated in Scheme 1, for the three general preparative methods of polymer/silica nanocomposites, silica nanoparticles are generally introduced directly in the blending and in situ polymerization methods, whereas silica precursors are used in the sol−gel process, among which the most widely used ones are silicon alkoxides, TEOS and TMOS. Sometimes, alkoxysilane-containing polymers[38–42] are also used in the sol−gel process as silica precursors. In addition, in some special cases, silica in the nanocomposites can originate from precursors PHPS,[43] water glass[44]/sodium silicate,[45,46] silicic acid,[47] etc.[48–50]

Two classes of techniques have been developed for silica nanoparticle formation: the sol−gel method and the microemulsion method.[51] In 1968, Stöber and Fink[52] reported a simple synthesis of monodisperse spherical silica particles by means of hydrolysis of a dilute solution of TEOS in ethanol at high pH as observed earlier by Kolbe.[53] Uniform amorphous silica spheres whose sizes ranged from 10 nm to 2 μm were obtained simply by changing the concentrations of the reactants. This Stöber method was later improved by many others[54–58] and appears to be the simplest and most effective route to monodispersed silica spheres.[59] In 1990, Osseoasare and Arrigada[60] prepared nanosized and monodisperse silica particles by controlled hydrolysis of TEOS in an inverse microemulsion. This microemulsion method is also widely used to synthesize silica nanoparticles.

Silica nanoparticles are also available from commercial sources now, and they usually exist as powder or colloid. Nanosilica powder is mainly produced by the fuming method and the precipitation method in industry. Fumed silica is a fine, white, odorless, and tasteless amorphous powder. It is manufactured by a high-temperature vapor process in which $SiCl_4$ is hydrolyzed in a flame of oxygen−hydrogen according to the reaction[61]

$$SiCl_4 + 2H_2 + O_2 \rightarrow SiO_2 + 4HCl \quad (1)$$

The silica has an extremely large surface area and smooth nonporous surface, which could promote strong physical contact between the filler and the polymer matrix.[62] Precipitated silica is manufactured by a wet procedure by

Scheme 1. The Three General Approaches To Prepare Polymer/Silica Nanocomposites

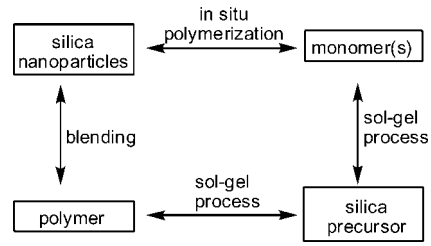

Scheme 2. Schematic Illustrations of Three Types of Surface Silanol

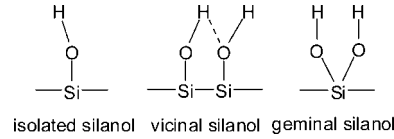

Scheme 3. Schematic of Aggregate Formation between Adjacent Fumed Silica Particles through Hydrogen Bonding among the Silanol Groups[a]

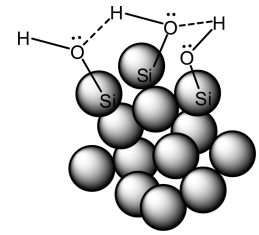

[a] Reprinted with permission from Jana, S. C.; Jain, S. Polymer 2001, 42, 6897. Copyright 2001 Elsevier Science Ltd.

treating silicates with mineral acids to obtain fine hydrated silica particles in the course of precipitation.[63] For the preparation of silica nanocomposites, fumed silica is commonly used and precipitated silica is seldomly used since the precipitated one has more silanol (Si−OH) groups on the surface and consequently it is much easier to agglomerate than fumed one. As for commercial colloidal silica spheres, they are usually in the form of a sol, with water or alcohol as the dispersing medium.

The structure of nanosilica shows a three-dimensional network. Silanol and siloxane groups are created on the silica surface, leading to hydrophilic nature of the particles. The surfaces of the silica are typically terminated with three silanol types: free or isolated silanols, hydrogen-bonded or vicinal silanols and geminal silanols (Scheme 2).[59] The silanol groups residing on adjacent particles, in turn, form hydrogen bonds and lead to formation of aggregates, as shown in Scheme 3. These bonds hold individual fumed silica particles together and the aggregates remain intact even under the best mixing conditions if stronger filler−polymer interaction is not present.[64]

The dispersion of nanometer-sized particles in the polymer matrix has a significant impact on the properties of nanocomposites. A good dispersion may be achieved by surface chemical modification of the nanoparticles or physical methods such as a high-energy ball-milling process and ultrasonic treatment.

The great differences in the properties of polymer and silica materials can often cause phase separation. Therefore, the interfacial interaction between two phases of nanocomposites is the most decisive factor affecting the properties of the resulting materials.[4b] A variety of methods have been

Table 1. Typical Silane Coupling Agents Used for Surface Modification of Silica Nanoparticles

abbreviation	name	chemical struture
APMDES	aminopropyl methydiethoxysilane	$H_2N(CH_2)_3(CH_3)Si(OC_2H_5)_2$
APMDMOS	(3-acryloxypropyl)methydimethoxysilane	$CH_2{=}CHCOO(CH_2)_3(CH_3)Si(OCH_3)_2$
APTES (APTS, APTEOS, APrTEOS)	3-aminopropyltriethoxysilane	$H_2N(CH_2)_3Si(OC_2H_5)_3$
APTMS (APTMOS, APrTMOS)	3-aminopropyltrimethoxysilane	$H_2N(CH_2)_3Si(OCH_3)_3$
APTMS (APTMOS)	(3-acryloxypropyl)trimethoxysilane	$CH_2{=}CHCOO(CH_2)_3Si(OCH_3)_3$
APTMS (APTMOS)	aminophenyltrimethoxysilane	$H_2NPhSi(OCH_3)_3$
TESPT	bis(triethoxysilylpropyl)tetrasulfane	$(C_2H_5O)_3Si(CH_2)_3S_4(CH_2)_3Si(OC_2H_5)_3$
DDS	dimethyldichlorosilane	$(CH_3)_2SiCl_2$
GPS (GPTS, GOTMS, GPTMOS, KH560)	3-glycidoxypropyltrimethoxysilane, 3-glycidyloxypropyltrimethoxysilane	$CH_2(O)CHCH_2O(CH_2)_3Si(OCH_3)_3$
ICPTES	3-isocyanatopropyltriethoxysilane	$OCN(CH_2)_3Si(OC_2H_5)_3$
MMS	methacryloxymethyltriethoxysilane	$CH_2{=}C(CH_3)COOCH_2Si(OC_2H_5)_3$
MPS (MPTMS, MPTS, MAMSE, MATMS, MSMA, TPM, MEMO, KH570)	methacrylic acid 3-(trimethoxysilyl) propyl ester, 3-(trimethoxysilyl)propyl methacrylate, 3-methacryloxypropyltrimethoxysilane	$CH_2{=}C(CH_3)COO(CH_2)_3Si(OCH_3)_3$
MPTES	methacryloxypropyltriethoxysilane	$CH_2{=}C(CH_3)COO(CH_2)_3Si(OC_2H_5)_3$
MPTS	mercaptopropyl triethoxysilane	$SH(CH_2)_3Si(OC_2H_5)_3$
MTES	methyltriethoxysilane	$CH_3Si(OC_2H_5)_3$
PTMS	phenyltrimethoxysilane	$PhSi(OCH_3)_3$
VTES	vinyltriethoxysilane	$CH_2{=}CHSi(OC_2H_5)_3$
VTS	vinyltrimethoxysilane	$CH_2{=}CHSi(OCH_3)_3$

used to enhance the compatibility between the polymer (hydrophobic) and nanosilica. The most frequently used method is to modify the surface of silica nanoparticles (especially for the blending and in situ method), which can also improve the dispersion of nanosilica in the polymer matrix at the same time. In general, surface modification of nanosilica can be carried out by either chemical or physical methods.[13]

2.2. Modification by Chemical Interaction

Much attention has been paid to modification of the surface of the nanosilica by chemical interaction since it can lead to much stronger interaction between modifiers and silica nanoparticles. Chemical methods involve modification either with modifier agents or by grafting polymers. Silane coupling agents are the most used type of modifier agents. They generally have hydrolyzable and organofunctional ends. The general structure of the coupling agents can be represented as[65] $RSiX_3$, where the X represents the hydrolyzable groups, which are typically chloro, ethoxy, or methoxy groups. The organo, R, group can have a variety of functionalities chosen to meet the requirements of the polymer. The functional group X reacts with hydroxyl groups on the SiO_2 surface, while the alkyl chain may react with the polymer. Hydrophobic silica can thus be obtained. Some typical silane coupling agents used for surface modification of nanosilica are listed in Table 1, among which the most commonly used one is MPS. In addition, polymeric silane coupling agents such as trimethoxysilyl-terminated P(MA-St)[66] have also been developed.

Other modifier agents, such as epichlorohydrin,[67] TDI,[67] 2-(methacryloyloxy)ethyl isocyanate,[68] DGEBA,[69a] GMA,[69a] AGE,[69a,b] glycidyl phenyl ether (GPE),[69c–e] and octadecylamine,[70] are also used.

Grafting of polymer chains to silica nanoparticles is also an effective method to increase the hydrophobicity of the particles and to bring about tunable interfacial interactions in nanocomposites. Generally, there are two main approaches to chemically attaching polymer chains to a surface: covalent attachment of end-functionalized polymers to the surface ("grafting to" method) and in situ monomer polymerization with monomer growth of polymer chains from immobilized initiators ("grafting from" method). In a sense, the polymer-grafted silica nanoparticles can also be viewed as polymer/silica nanocomposites. It will be discussed in detail in section 5.3.

Besides above-described chemical methods, grafting of polymers to nanoparticles can also be realized by irradiation. Zhang and co-workers[63,71] have published a series of studies on irradiation-grafted nanosilica-filled nanocomposites. It was found that modification of nanoparticles through graft polymerization was very effective to construct nanocomposites because of (i) an increase in hydrophobicity of the nanoparticles that is beneficial to the filler/matrix miscibility, (ii) an improved interfacial interaction yielded by the molecular entanglement between the grafting polymer on the nanoparticles and the matrix polymer, and (iii) tailorable structure−properties relationship of the nanocomposites provided by changing the species of the grafting monomers and the grafting conditions since different grafting polymers might bring about different interfacial characteristics.

2.3. Modification by Physical Interaction

Surface modification based on physical interaction is usually implemented by using of surfactants or macromolecules adsorbed onto the surface of silica particles. The principle of surfactant treatment is the preferential adsorption of a polar group of a surfactant to the surface of silica by electrostatic interaction. A surfactant can reduce the interaction between the silica particles within agglomerates by reducing the physical attraction and can easily be incorporated into a polymer matrix. For example, silica was treated with CTAB to improve the chemical interaction between SiO_2 and polymer;[72] SiO_2 nanoparticles were modified with stearic acid to improve their dispersion and the adhesion between the filler and polymer matrix;[73,74] nanosized silica was modified with oleic acid, which was bonded to the silica surface with a single hydrogen bond.[75–77]

Adsorption of polymer can also promote the surface hydrophobicity of silica particles. Reculusa et al.[78] modified a silica surface by adsorption of an oxyethylene-based macromonomer. This macromonomer is mainly hydrophilic

Scheme 4. Schematic Drawings of (a) Agglomerated Nanoparticles Dispersed in a Polymer Matrix and (b) the Possible Structure of Grafted Nanoparticles Dispersed in a Polymer Matrix[a]

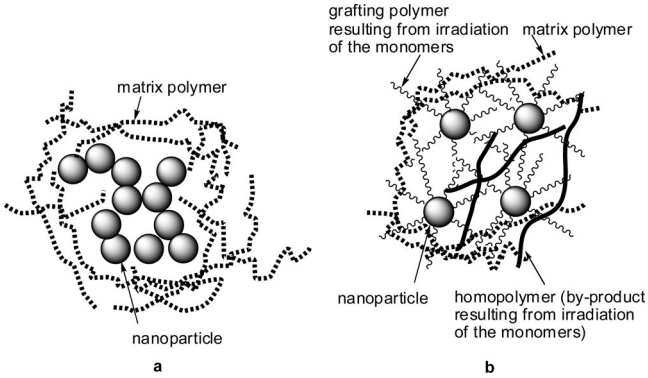

[a] Reprinted with permission from Rong, M. Z.; Zhang, M. Q.; Zheng, Y. X.; Zeng, H. M.; Walter, R.; Friedrich, K. Polymer 2001, 42, 167. Copyright 2001 Elsevier Science Ltd.

due to the presence of ethylene oxide groups, which are able to form hydrogen bonds with silanol functions present on the silica surface. At one of its ends, this molecule also contains a methacrylate group, which constitutes a polymerizable group for the later reaction of styrene. Lu et al.[79] chose a natural biomacromolecule, chitosan, as an adsorbent to alter the surface properties of silica. The acetylamino group in chitosan is considered to form hydrogen bonds with the hydrogen atom on nitrogen of PPy and ensures the fixed-site growth of PPy on silica.

3. Blending

The traditional and simplest method of preparing polymer/silica composites is direct mixing of the silica into the polymer. The mixing can generally be done by melt blending and solution blending. The main difficulty in the mixing process is always the effective dispersion of the silica nanoparticles in the polymer matrix, because they usually tend to agglomerate.

3.1. Melt Blending

Melt blending is most commonly used because of its efficiency, operability, and environmental containment.[13a] Polymers and polymer blends like PP,[63,70,71a–m,80–87] PP-based copolymer,[88] PE,[71n,89–93] PE-based copolymer,[94,95] PS,[95–97] PMMA,[97,98] PC,[97] PC-based copolymer,[99] PEN,[62,73] perfluoropolymer,[100] PET,[101–103] PES,[64] PA 6,[104,105] PA 66,[106] PEI,[107] PDMS,[108] PVAc,[109] copolyetherester,[110] styrene−butadiene rubber,[111,112] EVA,[113] thermoplastic olefin (TPO),[114] thermoplastic vulcanizate (TPV),[72] PP/PS,[115a,116] PP/EPDM,[115b,c] PET/PA 6[115d] liquid crystalline polymer (LCP)/PP,[117] LCP/PC,[118a,b] LCP/PSF,[118c] PET/PS,[119] PCL,[120] polyhydroxyalkanoate,[121] and poly(L-lactide)[122] have been reported as the matrices.

As indicated several times before, making a homogeneous dispersion of nanoparticles in a polymeric matrix is a very difficult task due to the strong tendency of nanoparticles to agglomerate. Consequently, the so-called nanoparticle filled polymers sometimes contain a number of loosened clusters of particles (Scheme 4a) and exhibit properties even worse than conventional particle/polymer systems.[71b] To break down these nanoparticle agglomerates and to produce nanostructural composites, an irradiation grafting method was applied for the modification of nanoparticles and then the grafted nanoparticles were mechanically mixed. A series of works on irradiation grafted nanosilica filled PP composites have been reported by Zhang and co-workers[63,71a–m] since 2000. Through irradiation grafting polymerization, nanoparticle agglomerates turned into a nanocomposite microstructure (comprising the nanoparticles and the grafted, homopolymerized secondary polymer, Scheme 4b), which in turn built up a strong interfacial interaction with the surrounding, primary polymeric matrix during the subsequent mixing procedure. Because different grafting polymers brought about different nanoparticle/matrix interfacial features, microstructures and properties of the ultimate nanocomposites could be tailored. It was found that the reinforcing and toughening effects of the nanoparticles on the polymer matrix could be fully brought into play at a rather low filler loading (typically less than 3 vol %) in comparison with conventional particulate filled composites. The technique was characterized by many advantages, such as being simple, low cost, easy to control and broadly applicable.[71b] A double percolation of stress volumes around the nanoparticles and their agglomerates, which was characterized by the appearance of connected shear yielded networks throughout the composite, explained the reinforcing and toughening effects of the treated nanoparticles.[71d] The cases of industrial-scale twin screw extruder and injection molding machine[71k] instead of laboratory-scale single screw extruder and compression molding, PE[71n] instead of PP, and precipitated nanosilica[63] instead of fumed nanosilica have also been successfully investigated. All proved that the method was still effective. When graft pretreatment and drawing techniques were combined with melt mixing to prepare the composites, separation of the nanoparticles was induced, β-crystals in the PP matrix were formed, and the resultant PP-based nanocomposites were much tougher than the unfilled polymers.[71i]

In a recent publication[71m] of the same group, *p*-vinylphenylsulfonylhydrazide, a polymerizable foaming agent, was synthesized and grafted onto the silica nanoparticles. It was found that the grafted poly(*p*-vinylphenylsulfonylhydrazide) played dual roles when melt mixed with PP. The side sulfonylhydrazide groups were gasified to form polymer bubbles, leading to rapid inflation of the surrounding matrix that pulled apart the agglomerated nanoparticles, while the remaining backbone of the grafted polymer helped to improve the filler/matrix interaction through chain entanglement and interdiffusion at the interface. Furthermore, a route that combined in situ bubble-stretching and reactive compatibilization techniques was also proposed.[71l]

Karayannidis et al.[80a] prepared iPP/SiO_2 nanocomposites with untreated and surface-treated silica nanoparticles by melt compounding using a corotating screw extruder. SiO_2 contents of 1, 2.5, 5, 7.5, and 10 wt % were used. All nanocomposites were transparent as pure iPP, indicating fine dispersion of the silica nanoparticles into iPP matrix and the retention of their nanosizes. However, scanning and transmission electron microcopy indicated that silica nanoparticles were dispersed not as individual particles but more or less as agglomerates. The extent of the agglomeration depended on the amount of SiO_2 as well as on its hydrophobic or hydrophilic character. When PP-*g*-MA copolymer was added as a compatibilizer,[80c] it resulted in a higher adhesion between the iPP matrix and SiO_2 nanoparticles, due to the interactions that took place between the reactive groups. Thus

Scheme 5. Schematic Representation of PET/SiO_2 Cross-Linked Macromolecules[a]

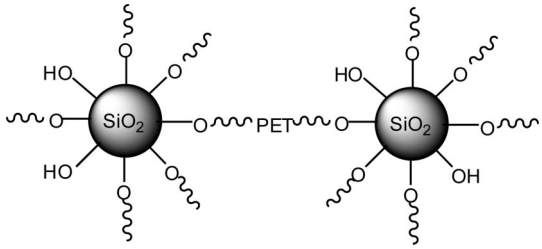

[a] Reprinted with permission from Bikiaris, D.; Karavelidis, V.; Karayannidis, G. Macromol. Rapid Commun. 2006, 27, 1199. Copyright 2006 Wiley-VCH.

the size of silica aggregates decreased, inducing a further enhancement in mechanical properties.

Kim et al.[62] prepared silica nanoparticle-filled PEN composites by melt-blending to improve the mechanical and rheological properties of PEN. The melt viscosity and total torque values of the composites were reduced by the silica content because it acted as a lubricant in the PEN matrix. Such additions could be proposed as possibly improving the processability and various applications of PEN. A further study[73] investigated the effect of stearic acid modification on the dispersity of silica nanoparticles and the adhesion between the filler and polymer matrix with stearic acid concentration. The wettability of silica nanoparticles could be improved by modification with stearic acid. From contact angle measurements, it was found that the stearic acid modification enabled the filler's surface to become hydrophobic, and thus the stearic acid-modified filler was more easily wetted by the polymeric matrix melt. The presence of adsorbed stearic acid on the surface of the silica nanoparticles reduced the interactions between the silica nanoparticles within any agglomerates, and these agglomerates could be broken down more easily.

The commercial production of PET polyesters requires a subsequent postpolymerization process in the solid state, in order to reach intrinsic viscosity values greater than 0.80 $dL \cdot g^{-1}$ and make the polyester appropriate for blown bottle production. Karayannidis et al.[102] unexpectedly found that solid-state polycondensation (SSP) could act as a facile method to prepare PET/SiO_2 nanocomposites with high molecular weight and an adjustable degree of branching or cross-linking. Fumed silica, with its surface silanol groups, seemed to participate in some kind of reaction, probably esterification with the hydroxy end groups of PET, during SSP to act as a multifunctional chain extender. Silica agglomerates reacted with the surrounding end group macromolecules of PET. The PET/SiO_2 cross-linked macromolecules are schematically presented in Scheme 5. The molecular weight increase depended on the temperature used in SSP, as well as on the amount of SiO_2 added. As the amount of silica increased the rate of increase of the intrinsic viscosity slowed because of the higher extent of branching. At 5 wt % SiO_2, the extensive branching produced a cross-linked polymeric material. Such polyesters with increased molecular weight and low silica content could be suitable for blown bottle production, while the high SiO_2 content and adjustable branching or cross-linking could make them ideal high-melt strength resins suitable for the preparation of low-density closed-shell foams.

Melt mixing of nanoparticles with high-performance polymers is not feasible due to severe shear heating and formation of particle aggregates. Jana and Jain[64] proposed an alternative method involving the use of low molecular weight reactive solvents as processing aids and dispersing agents. Dispersion of nanosized fumed silica particles in a PES matrix was conducted with the aid of small amounts of low molecular weight epoxy. Viscosity and processing temperature of PES were significantly reduced, and fumed silica particles were successfully dispersed to nanoscales. The epoxy component was polymerized after dispersion of fumed silica to recover the mechanical properties. Significant improvement in barrier resistance and deflection temperature over neat PES was observed.

Garcìa et al.[104] prepared nylon 6/silica nanocomposites by large-scale extrusion processing. The filler used was added as sol in a twin screw extruder apparatus, providing bulk amounts of composite material at industrial scale. The XRD spectra showed a constant degree of crystallinity for all the composites. The behavior illustrated by the DMA curves indicated that in general when a filled system was compared with an unfilled material, the values of the moduli (E' and E'') increased and the damping decreased. Furthermore, the values measured experimentally were found to be above of the theoretical predictions.

Polymer blends have been widely used in many fields. However, most polymer blends are immiscible. In recent years, some work has focused on the possibility of using silica nanoparticles as a compatibilizer for polymer blends. Blends of PP and dynamically vulcanized EPDM rubber are called TPVs. Wu and Chu[72] prepared nanocomposites of TPV/SiO_2. The CTAB-treated SiO_2 was melt-blended with TPV in the presence of MA grafted PP (mPP), which acted as a functionalized compatibilizer. During melt blending, CTAB and mPP tethered themselves onto the TPV backbone by a grafting reaction. The strong interaction caused by the grafting reaction improved the dispersion of silica in the TPV matrix.

Fu et al.[115a] reported the change of phase morphology and properties of immiscible PP/PS blends compatibilized with nano-SiO_2 particles. The compatibility of PP/PS blends was dramatically improved with the addition of nano-SiO_2 particles, which possess excellent hydrophobicity and contain a large number of alkyls on their surface. The SiO_2 content and mixing time also had profound effects on the compatibility of PP/PS blends. A drastic reduction of PS phase size and a very homogeneous size distribution were observed by introducing nano-SiO_2 particles in the blends at short mixing time. However, at longer mixing time an increase of PS size was seen again, indicating a kinetics-controlled compatibilization.

LCPs consist of linear semirigid rod-like molecules that are capable of forming well-ordered fibrillar structures with anisotropic properties. In recent years, blends of thermoplastics and LCPs have been the focus of intense academic and industrial interest. LCP/PP/SiO_2 composites with various silica concentrations were reported by Hu et al.[117] Results revealed the transformation of short LCP fibrils to high aspect ratio fibrous structures upon the addition of the nanofillers. The silica particles had promoted the shear-induced fibrillation of the LCP phase. The WAXD results indicated that high orientation was achieved with rising silica content. The injection molded samples also showed increased mechanical anisotropy with rising filler content. Consequently, both the in situ fibrillation of LCP and silica reinforcements imparted good tensile strength and modulus to the composites along

the flow direction. Such an improvement was achieved basedon increasing the matrix viscosity and raising the capillary number, which was a dimensionless factor governing the fibrillation process. LCP/PC/SiO_2[118a,b] and LCP/PSF/SiO_2[118c] ternary blends were also prepared.

As the interest in industrial application of biodegradable polymers is growing, biodegradable polymer/silica nanocomposites have attracted much attention. PCL/SiO_2,[120] poly(3-hydroxybutyrate-*co*-3-hydroxyhexanoate)/SiO_2,[121] and poly(L-lactide)/SiO_2[122] prepared by melt compounding have been reported.

3.2. Solution Blending

Solution blending is a liquid-state powder processing method that brings about a good molecular level of mixing and is widely used in material preparation and processing. Some of the limitations of melt mixing can be overcome if both the polymer and the nanoparticles are dissolved or dispersed in solution but at a cost depending on the solvent and its recovery.[4a,13a] The location for solution blending herein is not limited to a solution[69c–e,74,107,123–152] and can include a latex[153,154] or a suspension.[155–161] A method through solution blending and then compression molding is also applied.

Polymer/silica nanocomposite membranes have received much attention in the past decade, and such membranes are typically prepared by solution-casting mixtures of nanosilica and polymer. The membranes can be applied in gas separation such as reverse-selective process, in liquid separation such as pervaporation, and as a proton exchange membrane for fuel cell, among other uses.

It is well-known that the presence of nonporous particles in conventional filled polymer systems typically reduces the permeability of a polymer by reducing the volume of polymer available for transport and increasing the tortuosity of the diffusion path available to gas molecules. However, in 2001, it was discovered by Merkel et al.[123] that the addition of nanometer-sized fumed silica particles to certain high-free-volume, glassy polymers could systematically increase gas permeability. Such high-permeability polymers included poly(4-methyl-2-pentyne) (PMP),[123,124] poly[1-(trimethylsilyl)-1-propyne] (PTMSP),[125–128] and poly(2,2-bis(trifluoromethyl)-4,5-difluoro-1,3-dioxole-*co*-tetrafluoroethylene).[129,130] PMP and PTMSP are both members of a family of substituted acetylene polymers that exhibit poor polymer chain packing in part due to rigid backbones, low interchain cohesion, and bulky substituents. These glassy polymers are characterized by low densities, high fractional free volumes, high gas permeabilities, and in some cases vapor selectivity (i.e., they are more permeable to large organic vapors than to small permanent gases), which in glassy polymers is unusual (most conventional glasses are size-selective, i.e., more permeable to small molecules than to larger ones). Such unusual transport properties make them particularly well suited for vapor separation applications. PTMSP is a material possessing the highest organic-vapor permeability and vapor/permanent gas selectivity of all known polymers. It is approximately an order of magnitude more permeable than PMP and has roughly double the vapor/permanent gas selectivity of PMP, but its high solubility in hydrocarbon solvents restricts its use. However, PMP has better solvent resistance than PTMSP.[125b]

Upon addition of nonporous, nanoscale fumed silica particles to PMP, both permeability and vapor/permanent gas selectivity simultaneously increased (Figure 1). For example, incorporation of 30 wt % FS into PMP doubled mixed-gas *n*-butane/methane selectivity and increased *n*-butane permeability by a factor of 3. This highly unusual result suggested that the volume filling and tortuosity effects were offset by the ability of these tiny particles to disrupt packing of rigid polymer chains, thereby subtly increasing the amount of free volume in the polymer.[123]

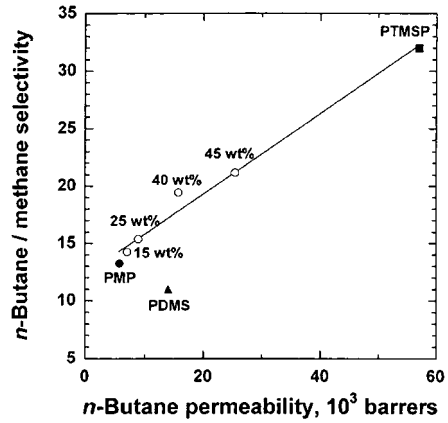

Figure 1. Effect of FS content on *n*-butane permeability and *n*-butane/methane selectivity of PMP (●, pure PMP; ○, filled PMP containing 15, 25, 40, and 45 wt % FS; 1 barrer = 10^{-10} cm^3 (STP) cm/(cm^2 s cmHg). All data have been collected at 25 °C from mixed-gas experiments with an upstream pressure of 11.2 atm, a permeate pressure of 1 atm, and a feed composition of 2 mol % *n*-butane in methane. Data for PDMS (▲) and PTMSP (■) are provided for comparison. Reprinted with permission from ref 123c. Copyright 2003 American Chemical Society.

Similar to PMP, incorporation of FS into PTMSP increased penetrant permeability. However, in contrast to PMP, the permeability of PTMSP to relatively small gases increased more upon filling than that of larger penetrants. This resulted in a reduction in vapor/permanent gas selectivity for filled PTMSP. In fact, mixed-gas *n*-butane/methane selectivity was 64% lower in PTMSP containing 50 wt % FS than in pure PTMSP. This result was ascribed to PTMSP having larger and more interconnected free volume elements than PMP. Addition of FS increased the size of these free volume elements to the point where free phase transport mechanisms that favored light gas transport, such as Knudsen diffusion, appeared to become important.[125b] At a constant volume fraction of nonporous fumed silica nanoparticles with essentially equivalent surface chemistries, gas permeability of PTMSP/silica nanocomposites increased linearly with decreasing primary particle size.[125c]

Unlike PMP and PTMSP, poly(2,2-bis(trifluoromethyl)-4,5-difluoro-1,3-dioxole-*co*-tetrafluoroethylene), a random copolymer containing of the packing-disrupting dioxole monomer, is size-selective. The addition of nanoscale, nonporous fumed silica particles to it (AF2400, containing 87 mol % of the packing-disrupting dioxole monomer) systematically increased penetrant permeability coefficients, similar to behavior observed in PMP and PTMSP but contrary to results in traditional filled polymer systems. Permeability coefficients of large penetrants increased more than those of small molecules in filled AF2400, thereby decreasing the size selectivity of this polymer. As a result, AF2400 exhibited a selectivity reversal for the vapor−gas pair *n*-C_4H_{10}/CH_4, becoming *n*-butane selective above 18 wt % FS (Figure 2). FS addition modified AF2400, allowing *n*-butane to be accommodated without swelling the matrix,

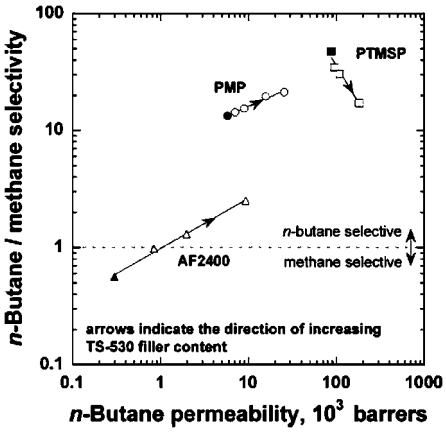

Figure 2. Mixed-gas *n*-butane/methane permselectivity vs *n*-butane permeability in AF2400 (▲), FS-filled AF2400 (△, 18, 30, and 40 wt %), PMP (●), FS-filled PMP (○; 15, 25, 40, and 45 wt %), PTMSP (■), and FS-filled PTMSP (□; 30, 40, and 50 wt %) (1 barrer = 10^{-10} cm^3 (STP) cm/(cm^2 s cmHg). Reprinted with permission from ref 129. Copyright 2003 American Chemical Society.

thereby mitigating penetrant-induced plasticization, whereas unfilled AF2400 was readily plasticized by *n*-butane. This finding implied that all of the increase in penetrant permeability in filled AF2400 was a result of increased diffusion coefficients.[129]

Kim et al.[135a] prepared an organic/inorganic nanocomposite membrane using a reactive polymeric dispersant and compatibilizer urethane acrylate nonionomer (UAN). Sulfonated styrene copolymer (PSSU) membranes were prepared over a wide range of sodium styrene sulfonate and styrene compositions using UAN as a compatibilizer to overcome the synthetic limitations derived from the solubility difference and immiscibility of each monomer. UAN also played a role as a dispersant to uniformly distribute the silica nanoparticles of different hydrophilicity and to obtain subsequent sulfonated PS/SiO_2 nanocomposite membranes.Similarly, sulfonated PI/SiO_2 nanocomposite membranes containing IPN were also fabricated. UANs were used as dispersants to homogeneously distribute nanosized SiO_2 and, simultaneously, as cross-linkers to induce IPN structure formation.[135b]

van Zyl et al.[136] reported the preparation of PA/silica nanocomposites via solution blending. Nylon 6 was first dissolved in formic acid, the pH was controlled at ca. 2, and the silica sol with particle sizes 10−30 nm was added to the nylon solution and stirred gently at room temperature. The solution was then casted, and the solvent was evaporated. The procedure was based on selecting appropriate reaction conditions, particularly with regard to solvent choice and pH control. Formic acid not only dissolves nylon 6 but compared with the other solvents is a much stronger Brønsted acid and hence effective in keeping the charge on the silica surface, prohibiting dissipation of charge and consequent gel formation. Through addition of small amounts of aqueous HCl, a positive charge on the silica surface was maintained at ca. pH 1−2. Such a low pH was necessary since the isoelectric point of silica is in the pH 2−3 range. The composite was examined with TEM, which revealed that the silica particles were well-dispersed and nonaggregated.

Oberdisse and Demé[153] synthesized silica-filled latex films. Samples were prepared by mixing appropriate amounts of colloidal silica and latex stock solutions (previously brought to the desired pH) in order to obtain a given volume fraction

Scheme 6. Drawing Illustrating the Latex Route for Incorporation of Nanoscopic Colloidal Silica Beads in Polymer Films by Latex Film Formation[a]

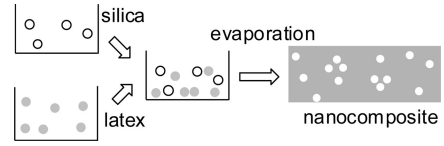

[a] Reprinted with permission from Oberdisse, J. Soft Matter 2006, 2, 29. Copyright 2006 The Royal Society of Chemistry.

of silica in the final composite film. The nanolatex was a core−shell latex of PMMA and PBA, with a hydrophilic shell containing methacrylic acid. The main stage of the synthesis consists of physicochemical manipulations of colloidal solutions of nanosilica and nanolatex beads, followed by drying and film formation (Scheme 6).

Zhang and Archer[155] prepared PEO/silica nanocomposites using a "freeze-drying" method to guarantee homogeneous dispersion of silica. A three-step procedure was followed to disperse silica nanoparticles in the PEO matrix. In the first step, colloidal silica was diluted with deionized water to produce a colloidal dispersion. The dilute suspension was mixed with an aqueous PEO solution. Sterically stabilized silica nanoparticles were homogeneously dispersed by continuously stirring. In the second step, the suspension was frozen rapidly with liquid nitrogen and freeze-dried to remove water and NH_4OH. The freeze-drying procedure yielded a porous hybrid that was finally compressed in a vacuum to form nanocomposite films. The compressive force used in the final step was deliberately kept small to avoid creation of voids in the film.

Occasionally, a specific silica precursor is used in the blending method instead of silica nanoparticles. In 2002, Saito et al.[43a] discovered organic/silica nanocomposites with well-ordered micro-phase separation with PHPS, which is highly soluble in many organic solvents and is highly multireactive with hydroxyl groups. Thus, it is possible to graft PHPS onto organic polymers that contain hydroxyl groups. When the organic polymer is soluble in the organic solvent in which PHPS is dissolved, the graft copolymer will be soluble in the organic solvent. By blending PHPS and the organic polymer with hydroxyl groups in the organic solvent and casting the blend solution resulted in convenient formation of the organic/PHPS film with organic polymer and PHPS microdomains. The general procedure to prepare the organic/silica nanocomposites is as follows: a PHPS/xylene solution (PHPS concentration 20 wt %) was added to an organic polymer solution. To prevent gelation, polymer concentration was set at 1 wt %. The blend solution was stirred at room temperature for 12−24 h. Then, the solution was casted on a substrate and gradually dried. By calcination at 100 °C for 4 h under steam, organic/silica nanocomposites were obtained. A series of polymer/silica nanocomposites have been prepared by blending PHPS and PMMA,[43a–d,h] P2VP,[43e,f] P4VP,[43e] and PS[43g] containing hydroxyl groups. Scheme 7 shows the synthetic concept of nanocomposites of organic polymer and silica glass by hybridization of PHPS and random copolymers containing hydroxyl groups.

Conversely, specific polymer precursors instead of polymers were also used infrequently in the blending method.[145,146] Ho et al.[145] obtained thin films of the semiconducting poly(*p*-phenylenevinylene) (PPV)/SiO_2 composite that exhibited composition-tunable optical constants. The method comprises

Scheme 7. Synthetic Scheme of Organic/Silica Nanocomposites with PHPS[a]

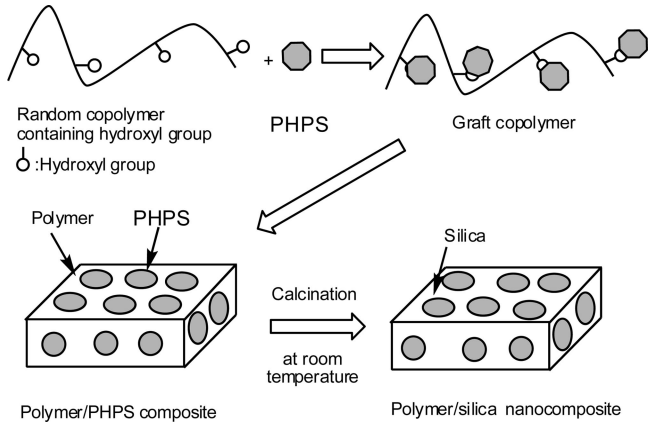

[a] Reprinted with permission from Saito, R. J. Polym. Sci., Part A: Polym. Chem. 2006, 44, 5174. Copyright 2006 Wiley Periodicals, Inc.

Scheme 8. A Schematic Diagram for the Preparation of Homogeneous PPV/SiO_2 Nanocomposites[a]

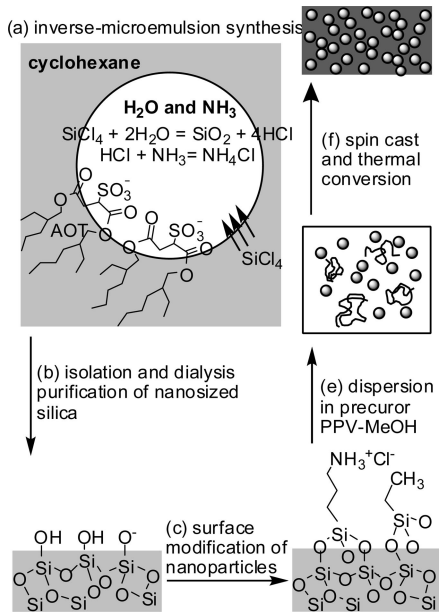

[a] Reprinted with permission from Ho, P. K. H.; Friend, R. H. J. Chem. Phys. 2002, 116, 6782. Copyright 2002 American Institute of Physics.

a microemulsion nanoparticle synthesis, followed by surface functionalization and homogeneous blending with the polymer precursor solution for subsequent processing (Scheme 8).

3.3. Other Blending Methods

Even the melt or solution route becomes infeasible when the particle load is high, the polymer melt is viscous, or the polymer just does not melt at all. One way to overcome these problems is to process the polymer in the solid state, which avoids the thermal and solvent problems encountered with traditional technologies while providing almost infinite design flexibility and processing simplicity. Cryogenic mechanical alloying or cryogenic ball milling (cryomilling) is such a solid-state method that can effectively improve blending intimacy and enhance compatibility. Li et al.[162] prepared PET/SiO_2 nanocomposites by cryomilling. A three-stage model to illustrate the formation mechanism of PET/SiO_2 nanostructures was deduced. The first stage was characterized by the great reduction of particle size and the transformation of PET from big blocks into flakes; meanwhile the SiO_2 conglomerations were broken up and dispersed in PET flakes forming the primary composite particles. The second stage was characterized by the gradual dispersion of single SiO_2 nanoparticles into PET flakes, and the formation of the secondary composite particles due to the conglomeration of the refined PET/SiO_2 primary composite particles. The third stage was characterized by the constant size of the secondary composite particles and the further homogeneous dispersion of nanometer SiO_2 in PET matrix. It was shown that, upon cryomilling for 10 h, SiO_2 nanoparticles were well-separated into single particles (~30 nm) that get homogeneously dispersed in PET matrix. The resulted PET/SiO_2 primary particles were flake-shaped with a size of 400 nm. These primary composite particles agglomerated to form secondary composite particles with an average size about 7.6 μm. The dispersion homogeneity of SiO_2 nanoparticles in PET matrix was far beyond the capability of conventional methods, which was ascribed to solid processing, high mechanical energy of ball milling, and cryogenic temperature.

The solid-state method of high-energy blending by ball milling was reported by González-Benito et al.[163] Fumed silica nanoparticles of 14 nm diameter were blended with PMMA. It was observed that the properties of the composite were highly dependent on the active milling time.

Another excellent solution to the processing limitations of polymer/ceramic nanocomposites, such as the use of solvents, is thermal spraying. Thermal spray generally is a process in which a material is heated, accelerated, and propelled by a high-temperature jet through a confining nozzle toward a surface. The individual molten or softened droplets impact, spread, cool, and solidify to form continuous coatings. High-velocity oxy-fuel (HVOF) provides thermal energy for heating provided by combusting fuels with oxygen. Petrovicova et al.[164] produced nylon 11 coatings filled with nanosized silica using the HVOF combustion spray process. Powders were prepared for spraying by dry ball-milling nylon 11 together with the nanoparticulate phase for 48 h in a ball mill using zirconia balls to create a composite powder. The composite powder aided both the distribution of the filler in the coating and the simultaneous powder feeding into the HVOF spray jet.

4. Sol−Gel Process

Sol−gel reactions have been extensively studied for several decades as a method to prepare ceramic precursors and inorganic glasses at relatively low temperatures. The major advantage of the process is that mild conditions, such as relatively low temperature and pressure, are used in this type of processing of ceramics. Within the past decades, the sol−gel process has been widely used to create novel organic−inorganic composite (hybrid) materials, which were termed "ceramers" by Wikes et al.[165] and "ormosils" or "ormocers" by Schmidt et al.[166] In the case of composites, the goal is to carry out the sol−gel reaction in the presence of organic molecules that are typically polymeric and contain functional groups to improve their bonding to the ceramic-like phase. This is a very useful novel reinforcement technique, which can generate reinforcing particles within a polymer matrix. Moreover, these novel hybrid sol−gel materials are normally nanocomposites and have the potential for providing unique combinations of properties that cannot

be achieved by other materials.[167] Several comprehensive reviews on the research activities in the field of organic/inorganic hybrid materials by the sol−gel approach have been published.[14–20]

As is well-known, the sol−gel process can be viewed as a two-step network forming process, the first step being the hydrolysis of a metal alkoxide and the second consisting of a polycondensation reaction. Most of the interest in this method is concentrated on metal−organic alkoxides, especially silica, since they can form an oxide network in organic matrices. The sol−gel reactions of alkoxysilane can be described as follows:
hydrolysis:

$$\geq Si{-}OR + H_2O \xrightarrow{H^+ \text{ or } OH^-} \geq Si{-}OH + ROH, \quad R = \text{alkyl groups} \qquad (2)$$

polycondensation:

$$\geq Si{-}OH + OH{-}Si\leq \xrightarrow{H^+ \text{ or } OH^-} \geq Si{-}O{-}Si\leq + H_2O \qquad (3)$$

and/or

$$\geq Si{-}OH + RO{-}Si\leq \xrightarrow{H^+ \text{ or } OH^-} \geq Si{-}O{-}Si\leq + ROH \qquad (4)$$

If these sol−gel reactions are complete, full condensed silica is obtained in this process that can be summarized by the following equation:

$$Si(OR)_4 + 2H_2O \xrightarrow{H^+ \text{ or } OH^-} SiO_2 + 4ROH \qquad (5)$$

The most common ceramic precursor is TEOS because it is readily purified and has a relatively slow and controllable rate of reaction.[167]

Many factors influence the kinetics of the hydrolysis and condensation reactions in the sol−gel process, which include the water/silane ratio, catalyst, temperature, the nature of solvent, and so forth. The sol−gel process surpasses the traditional blending method since it can subtly control the morphology or surface characteristics of the growing inorganic phase in the polymer matrix by control of these reaction parameters. The poor reactivity of silicon is generally activated by using acid or base catalysts. Acid catalysis results in a faster hydrolysis of TEOS and in an open weakly ramified polymer-like structure. In contrast, slower hydrolysis and faster polycondensation were observed in the case of base catalysis leading to compact colloidal particles. Large spherical particles are expected in the case of base-catalyzed reaction, while linear chain growth is expected via acid catalysis. It has been shown that basic catalysis usually yields opaque composites with phase dimensions well above 100 nm and more generally in the micrometer range. These materials can definitely not be considered as nanocomposites. Alternatively, if acid catalysis is used, transparent nanocomposites with characteristic morphology sizes below 100 nm are generally obtained. Therefore, the polymer/silica nanocomposites prepared by sol−gel processes are generally obtained by acid-catalysis.[6]

There are many different synthetic techniques used in the sol−gel process to generate polymer/silica hybrid materials, two approaches are normally utilized, as indicated in Scheme 1: (i) In situ formation of an inorganic network in the presence of a preformed organic polymer.[168–238] To obtain optically transparent materials, conditions need to be identified under which phase separation will not occur during both the gel forming and the drying processes. Introduction of covalent bonds between the inorganic and organic phases is common to reduce phase separation. The most important adjustable parameter in controlling polymer solubility is the cosolvent used. Solvents commonly used are alcohol, THF, and DMF. (ii) Simultaneous formation of both organic polymer and SiO_2 leading to IPN.[6,239–247] The two organic−inorganic synthetic techniques are distinguished by the sequence of formation of the organic and inorganic components.

For the sol−gel process, the properties of the resulting nanocomposites are in general influenced by particle sizes and interaction between the dispersed and continuous phases. According to the nature of interfacial interaction, hybrid materials can be grossly divided into two distinct classes, as defined by Sanchez and Ribot[15a] earlier. The class 1 hybrid involves physical or weak phase interactions, for example, hydrogen bonding or van der Waals. Meanwhile, in class 2, the hybrid possesses strong chemical bonds (covalent or ionocovalent bonds) between the organic and inorganic phases. Within many class 2 hybrid materials, organic and inorganic components can also interact via the same kind of weak bonds that define the class 1 hybrids.[17]

4.1. Class 1: Interfacial Interaction with Physical or Weak interaction

In order to prepare class 1 hybrid materials where hydrogen bonding is prevalent, the organic species usually need to bear functional groups that could form hydrogen bonds. Many kinds of polymers such as PHEMA,[6,141] acrylic copolymer/terpolymer,[168] PVA,[169,170] PDMS,[171,172] PA 66,[173] PAAm,[174] PU,[175] PVP,[176] PANI,[177] polysaccharide,[178] and other polymers[179–189] containing functional groups that can form hydrogen bonds with silica have been successfully used to prepare silica nanocomposites.

Huang et al.[141] used two methods to prepare the silica/PHEMA nanocomposites: one was the direct mixing of colloidal silica with PHEMA using methanol as a cosolvent (colloidal silica/PHEMA) and the other was the adding TEOS to the PHEMA/methanol solution, followed by the sol−gel process with an acid catalyst (TEOS/PHEMA). The structure of the colloidal silica/PHEMA hybrid consisted of nanosilica uniformly dispersed in the PHEMA phase with slight intermolecular hydrogen bonding. The structure of the TEOS/PHEMA hybrid was similar to a semi-interpenetrated network with PHEMA chains tethered into the nanosilica network by inter- and intramolecular hydrogen bonding. Consequently, the TEOS/PHEMA hybrid gels exhibited a smoother surface, higher transparency, and better thermal stability than the colloidal silica/PHEMA hybrid gels.

PVA is a hydrophilic polymer in nature and contains pendant hydroxyl groups. The hydroxyl groups in the repeating units of the polymer are expected to produce strong secondary interactions with the residual silanol groups generated from acid-catalyzed hydrolysis and polycondensations of TEOS. The relationships between the properties and structure of PVA/silica composites were discussed by

Scheme 9. The Tentative Modes of Hydrogen Bonding in the Monomer (Structure 1) and Polymer (Structure 2) Suggested from the FTIR Results[a]

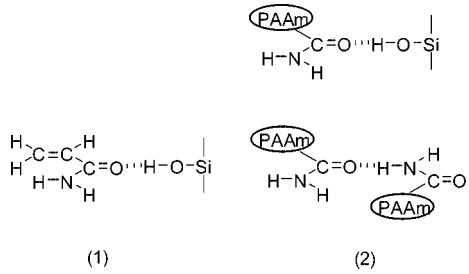

[a] Reprinted with permission from Jang, J.; Park, H. J. Appl. Polym. Sci. 2002, 83, 1817. Copyright 2002 John Wiley & Sons, Inc.

Suzuki et al.[169] The composites became stiff and brittle with increasing the silica content. The properties of the composites were changed drastically around the composition of PVA/silica = 70/30 wt %. Consequently, it was considered that the three-dimensional network structure of silica could be formed in the composite with more than 30 wt % of silica in PVA.

PDMS with a repeat unit [$-Si(CH_3)_2O-$] is the most commonly used member of the polysiloxanes polymers. However, PDMS elastomers exhibit very poor mechanical properties, particularly low tensile strengths, so they need to be reinforced by mineral fillers in order to improve mechanical properties required in almost all commercial applications. PDMS is traditionally reinforced with silica, and the chemical bonding between the two phases is ensured via hydrogen bonds between the silanols on the silica surface and the oxygen atoms of the polymer chains. Bokobza et al.[171] synthesized PDMS/silica nanocomposites by filling PDMS networks with in situ generated silica particles under the presence of two different catalysts: dibutyltin diacetate and dibutyltin dilaurate. In each case, the generated inorganic structures were uniformly dispersed in the polymer phase, but different morphologies were revealed reflecting two different types of growth processes.

Amide polymers such as PA, PAAm, and PU have been found to be most suitable for the preparation of hybrids with silica due to the $-NHCO-$ groups in the polymer chains, which very easily form hydrogen bonds with silanol groups. Bhowmick et al.[173] synthesized hybrid nanocomposites composed of PA 66 and SiO_2 through a sol−gel technique at ambient temperature. The inorganic phase was generated in situ by hydrolysis−condensation of TEOS in different concentrations under acid catalysis in presence of PA 66 dissolved in formic acid.

Jang and Park[174] studied the formation of nanocomposites by the sol−gel reaction of TEOS in PAAm. Since the solubility of PAAm in a solvent was very restrictive, the nanocomposites were prepared in aqueous solution. The aqueous solution of PAAm was diluted with distilled water to 25 wt %. A mixture of TEOS, HCl, and water was stirred vigorously to produce a homogeneous and transparent solution. Then the two solutions were mixed and stirred. The solution was placed in a PE bottle to undergo gelation and drying at room temperature. FTIR spectroscopy showed that substantial hydrogen bonding occurred in the nanocomposites. The tentative hydrogen bonding modes (Scheme 9) were suggested from the FTIR results.

Since the common precursors TEOS and TMOS do not dissolve enough in water, it is often necessary to add an organic solvent. However, its addition can have a denaturating effect and/or decrease the solubility of biopolymers, which sets limits on the possibility of the sol−gel technique to prepare biomaterials. As an alternative to TEOS and TMOS, tetrakis(2-hydroxyethyl)orthosilicate (THEOS) is completely water-soluble, which obviates the need for organic solvent addition. Shchipunov and Karpenko[178] synthesized monolithic nanocomposite silica biomaterials on the basis of various natural polysaccharides and completely THEOS. The sol−gel processes were performed in aqueous solutions without the addition of organic solvents and catalysts. The silica polymerization was promoted by the polysaccharides through acceleration and catalytic effect on the processes. The polysaccharides are polyhydroxy compounds because they are composed of numerous monosaccharide residues. Their hydroxyl groups could form hydrogen bonds or enter into the condensation reaction with silanols produced in the course of hydrolysis of the precursor, thus providing silica nucleation on macromolecules.

PCL can be end-capped with functional groups such as hydroxyl groups or vinyl groups reactive in the sol−gel process. Transparent hybrid materials that combine TEOS and PCL known for biodegradability and biocompatibility have accordingly been prepared.[179] The thermal stability of PCL was improved by incorporation into the silica network. Conversely, the thermal stability of the ceramer depended on the effective PCL content. The extent of PCL incorporation into the silica network depended on PCL molecular weight and number and reactivity of the PCL functional groups. IR spectroscopy showed that hydrogen bonding occurred between the ester groups of PCL and residual OH groups of the silicate component.

The $-COO-$ groups in the polyester chains are not strong enough to form hydrogen bonds with silanol groups. To improve the compatibility between the silica network and the polyester, Hsu et al.[181] prepared a type of linear polyester that contained hydroxy groups in the polymer chain to increase hydrogen bonding. This hydroxy-containing linear polyester (HLP) was obtained by a ring-opening reaction of DGEBA with adipic acid in xylene at 135 °C under the catalyzation of triphenylphosphine (TPP) (Scheme 10). The hybrid material, HLP/SiO_2, was obtained by the incorporation of HLP with TEOS through a sol−gel process. The hydroxyl groups in polyester not only form hydrogen bonds with silanol groups but can also form Si−O−C bonds by dehydrating with silanol groups at high temperature.

Similarly, PAAs with pendent hydroxyl groups were synthesized, and the corresponding PI/silica hybrid materials were prepared via a sol−gel process. Transparent hybrid films with higher silica contents were obtained, because the presence of hydroxyl groups improved the compatibility of the two components due to the formation of hydrogen bonds and chemical bonds between the organic and inorganic phases.[182]

Retuert et al.[187] synthesized hybrid compounds based on silica and a polyelectrolyte complex between chitosan (CHI) and poly(monomethyl itaconate) (PMMI). The inorganic phase was prepared by a sol−gel process of TEOS. PMMI has polar functional groups that could interact with residual silanol groups of the silica gel through hydrogen bonding. Most of the amine groups from CHI (pK_b 7.7) were quaternized in the acidic medium used in the preparations (pH = 2), where a physical cross-linking via hydrogen bonding could occur through carboxyl groups from PMMI.

Scheme 10. Ring-Opening Polymerization of DGEBA with Adipic Acid To Synthesize the HLP[a]

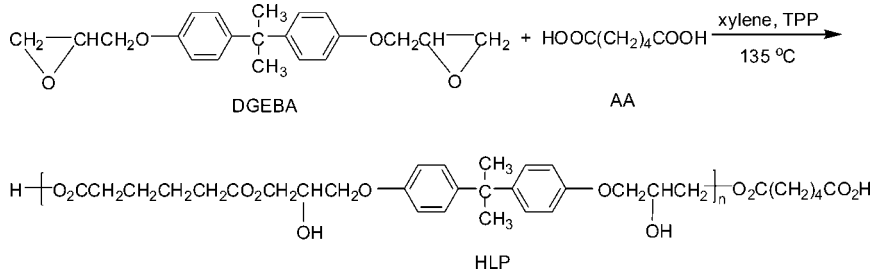

[a] Reprinted with permission from Hsu, Y. G.; Chiang, I. L.; Lo, J. F. J. Appl. Polym. Sci. 2000, 78, 1179. Copyright 2000 John Wiley & Sons, Inc.

Silica gel obtained from TEOS was intercalated as a very fine dispersion in the polymer complex formed between CHI and PMMI.

Ionomers have unique properties due to their unique architecture. Choudhury et al.[189] prepared transparent ionomer/silica hybrid materials from polyethylene-*co*-acrylic acid neutralized by a zinc salt and TEOS via the sol−gel reaction. The effects of various experimental parameters such as solvents, H_2O/Si ratio, and the amount of TEOS in the ionomer solution on the hybrid structure and properties were examined. The results showed that the structure of the hybrids did not change with the change in these parameters, but the silica substructures and the thermal properties of the hybrids changed.

4.2. Class 2: Interfacial Interaction with Strong Interaction

Since the number of polymers bearing functional groups that could form hydrogen bonds is rather limited, class 2 hybrid materials have been paid much attention. In order to introduce covalent bonds between two phases to decrease the extent of phase separation or to increase compatibility of the polymer/silica nanocomposites, coupling agents are widely used in the sol−gel process. Addition of the coupling agents can be accomplished by several paths: (i) copolymerization with the monomer(s) to obtain functionalized polymer;[38,202–210] (ii) reaction with the preformed polymer to modify it;[40–42,211–226] (iii) addition to the silica precursor to modify it;[217,227–229] (iv) addition to the mixture of polymer and silica precursor.[44a–c,230–235] The most popular method is the second path. When polycondensation takes place between trialkoxysilyl groups on the polymer and TEOS, covalent bonds between two phases can be formed.[213]

PI is one of the most extensively studied polymers for the preparation of polymer/silica nanocomposites.[236] The PI/silica hybrids are generally prepared by a two-stage sol−gel process: poly(amic acid) (PAA) is first synthesized from dianhydrides and diamines; then hydrolyzed TEOS is added to proceed to the sol−gel process.[217] Typical dianhydrides and diamines used for preparation of PAA are shown in Chart 1, and some examples of the PI/silica nanocomposites prepared by the sol−gel process are listed in Table 2.

4.2.1. Path i: Copolymerization with the Monomer(s) To Obtain Functionalized Polymer

Hsiue et al.[38] prepared a series of organic/inorganic hybrid materials by copolymerizing St and alkoxysilane−methacrylate via the sol−gel process (Scheme 11). The alkoxysilane-containing copolymer precursors were synthesized by free-radical copolymerization of St with MAMSE at several feeds. The copolymer precursors were then hydrolyzed and condensed to generate PS/SiO_2 hybrid materials. It was found that compatibility between copolymer and silica mainly came from incorporating the polymer with silica covalently. Moreover, MAMSE could be hydrolyzed to methacrylic acid and ester-interchanged to silyl methacrylate during heat treatment. This also enhanced the compatibility between the copolymer and silica.

Jang et al.[203] fabricated two series of hybrid composite materials, P(VA-*co*-VTS)/TEOS and P(VA-*co*-MPS)/TEOS using a modified sol−gel process. This method consisted of separate polymerization and gelation steps. The overall process was simplified by omitting the precipitation of copolymers, and this made it possible to prepare hybrids in one solution. Using this method, they were able to efficiently introduce covalent bonds between organic polymer and inorganic silica during gelation. Moreover, it was also possible to improve the thermal, mechanical, and morphological properties by controlling the processing conditions. Two kinds of silane coupling agents, VTS and MPS, were used to prevent macrophase separation through formation of covalent bonds. Thermal analysis showed that MPS was more effective than VTS for the formation of covalent bonds.

Ahmad et al.[204a] prepared PI/silica nanocomposites from an aromatic PAA derived from PMDA and ODA and a silica network using the sol−gel reaction. Compatibility of the two components was achieved by modifying the silica network with imide linkages. The AA dimers were prepared by reacting APTMOS with PMDA. The APTMOS located at the end groups was used to link AA with TEOS, which on further hydrolysis and condensation reactions produced a silica network in high molecular weight PAA solution. The resulting material was imidized by heating the hybrid films. The imide spacer group in the silica network was supposed to reduce the agglomeration tendencies in silica, particularly at high silica contents in the matrix, and also increase the interaction between the inorganic network and the organic polymer chains.

4.2.2. Path ii: Reaction with the Preformed Polymer To Modify It

The trialkoxysilyl groups incorporated onto the polymer in advance by copolymerization are not stable. The more popular method is to take advantage of a coupling agent with trialkoxysilyl groups to modify preformed polymer before the sol−gel process.

Tan et al.[211a] synthesized polyethercarbonate/silica nanocomposites by copolymerization of AGE with CO_2 followed by the sol−gel process. AGE with CO_2 copolymerized at 60 °C and 400 psi under the catalyst system consisting of $Y(CF_3CO_2)_3$, $Zn(Et)_2$, and pyrogallol in the solvent of 1,3-

Chart 1. Chemical Structures of Typical Dianhydrides and Diamines Used for the Preparation of PAA

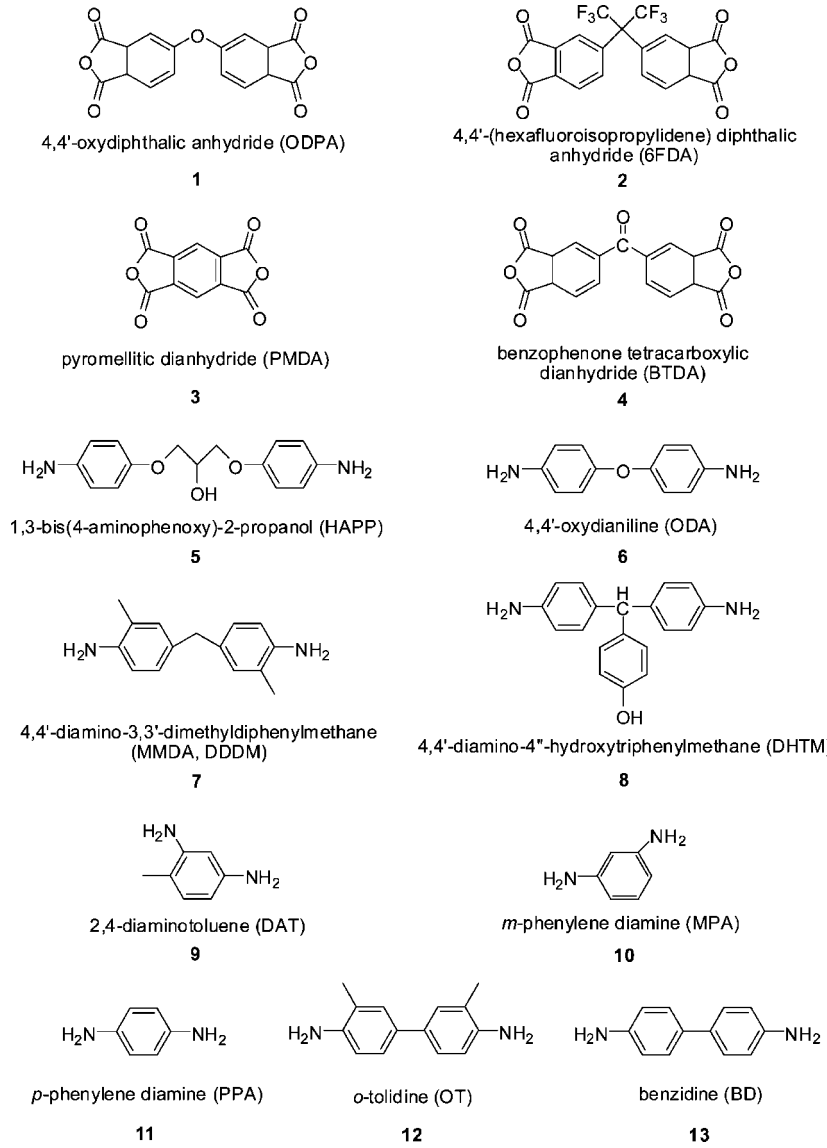

Table 2. Examples of the PI/Silica Nanocomposites Prepared by the Sol−Gel Process

monomers	solvent	coupling agent (s)	ref
ODPA, HAPP	NMP		182
6FDA, BATB[a]/DBAPB[b]/ BAPPH[c]/BAPN[d]	DMAc	APrTEOS, GOTMS	183
ODPA, DDDM, APN	DMAc		191
PMDA, two of PPA/ MPA/BD/DAT/OT	NMP		192
PMDA, ODA	DMAc		193
BTDA, ODA, DDS,	DMAc		194a
BTDA, ODA	DMAc		194b
PMDA, ODA	DMAc	APTMOS	204a
PMDA/6FDA, ODA	DMAc	APrTMOS	214
PMDA, DHTM	NMP	GPTMOS	217
BTDA, MMDA	NMP	GOTMS	227
PMDA, ODA	NMP + xylene	GOTMS	228

[a] BATB = (1,4-bis(4-aminophenoxy)-2-*tert*-butylbenzene). [b] DBAPB = (2,2′-dimethyl-4,4′-bis(4-aminophenoxy) henyl). [c] BAPPH = (2,2-bis[4-(4-aminophenoxy)phenyl] hexafluoropropane). [d] BAPN = (2,2′-bis[4-(4-aminophenoxy)phenyl]norbornane), APN (4-aminophenol).

dioxolane. The resulting polyethercarbonate could react with MPS via a free radical reaction to generate the alkoxysilane-containing copolymer precursors that were used in the subsequent sol−gel process to result in the nanocomposites. Similarly, the copolymerization of CO_2, AGE, and cyclohexene oxide (CHO) followed by the sol−gel process was also carried out.[211b]

Scheme 11. Preparation of PS/SiO_2 Hybrid by Sol−Gel Process[a]

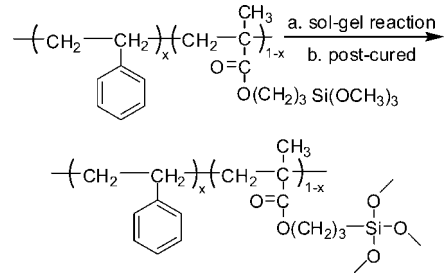

[a] Reprinted with permission from Hsiue, G. H.; Kuo, W. J.; Huang, Y. P.; Jeng, R. J. Polymer 2000, 41, 2813. Copyright 2000 Elsevier Science Ltd.

Ma and co-workers[212a] prepared novolac-type phenolic resin/silica hybrid nanocomposites with a sol−gel process. The coupling agent GPTS was used to improve the interface between the organic and inorganic phases. The hybrid

Scheme 12. Synthesis of P(St-*co*-MA)/Silica Hybrid Material[a]

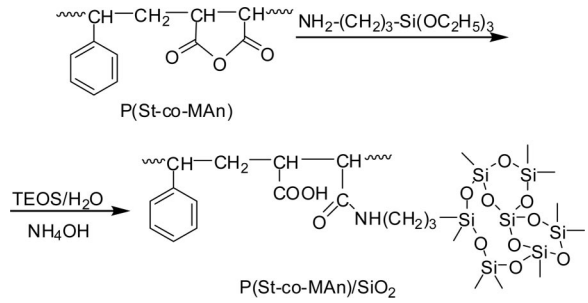

[a] Reprinted with permission from Zhou, W.; Dong, J. H.; Qiu, K. Y.; Wei, Y. J. Polym. Sci., Part A: Polym. Chem. 1998, 36, 1607. Copyright 1998 John Wiley & Sons, Inc.

materials were prepared by mixing two solutions, A and B. Solution A was GPTS-modified phenolic resin/THF solution. Hexamethylene tetramine was used as a curing agent and added into solution A. Solution B consisted of TEOS/H_2O/THF/HCl. The coupling agent reacted with the resin to form covalent bonds.The preparation of the phenolic resin/silica nanocomposites using ICPTES as the coupling agent and DGEBA-type epoxy as the curing agent was also conducted.[212b]

Wei et al.[213] prepared P(St-*co*-MA)/silica hybrid from St-MA copolymer and TEOS in the presence of a coupling agent APTES by an in situ sol−gel process (Scheme 12). It was observed that the gel time of sol−gel solution was dramatically influenced by the amount of APTES. The covalent bonds between organic and inorganic phases were introduced by the aminolysis reaction of the amino group with MA units of copolymer to form a copolymer bearing trimethoxysilyl groups, which underwent hydrolytic polycondensation with TEOS.

Chen et al.[183] prepared a PI/silica hybrid based on the organosoluble PIs of 6FDA and four diamines. APrTEOS and GOTMS were used to increase the intrachain chemical bonding and interchain hydrogen bonding between the PI and silica moieties, respectively. The chemical interaction would significantly affect the morphologies and properties of the prepared films. From the TEM picture, the size of the silica appeared to be smaller than 5 nm. The thermal properties of the organosoluble PI were significantly enhanced by only hybridizing 6.30−7.99 wt % of silica. It was found that the intrachain chemical bonding could effectively enhance the glass transition temperature or CTE in comparison with the interchain interaction.

Two series of the PI/silica hybrid optical thin films, PMDA−ODA/SiO_2 and 6FDA−ODA/SiO_2, were synthesized using an in situ sol−gel reaction combined with spin coating and multistep curing.[214] The hybrid thin films were prepared from the aminoalkoxysilane-capped PAAs and TMOS as the precursors. The prepared hybrid thin films had a homogeneous structure and nanoscale size domain of the silica moieties. Excellent surface planarity and optical transparence were obtained at a high silica content.

Jain et al.[225] prepared PP/silica nanocomposites via solid-state modification (SSM) and sol−gel reactions. VTES was grafted via SSM in porous PP particles. Solid-state grafting of VTES onto PP enabled the interfacial interaction between filler and matrix. Grafted monomeric VTES was then incorporated in the silica during the sol−gel reaction to control the interaction. Bulk polymerization with the same

Scheme 13. Preparation of PI/SiO_2 Hybrid Composites[a]

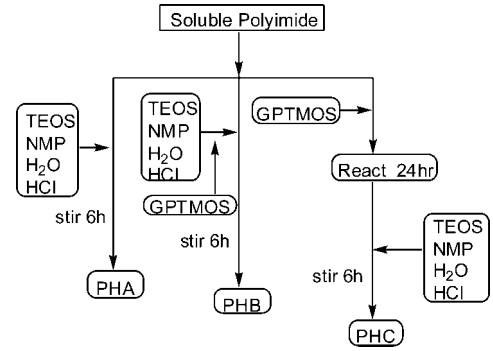

[a] Reprinted with permission from Chen, B. K.; Chiu, T. M.; Tsay, S. Y. J. Appl. Polym. Sci. 2004, 94, 382. Copyright 2004 Wiley Periodicals, Inc.

experimental conditions as in SSM showed that homopolymerization of VTES to high molecular weight occurred, but at limited conversions. This suggested that VTES could be grafted on PP as monomer, polymer, or both.

Xu et al.[42a] synthesized positively charged PMA/SiO_2 nanocomposites. PMA with pending trialkoxysilyl groups and quaternary ammonium groups was prepared through reacting PMA with diamine silane and quaternizing the silane afterward. The obtained polymer precursors then underwent hydrolysis and condensation reactions in the presence of an aqueous HCl catalyst. A series of positively charged hybrid membranes with both strong and weak base groups based on PPO were also prepared.[42b]

4.2.3. Path iii: Addition to the Silica Precursor To Modify It

The invention of soluble PI has made it possible to prepare a PI/silica composite directly from a PI solution. Shang et al.[227] prepared soluble PI/SiO_2 hybrid by the sol−gel process. The coupling agent GOTMS was chosen to enhance the compatibility between the PI and SiO_2. The results showed that the size of the silica particle was markedly reduced by the introduction of the coupling agent, which caused the PI/SiO_2 hybrid films to become transparent. The solubility of the PI/SiO_2 hybrid was also improved by the coupling agent. In addition, all of these effects became even more pronounced with increased amounts of the coupling agent. The compatibility of the two components was effectively improved by the coupling agent.

Chen et al.[217] also prepared PI/SiO_2 hybrid nanocomposites from a soluble PI. This soluble PI was synthesized from a diamine with a pendant phenylhydroxyl group, DHTM, and a dianhydride, PMDA, followed by cyclodehydration. Three ways of preparing PI/SiO_2 hybrid nanocomposites were investigated (Scheme 13). Two of them used the coupling agent GPTMOS to enhance the compatibility between PI and silica. The coupling agent could react with the PI to form covalent bonds. In the preparation of hybrid PHB, the epoxy group in GPTMOS was acid-hydrolyzed to form hydroxyl groups that could form hydrogen bonds with the carbonyl groups in PI. This led to increased compatibility. For the preparation of hybrid PHC, the epoxy group in GPTMOS reacted with the hydroxyl group in PI. Then, the other end of GPTMOS was hydrolyzed and reacted with TEOS to form a composite network.

Musto and co-workers[228] also prepared PI/silica hybrids by a sol−gel process. The alkoxysilane solutions were prepared first from either pure TEOS or TEOS/GOTMS

Scheme 14[a]

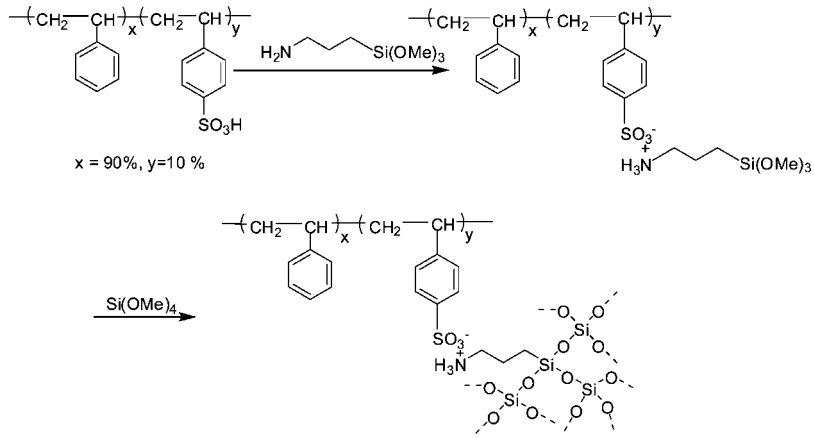

[a] Reprinted with permission from ref 237. Copyright 1999 American Chemical Society.

mixtures mixed with EtOH, H_2O, and HCl solution. The precursor hybrid solution was obtained by adding the hydrolyzed alkoxysilane solution dropwise to the poly(amic acid) solution under continuous stirring at room temperature.

4.2.4. Path iv: Addition to the Mixture of Polymer and Silica Precursor

Peinemann et al.[233] prepared membranes for gas separation based on PTMSP/silica nanocomposites by the copolymerization of TEOS with different organoalkoxysilanes in solutions of PTMSP. The butane permeability and the butane/methane selectivity increased simultaneously when high silica conversion was obtained and the size of particle was in the range 20−40 nm.

Du et al.[44a,b] reported a nonhydrolytic sol−gel method for the preparation of PI/silica hybrid materials using silicic acid oligomer extracted from water glass and proved that transparent PI/silica nanohybrids with silica content up to 40 wt % could be obtained by the addition of APTES as coupling agent. They also prepared the P(St-*co*-MA) and P(St-*co*-AN)/SiO_2 hybrids by mixing of polymer, silicic acid, and APTES, followed by the sol−gel process.[44c]

Only a few reports have been published with regard to the utilization of ionic interaction to synthesize silica-based hybrids. Tamaki and Chujo[237] investigated the synthesis of nanometer scale homogeneous PS and silica gel polymer hybrids utilizing ionic interactions. Partially sulfonated PS (10 mol %) was used as a starting organic polymer and APTMOS was used as a countercation as well as the precursor to the inorganic phase (Scheme 14). Since the strength of ionic interaction is much higher than that of hydrogen bonding, it should provide a better degree of homogeneity and order in the final hybrids. Amorphous and nanostructured cationic polyacetylene/silica hybrids with a conducting, π-conjugated polymer of poly(2-ethynylpyridinium chloride) (P2EPY-HCl) were also synthesized by using ionic interactions.[238] The strong ionic interaction between the cationic pyridinium moieties of P2EPY-HCl and anionic silanol groups resulting from hydrolysis of TMOS enabled the nanometer scale dispersion of P2EPY-HCl in a silica gel matrix.

5. In Situ Polymerization

5.1. General Polymerization

There are several advantages of using the in situ polymerization method. These include ease of handling, the speed of the process, and better performance of the final products.[248] Generally, the process of in situ polymerization involves three continuous steps. First, the nanoscale additives are pretreated with appropriate surface modifiers and then the modified additives are dispersed into monomer(s). This is followed by bulk or solution polymerization. Then the nanocomposites are formed in situ during the polymerization.

It is obvious that the most important factors that affect the properties of composites are the dispersion and the adhesion at the polymer and filler interfaces. Inorganic particles may disperse homogeneously in the polymer matrices when they are premodified by a coupling agent.[249a] The studied polymers include PA 6,[249–251] PET,[252–255] PI,[77,256–258] *N*,*N*′-bismaleimide-4,4′-diphenylmethane polymer,[259] PMMA,[68,69b,248,260,261] PHEMA,[6,262,263] PVA,[264] acrylic polymer,[265] epoxy polymer,[67,266–276] PU,[277–281] PCL,[61,282] and poly(butylene succinate).[283]

In 1998, Ou et al.[249a] reported the preparation of PA 6/silica nanocomposites through in situ polymerization. Silica particles were suspended in ε-caproamide first under stirring, and then this mixture was polymerized using a technique similar to bulk polymerization at high temperature under a nitrogen atmosphere. The silicas were premodified with aminobutyric acid prior to the polymerization. The results showed that the silicas dispersed homogeneously in the PA 6 matrix. The morphological investigation demonstrated the noninfluence of the particle presence on the crystalline phase of such composites. The introduction of filler led to an obvious reinforcement of the matrix elastic modulus: the observed increase was dependent on the modulus difference between the various phases present, the filler content, and its dispersion state. In the same way, the yield point, in both compressive and tensile tests, was found to be sensitive to the latter parameters.[250]

The influence of APS or GPS treatment on nylon 6/nano-SiO_2 in situ polymerization was studied by Yu et al.[251a] Functional silane treatment of nano-SiO_2 before in situ polymerization of nylon 6 did not bring about a significant difference in the reactivity of surface groups of silicas, as

shown by TGA of silicas isolated from the composites and an endgroup analysis of the composites. However, it could simultaneously improve the strength and toughness of the composites, as indicated by mechanical tests. This was mainly as a result of the introduction of a flexible layer in the interface. Three commercially available silane-, titanate-, and aluminate-based coupling agents were used to pretreat nano-SiO_2 to investigate the influence of interphase on the nanocomposites. As is the case with a silane-treated silica, the introduced amino functional groups could participate in the polymerization, resulting in graft polymers on silica surface, whereas for titanate- or aluminate-treated silicas, the hydrogen-bonding interactions along the interphase may have contributed to the interfacial interactions between silica and the matrix.[251b]

PET/silica nanocomposites were successfully fabricated by in situ polymerization of PET monomer dispersed with organic-modified silica nanoparticles.[252] Results showed that the nanoparticles were well-dispersed in the polymer matrix; the addition of nanoparticles could speed up the crystallization and melting point, and the addition had no significant effect on the synthesis process.

PMMA/silica nanocomposites have been prepared via bulk or solution polymerization methods. Kashiwagi et al.[260] prepared PMMA/silica nanocomposites made by in situ radical polymerization of MMA with colloidal silica. Homogeneous dispersion of the silica particles in the PMMA matrix was found. The addition of nanosilica particles (13% by mass) did not significantly change the thermal stability, but it made a small improvement in modulus, and it reduced the peak heat release rate by roughly 50%. Chen et al.[261] incorporated three different types of modified silica particles in a PMMA matrix using a bulk polymerization technique. Three organic silica groups, two modified with methyl groups and the third an octane, made these inorganic silica particles more hydrophobic. Nakanishi et al.[68] prepared PMMA/silica hybrid materials incorporating reactive silica nanoparticles. The nanoparticles were obtained by the reaction of 2-(methacryloyloxy)ethyl isocyanate with colloidal silica dispersed in ethyl acetate, and they were copolymerized in various ratios with MMA. The PMMA/silica hybrid copolymers maintained high transparency, and their storage elastic modulus and surface hardness increased with increasing silica content. Moreover, the hybrid copolymers had greater heat resistance and lower volume contraction in comparison with PMMA. Liu et al.[69b] prepared PMMA/silica nanocomposite films from copolymerizing MMA with AGE functionalized silica nanoparticles with THF as solvent and BPO as initiator. No alkoxysilane coupling agents and sol−gel reactions were employed in this preparation approach to result in nanocomposite films having silica contents higher than 70 wt %. Yang and Nelson[248] also prepared PMMA/silica nanocomposites by solution polymerization. Pretreated fumed silica solution and MMA were mixed together with toluene as the reaction medium and BPO as the initiator. Both APMDMOS and APTMOS served as reagents for the surface modification of silica; APTMOS performed better than APMDMOS for the modification of the silica surface.

Becker et al.[262] prepared thermoplastic nanocomposites containing MPS-functionalized silica nanoparticles by free radical polymerization of the monomers. MMA and HEMA mixtures contained approximately 2, 5 and 10 vol % silica.

Two types of polymer/silica nanocomposites have been prepared by free-radical polymerization of HEMA either in the presence of HEMA-functionalized SiO_2 nanoparticles (type 1) or during the simultaneous in situ growth of the silica phase through the acid-catalyzed sol−gel polymerization of TEOS (type 2). Type 1 systems exhibited a classical particle−matrix morphology, but the particles tended to form aggregates. Type 2 systems possessed a finer morphology characterized by a very open mass-fractal silicate structure, which was believed to be bicontinuous with the organic phase at a molecular level.[6]

Chen et al.[265a] synthesized hybrid thin films containing a nanosized inorganic domain from acrylic and monodispersed colloidal silica with coupling agent. The MSMA was bonded with colloidal silica first and then polymerized with acrylic monomer to form a precursor solution with THF as solvent and BPO as initiator. Then, the precursor was spin coated and cured to form the hybrid films. Three kinds of acrylic monomers were used in the study including a single functional acrylate of MMA, a bifunctional acrylate of ethylene glycol dimethacrylate (EDMA), and a trifunctional acrylate of trimethylolpropane triacrylate (TMPTA).The silica content in the hybrid thin films was varied from 0 to 50 wt %. The results showed that the coverage area of silica particles by the MSMA decreased with increasing silica content and resulted in the aggregation of silica particle in the hybrid films. Thus, the silica domain in the hybrid films was varied from 20 to 35 nm by the different mole ratios of MSMA to silica. For reducing the environmental pollution problem and the cost of solvent-based colloidal silica, acrylic/silica hybrid thin films containing nanosized silica were also successfully prepared from acrylic monomers and aqueous monodispersed colloidal silica with coupling agent.[265b]

A widely studied nanocomposite system is that of epoxy/silica. Epoxy resins as an organic matrix have excellent heat, moisture, and chemical resistance and good adhesion to many substrates. However, they cannot meet all the requirements of appplications such as epoxy molding compounds. This is due to their low mechanical properties and high CTE value compared with inorganic materials. Thus, silica particles are commonly used for the reinforcement of epoxy matrix to lower shrinkage on curing and CTE, to improve thermal conductivity, and to meet mechanical requirements. Epoxy/silica nanocomposites are generally prepared by blending the epoxy prepolymer and silica nanoparticles first and then adding the hardener to perform the curing reaction. Typical epoxy resins and hardeners used for the preparation of epoxy/SiO_2 nanocomposites are shown in Chart 2, and some examples of this type of nanocomposite prepared by in situ polymerization are listed in Table 3.

Kim et al.[67] prepared epoxy/silica nanocomposites filled with functionalized nanosilica particles. To investigate the interfacial effect on properties of epoxy composites, uniform sized silica particles (S) were synthesized by sol−gel reaction and then modified either by substituting surface silanol groups into epoxide ring (S-epoxide), amine (S-NH_2), or isocyanate (S-NCO) groups or by calcinating them to remove surface silanol groups (CS) (Scheme 15). The modified particles were then dispersed into epoxy resin with ultrasonic instruments. Subsequently, the resins were degassed and cured. It was found that surface-modified particles could be chemically reacted with epoxy matrix.

Zhang and co-workers[266] studied the improvement of tribological performance of epoxy by the addition of irradiation grafted nanosilica particles. PAAm-grafted SiO_2 (SiO_2-*g*-PAAm) with an average primary silica particle size of 9

Chart 2. Typical Epoxy Resins and Hardeners Used for the Preparation of Epoxy/SiO_2 Nanocomposites

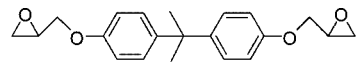

diglycidyl ether of bisphenol A or
bisphenol A diglycidyl ether (DGEBA, BADGE)

14

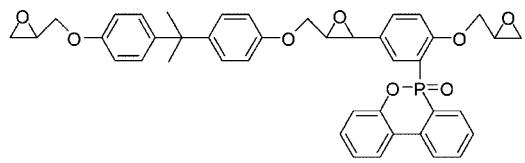

phosphorus-containing epoxy resin

15

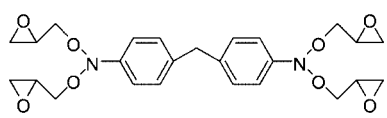

tetraglycidyl-4-4'-diaminodiphenylmethane (TGDDM)

16

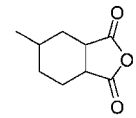

hexahydro-4-methylphthalic anhydride (HMPA)

17

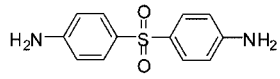

4,4'-diaminodiphenylsulfone (DDS)

18

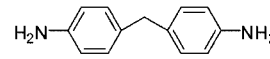

4,4'-diaminodiphenylmethane (DDM)

19

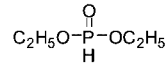

diethylphosphite (DEP)

20

Table 3. Examples of Preparation of Epoxy/SiO_2 Nanocomposites by in Situ Polymerization

epoxy resin type	hardeners	SiO_2	ref
DGEBA	Z	400 nm, functionalized particles	67
bisphenol A	DDS	9 nm, PAAM-grafted	266
DGEBA	aromatic hardener	15 nm	267
DGEBA	HMPA	100 nm	268
DGEBA	aliphatic polyamine	~330 or ~75 nm	269
DGEBA	piperidine	15−50 nm, surface-modified	270
DGEBA	HMPA	20 nm	271
DGEBA	DDA		272
DGEBA, P-containing epoxy	DDM, DEP	dispersed in MIBK, 10−20 nm	273a
DGEBA	SiO_2	dispersed in MIBK, 10−20 nm	273c
TGDDM	DDS	dispersed in isopropanol, 10−15 nm	274
DGEBA	polyamide−amine		275

nm was prepared first. It was then mixed with bisphenol-A epoxy resin and cured with DDS. Through irradiation grafting, the nanoparticle agglomerates turned into a nanocomposite microstructure (comprised of the nanoparticles and the grafted, homopolymerized secondary polymer), which in turn built up a strong interfacial interaction with the surrounding epoxy matrix through chain entanglement and chemical bonding during the subsequent mixing and consolidation.

Zheng et al.[267] studied the effects of nanoparticles of SiO_2 on the performance of nanocomposites. The nanoparticles were dispersed in epoxy resin in three different ways: (i) the epoxy resin was mixed with unpretreated SiO_2 nanoparticles using ultrasonic energy; (ii) the mixture of epoxy and nanoparticles pretreated with a coupling agent was treated with ultrasonic waves at the same temperature; (iii) the pretreated SiO_2 nanoparticles were dispersed in the epoxy resin by ultrasonic waves followed by a high-speed homogenizer. The properties of the nanocomposites prepared by the three approaches are listed in Table 4 to compare with those of the pure epoxy resin. From the macroscopic level, the mechanical testing results demonstrated that the properties of the nanocomposites with a uniform distribution of nanoparticles were greatly improved. Results demonstrated that with the assistance of coupling agent and high-speed homogenizer, a relative uniform distribution of nanoparticles could be achieved. Uniform dispersion of nanoparticles was

Scheme 15. The Surface Modification of Silica[a]

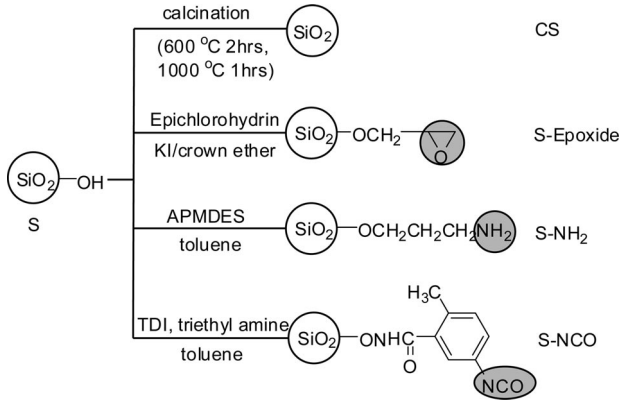

[a] Reprinted with permission from Kang, S.; Hong, S. I.; Choe, C. R.; Park, M.; Rim, S.; Kim, J. Polymer 2001, 42, 879. Copyright 2001 Elsevier Science Ltd.

Table 4. Effects of Nanoparticle Dispersion on the Properties of Nanocomposites[a]

epoxy resin/SiO_2 (g/g)	treatment methods	tensile strength (MPa)	tensile modulus (GPa)	impact strength ($kJ \cdot m^{-2}$)
100/0		35.33	3.17	10.2
100/3	1	38.33	3.21	11.2
100/3	2	45.88	3.43	12.68
100/3	3	75.68	3.57	15.94

[a] Adapted with permission from Zheng, Y. P.; Zheng. Y.; Ning, R. C. Mater. Lett. 2003, 57, 2940. Copyright 2003 Elsevier Science B.V.

critical to the morphological structure and impact strength of the nanocomposites.

Liu et al.[273a,b] prepared epoxy/silica nanocomposites from nanoscale colloidal silica dispersed in MIBK. DGEBA can dissolve in MIBK-ST (a commercial product of silica dispersed in MIBK) to result in a clear and transparent solution. Epoxy/silica nanocomposites were obtained from directly blending DGEBA and MIBK-ST and then curing with DDM or DEP. Epoxy/silica nanocomposites were obtained with high silica loadings of 70 wt % without employing silane coupling agents and surfactants. Experiments using silica nanoparticles as curing reagents for epoxy resins were also conducted. Nanoscale colloidal silica showed high reactivity toward curing epoxy resins to form epoxy/silica nanocomposites under mild conditions. The reactivity might be correlated to the special effect of the nanosize of the silica particles. Adding a certain amount (5000 ppm) of $MgCl_2$ lowered the activation energy of the reaction from 71 to 46 kJ/mol. Both increasing and decreasing the amount of $MgCl_2$ from this value had a negative effect on lowering the activation energy of the curing reaction. $SnCl_2$ and $Zn(AcO)_2$ were also added into the curing compositions; however, they showed no significant effect on promoting the curing reaction. Through this curing reaction, epoxy/silica nanocomposites containing high silica contents up to 70 wt % were obtained.[273c]

It is well-known that PU is produced by reaction of a polyol, an isocyanate, and a chain extender. Preparation of PU/silica nanocomposites by in situ polymerization is often carried out in a three-step process: mixing the polyol with nanosilica first and subsequently curing the mixture with diisocyanate to obtain the prepolymer, and then carring out a chain extension reaction on the prepolymer with a chain extender. The chemical structures of several polyols, isocyanates, and chain extenders are shown in Chart 3.

Petrović et al.[277a] prepared PU/silica nanocomposites by mixing polypropylene oxide glycol with silica dispersed in MEK and subsequent curing using MDI in the presence of the catalyst and extending with BD. The filler used was a well-defined, perfectly round silica with narrow size distribution. The nanosilica filler was amorphous, giving composites with the PU that were transparent at all concentrations. The nanocomposites displayed higher strength and elongation at break but lower density, modulus, and hardness than the corresponding micrometer-size silica-filled polyurethanes.

Wu and co-workers prepared polyester-based[278a,b] or acrylic-based[278c–f] PU with embedded nanosilica particles by directly dispersing nano-SiO_2 into monomers of polyester resins or polyester resins under stirring and then mixing with curing agent.

Infrequently, specific silica precursor of silica nanoparticles is also used in the in situ polymerization. Du et al.[44d] prepared PA 6/silica nanocomposites via an in situ polymerization route using silicic acid as the precursor of silica, which was extracted from water glass. APTES was used to introduce some chemical bonds between the PA 6 matrix and silica surface in order to improve their compatibility.

5.2. Photopolymerization

Photopolymerization technology has been selected in some works[284–304] for polymeric nanocomposites preparation. It is a process where UV light induces the polymer formation allowing a fast transformation of the liquid monomer into the solid film with tailored physicochemical and mechanical properties. In the process, radical or cationic species are generated by the interaction of the UV light with a suitable photoinitiator, which induce the curing reaction of reactive monomers and oligomers.[298] It is an environmentally friendly technique because it is a solvent-free process. The substrate does not need to be heated as in traditional thermal curing; therefore it saves energy. In addition, a similar method, electron beam (EB) induced polymerization technology, has also received widespread attention.[287–289,305]

In general, oligomers (e.g., acrylate, epoxy acrylate) and/or reactive dilutes (e.g., TMPTA, HDDA) are contained in the formulation of UV-curable nanocomposites (Chart 4). The nanocomposite films or coats could be formed via the cross-linking reaction of oligomers and/or reactive dilutes, and nanosilica particles acted as fillers.[297a] Acrylate polymers,[284–294] epoxy acrylate polymers,[295–297] and epoxy polymers[298,299] are common systems involved in UV photoloymerization.

Montes et al.[284] prepared model filled elastomers to vary separately the chemistry at the particle surface and the dispersion state in order to determine the relative weight of these two parameters on the mechanical behavior. Such samples were prepared following the procedure developed by Ford and co-workers,[285,286] which involved photopolymerization of a concentrated dispersion of grafted silica particles in acrylate monomers. It was shown that nanosized silica modified by trialkoxysilane in radiation-curable acrylate systems results in nanocomposite films with improved scratch and abrasion resistance.

In a series of papers, Bauer et al.[287–289] studied the preparation of radiation-cured polymeric nanocomposites. Silica nanoparticles were modified with trialkoxysilane and then used as fillers in UV/EB curable acrylates for polymer

Chart 3. Chemical Structures of Several Polyols, Isocyanates, and Chain Extenders Used for the Preparation of PU

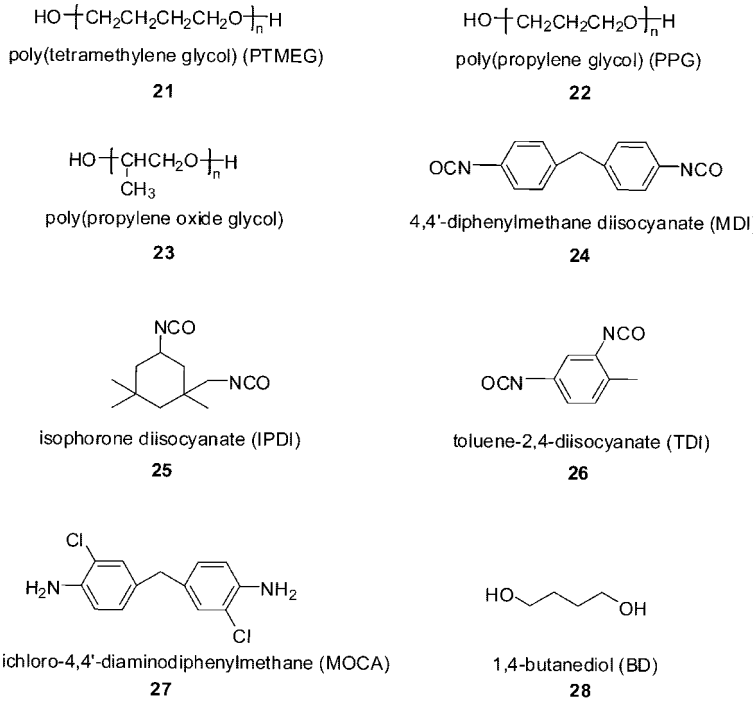

Chart 4. Chemical Structures of Several Oligomers and Reactive Dilutes Used in UV-Curable Formulations

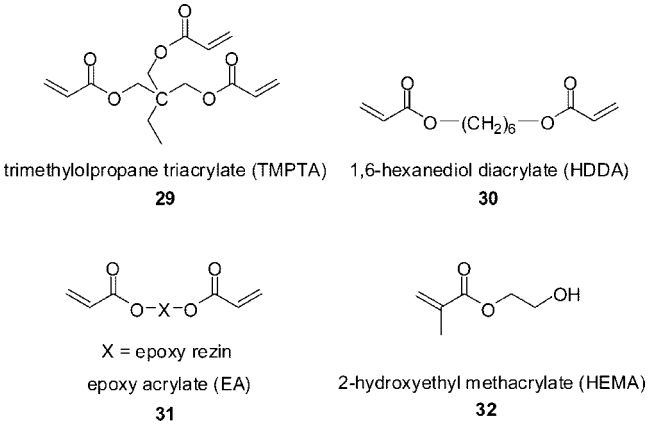

reinforcement. By in situ grafting of methacroyloxy functionalized silanes on commercial nanoglobular silica, polymerization-active silico-organic nanoparticles were prepared. Acid-catalyzed condensation of trialkoxysilanes on the surface of oxide nanoparticles formed a polysiloxane shell, yielding a core−shell nanocapsule. The cross-linked polysiloxanes were anchored onto the particle surface by condensation reactions with oxide OH groups. Radiation (UV, EB) induced polymerization reactions resulted in these modified nanoparticles forming covalent cross-links to acrylate substrates, thus efficiently modifying their viscoelastic properties.[287b] The transparent nanopowder composites could be used as scratch-resistant coatings. In a further study,[287c] the effect of methacroyloxypropyl-, vinyl-, and propyl-functionalized trimethoxysilanes as surface modifiers and pyrogenic silica as nanoparticles on the viscoelastic and surface mechanical properties of the corresponding radiation-cured polyacrylate nanocomposites was investigated. Nanoparticles modified with polymerization-active silanes, such as MEMO and vinyltrimethoxysilane, were found to form cross-links within UV and EB curable acrylate/nanoparticle systems, thus bringing on a pronounced modification effect of the viscoelastic data of the copolymerized composites. However, even the mere organophilation of nanosized pyrogenic silica by polymerization-inactive propyltrimethoxysilane resulted in transparent polyacrylate nanocomposite films with improved scratch and abrasion resistance. In the case of surface-modified pyrogenic silica, the comparison with commercially available acrylate suspensions using colloidal silica filler revealed a distinct improvement in the surface mechanical properties. It was assumed that the density and hardness of the fumed nanoparticles were higher, which led to an increase in the abrasion resistance at the same filler content.

Soloukhin et al.[290] prepared hybrid cross-linked coatings consisting of polymer (meth)acrylate matrices with dispersed nanosized silica particles. The coatings were deposited on PC substrates.

A study was carried out on nanocomposites consisting of nanometer silica fillers embedded in thermoset epoxy acrylate polymers by irradiation of UV light.[296] Due to the introduction of nanosilicas, the curing times were prolonged, but the mechanical properties of the nanocomposites, such as tensile strength and Young's modulus, increased, and the thermostability of the nanocomposites at temperatures lower than 400 K improved. TEM images showed that the nanometer silicas were well-dispersed within nanocomposites containing less than 3 wt % nanometer silicas.

In the case of the cationic polymerization, onium salts are used to generate very strong Brönsted acids upon photodecomposition. The cationic photoinduced process presents some advantages compared with the radical one, in particular, lack of inhibition by oxygen, low shrinkage, good mechanical properties of the UV cured materials and good adhesion properties to various substrates. Moreover, the monomers employed are generally characterized by being less toxic and irritant. Sangermano et al.[298] monitored the effect of the presence of the silica nanopowder on the kinetics of cationic photopolymerization of an epoxy-based system and studied the properties of the obtained photocured nanocomposite

films. The silica nanofiller induced both a bulk and a surface modification of UV-cured coatings with an increase on T_g, modulus, and surface hardness by increasing the amount of silica into the photocurable resin. TEM investigations confirmed that silica filler had a size distribution range between 5 and 50 nm without formation of aggregates. The strong decrease on water uptake in the presence of SiO_2 makes these nanocomposite materials particularly interesting for gas-barrier coatings applications.

Hong et al.[300] used photodifferential scanning calorimetry to investigate the photocuring kinetics of UV-initiated free-radical photopolymerizations of acrylate systems with and without silica nanoparticles. The kinetic analysis revealed that the silica nanoparticles apparently accelerated the cure reaction and cure rate of the UV-curable acrylate system, most probably due to the synergistic effect of silica nanoparticles during the photopolymerization process. However, a slight decrease in polymerization reactivity that occurred when the silica content increased beyond 15 wt % was attributed to aggregation between silica nanoparticles. It was also observed that the addition of silica nanoparticles lowered the activation energy for the UV-curable acrylate system and that the collision factor for the system with silica nanoparticles was higher than that obtained for the system without silica nanoparticles, indicating that the reactivity of the former was greater than that of the latter.The kinetics of cationic photopolymerizations of UV-curable epoxy-based negative photoresists with and without silica nanoparticles were also studied.[294]

The development of inorganic nanoparticle/thiol−ene nanocomposites is one of the most interesting areas in photopolymerization research. Lee and Bowman[301] investigated the effect of the functionalized silica nanoparticles on the thiol−ene photopolymerization kinetics by real-time FTIR spectroscopy. Nanoparticles were not found to significantly affect the polymerization of acrylate-based nanocomposites regardless of the functional group type attached to the particle surface, while significant changes in polymerization kinetics were observed with thiol−ene based nanocomposites. The thiol−ene polymerization rate decreased with increasing particle content for small amounts of particle loadings due to a stoichiometric imbalance of thiol and ene groups at the particle surface. However, the polymerization rates increased with larger particle loadings because of polymerization viscosity enhancements. Thiol−ene-based nanocomposites exhibited higher final conversions than acrylate systems and reduced oxygen inhibition relative to acrylate polymerizations and still reacted rapidly to form highly cross-linked, hard, high glass transition temperature materials.

Frey et al.[302] prepared organic/inorganic hybrid materials by a two-step curing procedure based on sol−gel condensation and subsequent photopolymerization. Bismethacrylate-based hybrid monomers with pendant, condensable alkoxysilane groups were prepared by Michael addition and possessed number-average molecular weights between 580 and 1600 g/mol. The formation of inorganic networks by sol−gel condensation of the alkoxysilane groups in the presence of aqueous methacrylic acid was monitored with rheological measurements. The condensation conversion was monitored with solid-state ^{29}Si cross-polarization/magic-angle spinning NMR spectroscopy. Subsequent photopolymerization led to organic/inorganic hybrid networks and low volume shrinkage, ranging from 4.2% to 8.3%, depending on the molecular weight of the hybrid monomer applied. Highly filled composite materials with glass filler fractions greater than 75% showed attractive mechanical properties with Young's moduli of 2700−6200 MPa.

Similarly but in reverse order, Sangermano et al.[303] reported the preparation of nanocomposite coatings through a dual-curing process, involving either radical or cationic photopolymerization and subsequent condensation of alkoxysilane groups. The sequence of the reactions involved in the adopted dual-curing process is shown in Scheme 16. This combines the advantages of both the curing methods. Hybrid systems containing PEO segments linked to an acrylate−methacrylate network were prepared.[303a−d] The evaluation of the acrylic and methacrylic groups and of the alkoxysilane groups (through the alcohol evaporation) indicated that an almost complete conversion of the reactive functional groups was achieved. The T_g values of the hybrids were found to increase by increasing the TEOS content and the alkoxysilane group condensation. TEM analyses indicated the formation of silica phases at a nanometric level. TGA curves revealed a higher thermal stability of the hybrid structures. From pursuit of this research, nanocomposite coatings were prepared by a dual-cure process involving cationic photopolymerization of epoxy systems, such as epoxy groups[303e] or hyperbranched epoxy-functionalized resin,[303f] or vinyl ether-based systems[303g] and subsequent condensation of alkoxysilane groups.

5.3. Surface-Initiated Polymerization

A key feature in the construction of nanocomposite systems is the development of specific interactions at the interface of the organic and inorganic components, because the interface plays a dominant role in the preparation and properties of nanocomposites. Therefore, the development of grafting strategies so as to tailor the surface properties of mineral substrates is of great current interest. As mentioned in section 2.2, two general routes have been used to graft linear polymer chains at the surface of the particles. One method is the "grafting-to" technique and the other method is the "grafting-from" technique.

The grafting of polymers to inorganic particles such as silica is effective at improving the surface, but contamination from nongrafted chains usually occurs. Then separation of the grafted chains from the nongrafted ones remains difficult. Also, strong hindrance between grafted polymer chains prevents attachment of further ones and then limits the graft density.

The "grafting-from" technique, also called surface-initiated polymerization, for example, polymerization performed in situ with monomer growth of polymer chains from immobilized initiators on mineral surfaces, leading to the formation of so-called "polymer brushes" or "hairy nanoparticles", appears to be a very promising and versatile method. A large variety of initiating mechanisms, including free radical polymerization, which involves conventional radical polymerizations[306,307] and controlled radical polymerization (CRP),[308−337] living anionic polymerization,[338] living cationic polymerization,[339,340] ring opening polymerization (ROP),[341−343] ring opening metathesis polymerization (ROMP),[344,345] and others,[346] have been applied. Among them, controlled CRP has become the most popular route, which is usually divided into three categories: atom transfer radical polymerization (ATRP),[308−328] nitroxide-mediated polymerization (NMP, also referred to as stable

Scheme 16. Scheme of the Sequence of Reactions Involved in the Dual-Curing Process[a]

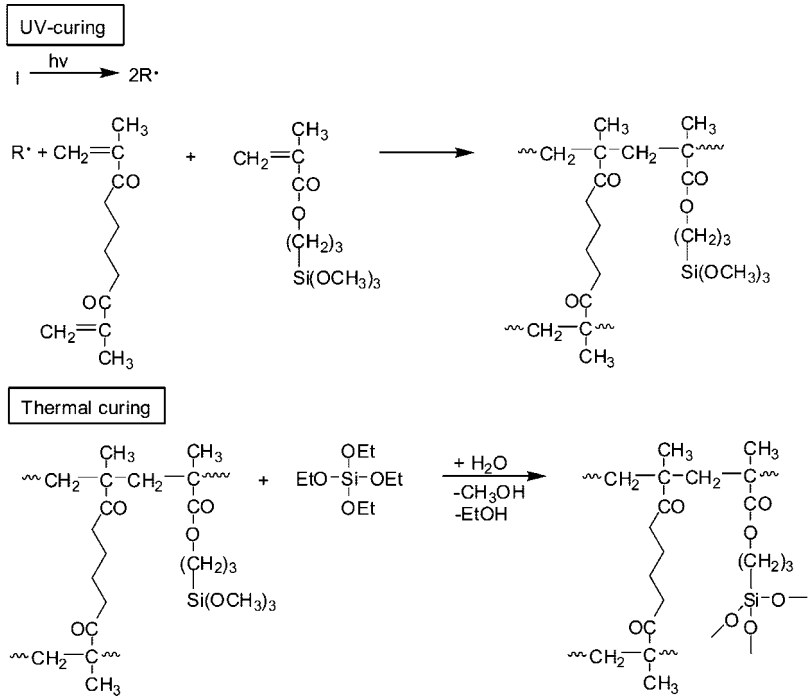

[a] Reprinted with permission from Malucelli, G.; Priola, A.; Amerio, E.; Pollicino, A.; di Pasquale, G.; Pizzi, D.; de Angelis, M. G.; Doghieri, F. J. Appl. Polym. Sci. 2007, 103, 4107. Copyright 2007 Wiley Periodicals, Inc.

free-radical polymerization),[329–332] and reversible radical addition, fragmentation, and transfer (RAFT) polymerization.[333–337] All three techniques permit the polymer molecular weight, the polydispersity, and the polymer architecture to be accurately controlled.

The preparation of organic/inorganic nanocomposites via surface-initiated polymerizations has been reviewed by several groups.[21–28] Especially, a comprehensive and special review[25] on surface-initiated polymerization from silica nanoparticles has been published in 2006, so this section will be omitted from this review.

5.4. Other Methods

In situ melt polycondensation of L-lactic acid (LLA) in the presence of acidic silica sol was proposed to prepare PLLA/SiO_2 nanocomposites.[347]

Frontal polymerization is a mode of converting a monomer into a polymer via a localized reaction zone that propagates through the monomer. Chen et al.[348] synthesized PU/nanosilica hybrids by this method. Structurally well-dispersed and stable hybrids were obtained via a two-step functionalization process: First, the silica was encapsulated with APTS. Second, poly(propylene oxide glycol), TDI, BD, and a catalyst (stannous caprylate) were dissolved in dimethylbenzene and mixed together at room temperature along with the modified nanosilica. A constant-velocity propagating front was initiated via the heating of the end of the tubular reactor. The PU hybrids produced by frontal polymerization had the same properties as those produced by batch polymerization with stirring, but the frontal polymerization method required significantly less time and lower energy input than the batch polymerization method.

García et al.[349] prepared PP composites containing nanosized (~10 nm) spherical silica particles in situ utilizing a 1 L slurry-phase polymerization reactor containing a $MgCl_2$-supported Ziegler−Natta catalyst. Composites were prepared with variable filler sizes ranging from the nano- to microsize domain. The surface of the silica particles was modified with a silane coupling agent to prevent catalyst deactivation and to achieve better polymer/filler synergy by decreasing the hydrophobicity surrounding the bulk particle surface.

The use of microwave irradiation in polymer chemistry is a rapidly expanding field of research.[350] A series of PS/silica nanocomposites with different contents of inorganic nanofillers were prepared by the in situ bulk radical copolymerization of St with macromonomers, methacryloxypropyl silica nanoparticles, under microwave irradiation. A percentage of grafting of 33.14% could be achieved under the optimized polymerizing condition with a conversion of St of 98.92%. The resulting product could be used as nanocomposites directly because of the complete conversion of St after a short reaction time.[351]

In situ anionic polymerization of ε-caprolactam in the presence of SiO_2 and silanated SiO_2 nanoparticles by a rotational molding technique for the synthesis of two series of nylon 6/SiO_2 nanocomposites was also reported. The process was performed at 160 °C, well below the melting temperature of the nylon 6 ($T_m \approx 225$ °C).[352]

Very recently, acetal copolymer/silica nanocomposites were prepared by in situ bulk cationic copolymerization of trioxane and 1,3-dioxolane in the presence of nanosilica.[353]

6. Colloidal Nanocomposites

In recent years, considerable effort has been spent on the elaboration of particulate or colloidal polymer/silica nanocomposite materials with defined morphologies and properties. These materials represent a new category of nanocomposites, which can exhibit remarkable properties (mechanical, electrical, optical, chemical, rheological, etc.) by an appropriate combination and structuration of the organic and inorganic components

Scheme 17. Schematic Representation of the Possible Nanocomposite Particle Morphologies[a]

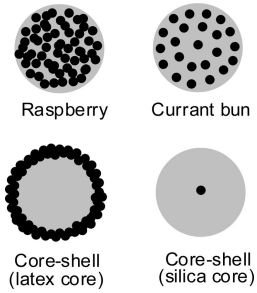

[a] Reprinted with permission from Percy, M. J.; Amalvy, J. I.; Barthet, C.; Armes, S. P.; Greaves, S. J.; Watts, J. F.; Wiese, H. J. Mater. Chem. 2002, 12, 697. Copyright 2002 The Royal Society of Chemistry.

inside the nanoparticles. These nanocomposite materials are particularly promising in applications such as catalysis, surface coatings, chromatography, and biotechnologies. Several articles have summarized recent developments on organic/inorganic nanocomposite colloids.[29–34]

Principally colloidal polymer/silica nanocomposites can be divided into systems with a polymer core and a silica shell or vice versa.[33] Various methods have been developed for their preparation, and they typically involve the sol−gel process (resulting in coating of polymer colloids with silica), in situ heterophase polymerization (usually resulting in polymer encapsulation of silica nanoparticles), and self-assembly technique. Among these methods, in situ heterophase polymerization is by far the most frequently used. It should be indicated that structurally well-defined polymer/silica nanocomposites by surface-initiated polymerization can also be reduced to colloidal nanocomposites.

As is well-known, in order to circumvent the inherent incompatibility of polymers and minerals, the synthetic procedures of nanocomposites commonly require significant affinity between silica surfaces and polymers, whichever preparative method was used. To establish a physicochemical or chemical link at the interface of the organic and inorganic constituents, many synthetic strategies have been developed, and the general synthetic approach to organic/inorganic colloids involves two successive steps: (i) synthesis of the core material with the desired surface group and chemical reactivity and (ii) coating of the template core with an organic or inorganic shell.[32b]

Controlling the morphology of colloidal particles is very important to master their physicochemical properties. Colloidal polymer/silica nanocomposites with different interesting morphologies, such as raspberry-like, core−shell, currant-bun-like, hedgehog, dumbbell-like, snowman-like, daisy-shaped, and multipod-like structures have been prepared depending on the surface chemistry and the size of the inorganic particles. Several possible nanocomposite particle morphologies are illustrated in Scheme 17.

6.1. Sol−Gel Process

In most cases of colloidal nanocomposites prepared by the sol−gel process, silica precursors are controllably precipitated onto the polymer core particles to form silica-coated hybrid colloids, which is termed sol−gel nanocoating. Polymer latexes (especially PS emulsion) are commonly used as colloidal templates,[355–364] and the nanocoating procedures generally involve surface modification of the polymer particles to increase chemical affinity with the shell. The following strategies have been employed: (i) functionalization of the polymer by the use of functional ingredients of polymerization, namely, the surfactant, the monomer,[355–358] or the initiator molecule;[359] (ii) functionalization or modification[360,361] of the preformed polymer latex particles. Polymer templates such as microgel,[365] block copolymer,[366] and other methods[367–370] have also been used. It is worth mentioning that an interesting expansion of the composite particles is that hollow silica spheres can be obtained following the synthesis of the core−shell particles by removing the core via calcination or dissolution.[355–357,361,365]

Bourgeat-Lami et al.[355] reported a route for the synthesis of latex particles coated with a silica shell, which was divided in two steps as schematically represented in Scheme 18. In a first step, PS latex particles containing silanol groups have been synthesized in emulsion polymerization using MPS as a functional comonomer. Then a silica layer was formed on the hybrid particle surface by reaction of TEOS in water[355a] or ethanol/water[355b] under basic conditions. The transmission electron micrograph reported in Figure 3a clearly shows that silica has grown radially outward from the seed latex particles giving silica-coated organomineral particles with a core−shell morphology. By increasing the concentration of the sol−gel precursor, they were able to increase and to control the thickness of the inorganic shell. When nonmodified PS latex particles were used as the seed, under otherwise identical experimental conditions, silica precipitation also occurred but as small silica beads deposited on the polymer particles as well as free silica particles (Figure 3b).

Xia et al.[357] also reported the synthesis of hybrid spherical colloids composed of PS cores and silica shells (Scheme 19). The Stöber method was adopted to prepare hybrid core−shell particles by coating the surfaces of monodisperse PS beads with uniform silica shells. PS beads with diameters in the range of 0.1−1.0 μm were successfully demonstrated for use with this process. The thickness of the silica coating could be controlled within the range of 50−150 nm by adjusting the concentration of TEOS, the deposition time, or both. The morphology and surface smoothness of the deposited silica were found to strongly depend on a number of parameters such as the surface functional groups on the polymer beads, the pH value of the medium, and the deposition time.

Silica layer deposited onto the surface of PS particle via electrostatic interaction between positively charged PS colloids and negatively charged silica was reported by Wu and co-workers.[359] In this approach, the positively charged PS colloids were first prepared via surfactant-free emulsion polymerization of St by using AIBA (cationic) as initiator; hydrolysis and condensation of TEOS were then carried out in acidic aqueous ethanol medium in the presence of PS colloids with positive surface charge. Since the silica sols were negatively charged and could be captured rapidly by the positively charged PS colloids, homogeneous nucleation of silica could be avoided. Neither a centrifugation/redispersion process of obtained dispersions nor surface modification or addition of surfactant (stabilizer) was needed in the whole process.

Graf et al.[360] described a general method to coat colloids with silica based on the use of the amphiphilic, nonionic polymer PVP that was adsorbed to positively or negatively charged PS colloidal particles. The general procedure to coat colloids with silica consisted of two steps: adsorption of PVP and growth of the silica shell after transfer of the particles to ethanol. An outline of the synthesis is shown in Scheme

Scheme 18. Scheme of the Different Steps Involved in the Coating Reaction of Organomineral Latex Particles with Silica[a]

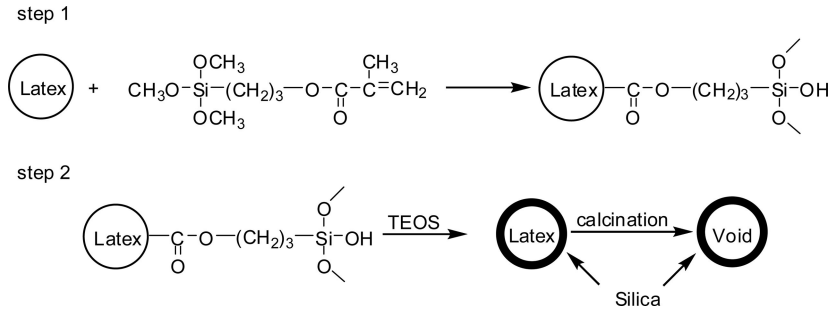

[a] Reprinted with permission from ref 355b. Copyright 2002 American Chemical Society.

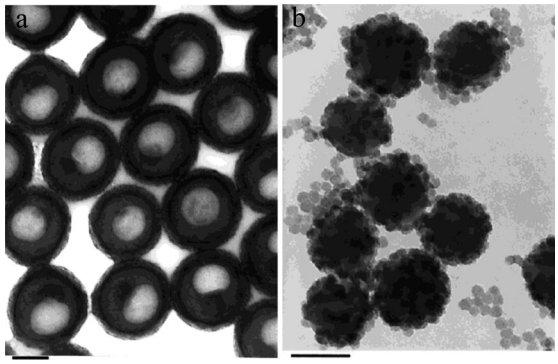

Figure 3. TEM micrographs of silica-coated latex particles using (a) MPS functionalized PS latex particles and (b) bare PS latex particles as the seed. Scale bar = 100 nm. Reprinted with permission from ref 355a. Copyright 2001 American Chemical Society.

Scheme 19. Schematic Illustrating the Difference in Silica Coating when PS Beads Terminated in (A) SO_3H and (B) NH_2 Groups Were Used as the Cores[a]

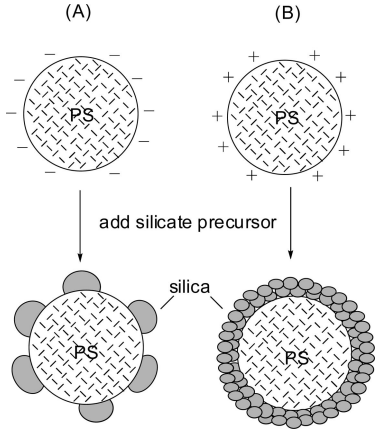

[a] Reprinted with permission from ref.[357] Copyright 2004 American Chemical Society.

20. After this functionalization, the stabilized particles could be transferred to a solution of ammonia in ethanol and directly coated with smooth and homogeneous silica shells of variable thickness by addition of TEOS in a seeded growth process. The length of the polymer used strongly influenced the stability of the colloids and the homogeneity and smoothness of the initial silica coating. This method is especially useful for colloidal particles that cannot be covered directly with SiO_2 by a Stöber-like growth process. This method is faster and requires neither the use of silane coupling agents nor a precoating step with sodium silicate.

Chen et al.[361] reported a method for preparing hollow silica nanopheres from the silica-coated poly(vinylbenzyl chloride)

Scheme 20. Diagram of the General Procedure for the Coating of Colloids with Silica[a]

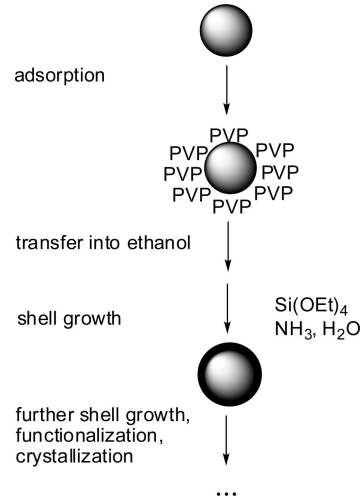

[a] In the first step PVP is adsorbed onto the colloidal particles. Then these stabilized particles are transferred into a solution of ammonia in ethanol. A silica shell is grown by consecutive additions of TEOS. Reprinted with permission from ref 360. Copyright 2003 American Chemical Society.

(PVBC) nanoparticles. PVBC latex particles of about 100 nm in size were prepared by emulsion polymerization. Silyl functional groups were introduced onto the PVBC nanoparticle templates via surface-initiated ATRP of MPS. The silyl groups were then converted into a silica shell, approximately 20 nm thick, via a reaction with TEOS in ethanolic ammonia. Hollow silica nanopheres were finally generated by thermal decomposition of the PVBC core.

Acrylic polymer/silica hybrids as a group of functional materials prepared by the sol−gel technique have also been of interest. Tang et al.[363] reported an approach of using an emulsion polymerized polymer in preparing organic/inorganic nanocomposites through a sol−gel technique. By mixing a polymer emulsion with TEOS prehydrolyzed under an acid condition, they prepared transparent PMMA/SiO_2,[363a] PBMA/SiO_2,[363b] and PEA/SiO_2[363c] nanocomposites. Results showed that there was a strong interaction between polymer latex particles and the SiO_2 network. Tamai and Watanabe[364] synthesized acrylic polymer/silica organic/inorganic hybrid emulsions by an acidic condition sol−gel reaction using a silane coupling agent containing acrylic polymer emulsion and TEOS. The acrylic polymer emulsions containing triethoxysilyl groups were synthesized by emulsifier-free[364a] or conventional[364b] emulsion polymerization. The acrylic polymer/silica hybrid films prepared from the acrylic polymer emulsions and TEOS were transparent and solvent-resistant. Recently, the effect of particle surface charge on the sol−gel

reaction in acrylic polymer emulsions was studied.[364c] The hybrid emulsions were synthesized from both anionic and cationic polymer emulsions by simple postaddition of TEOS. It was revealed that the hybrid emulsion from the anionic polymer emulsion was a mixture of anionic polymer particles and homogeneously dissolved silicate oligomer−polymer. In contrast, the hybrid emulsion from cationic polymer emulsion consisted of polymer core/silica shell particles. The electrostatic interaction between the cationic polymer particle surface and the silicate would be responsible for the accumulation of the silicate onto the particle surface, leading to the silica shell layer formation. The sol−gel condensation reaction of silicate in the acidic emulsion phase was revealed to be controllable by the surface charge of the coexisting particles.

Hu et al.[365] proposed a polymeric microgel template method for preparation of structural hybrid microspheres with poly(*N*-isopropylacrylamide-*co*-acrylic acid) (P(NIPAM-*co*-AA)) as the core and nanosilica particles as the shell. The microhydrogel of P(NIPAM-*co*-AA) swelled with ammonium hydroxide was used as microreactor. Nanosilica particles gradually deposited on the microhydrogel from the surface to the inner part via hydrolysis and condensation of TEOS in an *n*-heptane medium. The results indicated that the shell of the complex microspheres consists of SiO_2 microspheres with about 300 nm. Moreover, the thickness of the shell could be controlled by the depositing reaction of SiO_2.

Cationic diblock copolymer micelles have also been used as colloidal templates for the deposition of silica at ambient temperature and neutral pH. The diblock copolymer micelles comprised cationic poly(2-(dimethylamino)ethyl methacrylate) (PDMA) coronas and hydrophobic poly(2-(diisopropylamino)ethyl methacrylate) (PDPA) cores, and the hybrid copolymer/silica particles were obtained by the in situ hydrolysis of TMOS from aqueous solution at pH 7.2 at 20 °C. Both non-cross-linked and shell cross-linked (SCL) micelles could be coated with silica without loss of colloid stability. Under optimized conditions, the silica deposition was confined to the partially quaternized cationic PDMA chains, leading to hybrid copolymer/silica particles of around 35 nm diameter with well-defined core−shell morphologies.[366]

PE is perhaps the simplest and most common organic polymer. In 2007, Avnir et al.[367] developed a method for the preparation of physically interpenetrating nanocomposites of PE and silica, which was based on the entrapment of dissolved PE in a TEOS system for the first time. The preparation of particles of low-density PE@silica and high-density PE@silica was carried out by a silica sol−gel polycondensation process within emulsion droplets of TEOS dissolved PE, at elevated temperatures. The key to the successful preparation of this composite was the identification of a surfactant, PE-*b*-PEG, that was capable of stabilizing the emulsion and promoting the dissolution of the PE. A typical TEM picture of the composite particles is shown in Figure 4.

Kaskel et al.[368] developed a microemulsion method for the in situ generation of bulk nanocomposites using the pure monomer MMA as the oil phase. Reverse water-in-oil (w/o) microemulsions composed of MMA forming the oil phase, nonionic surfactants, and water were used for the synthesis of transparent SiO_2/PMMA nanocomposites. TEOS was hydrolyzed in the reverse micelles containing aqueous

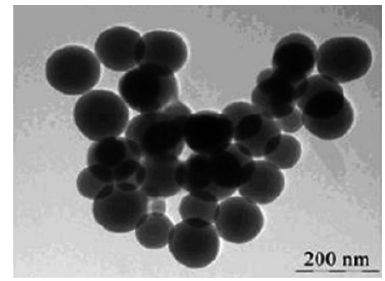

Figure 4. TEM of LDPE@silica. Reprinted with permission from ref 367. Copyright 2007 American Chemical Society.

Scheme 21. Representation of the Synthesis of SiO_2 Coated Latex Particles[a]

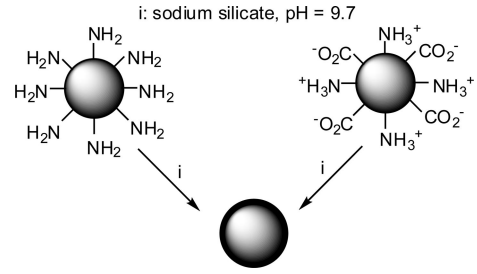

[a] Reprinted with permission from Cornelissen, J. J. L. M.; Connor, E. F.; Kim, H. C.; Lee, V. Y.; Magibitang, T.; Rice, P. M.; Volksen, W.; Sundberg, L. K.; Miller, R. D. Chem. Commun. 2003, 1010. Copyright 2003 The Royal Society of Chemistry.

ammonia. During the hydrolysis of TEOS, polymerization of the continuous MMA phase was initiated using AIBN, and after thermal polymerization at 60 °C for 12 h, solid blocks of PMMA were obtained in which nanometer-sized silica particles were trapped in the solid polymer matrix. The water droplets in MMA microemulsions were 12 nm in diameter, whereas after polymerization of the microemulsion, the SiO_2 particles in the transparent SiO_2/PMMA composites were 26 nm in diameter. TEM demonstrated a low degree of agglomeration in the composites. In comparison with materials generated from micelle-free solutions, the particle size distribution was narrow. The reverse micelle-mediated approach produced composites of high transparency comparable with that of pure PMMA.

It should also be mentioned that Miller et al.[45] prepared nanometer-sized silica-coated spheres using the controlled precipitation of silicic acid on functionalized PS latexes. They found that using PS latexes with either an amine functionalized or a zwitterionic surface, the latter consisting of amine and carboxylate groups, could be used to template the deposition of SiO_2 (Scheme 21). When a completely positively charged latex (i.e., PS stabilized with hexadecyl trimethyl ammonium bromide surfactant) or a negatively charged one (i.e., having sulfonate surface groups) was used, no formation of coated spheres was observed. This indicated that an attractive interaction between the surface groups and the precipitating silicate oligomers must be present. It was found that control of the pH of the sodium silicate solution was critical. An optimum was found at pH = 9.7, giving the desired coating in 24 h with limited formation of silica particles containing no latex core formed by the nontemplated precipitation of silica.

6.2. In Situ Polymerization

In this method, the nanocomposite particles are prepared via heterophase polymerization (including emulsion,[75,76,78,371–384]

emulsifier-free emulsion,[385–392] miniemulsion,[393–399] and dispersion polymerization;[400–405] postscript suspension polymerization may also be feasible but no report is found in recent literature) in the presence of silica nanoparticles as fillers or seeds, which is different from the previously mentioned in situ polymerization (homogeneous polymerization, i.e., bulk and solution polymerization).

Organic functionalization of the inorganic nanoparticles is usually necessary in the heterophase polymerization method. Two strategies[32a,b] are often employed: (i) modification of the inorganic particles by chemical interaction[78b,371–381,390,396,398a,b,400–402,405] (prevalently using coupling agents) or physical interaction;[75,76,78] (ii) absorption of the main ingredients of polymerization, namely, the monomer[385a–c,386,397,398c,403] or the initiator molecule,[383,384,388,404b,c] on the inorganic surface. After this functionalization, polymer encapsulation of silica could be realized by different polymerization processes. Several typical examples of polymer/silica nanocomposites prepared via heterophase polymerization are listed in Table 5.

6.2.1. Emulsion Polymerization

In fact, emulsion polymerization (normally referred to as seeded emulsion polymerization since silica nanoparticles are generally used as seeds) is the most important method for polymer encapsulation of inorganic particles by far. Early in the 1990s, Espiard et al.[371] reported results on the encapsulation of silica particles through emulsion polymerization using MPS as coupling agent. The silane molecule allowed the grafting of a significant amount of polymer from the early stages of polymerization; thus MPS provided reactive double bonds for covalent attachment of the growing polymer chains on the silica surface. This strategy has since been widely applied.[372–381]

Reculusa et al.[373] demonstrated the highly controlled synthesis of daisy-shaped and multipod-like PS/silica nanocomposites through an emulsion polymerization. The silica seeds were previously functionalized with an appropriate coupling agent carrying polymerizable groups. Following classical recipes, emulsion polymerization of St was achieved in the presence of these surface-modified particles, and PS was formed exclusively at the surface of the inorganic precursors. The density of the coupling agent and the silica seed diameter had a strong influence on the particle morphology. In the case when the density was equal to 0.1 molecule nm^{-2} (that is around 0.17×10^{-6} mol m^{-2}) and the seed size was close to 170 nm, an interesting evolution of the morphology with the reaction time, from daisy-like toward multipod-like, was observed. The Scheme 22 representation of the process involved in the synthesis of the daisy-shaped nanocomposites allows one to better understand the formation of this morphology.

Dissymmetrical colloidal particles, each of which consists of one PS nodule attached to a single silica nanoparticle, were synthesized through a seeded emulsion polymerization process.[78a] Silica seed particles from 50 to 150 nm were first surface-modified by adsorption of an oxyethylene-based macromonomer or covalent grafting of a trialkoxysilane derivative. Then, emulsion polymerization of St was carried out in the presence of these particles, the formation of PS nodules being highly favored at the silica surface in such conditions. Variation of different experimental parameters demonstrated that the ratio between the number of silica seeds and the number of growing nodules was a key

Table 5. Typical Examples of Colloidal Polymer/Silica Nanocomposites Prepared via Heterophase Polymerization

polymerization method	monomer(s)	morphology	comments	ref(s)
emulsion polymerization	St	raspberry-like	silica nanoparticles modified by adsorption of an oxyethylene-based macromonomer	78a
		controlled morphology such as dumbbell-like, snowman-like, decentered core−shell	silica nanoparticles modified by adsorption of an oxyethylene-based macromonomer or modified by MPS or APTES	78b
		controlled morphology such as snowman-like morphology, daisy-shaped, raspberry-like	silica nanoparticles modified by adsorption of an oxyethylene-based macromonomer	78c
	St	daisy-shaped and multipod-like	silica nanoparticles modified by MPS or MMS	373
	St	core−shell	silica nanoparticles modified by MPS	374a
	MMA	raspberry-like or core−shell	using a cationic initiator AIBA	383a
emulsifier-free emulsion polymerization	vinyl monomers	currant-bun	using a basic (co)monomer 4VP	385
	MMA	raspberry-like	using a basic comonomer 1-vinylimidazole	386a
	MMA	raspberry-like	using a cationic comonomer 2-(methacryloyl)ethyltrimethyl-ammonium chloride	386b
	2VP	core−shell	using a cationic initiator AIBA	388
miniemulsion polymerization	vinyl monomers	hedgehog, raspberry	using a basic comonomer 4VP or vinylimidazole	396
	St	core−shell and other such as raspberry-like	silica nanoparticles modified by MPS	398a
	St + BA	various morphologies (e.g., multicore−shell, core−shell, and raspberry-like)	silica nanoparticles modified by MPS	398b
	St	different asymmetrical morphology	silica particles partially modified with *n*-octadecyltrimethoxysilane	400
dispersion polymerization	St	core−shell, containing one or more silica particles in its core	silica nanoparticles modified by MPS	401a,b
	BA	core−shell	silica nanoparticles modified by MPS	402
	HPMA	core−shell	using a basic comonomer 4VP	403
	St	core−shell	using a cationic initiator AIBA	404b,c

Scheme 22. Schematic Representation of the Formation of the Daisy- and Multipod-like Nanocomposites Taking into Account That the Polymer Nodules Do Not Grow Exactly at the Same Rate and That the Silica Colloids Are Not Perfectly Monodisperse in Size[a]

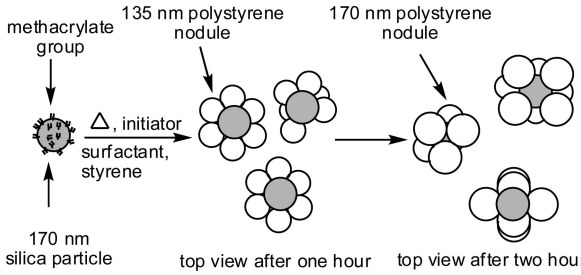

[a] Reprinted with permission from ref 373. Copyright 2004 American Chemical Society.

parameter in controlling the morphology of the final hybrid nanoparticles. For instance, in the particular case when this ratio was close to 1, dumbbell-like or snowman-like particles were obtained.

Yang et al.[374a] described a flexible method for preparing monodisperse silica/PS core−shell microspheres. The silica nanoparticles grafted by MPS were synthesized by the Stöber method and used as seeds in the emulsion polymerization. Monodisperse silica PS core−shell microspheres were then obtained through the emulsion polymerization of St on the surface of grafted silica nanoparticles. This method is useful to obtain narrowly distributed particles with well-defined particle morphology. The diameters of the core−shell microspheres increased as the content of monomer St is increased; the diameters of core−shell microspheres (from 212 to 369 nm) changed with those of the grafted silica (from 120 to 181 nm); the amount of emulsifier was directly related to the monodispersity and size of the core−shell microspheres. Monodisperse silica/PMMA core−shell nanospheres were obtained through the same method.[374b]

Yu et al.[375a] prepared silica/epoxy-functionalized PS core−shell composite nanoparticles via emulsion polymerization by the postaddition of GMA. The outermost shell of the multilayered core−shell particles was made up of PGMA. A semicontinuous process involving the dropwise addition of GMA was used to avoid demulsification of the emulsion system. The amount of grafted PGMA was altered within a wide range (for PGAA 1−50 wt % to St). The binding efficiency was usually high (ca. 90%), indicating strong adhesion between the silica core and the polymer shell. For epoxy-functionalized core−shell composite nanoparticles, there were approximately four or five original silica beads, which formed a cluster, per composite of nanoparticles whose size was about 60−70 nm. Similarly, silica/carboxyl-functionalized PS core−shell composite nanoparticles were also prepared.[375b]

As mentioned before, silica modified by physical interaction was also used in the emulsion polymerization.[75,76,78] Ding et al.[75] prepared monodisperse SiO_2/PS composite particles with core−shell structure by in situ emulsion polymerization of St on the surface of grafted silica nanoparticles. Nanosized silica particles modified with oleic acid could be coated by in situ emulsion polymerization of St monomer. Colloidal particles with a controlled morphology have been synthesized through an emulsion polymerization process using silica particles surface-modified by the adsorption of an oxyethylene-based macromonomer as seeds.[78c]

Luna-Xavier et al.[383a] described the preparation of silica/PMMA nanocomposite latex particles using an electrostatically adsorbed cationic initiator to promote polymerization at the surface of an anionic silica sol. The role of initiation in the synthesis of silica/PMMA nanocomposites was determined first using a nonionic surfactant, nonylphenol poly(oxyethylene) (NP30), and three different initiators, AIBA, KPS, and AIBN (cationic, anionic, and nonionic, respectively). A silica sol with an average diameter of 68 nm was used as the seed. The polymerization reaction was conducted under alkaline conditions in order to evaluate the role of the surface charge of the hydrophilic silica on the coating reaction. AIBA was found to be adsorbed on the silica surface owing to electrostatic interactions of the amidine function of the cationic initiator with the silanolate groups of the oxide surface, while the anionic and the nonionic initiators did not adsorb on silica under the same conditions. Nonetheless, whatever the nature of the initiator, polymerization took place on the silica particles as evidenced by TEM. As much as 65% by weight of the total polymer formed was found to be present at the silica surface using AIBA, while only 40% for KPS and 25% for AIBN were found to cover the silica particles under alkaline conditions. It was demonstrated that by use of a cationic initiator and by control of the pH of the suspension it was possible to significantly decrease the amount of free polymer. Coating of the silica particles took place through a kind of in situ heterocoagulation mechanism.

The effect of size and concentration of silica on morphology of composite particles were further studied using AIBA, NP30, and silica beads with diameters of 68, 230, and 340 nm, respectively (Scheme 23). Coating of the silica particles with PMMA occurred in situ during polymerization, resulting in the formation of colloidal nanocomposites with either a raspberry-like or core−shell morphology, depending on the size and nature of the silica beads. Electrostatic attraction between the positive end groups of the macromolecules and the inorganic surface proved to be the driving force of the polymer assembly on the seed surface at high pH, while polymerization in adsorbed surfactant bilayers (so-called admicellar polymerization) appeared to be the predominant mechanism of coating at lower pH.[383b] Three synthetic routes were also compared. In the first route, emulsion polymerization of MMA, initiated by AIBA, was performed directly in an aqueous suspension of the silica beads using NP30. In the second route, AIBA was first adsorbed on the silica surface, and the free amount of initiator was discarded from the suspension. The silica-adsorbed AIBA adduct was suspended in water with the help of surfactant and used to initiate the emulsion polymerization of MMA. In the third route, cationic PMMA particles were synthesized separately and subsequently adsorbed on the silica surface. Whatever the approach used for their elaboration, the colloidal nanocomposites were shown to exhibit a raspberry-like morphology.[383c]

Following a similar strategy, Bao et al.[384a] synthesized PBA/PMMA core−shell particles embedded with nanometer-sized silica particles by emulsion polymerization of BA in the presence of silica particles preabsorbed with AIBA initiator and subsequent MMA emulsion polymerization using PBA/silica composite particles as the seeds. It showed that AIBA could be absorbed effectively onto silica particles when the pH of the dispersion medium was greater than the isoelectric potential point of silica. The PBA/silica composite

Scheme 23. Schematic Representation of the Polymerization Reaction Initiated with AIBA at the Surface of the Silica Beads[a]

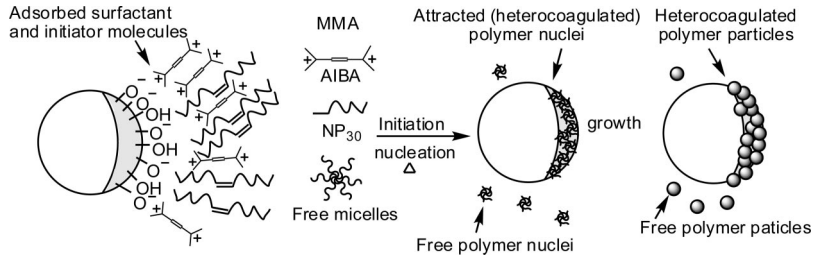

[a] Reprinted with permission from Luna-Xavier, J. L; Guyot, A.; Bourgeat-Lami, E. J. Colloid Interface Sci. 2002, 250, 82. Copyright 2002 Elsevier Science (USA).

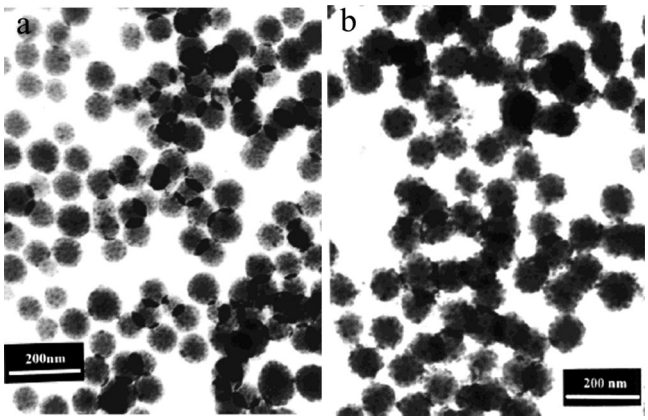

Figure 5. TEM micrographs of (a) 4VP/SiO_2 nanocomposites and (b) 90:10 St-4VP/SiO_2 nanocomposites. Note the "currant-bun" morphology due to the darker ultrafine silica sol within the interior of the particles in panel a. In contrast, panel b suggests a "raspberry" morphology. Reprinted with permission from ref 385b. Copyright 2000 American Chemical Society.

particles exhibited a raspberry-like morphology, with silica particles "adhered" to the surfaces of the PBA particles, whereas the PBA/silica/PMMA composite latex particles exhibited a sandwich morphology, with silica particles mainly at the interface between the PBA core and the PMMA shell.

6.2.2. Emulsifier-Free Emulsion Polymerization

Emulsifier-free emulsion polymerization has been receiving considerable attention in recent years because it can produce clean and monodisperse latexes. In 1999, Armes and co-workers[385a] reported the synthesis of colloidal dispersions of polymer/silica nanocomposite particles in high yield by homopolymerizing 4VP in the presence of an ultrafine silica sol using a free-radical initiator in aqueous media at 60 °C. The 4VP/silica nanocomposites have a "currant-bun" particle morphology, with the ultrafine silica sol being located primarily within the interior of the particles rather than at their surface (Figure 5). Copolymerization of 4VP with MMA and St also produced colloidally stable nanocomposite particles, in some cases for comonomer feeds containing as little as 6 mol % 4VP.[385b] However, homopolymerization of St or MMA in the presence of the silica sol did not produce nanocomposite particles in control experiments. Thus a strong acid−base interaction between the silica sol and the (co)polymer appears to be essential for nanocomposite formation. Film-forming vinyl polymer/silica colloidal nanocomposites were obtained by copolymerization of 4VP with either BA or BMA in the presence of an ultrafine aqueous silica sol.[385c] Highly transparent, free-standing nanocomposite films were readily obtained by solution-casting from aqueous media at room temperature. Reducing the initial silica concentration at constant monomer concentration led to an increase in the particle size and reduced colloid stability, indicating that the ultrafine silica sol stabilized the colloidal nanocomposites. Colloidal nanocomposites were also prepared using a methacrylate-capped PEG (MPEGMA) macromonomer as a reactive steric stabilizer. The resulting sterically stabilized nanocomposites exhibited enhanced colloid stability. In addition, this polymeric stabilizer led to an increase in the silica content of the nanocomposites and lower minimum film-forming temperatures due to its plasticizing effect. Typically these nanocomposite particles ranged from 100 to 200 nm diameter and contained approximately 10−50% silica by mass. This synthetic route has several advantages: (i) it is a simple, one-pot protocol based on readily available starting materials, (ii) no surface pretreatment of the silica sol is required, and (iii) no addition of surfactant is necessary. However, the use of 4VP has some disadvantages: (i) it is a relatively expensive monomer, (ii) it is a rather inefficient auxiliary, and (iii) it is somewhat malodorous.[402]

Following a similar route, Wu and co-workers[386a] also successfully prepared raspberry-like PMMA/SiO_2 hybrid microspheres with 1-vinylimidazole (1-VID) as auxiliary monomers. Waterborne raspberry-like PMMA/SiO_2 nanocomposite particles were synthesized via a free-radical copolymerization of MMA with 1-VID in the presence of ultrafine aqueous silica sols. The strong acid−base interaction between hydroxyl groups (acidic) of silica surfaces and amino groups (basic) of 1-VID was strong enough for promoting the formation of long stable PMMA/SiO_2 nanocomposite particles when 10 mol % or more 1-VID as auxiliary monomer was used. The average particle sizes and the silica contents of the nanocomposite particles could range from 120 to 350 nm and 5% to 47%, respectively, depending upon reaction conditions. Stable nanocomposite particles could only be obtained under basic conditions, and the silica content in the nanocomposite particles reached the maximum when the pH value was 8.0.

A cheap cationic monomer 2-(methacryloyl)ethyl trimethylammonium chloride (MTC) was also used as an auxiliary monomer to prepare raspberry-like hybrid microspheres. Only around 3% MTC based on monomer mass was copolymerized with MMA in the presence of aqueous silica particles, and simultaneously nanosilica particles were deposited onto the surfaces of organic particles in aqueous medium via electrostatic interaction between nanosilica particles and MTC. Since the surface hydroxyl groups of silica particles were hydrophilic, they could act as an emulsifier to stabilize the organic particles. The whole process required neither surface treatment for nanosilica particles nor addition of surfactant or stabilizer. The elec-

Scheme 24. Schematic Representation for the Formation of PMMA/Silica Nanocomposite Particles by the Free-Radical Polymerization of MMA at 25 °C in the Presence of an Ultrafine Silica Sol but in the Absence of Any Added Surfactant or Comonomer Auxiliaries[a]

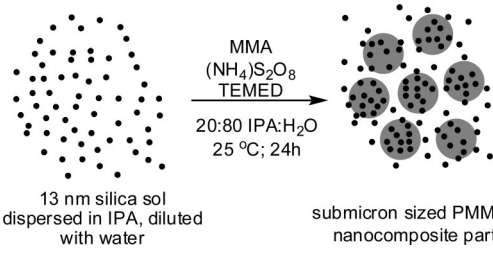

[a] Reprinted with permission from ref 387a. Copyright 2002 American Chemical Society.

trostatic interaction between negatively charged silica and positively charged MTC was sufficient to promote the formation of long-stable hybrid microspheres with raspberry-like morphology. The average particle sizes and the final silica contents of the hybrid microspheres ranged from 180 to 600 nm and 15 to 60 wt %, respectively.[386b]

Armes and co-workers[387a] also reported the surfactant-free synthesis of PMMA/silica nanocomposite particles in aqueous alcoholic media at ambient temperature without the use of auxiliary comonomers (Scheme 24). Stable colloidal dispersions with reasonably narrow size distributions could be obtained with silica contents of up to 58% by mass. Studies indicated that these nanocomposite particles had silica-rich surface compositions. This initial work was extended to include St, acrylates, and other methacrylate monomers and also two further commercial silica sols, thus providing access to a wide range of vinyl polymer/silica nanocomposite particles.[387b]

Very recently, Armes et al.[388] described the surfactant-free synthesis of colloidally stable P2VP/SiO_2 nanocomposite particles for the first time in purely aqueous media by emulsion polymerization at 60 °C using a commercial 20 nm aqueous silica sol as the sole stabilizing agent. Unlike previously reported P4VP/SiO_2 colloidal nanocomposite syntheses (typical silica aggregation efficiencies estimated for the successful syntheses were relatively low at 19−60%, thus the desired nanocomposite particles were always contaminated with excess nonaggregated silica sol),[385] TEM studies indicated very high silica aggregation efficiencies (88−99%) in this case. The key to success was simply the selection of a suitable cationic azo initiator. In contrast, the use of an anionic persulfate initiator led to substantial contamination of the nanocomposite particles with excess silica sol. The cationic azo initiator was electrostatically adsorbed onto the anionic silica sol at submonolayer coverage, which suggested that surface polymerization may be important for successful nanocomposite formation. Moreover, the 2VP could be partially replaced with either St or methacrylic comonomers to produce a range of copolymer silica nanocomposite particles. The P2VP/SiO_2 nanocomposite particles had a well-defined core−shell morphology, with P2VP cores and silica shells; mean diameters typically vary from 180 to 220 nm, and mean silica contents range from 27% to 35% by mass.

The emulsifier-free systems are often not truly free of an emulsifier in the strictest sense as the name indicates. The monomer or comonomer usually contains a part that resembles the structure of an emulsifier at one end of the molecular chain. Such a monomer or comonomer can play the role of an emulsifier while polymerizing. Sodium methacrylate (NaMA) is one such comonomer. It is an ionic vinyl monomer with sodium carboxylate salt at one end of the molecule and a double bond at the other end, and it has been used to conduct emulsifier-free emulsion copolymerization. Yu et al.[390] prepared polymer/silica composite nanoparticles bearing carboxyl groups on the surface via the emulsifier-free emulsion copolymerization of MMA and NaMA. Carboxyl groups were generated by the addition of hydrochloric acid at the end of the copolymerization. Two methods of NaMA addition were studied, batch and two-stage procedures. The batch procedure allowed only a limited number of carboxyl groups to effectively bond to the composite nanoparticles. In contrast, the number of carboxyl groups could be altered over a wide range with the two-stage procedure.

Scheme 25. The Principle of Miniemulsion Polymerization[a]

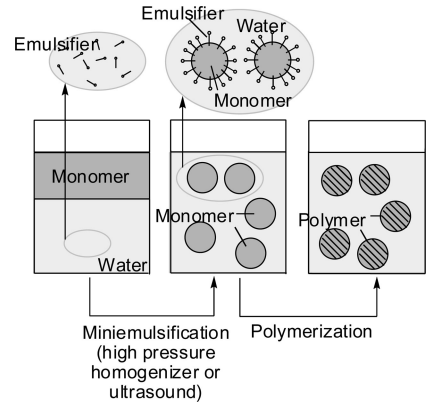

[a] Reprinted with permission from Antonietti, M.; Landfester, K. Prog. Polym. Sci. 2002, 27, 689. Copyright 2002 Elsevier Ltd.

6.2.3. Miniemulsion Polymerization

Recently, miniemulsion polymerization has turned out to be an attractive way to obtain nanocomposites particles, especially when the synthesis of more complex particles is involved. The miniemulsion is typically obtained by shearing a system containing monomer(s), water, surfactant, and a costabilizer. Because of their small size, the large overall surface area of the droplets, typically 50 to 500 nm in diameter, can effectively compete for radical capture. As a result, monomer droplets in a miniemulsion become the dominant site for particle nucleation. Scheme 25 shows the principle of miniemulsion polymerization. If the inorganic particles could be dispersed in the monomer phase followed by miniemulsification, each submicrometer droplet could indeed act as a nanoreactor, which produces nanocomposite particles with great encapsulation efficiencies of inorganic particles. The size of nanocomposite particles can be adjusted by varying the surfactant concentration and shear intensity during the miniemulsification. Therefore, miniemulsion polymerization is a powerful tool in preparing nanocomposite particles.[394–396]

In 2001, Landfester et al.[397] first reported the preparation of polymer/silica nanocomposites by using miniemulsion polymerization. Polymer dispersions made of a variety of monomers, including St, BA, and MMA were generated by the miniemulsion process in the presence of a coupling comonomer 4VP, hexadecane, hydrophobe, and silica nanoparticles. The anionic sodium dodecyl sulfate (SDS) and the

cationic cetyltrimethylammonium chloride (CTMA-Cl), as well as the nonionic surfactant Lutensol AT50 (which is a PEO-hexadecyl ether with an EO block length of about 50 units), were chosen. Depending on the reaction conditions and the surfactants employed, different hybrid morphologies were obtained, comprising a "hedgehog" structure where the silica surrounded the latex droplet and provided stabilization even without any low molecular weight surfactant. In other parts of the composition diagram noncoupled structures as well as "raspberry" hybrids could be made.

The size and morphology control of the nanocomposite particles by miniemulsion polymerization was studied by Wu and co-workers.[398a] SiO_2/PS nanocomposite particles were synthesized through miniemulsion polymerization by using sodium lauryl sulfate (SLS) surfactant and hexadecane costabilizer in the presence of silica particles coated with MPS. By adjusting the size of the silica particles and the surfactant concentration employed, they were able to control the size and morphology of the composite particles. For 45 nm silica particles, the size of the nanocomposite particles decreased from 200 to 80 nm with increasing surfactant concentration from 20 to 40 mM, and the numbers of silica particles entrapped in each polymer particle gradually decreased and finally formed core−shell morphology. For 90 nm silica particles, the size of the nanocomposite particles also decreased from 180 to 130 nm with increasing surfactant concentration from 20 to 40 mM, but the core−shell morphology remained unchanged. For 200 nm silica particles, some "raspberry-like" morphology was observed. Furthermore, SiO_2/P(St-BA) nanocomposite particles with various morphologies (e.g., multicore−shell, normal core−shell, and raspberry-like)[398b] and raspberry-like silica/PS/silica[398c] multilayer hybrid particles were also prepared via miniemulsion polymerization.

Zydowicz et al.[399] synthesized silica/PA nanocomposites via an original double emulsification process in miniemulsion. Silica was first synthesized in cyclohexane using a sol−gel process in an inverse microemulsion, and then the coupling agent APTES was grafted onto the surface of the silica nanoparticles. In a third step, direct miniemulsions were prepared from the microemulsion containing the functionalized silica nanoparticles. The miniemulsions were prepared using SDS as the surfactant and cetyl alcohol as the costabilizer. Finally, an interfacial polycondensation occurred between a diamine added to the external phase and sebacoyl chloride in solution in the dispersed phase.

Very recently, asymmetric nanocomposite particle pairs of PS and silica were prepared via one-step miniemulsion polymerization.[400] The TEM images showed that these nanocomposite particle pairs were monodisperse and highly asymmetric in morphology. Nanocomposite particles with different asymmetrical morphology were obtained by controlling the concentration of St. When the amount of St was changed from 2.2 to 4.8 g, the shape of the nanocomposite particles varied from mushroom-like to swaddle-like, as shown in Figure 6. Hence, even over this wide range of concentration, the asymmetric morphology of the nanocomposite particles could be well maintained. The key to obtaining the asymmetric nanocomposite particle pairs was the combination of miniemulsion polymerization and the local surface modification of silica substrates. Because of localized surface modification on the silica surface, the nucleation and formation of the polymer nodule in miniemulsion polymerization took place only in the modified area on the silica surface, thus ensuring the asymmetric morphology.

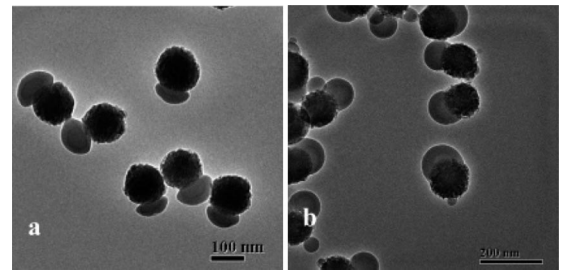

Figure 6. TEM images of asymmetric silica/polystyrene nanocomposite particles: (a) 2.2 g of styrene; (b) 4.8 g of styrene. Reprinted with permission from ref 400. Copyright 2008 American Chemical Society.

6.2.4. Dispersion Polymerization

In 1998, the pioneering work of Bourgeat-Lami and Lang[401a] demonstrated the encapsulation of silica nanoparticles by dispersion polymerization of St in polar media. The dispersion polymerization was carried out in a water−ethanol (5/95 wt/wt) medium, with PVP as stabilizer in the presence of small colloidal silica particles produced by the Stöber method. The silica particles were either unreacted (hydrophilic character) or coated with MPS (hydrophobic character). When the bare silica particles were used as the seed, obviously encapsulation did not occur. In contrast, when the silica surface was made hydrophobic by coating, the inorganic particles were entirely contained in the PS particles. Under the experimental conditions, each PS latex particle contained, on average, 4−23 silica beads with diameters between 49 and 120 nm depending, in particular, on the size of the silica. It was possible to control the composite particle size and morphology by a convenient choice of the composition of the system. The evolution of the shape and composition of the composite particles was a function of three main parameters, namely, the silica bead size and concentration, the solvent composition, and the nature or amount of stabilizer.[401d,e]

The effect of silica size and concentration on the morphology of silica/PS composite particles was further studied using larger silica beads with diameters between 191 and 629 nm.[401b] Figure 7 shows TEM micrographs of samples obtained with silica beads with diameters of 72, 120, 352, and 629 nm, respectively. All the micrographs show that the silica beads are embedded inside the PS latexes, and no free silica beads are present. This observation indicated that the encapsulation for the small silica beads was also successfully achieved with larger silica beads under the same experimental conditions. However, some important changes in composite particle size and morphology, as well as in the number of silica beads per composite particle, were observed when the size of the silica beads was changed from small (<200 nm) to larger ones (>200 nm). It appeared that the morphology of the composite particles changed from quasispherical to nonspherical shapes when the silica bead size increased. Furthermore, one can see in Figure 7 that the average number of silica beads per composite particle decreases when the silica bead size increases. It clearly appeared that the encapsulation of only one silica bead could be obtained simply by increasing the size of the beads. Under the experimental conditions, the optimal bead diameter for achieving composite particles containing only one silica bead

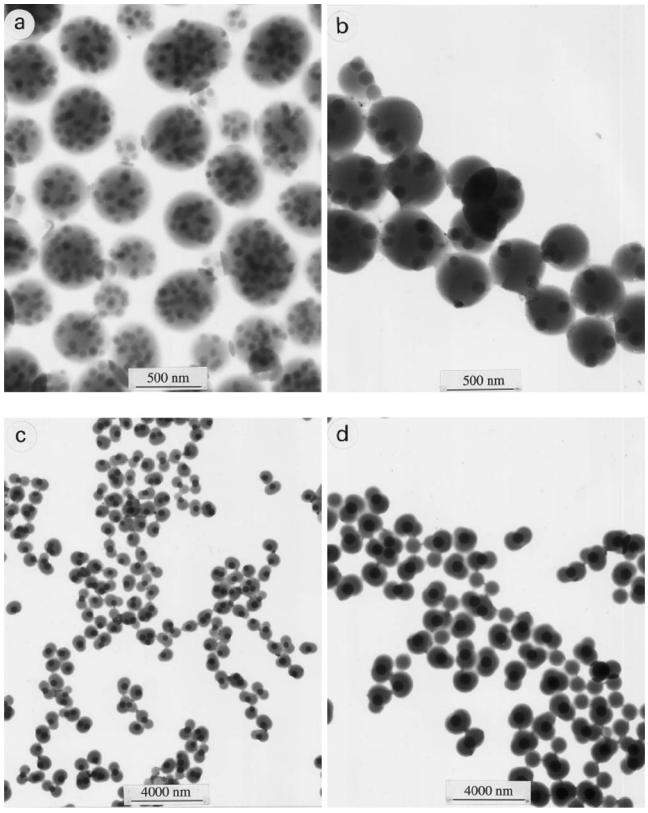

Figure 7. TEM micrographs of samples obtained with silica beads with diameters of (a) 72, (b) 120, (c) 352, and (d) 629 nm. Reprinted with permission from Bourgeat-Lami, E.; Lang, J. J. Colloid Interface Sci. 1999, 210, 281. Copyright 1999 Academic Press.

turned out to be around 450 nm. It showed that increasing the silica bead size above this value resulted in an increased number of composite particles without silica beads. In contrast, the number of composite particles with two, three, four, or more than four silica beads increased with decreasing silica bead size.

In order to have real control of the morphology of the composite particles, and in particular to obtain only one silica bead per composite particle, P(St-*b*-EO) block copolymer was used as a stabilizer for the synthesis of silica/PS core−shell particles.[401c] The polymerization of St in the presence of 29−300 nm diameter MPS-grafted silica beads had the following characteristics: (i) all the silica beads were encapsulated with PS; (ii) there was only one silica bead per composite particle; (iii) free latex particles were formed, but their number decreased as the diameter of the silica beads decreased and became very small compared with the number of composite particles when the diameter of the silica beads was 29 nm, and then almost all the polymer synthesized constituted the shell of the composite particles. It clearly appears from Figure 8 that the thickness of the shell increases when the diameter of the silica beads decreases.

Matijević et al.[402] reported the formation of an organic shell on extremely small silica nanoparticles (<10 nm) by the same method. Stable dispersions of nanosilica ranging in size between 8 and 11 nm were coated with BA polymer by in situ polymerization of monomer adsorbed on the particles in 2-propanol. The system was developed for use in the encapsulated inorganic resist technology. To achieve a high coating efficiency, silica was first modified with the MPS coupling agent at two different degrees of grafting. Under studied conditions, the encapsulation efficiency was

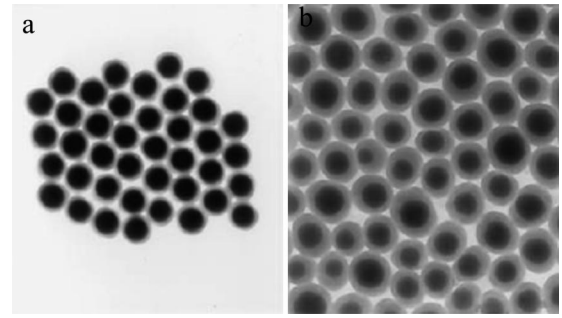

Figure 8. TEM micrographs of composite particles obtained after elimination of the free latex particles by centrifugation/redispersion in the aqueous alcoholic medium. Diameters of the silica beads were (a) 300 and (b) 108 nm. Stabilizer concentrations were 2 wt % relative to the solvent. Reprinted with permission from Corcos, F.; Bourgeat-Lami, E.; Novat, C.; Lang, J. Colloid Polymer Sci. 1999, 277, 1142. Copyright 1999 Springer-Verlag.

governed by the degree of MPS grafting and by the initial concentration of the monomer. The dissolution rate of these particles in aqueous base, a key parameter in photoresist application, was drastically reduced with increasing amount of grafted *tert*-BA polymer at the silica surface.

An aqueous dispersion polymerization route to colloidal polymer nanocomposites via the free radical copolymerization of HPMA and 4VP in the presence of an ultrafine silica sol was reported by Armes et al.[403] In the work, HPMA was copolymerized with 4VP using APS in the presence of an ultrafine silica sol. 4VP was used as an auxiliary in these syntheses; the strong interaction of this basic monomer with the acidic surface of the silica particles was essential for successful nanocomposite particle formation. HPMA monomer was selected since it has appreciable water solubility (up to 13% at 20 °C), but HPMA homopolymer is water-insoluble. This unusual solubility behavior ensured that these nanocomposite syntheses were conducted under true dispersion polymerization conditions. In view of the success of these syntheses, it was concluded that emulsion monomer droplets and micelles are not a prerequisite for the formation of nanocomposite particles. Under the conditions investigated, the minimum amount of 4VP auxiliary required was around 15%.

In 2005, Armes and co-workers[404a] reported the serendipitous discovery that using 13 or 22 nm commercial alcoholic silica sols as the sole stabilizing agent in purely alcoholic media led to the production of micrometer-sized PS latex particles (rather than the anticipated nanocomposite particles) via dispersion polymerization using the AIBN initiator. These resulting surfactant-free PS particles had relatively narrow particle size distributions and contained surprisingly low levels of silica (≤1.1% by mass). The silica sol was located exclusively at the particle surface and was solely responsible for the colloidal stability, which presumably involved a charge stabilization mechanism. The effect of the nature of the initiator on the size and morphology of the resulting particles was further studied (Scheme 26).[404b] Using an anionic 4,4′-azobis(4-cyanovaleric acid) (ACVA) initiator led to gross precipitation of PS, with little or no particle formation. In contrast, using a cationic initiator AIBA led to the formation of submicrometer-sized PS/silica nanocomposite particles. The key to the formation of colloidally stable nanocomposite particles was the selection of a cationic azo initiator. Neither surface modification of the silica sol nor the addition of surfactant or polymeric stabilizers was required for successful nanocomposite syntheses. Mean

Scheme 26. Schematic Representation of the Effect of Varying the Initiator Type in the Attempted Dispersion Polymerization of Styrene at 60 °C in the Presence of a Ultrafine Silica Sol[a]

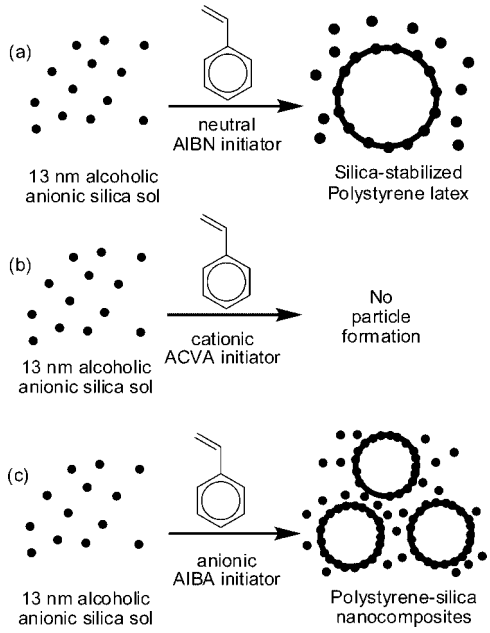

[a] Reprinted with permission from ref 404b. Copyright 2006 American Chemical Society.

particle diameters varied between 262 and 464 nm, and silica contents ranged between 13 and 29 wt %, depending on the precise reaction conditions and the silica sol type used.[404c] Variation of the silica sol concentration and initiator concentration, as exemplified for the 22 nm silica sol, had surprisingly little influence over both the final silica content and particle diameter. XPS and ESI/TEM studies confirmed well-defined core−shell morphologies for these nanocomposite particles (i.e., PS cores and thin silica shells). Hollow silica particles could be formed after calcination, suggesting that the surface layer of silica nanoparticles was reasonably contiguous.

6.2.5. Other Polymerization Methods

Ultrasound is a wave of frequency 2×10^4 to 10^9 Hz. Ultrasound has been extensively applied in dispersion, crushing, and activation of particles, as well as initiation of polymerization. Wang and co-workers[406] reported ultrasonic induced encapsulating emulsion polymerization in the presence of nanoparticles. The polymerization reaction occurred in the bilayer admicelle formed on the surface of nanoparticles. The process can be depicted as Scheme 27. The experimental results suggested that the pH value, the type of monomers, the type, content, and surface properties of nanoparticles, and the type and concentration of surfactant had great influence on the ultrasonic induced encapsulating emulsion polymerization and the obtained latex stability. If cationic emulsifier (such as CTAB), low water soluble monomer (such as BA and St), and hydrophobic nanosilica were selected, the inorganic nanoparticles could be encapsulated by polymers through ultrasonic irradiation successfully under alkalescent conditions, forming novel polymer/inorganic nanoparticle composites.

Recent studies have demonstrated the feasibility of non-free-radical routes in polymerization in aqueous systems.

Scheme 27. Schematic Illustration of the Ultrasonic Induced Encapsulating Emulsion Polymerization in the Admicelles Formed on the Nanoparticles[a]

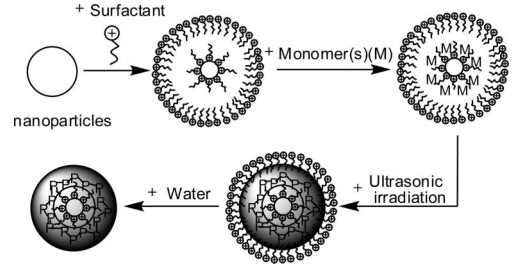

[a] Reprinted with permission from Xia, H. S.; Zhang, C. H.; Wang, Q. J. Appl. Polym. Sci. 2001, 80, 1130. Copyright 2001 John Wiley & Sons, Inc.

Catalytic polymerizations are of particular interest, because they enable a broad control of polymer microstructures.[407,408] Mecking et al.[407b] prepared silica/PE nanocomposite particles from catalytic emulsion polymerization of ethylene with nickel catalysts in the presence of silica nanoparticles affording stable dispersions of silica/PE nanocomposite particles. The modification of the surface of silica particles by grafting upon their surface of octenyl- or octylsilanes was a prerequisite for obtaining composites. Different morphologies of composites particles were observed depending on the microstructure and crystallinity of the PE part, controlled by different catalyst precursors.

The term phase inversion originally referred to transformation of the continuous phase from the oil to the water phase (or vice versa) in emulsions composed of small molecular species. In the vicinity of the phase inversion point (PIP), interfacial tension between the oil and the water phases reaches a minimum and an emulsion of small particle size is obtained. In 2002, Yang et al.[409] reported the preparation of waterborne dispersions of an epoxy resin-encapsulated inorganic particle nanocomposite with narrow size distribution by phase-inversion emulsification (Scheme 28). Microscopy results indicated that all the silica nanoparticles were encapsulated within the composites and uniformly dispersed therein. Curing of the nanocomposite dispersions proceeded in a controlled manner.

Microemulsion polymerization is seldomly reported for the in situ preparation of polymer/silica nanocomposites.[410–412] Depending on the composition of the oil, water, and surfactant, the nanostructure of microemulsion may be described as water droplets dispersed in oil medium or oil droplets dispersed in water. By choosing the right concentrations, both the oil and water phases can be a continuum, thus forming a bicontinuous microemulsion. The oil phase can then be polymerized together with the polymerizable surfactant, and the water phase be used to host organic/inorganic species. Chow and Gan[411] presented a simple and convenient method for the preparation of silica/polymer nanocomposites with a polymerizable bicontinuous microemulsion as a template for directing nanoparticles of SiO_2 to disperse uniformly in the polymerized microemulsion system. In the approach, nonfunctionalized/functionalized silica particles are first introduced into the aqueous channels of the bicontinuous microemulsion system, followed by in situ polymerization. The nonfunctionalized silica−polymer nanocomposites exhibited better mechanical properties. Further improvement of the properties was achieved for the functionalized silica/polymer by cross-polymerization of the

Scheme 28. Illustration of Polymer-Encapsulating Nanoparticles Obtained by Phase-Inversion Emulsification To Prepare Nanocomposite Waterborne Dispersions[a]

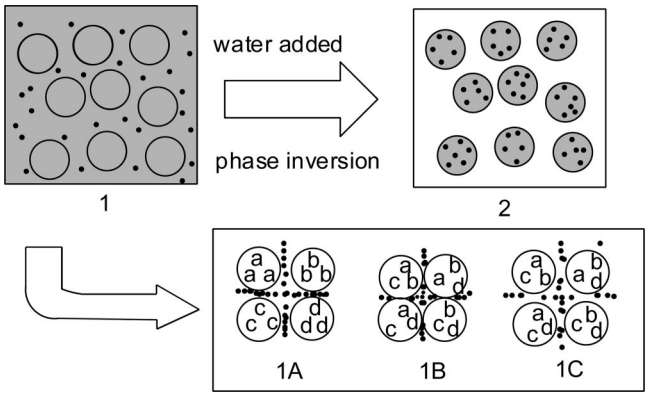

[a] (1) Water in resin system before phase-inversion point (PIP), (2) nanocomposite waterborne dispersions (resin in water system) obtained after PIP; (1A) nearest contact of the water droplets, (1B) transiently coalescent water droplets and scissored nanoparticle clusters, (1C) transiently coalescent structure broken up into water droplets and smaller patches re-dispersed in the matrix. The repeatedly dynamic coalescence and break-up of water droplets along pathway 1A−1B−1C−1A cuts the clusters into individual nanoparticles and guarantees re-dispersion in the matrix (gray, organic phase including epoxy resin, emulsifier, and curing agent; white, water phase; solid dots, silica nanoparticles.) Reprinted with permission from Yang, Z. Z.; Qiu, D.; Li, J. Macromol. Rapid Commun. 2002, 23, 479. Copyright 2002 Wiley-VCH.

Scheme 29. Illustration of the VDP for the Encapsulation of the Inorganic Nanoparticles[a]

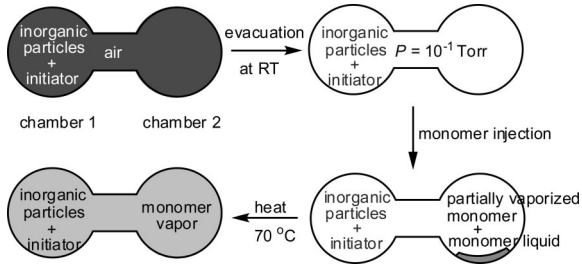

[a] Reprinted with permission from Jang, J.; Lim, B. Angew. Chem. Int. Ed. 2003, 42, 5600. Copyright 2003 Wiley-VCH.

functionalized silica nanoparticles and microemulsion components.

Vapor deposition techniques (VDP) can provide the creation of a smoother and more uniform polymer layer by the consecutive polymerization of vaporized monomer under a vacuum onto the desired surface. Jang and Lim[413] reported a facile route for the fabrication of various inorganic colloid−vinyl polymer core−shell nanostructures by one-step VDP. The overall synthetic procedure is represented in Scheme 29. The reactor containing the inorganic nanoparticles and a solid initiator was evacuated at room temperature until the pressure inside reached about 10^{-1} Torr, which put the system under a static vacuum. Then the liquid monomer was introduced into the reactor by injection. The monomers were partially vaporized as soon as they were injected inside the reactor at room temperature and completely vaporized by heating the reactor at 70 °C. Polymerization was initiated by thermal decomposition of a radical initiator, and the inorganic particles were stirred with a magnetic stirrer to prevent the formation of particle−particle aggregations. They applied it to encapsulate silica nanoparticles with PMMA and polydivinylbenzene (PDVB).

Chart 5. Chemical Structures of Typical Monomers for Conducting Polymers

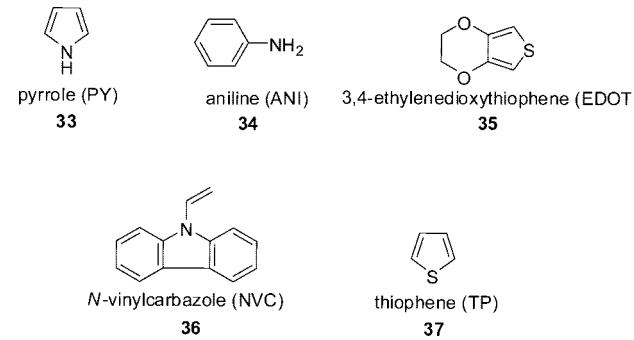

6.2.6. Conducting Nanocomposites

Inorganic nanoparticles can be combined with conducting polymers giving rise to nanocomposites with interesting properties and important application potential. Such nanocomposites have been overviewed by Gangopadhyay and De[35] and Jang.[36] Among them, the preparation and evaluation of silica nanocomposites of intractable conducting polymers formed the subject of a considerable amount of research during the past decade. Such nanocomposites are readily prepared by synthesizing the conducting polymers such as PPy,[414a–h,415–421] PANI,[414i–k,415,422–428] PANI derivates,[429–431] PEDOT,[432,433] PNVC,[434] and PT[435] in the presence of ultrafine silica in aqueous or other media. The chemical structures of typical monomers for conducting polymers are shown in Chart 5

The most widely used monomers are pyrrole (PY) and aniline (ANI), both of which are soluble in water and can be fast-polymerized in water by $FeCl_3$ or $(NH_4)_2S_2O_8$, respectively, to yield conducting nanocomposites. From the early 1990s, Armes and co-workers[414] have reported the preparation and characterization of PANI/silica and PPy/silica particles using ultrafine silica sol as particulate dispersants in aqueous media. It was shown that these polymer/silica nanocomposites had a "raspberry" morphology, with the silica particles being "glued" together by the precipitating PANI or PPy.

Surface functionalization of the PPy/silica nanocomposites, particularly with certain hydrophilic groups such as carboxylic acids or amines, can be highly desirable in application since it can provide specific binding. Carboxylic acid functionalized PPy/silica nanocomposites were successfully synthesized by copolymerizing a functional pyrrolic comonomer (either 1-(2-carboxyethyl) pyrrole or pyrrole-3-acetic acid) with PY.[414d,e] Amine-functionalized PPy/silica nanocomposites were synthesized via two routes: (i) initial synthesis of homopolypyrrole/silica particles, followed by surface amination using APTES, and (ii) copolymerization of an N-substituted aminopyrrole comonomer with PY in the presence of an ultrafine silica sol.[416] Ester-functionalized PPy/silica nanocomposite particles were prepared by oxidative copolymerization of PY and *N*-succinimidyl ester pyrrole (50/50 initial concentrations), using $FeCl_3$ in the presence of ultrafine silica nanoparticles. XPS studies of a series of conducting polymer/silica nanocomposites confirmed that the conducting polymer component was always present at (or very near) the surface of the particles. On the other hand, their surface compositions were invariably silica-rich, as judged from their Si/N atomic ratios. Aqueous electrophoresis measurements supported these observations since ζ potential vs pH curves obtained for various PANI/silica and PPy/silica

Scheme 30. Synthetic Procedure of Silica/PANI Core-Shell Nanoparticles[a]

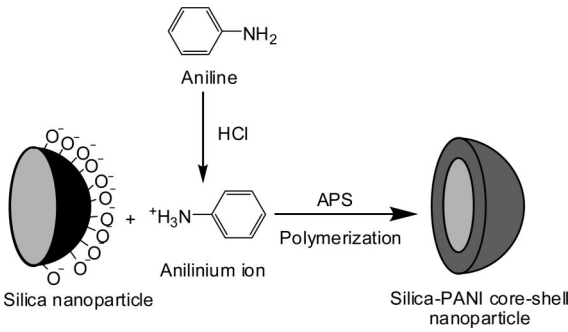

[a] Reprinted with permission from Jang, J.; Ha, J.; Lim, B. Chem. Commun. 2006, 1622. Copyright 2006 The Royal Society of Chemistry.

Scheme 31. Schematic Representation of the Formation of PEDOT/Silica Nanocomposites by the Oxidative Polymerization of EDOT in the Presence of an Ultrafine Methanolic Silica Sol[a]

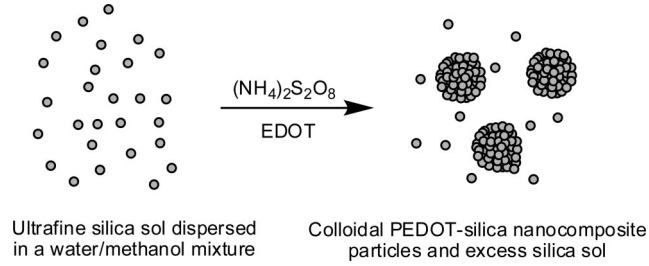

[a] Reprinted with permission from ref 432. Copyright 2003 American Chemical Society.

nanocomposites were essentially superimposable on that of a silica sol.[417]

The effect of methanol cosolvent on the synthesis of PPy/silica colloidal nanocomposites using ultrafine silica sols in combination with either the $FeCl_3$ or the APS oxidant was investigated. Two protocols were evaluated: the addition of methanol to an aqueous silica sol and the addition of water to a methanolic silica sol. The latter protocol proved to be more robust, since it allowed colloidally stable dispersions to be prepared at higher methanol contents (up to 50 vol % with the APS oxidant).[419]

Recently, Lu et al.[79] prepared sunflower-like PPy/silica nanocomposites via self-assembly polymerization. A natural biomacromolecule, chitosan, was chosen as an adsorbent to alter the surface properties of silica. The adsorption of chitosan was achieved on the silica surface to provide active sites for in situ self-assembly polymerization of PY monomer. Evidence was given that the final morphology of the composites was strongly dependent on the presence of the adsorbed chitosan, which ensured the formation of PPy particles on the silica surface.

Ultrasonic irradiation was also used to prepare PANI/nano-SiO_2 particle composites.[422] Polymerization of aniline was conducted under ultrasonic irradiation in the presence of two types of nano-SiO_2, porous nanosilica and spherical nanosilica. By taking advantage of the multiple effects of ultrasound, the aggregates of nano-SiO_2 particles could be broken down and the nanoparticles re-dispersed while polymerization of aniline proceeds. Synthesized PANI was deposited on the nano-SiO_2 particles, forming PANI-coated nanosilica composite particles. It was found that the aggregation of nano-SiO_2 could be reduced under ultrasonic irradiation and that nanoparticles were re-dispersed in the aqueous solution. The formed PANI deposited on the surface of the nanoparticles, which led to a core−shell structure.

Jang et al.[426] demonstrated the simple synthesis of silica/PANI core−shell nanoparticles by in situ polymerization of positively charged anilinium ions adsorbed on the negatively charged silica surfaces. The overall synthetic procedure is represented in Scheme 30. In this approach, aniline monomers were converted to cationic anilinium ions under acidic conditions with a pH of 3 and adsorbed onto the negatively charged silica surface. Since aniline has a known pK_a of 4.63, it is expected to be primarily positively charged at pHs below this value. On the other hand, the silica nanoparticles possess negative charges on their surfaces at pHs greater than 2, that is, the isoelectric point of silica. The aniline monomers electrostatically complexed to the silica surface were then polymerized by APS as an oxidizing agent at room temperature. This simple process allowed the formation of uniform PANI shells as thin as 2 nm on the silica cores, resulting in monodisperse core−shell nanoparticles. These silica/PANI core−shell nanoparticles also showed pH-responsive redox reversibility and relatively high electrical conductivity. This synthetic approach provided the formation of very thin layer shells with nanometer precision in thickness via electrostatic interactions.

A relevant work was the preparation of PANI and PPY modified water-dispersible conducting nanocomposites of polyacrylonitrile (PAN) with silica reported by Maity and Biswas.[436a] Stable aqueous suspension of a nanocomposite of PAN with SiO_2 was prepared via aqueous polymerization of AN by the K_2CrO_4−$NaAsO_2$ redox system first. A simple procedure for improving the conductivity of PAN/SiO_2 suspensions via incorporation of a second conducting polymer, such as PPY or PANI, onto the PAN/metal oxide suspensions was developed. The special advantage of the K_2CrO_4−$NaAsO_2$ redox pair used in this work for the aqueous polymerization of AN was that any excess of K_2CrO_4 in the system led to the facile initiation of ANI or PY monomers at selective pH thereby facilitating composite formation between PAN/SiO_2 and PANI or PPY. Such encapsulation was found to improve the conductivity of PAN/SiO_2 appreciably.[436b]

Several studies related to the composites of PANI derivatives and silica nanoparticles have been reported. These derivatives include poly(2-chloroaniline),[429] poly(*N*-[5-(8-quinolinol)ylmethyl]-aniline),[430] polydiphenylamine,[431a] and poly(3-aminophenylboronic acid).[431b]

Unlike PPy and PANI, due to the relatively low solubility of the EDOT monomer in aqueous solution, it has proven relatively difficult to prepare PEDOT in the form of colloidal dispersions. Ultrafine methanolic silica sol in place of the aqueous silica sol was used to synthesize of PEDOT/silica colloidal nanocomposites.[432] Using a methanolic ultrafine silica sol in combination with 4-toluenesulfonic acid facilitates the synthesis of colloidally stable, electrically conductive PEDOT/silica nanocomposites (Scheme 31). Raspberry-shaped PEDOT/silica nanocomposites of submicrometer dimensions were obtained. The mean nanocomposite particle diameter could be varied from 150 to 510 nm, and the silica content ranged from 19% to 80% by mass. Four-point probe measurements on pressed pellets indicated conductivities as high as 0.2 S cm^{-1}.

Core−shell PEDOT/silica nanoparticles and their corresponding hollow particles were also prepared (Scheme 32).[433]

Scheme 32. Schematic Illustration of the Procedure for Generating PEDOT/Silica Core-Shell Particles and PEDOT Hollow Particles[a]

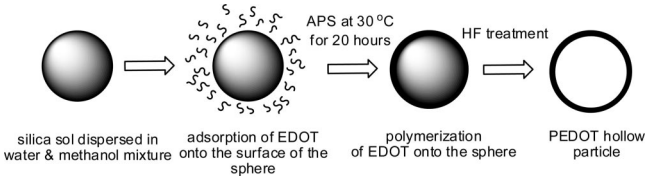

[a] Reprinted with permission from Han, M. G.; Foulger, S. H. Chem. Commun. 2004, 2154. Copyright 2004 The Royal Society of Chemistry.

For water-insoluble monomers, such as *N*-vinylcarbazole (NVC) and thiophene (TP), novel procedures were proposed. Ray and Biswas[434] conducted NVC polymerization in the presence of $FeCl_3$-impregnated ultrafine silica powder in benzene solution. The precipitation of polymer followed by benzene extraction of the PNVC/silica mass afforded a PNVC/silica nanocomposite. The composite exhibited a higher thermal stability and higher DC conductivity relative to PNVC homopolymer. The nanocomposite could be dispersed in water, dimethyl sulfoxide, or propanol in the presence of PVP to yield a stable suspension. Gök et al.[435] synthesized PT/PS/SiO_2 nanocomposite by chemical polymerization using $FeCl_3$ oxidant in $CHCl_3$.

6.3. Self Assembly

Self-assembled organic/inorganic nanocomposites are composed of discrete nanoscale organic and inorganic components that have been spontaneously organized based on noncovalent interactions. These organic/inorganic nanocomposites often demonstrate interesting properties because of the nanoscale size effects in constituent phases, high interfacial area, and synergic properties of these components.[37]

An alternative and remarkably adaptable approach termed the layer-by-layer (LbL) self-assembly technique, introduced by Decher and Hong[437] in 1991, has been widely applied to the coating of colloids. The basis of this method is the electrostatic association between alternately deposited, oppositely charged species.

The famous work concerning preparation of polymer/silica nanocomposites using LbL technology was reported by Caruso et al.[438] The work demonstrated that a homogeneous and highly regular nanoparticle multilayer coating of submicrometer-sized PS latex core particles was achieved by the controlled, stepwise adsorption of SiO_2 nanoparticles and polyelectrolyte poly(diallyldimethylammonium chloride) (PDADMAC) under deposition conditions where the nanoparticles and polyelectrolyte were oppositely charged (Scheme 33).

Although the driving forces in the self-assembly technique are dominated by electrostatic attractive interactions between positive and negative charges, other interactions, such as hydrophobic interactions, hydrogen bonding, coordination bonding, or chemical and biomolecular interactions have also been applied successfully. Kong et al.[439a–h] recently synthesized a PVA/SiO_2 nanocomposite with a self-assembly technique. Positively charged poly(allylamine hydrochloride) (PAH) molecular chains were adsorbed onto the surface of negatively charged SiO_2 nanoparticles through electrostatic adsorptive interactions. Afterward, PVA molecular chains were attracted to the surface of the SiO_2 nanoparticles through hydrogen-bonding interactions between the hydroxy groups of PVA and the amido groups of PAH. Finally, the SiO_2 nanoparticles were well-dispersed in the PVA matrix. Similiarly, a natural rubber/silica nanocomposite[439i,j] was also prepared.

Apart from the LbL self-assembly technique described, other self-assembly techniques are also used. In 2001, Walt et al.[440] reported a method for core−shell materials preparation by nanosphere−microsphere assembly. They demonstrated colloidal assembly using 100 and 200 nm diameter amine-modified PS nanospheres assembled onto 3−10 μm diameter glutaraldehyde-activated silica microspheres. The assembly process was controlled by specific chemical and biochemical interactions. The assembled composite was subsequently heated at temperatures above the T_g of the polymer nanospheres, allowing the polymer to flow over the silica microsphere surface and resulting in a uniform core−shell composite.

Recently, Mori et al.[441] developed novel intelligent colloidal polymer/silica nanocomposites, in which the complexation of cationic silica nanoparticles and a weak anionic polyelectrolyte could be manipulated simply by pH change in aqueous medium through hydrogen-bonded interaction and ionic complexation caused by hydrogen-transfer interactions between the constituents (Scheme 34). To provide an effective route for the controlled self-ordering of nanoparticles with polymers and for the achievement of characteristic stimuli-responsive properties in aqueous medium, they developed special silica nanoparticles (diameter $\sim$ 3.0 nm) that had two independent proton-accepting sites, oxygen or nitrogen atoms. Because of the tiny size and high functionality, the silica particles could be uniformly dispersed in water and behaved as single dissolved molecules to form a transparent colloidal solution. Poly(acrylic acid) was selected as a weak polyelectrolyte because the degree of ionization of carboxylic acids could be easily controlled by the pH value. In this system, both poly(acrylic acid) and the silica nanoparticles formed visually transparent solutions in water, while a white turbid dispersion was obtained just after mixing the two solutions at room temperature.

A precision-assembly methodology was described on the basis of the controlled, simultaneous assembly (CSA) of polyethylenimine onto nanoparticle silica colloids.[442] The CSA procedure involved the simultaneous addition at controlled rates of two or more fluids into a region of controlled geometry with constant mixing. The resulting dispersions were highly homogeneous, had a low viscosity and narrow particle-size distribution, and were stable colloids, even at solid concentrations of at least 33 wt %.

7. Other Preparative Methods

As mentioned in section 2.2, "grafting to" technology can be used to prepare polymer/silica nanocomposites.[443–446] Directly grafting preformed linear polymers onto a multifunctional core provides convenience in the preparation of star polymers. PDMS star polymers having a nanosized silica particle as a core were prepared by reacting silica nanoparticles with monoglycidylether-terminated PDMS (Scheme 35).[444] This star polymer was a hybrid material having an extremely high content of silica. The PDMS arms formed an organic domain to separate the silica particles and to prevent particle aggregation. The star polymers exhibited good thermal stability and high activation energy of their

Scheme 33. Schematic Illustration of the Assembly of SiO_2/PDADMAC Multilayers on PS Latexes To Form Core−Shell Particles[a]

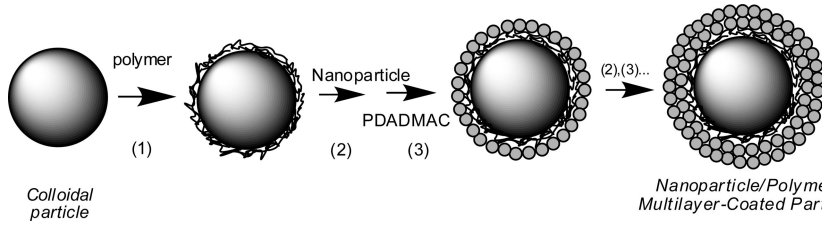

[a] The first stage involves the formation of a three-layer polyelectrolyte multilayer film (poly(diallyldimethylammonium chloride) (PDADMAC)/poly(sodium 4-styrenesulfonate) (PSS)/PDADMAC), formed by the sequential adsorption of PDADMAC and PSS under conditions where they are oppositely charged (step 1). The outermost layer, PDADMAC, positively charged, aids the subsequent adsorption of negatively charged SiO_2 nanoparticles. SiO_2/PDADMAC multilayer shells on the PS latexes are then formed by the sequential adsorption of SiO_2 (step 2) and PDADMAC (step 3). Additional SiO_2 and PDADMAC cycles result in further growth of the multilayer shell thickness on the PS latexes. The excess/unadsorbed polyelectrolyte and nanoparticles are removed by a series of centrifugation/water wash/re-dispersion cycles before additional layers are deposited. Reprinted with permission from ref 438c. Copyright 1999 American Chemical Society.

Scheme 34. Postulated Mechanism of the Reversible pH-Induced Association and Dissociation Behaviors of the Silica Nanoparticles with Poly(acrylic acid) through (a) Ionic Complexation and (b) Hydrogen-Bonded Complexation[a]

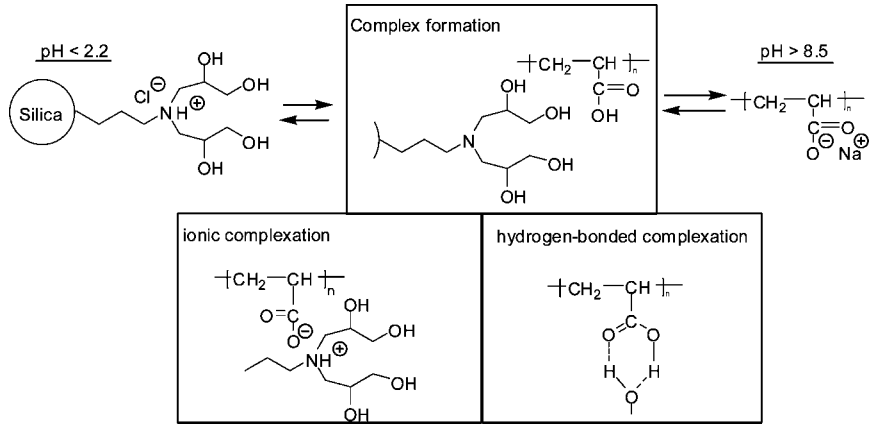

[a] Reprinted with permission from ref 441a. Copyright 2003 American Chemical Society.

Scheme 35. Preparation of PDMS Star Polymer Having a Nanosized Silica Core[a]

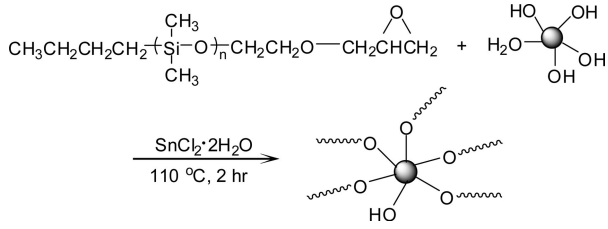

[a] Reprinted with permission from Liu, Y. L.; Li, S. H. Macromol. Rapid Commun. 2004, 25, 1392. Copyright 2004 Wiley-VCH.

degradation reaction, in comparison to the linear PDMS polymer and the PDMS/silica blending materials.

Chemical cross-linking of PEG diacrylate (PEGda) with fumed silica was reported by Spontak et al.[447a–c] The nanocomposite membranes composed of PEGda and FS nanoparticles were prepared by free-radical cross-linking in the presence of AIBN as cross-linking agent. Incorporation of nanoscale fumed silica modified with methacrylate surface groups to permit covalent coupling with the acrylate-terminated polymer chains, thereby forming tough hybrid nanocomposite membranes, was found to improve the bulk modulus without adversely affecting CO_2/H_2 selectivity or optical clarity. Similarly, cross-linked poly(propylene glycol) diacrylate (PPGda) nanocomposite membranes were also investigated.[447d]

A nanocomposite photocurable material that can act both as a photoresist and a stress redistribution layer applied on the wafer level was synthesized and studied.[448] In the experiments, 20 nm silica fillers were modified by a silane coupling agent through a hydrolysis and condensation reaction and then incorporated into the epoxy matrix. A photosensitive initiator was added into the formulation, which can release cations after ultraviolet exposure and initiate the epoxy cross-linking reaction. The photo-cross-linking reaction of the epoxy made it a negative tone photoresist.

Much work has been focused on chemical vapor deposition (CVD) polymer thin films; however, they often suffer from poor resistance to metal diffusion and undesirable dielectric anisotropy. To overcome these limitations, a nanocomposite consisting of poly(chloro-*p*-xylylene) (PPXC) and SiO_2 was developed by Senkevich and Desu[48] utilizing a near-room-temperature thermal CVD method to deposit SiO_2. The composition of the nanocomposite thin films could be varied by increasing the vaporization temperature of the SiO_2 precursor, diacetoxy-di-*tert*-butoxysilane.

Very recently, in situ coating of silica nanoparticles with acrylate-based polymers by the application of a combined vapor phase decomposition and plasma polymerization process was reported by Suffner et al.[49] In the work, silica nanoparticles were synthesized by decomposition of dimethyldiethoxysilane (Me_2-Si$(OEt)_2$) in the vapor phase and subsequently coated with plasma-polymerized MMA or ethyl-2-cyanoacrylate.

Scheme 36. Cationic Polymerization of TFOS[a]

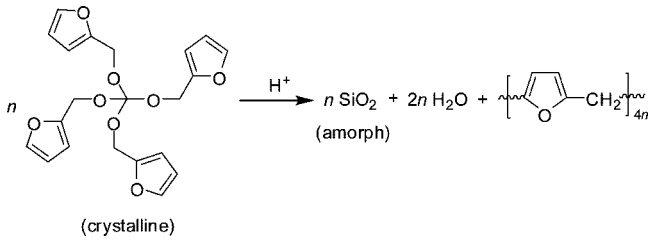

[a] Reprinted with permission from Grund, S.; Kempe, P.; Baumann, G.; Seifert, A.; Spange, S. Angew. Chem., Int. Ed. 2007, 46, 628. Copyright 2007 Wiley-VCH.

Spange et al.[50] described a new type of polymerization for the synthesis of nanocomposites in which one monomer underwent two different polymerization reactions simultaneously and on the same time scale. They demonstrated the principle of the method with the cationic polymerizations of tetrafurfuryloxysilane (TFOS). The functionality of the silane moiety of TFOS for cross-linking was four since all four furfuryloxy substituents could be cleaved hydrolytically. Since the formation of the SiO_2 network and the polymerization of furfuryl alcohol (FA) were mechanistically coupled, interpenetrating networks were formed as a polymer blend. As a result of this coupling, the two polymerization processes were synchronized. As shown in Scheme 36, the step-growth polymerization was initiated by cleavage of the Si−O−C bond.

8. Characterization and Properties

The characterization methods used in the analysis of the chemical structure, microstructure and morphology, as well as the physical properties, of the nanocomposites are varied. This section will focus on some techniques often used for the investigation of polymer/silica nanocomposites. Many of these techniques are specific for characterization of particular properties of nanocomposites, and the properties of nanocomposites are also discussed correspondingly. To fully understand structure−property relationships, several characterization techniques are often employed.

The properties of the nanocomposites strongly depend on their composition, the size of the particles, interfacial interaction, etc.[449] The interfacial interaction between polymer and silica (which depends on the preparative procedure) strongly affects the mechanical, thermal, and other properties of the nanocomposites. The internal surfaces (interfaces) are critical in determining the properties of nanofilled materials since silica nanoparticles have high surface area-to-volume ratio, particularly when the size decreases below 100 nm. This high surface area-to-volume ratio means that for the same particle loading, nanocomposites will have a much greater interfacial area than microcomposites. This interfacial area leads to a significant volume fraction of polymer surrounding the particle that is affected by the particle surface and has properties different from the bulk polymer (interaction zone). Since this interaction zone is much more extensive for nanocomposites than for microcomposites, it can have significant impact on properties.[92]

8.1. Chemical Structure

The chemical structure of polymer/silica nanocomposites is generally identified by FTIR and solid-state ^{29}Si NMR spectra. FTIR spectrometry is widely used to prove the formation of nanocomposites especially for those prepared by the sol−gel reaction, in which process a silica network can be formed. The major peak at about 1100 cm^{-1} (varying with different samples in the range of 1000−1200 cm^{-1}) that is attributed to the asymmetric stretching vibrations of Si−O−Si bonds of silica can be found in the hybrids. If the condensation reaction is not complete, Si−OH groups will also exist.

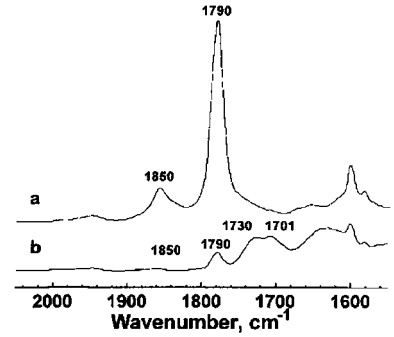

Figure 9. Magnified infrared spectra for the gel part of P(St-*co*-MAn)/SiO_2 (molar ratios of APTES over MA unit of copolymer = 1). Reprinted with permission from Zhou, W.; Dong, J. H.; Qiu, K. Y.; Wei, Y. J. Polym. Sci., Part A: Polym. Chem. 1998, 36, 1607. Copyright 1998 John Wiley & Sons, Inc.

The characteristic absorption bands of the hydrolysis product of TEOS in the PI/SiO_2 hybrids are as follows.[227] The FTIR spectrum shows absorption bands due to O−H bond stretching at 3480 cm^{-1} and Si−OH bond stretching at 882 cm^{-1}, as well as typical absorption bands for Si−O−Si network vibrations at 1130 and 823 cm^{-1}. The characteristic absorption band of Si−O−Si asymmetric stretching (1130 cm^{-1}) became stronger and moved to higher wavenumber (1180 cm^{-1}) with the addition of the coupling agent, indicating a more "condensed" silica network.

FTIR spectra can also supply evidence of the existence of hydrogen bonding or covalent bonding between organic and inorganic phases. The examples of hydrogen bonds between the polymer and the residual silanol of silica in the hybrids investigated by FTIR spectroscopy can be found in many references.[6,141,170,174,175,181] Figure 9 shows FTIR spectra of P(St-*co*-MAn) and the gels of P(St-*co*-MAn)/SiO_2.[213] New absorptions around 1730 and 1701 cm^{-1} appear, corresponding to the C═O stretching vibration in amido and carboxyl groups, respectively. This indicated the formation of amide bonds because of the aminolysis of the maleic anhydride unit of copolymer with the coupling agent APTES. It showed the existence of a covalent bond between the organic and inorganic phases due to the introduction of the coupling agent APTES in the synthesis of the hybrids.

ATR-IR spectra assess only the outmost 1−2 μm layer of the sample instead of the whole thickness of the film. It is very useful when the composite film is too thick to get a transmission IR spectrum with satisfactory resolution. Comparison of the ATR-IR and transmission IR is usually used to determine the structural difference between the surface and bulk.[200] The FTIR and ATR spectra for PAI−epoxysilane composites with 30 wt % silica were compared.[222] The intensity of the Si−O−Si peak near 1100−1000 cm^{-1} became stronger with the ATR method than with the transmittance method. This implied that abundant silica existed on the surface, and this was expected to improve the water resistance and abrasion resistance.

While FTIR results show the formation of Si−O−Si via a sol−gel reaction, ^{29}Si solid-state NMR gives further

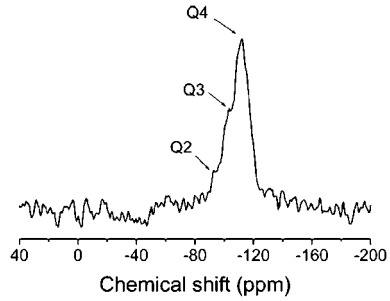

Figure 10. ^{29}Si solid-state NMR spectrum of hybrid with silica content of 11.0%. Reprinted with permission from ref 200. Copyright 2005 American Chemical Society).

information on the structure of silica and the degree of Si−OH condensation reaction. In principle high-resolution solid-state NMR spectra can provide the same type of information that is available from corresponding solution NMR spectra, but special techniques/equipment are required, including magic-angle spinning (MAS), cross polarization (CP), etc.[8b] In the ^{29}Si solid-state NMR spectra, peaks are generally denoted by the symbol Q^n to show un-, mono-, di-, tri-, and tetra-substituted siloxanes [$(RO)_{4-n}Si(OSi)_n$, R = H or an alkyl group]. For instance, a sample exhibiting a 100% Q^4 environment would possess a full condensed silica phase (i.e., corresponding to stoichiometric SiO_2). Such a deconvolution method displays only semiquantitative results but enables comparison of samples with each other in terms of the condensation state of their silicate phases. The degree of condensation within the SiO_2 particles can be evaluated from the Q^4 percent.[6,189a]

Figure 10 shows the ^{29}Si solid-state NMR spectra of the PP/silica nanocomposites prepared by sol−gel reaction with silica content of 11.0%.[200] The main peak appeared at −111 ppm adjacent with a minor peak at −101 ppm, which were Q^4 and Q^3, respectively. The strong Q^4 indicated that the degree of silicon condensation was very high. A weak peak at −92 ppm, which was assigned to Q^2, is also observed in the spectrum. The existence of Q^3 and Q^2 reflected the incomplete condensation of the TEOS.

Moreover, ^{29}Si CP MAS NMR proved to be useful for the characterization of the grafted structures formed at the silica surface. Figure 11 shows the ^{29}Si CP MAS NMR spectra of ungrafted SiO_2 and MEMO-treated silica (SIMA).[287a] The ^{29}Si CP MAS NMR spectrum of the untreated silica showed three signals at −91.2 (Q^2), −100.7 (Q^3), and −111.3 (Q^4) ppm, which are usually assigned to geminal silanols, free silanols, and siloxane groups, respectively. As expected, the grafting process reduced the intensities of the signals of geminal and free silanol groups in comparison with those of the siloxane groups. It was interesting to note that the peak assigned to geminal silanols disappeard to a greater extent than that of free silanols. For the organosilane-functionalized silica nanoparticles, two additional peaks were found at −58.8 and −66.8 ppm. The peaks observed in the range from −50 to −80 ppm proved that the silica surface was chemically modified, and they were assigned to different surface compounds. Based on peak area simulations, it was possible to determine the percentages of geminal and free residual silanol groups and to estimate their reactivities toward the functional groups of the coupling agent.

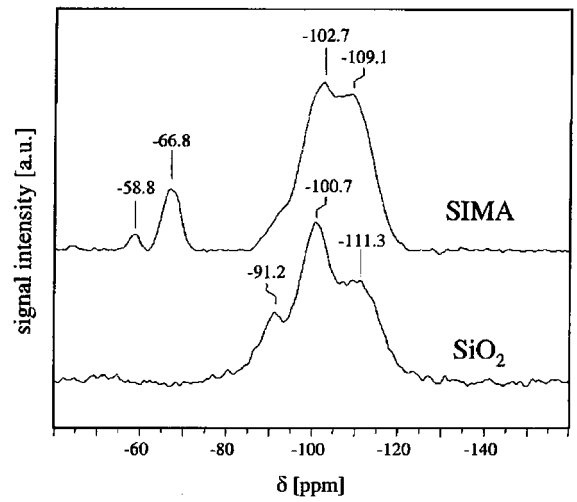

Figure 11. ^{29}Si CP MAS NMR spectra of ungrafted SiO_2 and MEMO-treated silica (SIMA). Reprinted with permission from Bauer, F.; Ernst, H.; Decker, U.; Findeisen, M.; Gläsel, H. J.; Langguth, H.; Hartmann, E.; Mehnert, R.; Peuker, C. Macromol. Chem. Phys. 2000, 201, 2654. Copyright 2000 Wiley-VCH.

8.2. Microstructure and Morphology

Crystallization behaviors of the silica nanoparticle-filled composites are usually studied by DSC. For the silica nanoparticle-filled PEN composites,[62] crystallization peaks were shifted to higher temperatures, and the overall crystallization time, which indicated the time to crystallize during nonisothermal crystallization process, was reduced by the silica content. The degree of crystallinity of the composites was increased with the silica content at a given cooling rate during the nonisothermal crystallization process, as listed in Table 6. These results could be explained by the supercooling temperature. In the research, fumed silica nanoparticles acted as nucleation agents in the PEN matrix under nonisothermal crystallization conditions, and the crystallization peak temperatures were shifted to higher temperatures, which indicated that the supercooling of the composites at a given cooling rate was reduced by the silica content. When the polymer crystallized with less supercooling, it crystallized more perfectly than with more supercooling; hence, the degree of crystallinity of silica nanoparticle-filled PEN composites was increased by the silica content at a given cooling rate.

The crystallization behavior of PP/silica nanocomposites prepared in situ via solid-state modification and sol−gel reaction was also investigated with DSC.[225b] Results showed that silica nanoparticles formed in situ acted as nucleating agents. The nonisothermal crystallization kinetics of the nanocomposites was studied using a combined Avrami−Ozawa approach and showed a two-stage crystallization process: the primary stage was characterized by nucleation and spherulitic growth, and the secondary stage was characteristic of the perfecting of crystals. Silica increased the rate of the primary stage, resulting in a more narrow lamellar thickness distribution. The crystallization activation energy decreased with increasing silica content in the PP/silica nanocomposites. The nucleating efficiency of the in situ prepared silica particles was found to be 20% in the low concentration range and was higher compared with silica nanoparticles as well as other nanofillers studied. The melting behavior indicated the formation of more perfect crystals with a narrow lamellar thickness distribution.

Table 6. DSC Data for PEN and Silica Nanoparticle-Filled PEN Composites at a Cooling Rate of 10 °C/min[a]

		T_c[b]		T_m				
sample	T_g (°C)	peak (°C)	ΔH_c (J/g)	peak (°C)	ΔH_f (J/g)	T_c[c] (°C)	ΔT (°C)	X_c[d] (%)
PEN, pure	119.2	181.9	17.2	266.0	40.3	212.8	53.2	22.3
PEN/silica 0.3%	119.7	177.4	15.1	266.9	40.2	214.5	52.4	24.2
PEN/silica 0.5%	119.5	177.9	17.2	266.7	44.7	216.4	50.3	26.5
PEN/silica 0.7%	119.3	175.1	13.5	266.5	44.1	219.9	46.6	29.4
PEN/silica 0.9%	119.5	172.0	8.4	266.5	46.5	221.8	44.7	36.8

[a] Adapted with permission from Kim, S. H.; Ahn, S. H.; Hirai, T. Polymer 2003, 44, 5625. Copyright 2003 Elsevier Ltd. [b] The crystallization temperature measured on the second heating at 10 °C/min. [c] The crystallization temperature measured on the second cooling at 10 °C/min. [d] The degree of crystallinity.

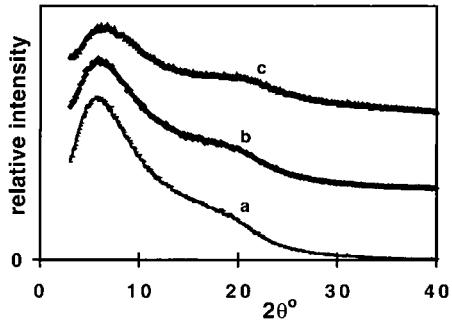

Figure 12. WAXD diffractograms of PU/silica nanocomposites with (a) 0%, (b) 10%, and (c) 30% nanosilica. Reprinted with permission from Petrović, Z. S.; Javni, I.; Waddon, A.; Bánhegyi, G. J. Appl. Polym. Sci. 2000, 76, 133. Copyright 2000 John Wiley & Sons, Inc.

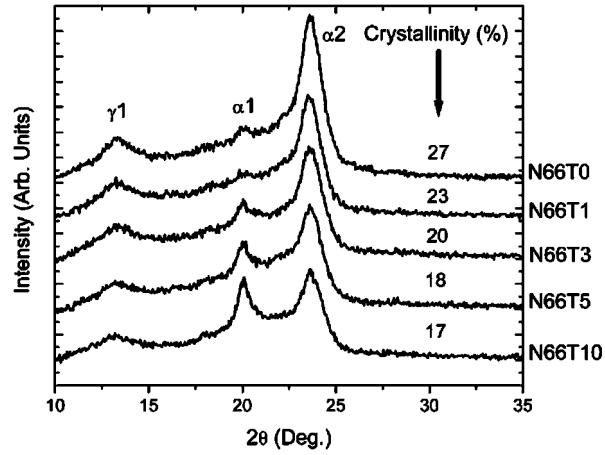

Figure 13. WAXS scans of the unannealed films as a function of TEOS loading (N66T0, N66T1, N66T3, N66T5, and N66T10 represent nanocomposites resulting from 0%, 1%, 3%, 5%, and 10% TEOS relative to PA 66, respectively). Reprinted with permission from Sengupta, R.; Bandyopadhyay, A.; Sabharwal, S.; Chaki, T. K.; Bhowmick, A. K. Polymer 2005, 46, 3343. Copyright 2005 Elsevier Ltd.

The microscopic structure of polymers is often studied by X-ray techniques (including WAXD/XRD, WAXS, and SAXS) and neutron scattering. The XRD technique is based on the elastic scattering of X-rays from structures that have long-range order, and it is an efficient analytical technique used to identify and characterize crystalline materials. For the nonlayered silica nanoparticle composites, WAXD was commonly performed to analyze the degree of crystallinity of the nanocomposites. The WAXD of nanocomposites of PU/silica showed a lower angle peak, at about $2\theta = 6°$, and most showed a distinct shoulder at $2\theta = 20°$.[277a] Figure 12 displays the diffractograms of the samples with 0%, 10%, and 30% nanosilica. In samples with 20% and 50% filler, the shoulder was less obvious but evident nonetheless. It is considered that these broad peaks came from the PU matrix. Clearly, the nanosilica did not display any crystalline peaks, which was consistent with the silica nanoparticles being noncrystalline at that size scale.

The crystallization behavior of PP/silica nanocomposites prepared via solid-state modification and sol−gel reaction was investigated.[225b] The WAXD patterns showed that silica nanoparticles induced the formation of crystals with the β-modification in PP at high silica content (ca. 5 wt %).

Scattering is a powerful tool to access the bulk structure in a nondestructive way. X-ray scattering is well-suited for many polymer/inorganic composites. WAXS, a technique that involves measuring scattering intensity at scattering angles 2θ larger than 5°, has been used to investigate the changes in crystalline structure. Figure 13 shows the WAXS scans of PA 66/silica nanocomposite samples.[173] On subsequent addition of TEOS, the α2 peak decreased in intensity and the α1 peak intensity slowly increased as evident from Figure 13. The decrease in the α2 peak intensity implied loss of hydrogen bonding between C═O and N−H groups, and this might be due to the interference of the silanol groups, which increased quantitatively with increase in TEOS loading from 0 to 10 wt % as mentioned in the IR discussion. The percent crystallinity from WAXS is mentioned in Figure 13 against the sample curves. This decreased with increase in TEOS loading. On addition of 1% TEOS, the drop in crystallinity was ∼15% from the neat polymer. The maximum drop in crystallinity occurred for N66T10 where the crystallinity was 37% less than that in N66T0. The decrease in crystallinity was probably due to the decrease in hydrogen bonding between the CaO and N−H groups situated on neighboring chains due to in situ generation of nanosized silica as mentioned previously.

Macromolecular scale structure has been widely studied by SAXS, which is a small-angle scattering technique where the source for the elastic scattering of the X-rays is the inhomogeneities in the sample. SAXS patterns are recorded at very low angles (typically <3−5°). In this angular range, information about the shape and size of the inhomogeneities is obtained.[8b] The scattering methods can also give geometrical descriptions of the structures using the concept of fractal geometry because random processes of polymerization or aggregation usually result in formation of fractal objects. The fractal structure has a mass fractal dimension, D_m, which can be experimentally determined by the scattering methods. D_m is a measure of the compactness of the mass fractal object and describes volume distribution of a mass, m, as $m \approx r^{D_m}$, where r is the radius of the fractal object and the relation $1 < D_m < 3$ holds for the mass fractal. The evolution of heterogeneous structure during polymerization in the epoxy/silica hybrid was followed by SAXS using a position-sensitive detector.[239b] The hybrid was composed of an

epoxide−amine system and the silica formed by the sol−gel process from TEOS. Silica structure evolution was determined by catalytic conditions and the method of preparation, one- or two-stage process. The one-stage polymerization was base-catalyzed by an amine used as a cross-linker of the epoxide. The reaction resulted in formation of large overlapping polysiloxane clusters from the very beginning of the reaction. During polymerization more branched domains gradually appearred within the structure. The polymer showed a compact structure with fractal dimension increasing during the polymerization to $D_m = 2.5$. The two-stage procedure consisting of acid prehydrolysis of TEOS and basic catalysis in the *m* second step led to an acceleration of gelation. Primary particles were formed in the first step followed by aggregation into clusters in the second step. The inner structure of the clusters described by a fractal dimension did not change during the polymerization. The diffusion-limited cluster−cluster reaction might be responsible for a more open structure with a fractal dimension $D_m = 1.7$.

Neutron scattering is preferred sometimes due to the extended *q*-range (with respect to standard X-ray laboratory sources), giving access to length scales between several and several thousand angstroms. Also, cold neutrons penetrate macroscopically thick samples more easily, and they offer the potential to extract the conformation of polymer chains inside the composite. SANS is therefore a method to unveil the structure of nanocomposites.[153e] Oberdisse et al.[153a] have analyzed the structure of the resulting filled latex films by means of this method. The scattered intensity varied enormously with the physicochemical parameters, indicating considerable structural modifications. To rationalize these results, they presented a unified description of the data that successfully accounted for the main characteristics of the scattered intensity: the form factor of beads at large *q* vectors, the position of the intra- and interaggregate structure factor peaks, the small-*q* upturn observed in some cases, and the overall intensity in absolute units. This allowed quantification of the degree of aggregation of the silica in the matrix. It was found that the latter can be varied in a systematic manner by changing pH, silica volume fraction, and quantity of added salt.

Montes et al.[284d] found by SANS that there were two opposite effects that control the final dispersion state of the filled elastomers that composed cross-linked polyethylacrylate chains reinforced with grafted silica nanoparticles during the polymerization. The first one was a depletion mechanism favoring the formation of aggregates. The second one was a repulsive steric interaction due to the growth of polymer chains from the particle surfaces avoiding contacts between the silica inclusions. Using these results, they could prepare sets of samples having the same particle/matrix interface but different dispersions states.

Carrot et al.[312b] described ATRP from silica nanoparticles and the dispersion of particles was checked using SANS at every stage of the functionalization. SANS measurements made on the polymer-grafted particles led to an understanding of the system behavior during the polymerization procedure. These observations permitted improvement of the synthetic conditions to get a better dispersion of the particles and a better control of the polymerization process. The SANS technique was well suited for the size range of interest, and due to the unique possibility of contrast variation, it was able to highlight independently the contributions of the polymer layer and of the silica beads or aggregates.

The ^{1}H NMR technique allows measurement of the total topological constraint density (such as entanglements or cross-links) in polymeric systems. By comparing the transverse magnetization relaxation of reinforced and nonreinforced matrices, one can estimate the topological constraints density at the particle/matrix interface. The cross-linking density at the filler−elastomer interface of model reinforced elastomers composed of grafted nanosilica particles and cross-linked ethylacrylate chains was analyzed by ^{1}H NMR measurements.[284c] Measurements performed at high temperature ($T > T_g + 120$ K) revealed that the relaxation of the bulk polymer matrix was affected by the topological constraints existing at the particle surface. It was deduced that the effect of particles in the bulk matrix could be interpreted as that of a homogeneous additional constraint density, which increased proportionally to the surface area introduced in the matrix.

In order to probe the nature of the molecular interactions between the polymer and silica phases, colloidal P4VP/silica and PS/silica nanocomposite particles comprising 38% and 48% silica by mass, respectively, were characterized by solid-state NMR spectroscopy.[385d] For P4VP/silica nanocomposite particles, the results indicated hydrogen bond formation between the pyridine nitrogen and a surface hydroxyl proton. In contrast, a π-interaction between the aromatic ring and the silica surface was the most likely model for the PS/silica nanocomposite particles. Nonspecific binding interactions did not appear to play an important role in nanocomposite particle formation in either case.

Gas transport in polymers is known to be strongly dependent on the amount of free volume in the polymer matrix. Positron annihilation lifetime spectroscopy (PALS) is a technique that probes the free volume cavities by measuring the lifetime of *ortho*-positronium (*o*-Ps) before annihilation in the free volume regions of the polymer. The lifetime of *o*-Ps (normally 2−5 ns) is a direct measure of the free volume size. The free volume sizes and interstitial mesopore sizes in PTMSP/silica nanocomposites and the correlation between nitrogen permeability and cavity sizes were studied by PALS at filler concentrations between 0 and 50 wt %.[126a] A bimodal free volume distribution was observed for PTMSP, and the size of the larger free volume cavities was significantly increased upon addition of hydrophobic fumed silica. Nanometer-sized interstitial cavities in filler agglomerates were observed in all PTMSP/fumed silica nanocomposites and in neat hydrophobic fumed silica. The radius of these interstitial mesopores in the nanocomposites decreased with decreasing filler concentration. A strong correlation between nitrogen permeability and the volume of the interstitial mesopores in the nanocomposite membranes was observed. Figure 14 shows the radius of the large polymer free volume cavities in PTMSP/SiO_2 nanocomposites as a function of filler content. The free volume cavity size increased significantly and systematically from 0.53 nm in unfilled PTMSP to 0.58 nm in PTMSP/SiO_2 nanocomposites with 50% SiO_2.

^{129}Xe NMR spectroscopy was also used to investigate the enhancement of free volume in nanosilica-filled PTMSP. Because of its high polarizability, the xenon atom is particularly sensitive to the density of its microenvironment. This attribute, combined with its small molecular size (4.4 Å atomic diameter), spherical symmetry, and chemical inertness, makes xenon an ideal probe of microstructure. In general, the chemical shift of ^{129}Xe gas sorbed in a solid is

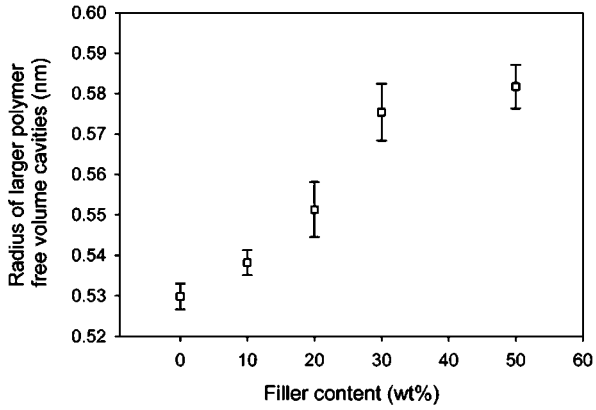

Figure 14. Large free volume cavity radius in PTMSP/hydrophobic fumed silica nanocomposite membranes at room temperature as a function of silica content. Reprinted with permission from ref 126a. Copyright 2005 American Chemical Society).

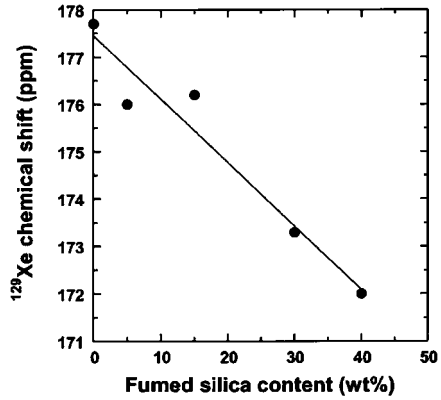

Figure 15. ^{129}Xe NMR chemical shift for PTMSP nanocomposite films as a function of fumed silica content. NMR measurements were conducted at 25 °C and 120 psig xenon. Reprinted with permission from ref 125a. Copyright 2003 American Chemical Society).

proportional to its collision rate within the free volume environment in the material. The ^{129}Xe NMR chemical shift decreased regularly with increasing fumed silica concentration, consistent with an increase in the average size of free volume elements or cavities through which molecular transport can occur. A relationship between the chemical shift and gas permeability in the filled polymer was reported.[125a] Figure 15 plots the observed chemical shift as a function of filler content in the polymer. A significant negative correlation was observed to exist between these two variables over the fumed silica concentration range of 0−40 wt %, indicating that free volume in the PTMSP nanocomposites increased as more and more silica is added.

TEM, SEM, and AFM are three powerful microscopy techniques to observe the morphology of nanocomposites. TEM is a microscopy technique whereby a beam of electrons is transmitted through an ultrathin specimen and carries information about the inner structure of the specimen. It is difficult to receive details of some samples due to low contrast resulting from weak interaction with the electrons; this can partially be overcome by the use of stains such as phosphotungstic acid and RuO_4. Sometimes the organic components of the sample would be decomposed by the electron beam; this can be avoided using cryogenic microscopy (cryo-TEM), where the specimen is measured at liquid nitrogen or liquid helium temperatures in a frozen state. High-

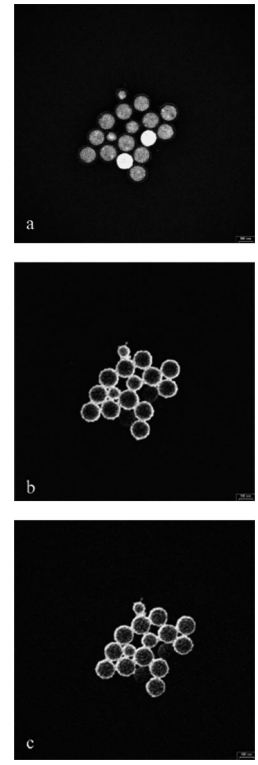

Figure 16. Elemental distribution maps obtained for carbon (a), silicon (b), and oxygen (c) from the PS/silica nanocomposite particles (scale bar = 100 nm). Reprinted with permission from ref 385e. Copyright 2005 American Chemical Society.

resolution TEM (HRTEM) can afford a much closer look at the samples.[8b]

The recent application of electron energy loss spectroscopy imaging techniques to TEM (ESI-TEM) can provide information on the composition of polymer surfaces. This is a powerful technique for the characterization of colloidal nanocomposite particles. The internal nanomorphologies of two types of vinyl polymer/silica (P4VP/silica and PS/silica) colloidal nanocomposites were assessed using ESI.[385e] This technique enables the spatial location and concentration of the ultrafine silica sol within the nanocomposite particles to be determined. The ESI data confirmed that the ultrafine silica sol was distributed uniformly throughout the P4VP/silica nanocomposite particles, which was consistent with the "currant-bun" morphology previously used to describe this system. In contrast, the PS/silica particles had pronounced "core−shell" morphology, with the silica sol forming a well-defined monolayer surrounding the nanocomposite cores. Specific elemental information can be obtained from Figure 16. In the carbon map, most of the particles have a uniform gray appearance with a diffuse halo. However, bright halos with darker particle interiors are observed in the silicon and oxygen maps. These images were consistent with a "core−shell" type particle morphology. Thus these ESI results provided direct verification of the two types of nanocomposite morphologies that were previously only inferred on the basis of XPS and aqueous electrophoresis studies. Moreover, ESI also allowed the unambiguous identification of a minor population of PS/silica nanocomposite particles that were not encapsulated by silica shells.

SAXS in combination TEM is a useful method to characterize the morphology of hybrid organic−inorganic materials. Combined TEM and SAXS investigations on thermoplastic nanocomposites poly(MMA-*co*-HEMA) co-

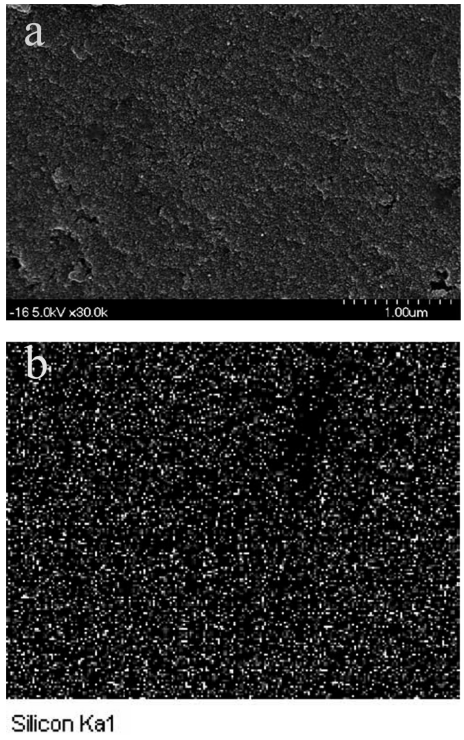

Figure 17. (a) SEM and (b) EDX-Si mapping microphotographs of a PMMA−silica nanocomposite film containing 50 wt % silica. Reprinted with permission from Liu, Y. L.; Hsu, C. Y.; Hsu, K. Y. Polymer 2005, 46, 1851. Copyright 2005 Elsevier Ltd).

polymer filled with 10 nm SiO_2 particles with different particle surface coatings have been shown to be important tools in gaining complete information about the morphology of the materials.[262] TEM analysis gave visible information on the extent of particle separation in the nanocomposites depending on the surface modification over a broad scale range including especially large sized aggregates. On the other hand, SAXS analysis enabled acquistion of more detailed information about size distributions of primary particles and "mean" size aggregates in the real nanosize range below 20 nm.

The scanning electron microscope (SEM) is a type of electron microscope that creates images by the electrons emitted when the primary electrons coming from the source strike the surface and are inelastically scattered by atoms in the sample. SEM images have a characteristic 3-D appearance and are therefore useful for judging the surface structure of the sample.[8b]

Besides the emitted electrons, X-rays are also produced by the interaction of electrons with the sample. These can be detected in a SEM equipped for energy-dispersive X-ray (EDX) spectroscopy.[8b] Figure 17 shows the SEM and EDX Si-mapping photography of a PMMA/silica nanocomposite film containing 50 wt % silica.[69b] From the SEM photography, aggregation of silica was not observed. The fracture surface was very dense. Both the SEM and EDX Si-mapping results indicated the homogeneous dispersion of the silica in the polymer matrix.

AFM is an effective tool to characterize nanocomposites by providing the morphological information. The AFM consists of a sharp tip (10−20 nm diameter) attached to a stiff cantilever. The tip is brought close to the surface, and the sample is scanned beneath the tip. The tip moves in response to tip−surface interactions, and this movement is measured by focusing a laser beam onto the back of the cantilever and detecting the position of the reflected beam with a photodiode. Different modes of operation can be used.[8b] A detailed investigation on the modified nanoparticles in the absence and presence of a PP matrix was carried out by AFM.[71c] The results indicated that the loosened agglomerates of the untreated SiO_2 became more compact due to the linkage between the nanoparticles offered by the grafting polymer. In addition, the molecules of the PP matrix were able to diffuse into the modified nanoparticle agglomerates during the melt processing. Entanglement between the molecules of the grafting polymer and the matrix was thus available, which in turn facilitated a strong particle−matrix interfacial interaction.

8.3. Mechanical Properties

Since one of the primary reasons for adding inorganic fillers to polymers is to improve their mechanical performance,[4a] the mechanical properties of polymer nanocomposites are most concerned.[15c,450] It is well-known that one of the major requirements of polymer nanocomposites is to optimize the balance between the strength/stiffness and the toughness as much as possible.[143] Therefore, it is usually necessary to characterize the mechanical properties of nanocomposites from different viewpoints. Several criteria, including tensile strength, impact strength, flexural strength, hardness, fracture toughness, and so forth, have been used to evaluate the nanocomposites.

8.3.1. Tensile, Impact, and Flexural Properties

Tensile test is the most widely used method to evaluate the mechanical properties of the resultant nanocomposites, and accordingly Young's modulus, tensile strength, and the elongation at break are three main parameters obtained. These vary with the silica content, but the variation trends are different. Furthermore, impact test is also widely used for the mechanical properties characterization.

Table 7 gives the mechanical properties of PP nanocomposites filled with SiO_2 particles grafted with various polymers at a fixed SiO_2 fraction.[71b] Although the monomers of the grafting polymers should have different miscibilities with PP, all the grafting polymers except PEA exhibited a reinforcement effect on the tensile strength of the nanocomposites. These results contributed to a further understanding of the modified nanoparticles and their role in the composites. That is, interdiffusion and entanglement of the grafting polymer segments with the PP molecules, instead of a miscibility between the grafting polymer and the matrix, dominated the interfacial interaction in the nanocomposites. This led to the conclusion that a PP matrix with a higher molecular weight should be entangled more effectively with the nanoparticle agglomerates, thus leading to a higher tensile strength increment. Typical tensile stress−strain curves of neat PP and its filled version are shown in Figure 18, indicating that both a reinforcing and a toughening effect of the nanoparticles on the polymeric matrix were fully brought into play.

iPP/SiO_2 nanocomposites with untreated and surface-treated silica nanoparticles were prepared by melt compounding.[80a] A small improvement in mechanical properties such as tensile and impact strength as well as elongation at break was observed after nanoparticle addition. A maximum in mechanical properties appeared at a silica content of 2.5 wt % in both surface treated and untreated

Table 7. Mechanical Properties of PP (Melting Flow Index = 8.5 g/10 min) Based Nanocomposites (Content of SiO_2 = 3.31 vol %) Filled with Different Polymer-Grafted SiO_2[a,b]

	nanocomposites						
grafting polymers	PS	PBA	PVA	PEA	PMMA	PMA	neat PP
tensile strength (MPa)	34.1	33.3	33.0	26.8	35.2	33.9	32.0
Young's modulus (GPa)	0.92	0.86	0.81	0.88	0.89	0.85	0.75
elongation-to-break (%)	9.3	12.6	11.0	4.6	12.0	11.9	11.7
area under tensile stress−strain curve (MPa)	2.4	3.3	2.3	0.8	3.2	2.9	2.2
unnotched Charpy impact strength (KJ/m^2)	19.8	19.4	22.9	14.6	20.5	4.7	8.0

[a] Adapted with permission from Rong, M. Z.; Zhang, M. Q.; Zheng, Y. X.; Zeng, H. M.; Walter, R.; Friedrich, K. Polymer 2001, 42, 167. Copyright 2001 Elsevier Science Ltd. [b] Irradiation dose =10 Mrad; weight ratio of monomer/SiO_2 = 20/100; all the systems used acetone as solvent when they were irradiated, except for methyl acrylic acid/SiO_2 system with ethanol as solvent.

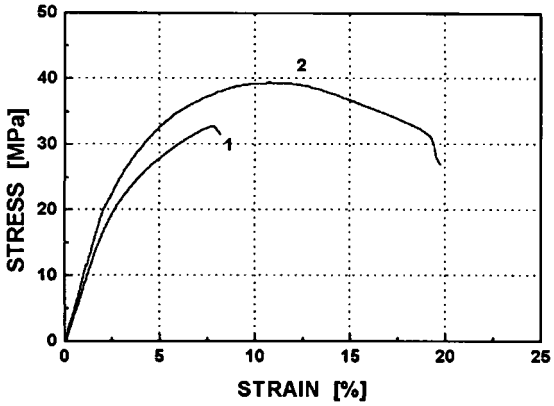

Figure 18. Typical tensile stress−strain curves of (1) the neat PP matrix resin (melting flow index = 6.7 g/10 min) and (2) the one filled with SiO_2-*g*-PS (content of SiO_2 = 1.96 vol %). Reprinted with permission from Rong, M. Z.; Zhang, M. Q.; Zheng, Y. X.; Zeng, H. M.; Walter, R.; Friedrich, K. Polymer 2001, 42, 167. Copyright 2001 Elsevier Science Ltd.

SiO_2 nanoparticles. A nanoparticle content higher than 2.5 wt % in the polymer matrix resulted in decreased mechanical properties. This was attributed to the increased tendency of SiO_2 nanoparticles to form agglomerates at higher concentrations. However, it was found that surface-treated nanoparticles produced larger aggregates than did those derived from untreated nanoparticles, despite the increased adhesion of the iPP matrix.

Silica nanoparticle-filled PEN composites were melt-blended to improve the mechanical properties of PEN.[62] However, the mechanical properties of the unmodified silica nanoparticle-reinforced composites tended to be worse than those of pristine PEN. A major problem of such materials was the nonuniformity of the resulting properties attributed to the poor dispersion of the filler in the polymer matrix, and no adhesion occurring at the polymer−filler interface. The mechanical properties of stearic acid-modified silica nanoparticle-reinforced PEN composites were further investigated.[73] The tensile moduli of the composites reinforced with unmodified silica nanoparticles increased with increasing silica content, whereas the tensile strength and elongation decreased. However, the stearic acid-modified silica nanoparticle-reinforced PEN composites exhibited increased elongation and decreased tensile moduli with increasing content because stearic acid, which adsorbed onto the surface of the silica nanoparticles in layers thicker than a monolayer, acted as a plasticizer during the melt-compounding stage.

The influence of the silica content on the mechanical properties of the PI/SiO_2 hybrids prepared by the sol−gel process is shown in Figure 19.[227] From Figure 19a, it can be observed that the Young's moduli (E) of the hybrid films

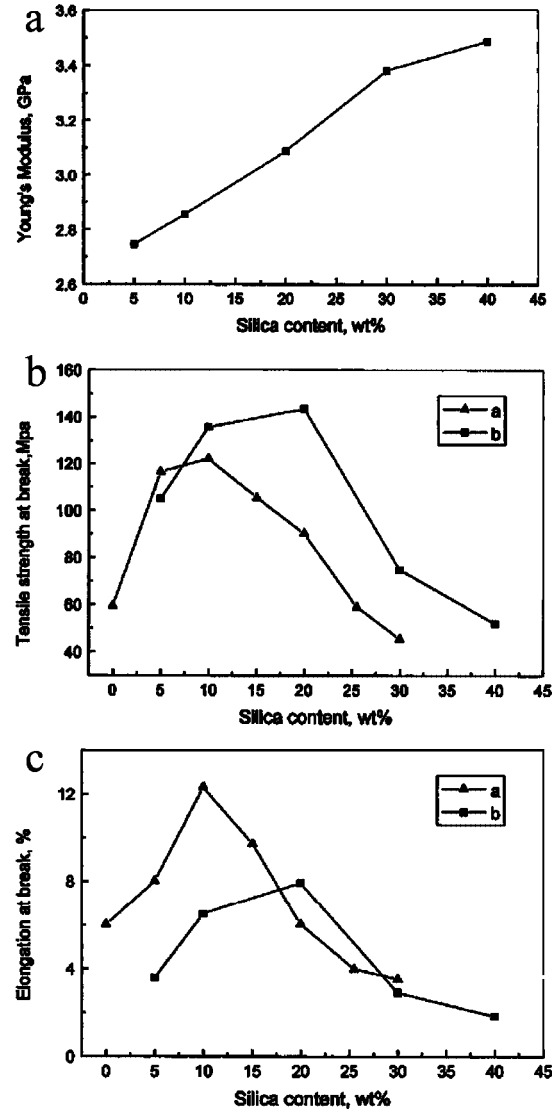

Figure 19. (a) Correlation between Young's modulus of the PI/SiO_2 hybrids and silica content (with GOTMS/TEOS = 0.10), (b) effect of coupling agent on the tensile strength at break of the PI/SiO_2 films (▲, without coupling agent; ■, with GOTMS/TEOS = 0.10), and (c) effect of coupling agent on the elongation at break of the PI/SiO_2 films (▲, without coupling agent; ■, with GOTMS/TEOS = 0.10). Reprinted with permission from ref 227. Copyright 2002 American Chemical Society.

increased linearly with the silica content. It can be seen in Figure 19b,c that when the silica content was less than 20 wt %, both the tensile strength (σ_b) and the elongation at break (ε_b) increased with increasing silica content. When the silica content exceeded 20 wt %, both the tensile strength and the elongation at break decreased. These phenomena

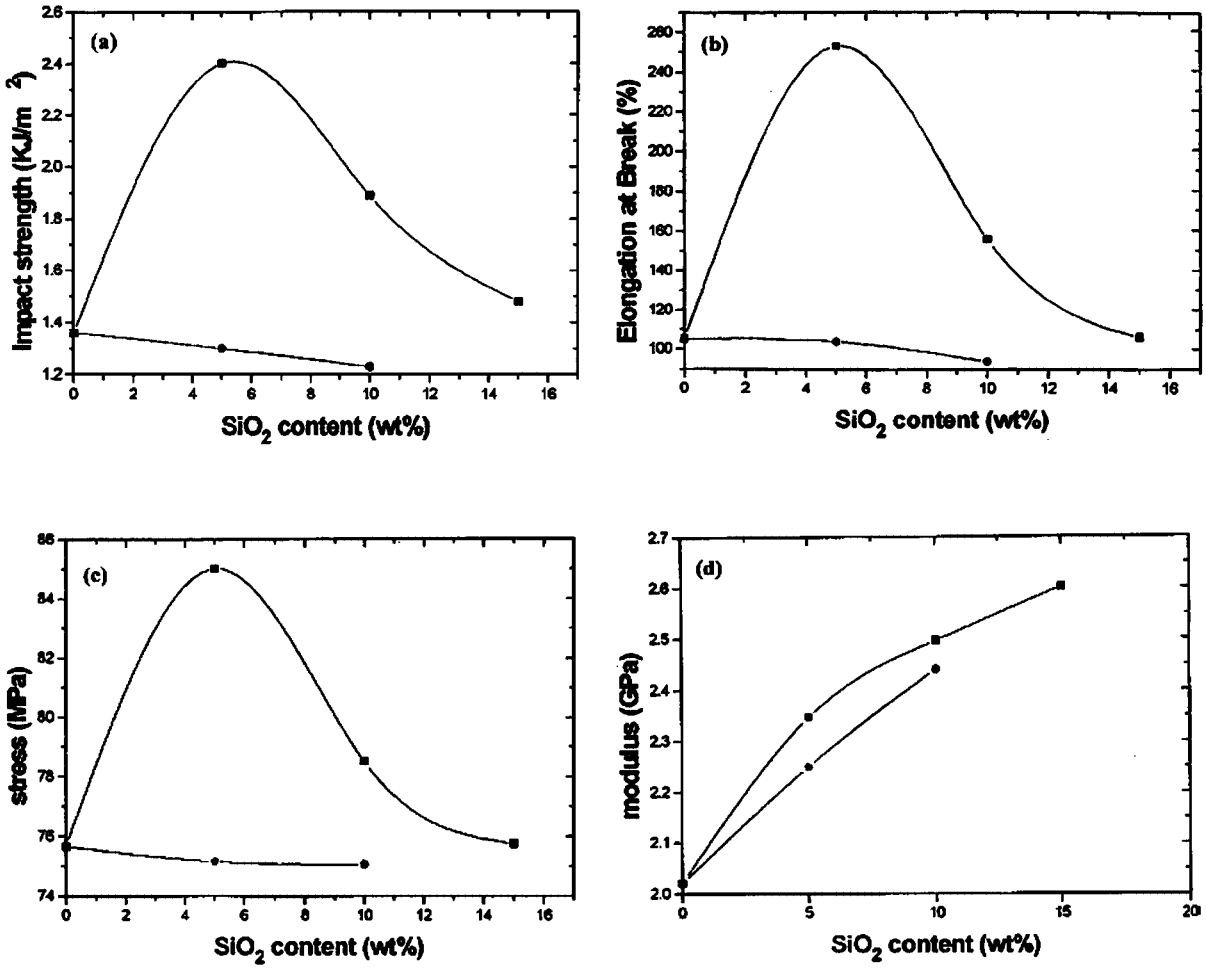

Figure 20. (a) Impact strength, (b) elongation at break, (c) tensile strength, and (d) modulus versus silica content for (●) unmodified and (■) modified silica-filled PA 6 nanocomposites. Reprinted with permission from Yang, F.; Ou, Y. C.; Yu, Z. Z. J. Appl. Polym. Sci. 1998, 69, 355. Copyright 1998 John Wiley & Sons, Inc.

might be distinctive features of a nanocomposite. However, this critical point was only 10 wt % for PI/SiO_2 hybrids without a coupling agent. Most of the moduli and tensile strengths were higher in the hybrids containing a coupling agent than in their counterparts without a coupling agent. This effect could be attributed to the improved interaction between the PI matrix and the silica resulting from the reduced size of the SiO_2 particles and to the chemical bonds introduced by the coupling agent. In contrast, the elongations at break (ε_b) of the hybrids decreased dramatically with the addition of coupling agent. This could be explained by an increased cross-linking density resulting from the reduced particle size. Similar mechanical behavior was observed in other PI/SiO_2 hybrids prepared by the sol−gel process.[192,217]

As shown in Figure 20, mechanical properties such as impact strength, tensile strength, and elongation at break of the PA 6/modified silica nanocomposites prepared by in situ polymerization also show a tendency to increase and then decrease with increasing silica content and have maximum values at 5% silica content, whereas those of the PA 6/unmodified silica system decrease gradually.[249a] The composites containing the modified silicas had good dispersion and interfacial adhesion, so when under tensile stress, the force was transferred to silica particles through the interphase and the silica particles became the receptor of the tensile force. When the tensile stress added on the composites was beyond a critical value, the damage to the composite resulted from the destruction of the interphase between PA 6 and the silica. Due to the different degree of interfacial adhesion, the modified and unmodified silicas showed different effects on the toughness of PA 6. The unique mechanical behavior of a silica-modified nanocomposite was mainly due to the agglomeration of silica particles for silica content above 5 wt %. The deterioration of the toughness of unmodified composites appeared to be related mainly to the bad interfacial adhesion between unmodified silica and nylon 6, which led to many defects and flaws in the interphase and, consequently, made the damage to the composites easier. In addition, the addition of silica particles improved the modulus of the resulting composites whether the silicas were modified or not. Based on the relationship between impact strength of the nanocomposites and the matrix ligament thickness τ, a criterion was proposed to explain the unique mechanical properties of nylon 6/silica nanocomposites.[249b]

In comparison with tensile and impact properties, there are very few reports concerning the flexural properties of the nanocomposites. Liu and Kontopoulou[114] compared the flexural properties of the unfilled thermoplastic olefin (TPO) with those of composites containing SiO_2 and modified nanosilica ($mSiO_2$) prepared by melt mixing, as shown in Table 8. Both nanosilica filled samples had higher flexural modulus and flexural stress than the unfilled TPO, which provided clear evidence of the reinforcing effect that the filler exerted on the PP matrix. The differences between untreated SiO_2 and surface-treated $mSiO_2$ were marginal.

Table 8. Flexural Properties of TPO/Nanosilica Composites[a,b]

sample	flexural modulus (MPa)	flexural stress[c] (MPa)
TPO	797 ± 24	25.5 ± 0.5
TPO−5 wt % SiO_2	920 ± 39	28.4 ± 1.3
TPO−5 wt % $mSiO_2$[d]	942 ± 64	28.7 ± 1.6

[a] Adapted with permission from Liu, Y. Q.; Kontopoulou, M. Polymer 2006, 47, 7731. Copyright 2006 Elsevier Ltd. [b] TPO composition (PP/PP-*g*-MAn)/POE 80/20, (POE, polyolefin elastomer). [c] Measured at 5% strain. [d] Trimethoxyoctylsilane-modified nanosilica.

Table 9. Flexural Strength and Modulus of Phenolic Resin/SiO_2 Hybrid Systems with Different TEOS Content[a]

Systems	flexural strength (MPa)	flexural modulus (MPa × 10^2)
neat phenolic resin	27.81 ± 0.62	19.60 ± 0.48
unmodified hybrid composite	36.06 ± 1.96	40.49 ± 2.13
modified hybrid nanocomposite	41.90 ± 0.92	37.98 ± 2.47

[a] Adapted with permission from Chiang, C. L.; Ma, C. C. M.; Wu, D. L.; Kuan H. C. J. Polym. Sci., Part A: Polym. Chem. 2003, 41, 905. Copyright 2003 Wiley Periodicals, Inc.

The mechanical properties of the hybrid phenolic/SiO_2 nanocomposites prepared by the sol−gel method were examined by measuring the flexural mechanical properties.[212a] Table 9 demonstrates the flexural strength and modulus of neat phenolic resin and hybrid phenolic composites. The sizes of silica particles and the compatibility between the organic and the inorganic phases improved the flexural mechanical properties of hybrid phenolic composites. The flexural strength and modulus of the hybrid phenolic nanocomposites were 50% and 100% higher than those of neat phenolic resin, respectively. The coupling agent, GPTS, reduced the serious phase separation from macrophase to microphase. Accordingly, the results concerning flexural mechanical properties revealed that phenolic nanocomposites containing fine silica particles (GPTS content 10 phr) had excellent mechanical properties, and incorporating silica inorganic ingredients into the novolac-type phenolic resin enhanced the mechanical properties of the hybrid phenolic composites.

8.3.2. Hardness

Hardness refers to the properties of a material resistant to various kinds of shape change when force is applied. It is fundamental for many applications and is an important mechanical parameter of materials. There are three principal types of hardness: scratch hardness (resistance to fracture or plastic deformation due to friction from a sharp object), indentation hardness (resistance to plastic deformation due to impact from a sharp object), and rebound hardness (height of the bounce of an object dropped on the material), and there are several different definitions of hardness, Brinell hardness, Knoop hardness, Vickers hardness, Shore hardness, etc.

The pencil hardness test is perhaps the simplest form of hardness test. A set of pencils for hardness test ranging from softest to hardest are as follows: 6B, 5B, 4B, 3B, 2B, B, HB, H, 2H, 3H, 4H, 5H, 6H, 7H, 8H, 9H. The hardness of the hybrid thin films prepared from acrylic polymer and aqueous monodispersed colloidal silica was measured by a pencil test.[265b] The hardness of the acrylic polymer film is HB and 3H for the cases of thin film and thick film, respectively. It increased to 5H (for the thin film case) or 9H (for the thick film case) with increasing the silica content for the hybrid materials. This suggested that hardness was enhanced by incorporating the silica moiety in the acrylic polymers.

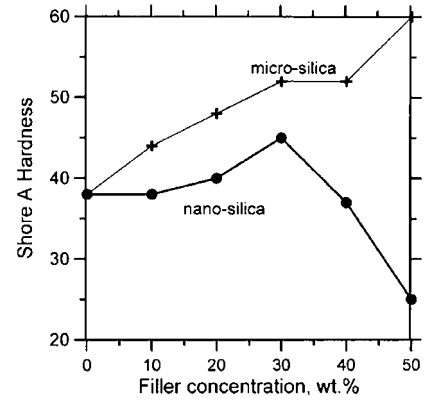

Figure 21. Shore hardness of nano- and microcomposites. Reprinted with permission from Petrović, Z. S.; Javni, I.; Waddon, A.; Bánhegyi, G. J. Appl. Polym. Sci. 2000, 76, 133. Copyright 2000 John Wiley & Sons, Inc.

The Shore A hardness is the relative hardness of elastic materials such as PU or soft plastics, and it can be determined with an instrument called a Shore A durometer. As shown in Figure 21, the Shore A hardness of the PU/silica nanocomposites increased steadily with increasing microsilica concentration, but with nanosilica this decreased after an initial increase.[277a] Obviously, microsilica is a hard filler, while it appears that nanosilica is not.

The microindentation hardness (microhardness) test is an indentation method for measuring the hardness of a material on a microscopic scale. A Vickers microhardness tester was applied to evaluate the microhardness enhancement of PEEK composites reinforced by nanosized SiO_2 particulates.[138] The PEEK polymer filled with nanosized silica 15−30 nm to 2.5−10 wt % was fabricated by vacuum hot press molding at 400 °C. The H_v microhardness readings increased all the way from 21.7 for the pure PEEK polymer to 32.5 for the 10 wt % 15 nm SiO_2 filled composites, implying a maximum increment percentage of 50%. Meanwhile, in comparison with the same SiO_2 particles but with different sizes of 15 and 30 nm, the composites with finer nanoparticles showed a continuous and linear hardness increment even at the highest SiO_2 content of 10 wt %. It seemed that the finer 15 nm particles could be more uniformly distributed and contributed the continuous hardness improvement.

The scratch resistance of coatings having a thickness in the range of micrometers can also be estimated by microhardness testing. The microhardness of transparent nanocomposites prepared from nanosized silica and radiation curable acrylates was measured.[287f] A standard diamond intender was impressed into the material under test at loads from 5 to 50 mN. The impression length was measured as a function of load. Obviously, the microhardness of acrylate nanocomposite coatings was more improved the higher the content of silica particles (Figure 22).

At present, load and depth sensing indentation, commonly referred to as nanoindentation, has proven itself as a powerful tool in hardness determination of thin films and coatings. In a nanoindentation test, a diamond indenter is forced into the coating surface. The load and depth of penetration (the indentation profile) is recorded, from which the hardness and elastic properties are calculated.[451] The mechanical properties

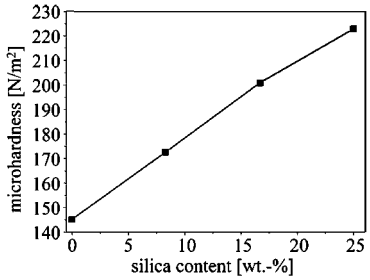

Figure 22. Microhardness of an acrylate coating as function of silica content. Reprinted with permission from Bauer, F.; Mehnert, R. J. Polym. Res. 2005, 12, 483. Copyright 2005 Springer.

of hybrid cross-linked silica/(meth)acrylate coatings on PC substrate were determined from indentation data.[290] It was shown that reliable elastic modulus and hardness data could be obtained from load and depth sensing indentation for a broad range of filler content when an indentation rate above 2 nm/s was used. Analyses showed that filler content and chemical composition influenced the mechanical properties of the silica/(meth)acrylate hybrid coatings in a complex way.

8.3.3. Fracture Toughness

Fracture toughness is a property that describes the ability of a material containing a crack to resist fracture. It is also one of the most important properties of materials. A parameter called the stress intensity factor is used to determine the fracture toughness of most materials. As the stress intensity factor reaches a critical value (K_{Ic}), unstable fracture occurs. This critical value of the stress intensity factor is known as the fracture toughness of the material. Fracture toughness can be measured by different methods, such as single-edge notch bend (SENB) and indentation fracture toughness (IFT).

The fracture toughness, K_{Ic}, of the silica nanoparticle-modified epoxy polymers was measured by the SENB.[271] A K_{Ic} of 0.59 MN $m^{-3/2}$ was recorded for the unmodified epoxy. Addition of nanoparticles increased the fracture toughness and a maximum value of 1.42 MN $m^{-3/2}$ was measured for the epoxy polymer with 13.4 vol % of nanoparticles. These values were converted to fracture energies, G_{Ic}, using the measured modulus. The unmodified epoxy polymer gave $G_{Ic} = 103$ J/m^2, and a maximum fracture energy of 460 J/m^2 was calculated. Hence there was a significant toughening effect due to the addition of silica nanoparticles.

It was shown by Rosso et al.[270a] that the addition of 5 vol % silica nanoparticles could improve the stiffness and the toughness of an epoxy resin at the same time. The elasticity modulus (E-modulus) from the tensile test was increased by more than 20%, whereas fracture toughness values, K_{Ic}, were improved by 70% and G_{Ic} by more than 140%. Moreover, the nanoreinforced material were more ductile and showed a greater yielding than the pure epoxy.

Fracture mechanics tests of epoxy/silica nanocomposites reported by Ragosta et al.[274] showed that the addition of silica nanoparticles up to 10 wt % brought about a considerable enhancement in fracture toughness and an increase in the critical crack length for the onset of crack propagation. This enhancement in toughness was larger than that achieved with microsized particles.

It is well-known that cracks are formed close to hardness impressions, especially for materials that have a low resistance to crack initiation. These cracks can be evaluated to determine the fracture toughness within the scope of indentation fracture mechanics. Kim et al.[143] demonstrated that the procedure of indentation fracture mechanics was a straightforward and cost-effective method for determination of both strength/stiffness and toughness of small samples of extremely brittle PMMA/SiO_2 nanocomposites. The nanocomposites studied in their work, which were prepared by solution blending, exhibited nanomorphology without any sign of agglomerates, even up to 20 wt %. While the stiffness and hardness were moderately affected by the concentration of SiO_2 nanoparticles, the fracture toughness was drastically affected by the filler contents, as seen in Figure 23. The significant reduction in fracture toughness at 20 wt % of SiO_2 nanoparticles was explained with a percolation of the bound layers, which was deduced by the results from DSC measurements. The effective particles, that is, particles plus their bound layer, came close to each other with increasing particle content, and percolation finally took place at 20 wt % of SiO_2 nanoparticles in the nanocomposite system. As a consequence, during the deformation processes, no material between the particles was available for energy dissipation. Thus, the system became more brittle.

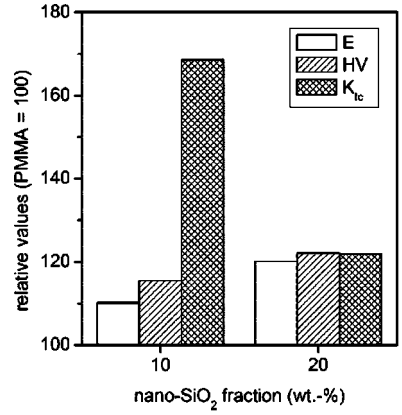

Figure 23. Relative mechanical values of PMMA/SiO_2 nanocomposites (the ratios between nanocomposites and pure PMMA; E, elastic modulus; H_V, Vickers hardness; K_{Ic}, fracture toughness). Reprinted with permission from Lach, R.; Kim, G. M.; Michler, G. H.; Grellmann, W.; Albrecht, R. Macromol. Mater. Eng. 2006, 291, 263. Copyright 2006 Wiley-VCH.

8.3.4. Friction and Wear Properties

Both friction and wear belong to the discipline of tribology. Friction is the force of two surfaces in contact or the force of a medium acting on a moving object, and wear is the erosion of material from a solid surface by the action of another solid. Factors that exert influence on friction and wear characteristics of polymer composites are the particle size, morphology, and concentration of the filler.[136b]

The addition of a second phase was one of the methods used to improve the tribological properties (such as coefficient of friction and wear rate) of the thermoplastic PA 6.[136b] The friction and wear properties of nylon 6/SiO_2 nanocomposites prepared by solution blending and subsequently compression molding were investigated on a pin on disk tribometer by running a flat pin of steel against a composite disk. The addition of 2 wt % nanosilica particles improved the coefficient of friction and wear resistance of nylon 6 composites. Table 10 shows the coefficient of friction (μ) and specific wear rate (K_w) of the PA 6, 2NS (containing 2 wt % silica particles, homogeneously dispersed), and 14NS

Table 10. Wear Rate and Coefficients of Friction of PA 6 Nanocomposites[a,b]

silica (wt %)	friction coefficient (μ)	wear rate [mm^3/nm] (k_w)
0	0.45	5.29×10^{-5}
2	0.20	2.0×10^{-7}
14	0.40	2.81×10^{-5}

[a] Adapted with permission from García, M.; de Rooij, M.; Winnubst, L.; van Zyl, W. E.; Verweij, H. J. Appl. Polym. Sci. 2004, 92, 1855. Copyright 2004 Wiley Periodicals, Inc. [b] Velocity = 0.1 m/s; load = 1 N; distance of sliding = 10 km.

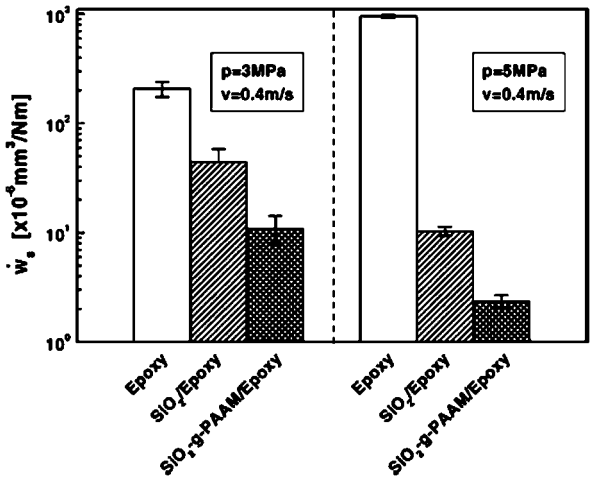

Figure 24. Frictional coefficient, μ, of epoxy and its composites at 2.17 vol % nanosilica content. Reprinted with permission from Zhang, M. Q.; Rong, M. Z.; Yu, S. L.; Wetzel, B.; Friedrich, K. Wear 2002, 253, 1086. Copyright 2002 Elsevier Science B.V).

nanocomposites (containing 14 wt % particles, more likely to be aggregated). Pure nylon showed a μ of 0.18 at the beginning of the friction measurements. During the test, the μ was gradually elevated up to a steady state of $\mu = 0.45$. At filler loadings of 2 wt %, the starting μ was 0.14. This nanocomposites rapidly reached a steady value of $\mu = 0.18$. The addition of 14 wt % of silica in the PA 6 resulted in an initial $\mu = 0.11$. After 0.1 km, a transient period resulted in $\mu = 0.2$, whereas after 1 km, a building up of μ was again observed up to almost the same steady-state value of the neat polymer (0.40). It was observed that the coefficient of friction for 2 wt % of SiO_2-filled composite was lower than that of unfilled nylon 6. Addition of 14 wt % of SiO_2 resulted in a coefficient of friction value (μ) slightly lower than pure nylon 6 after a few kilometers of wear track. Therefore, the 2NS composite had a lower wear rate and a lower coefficient of friction when compared with PA 6 and 14NS.

The effect of particle surface treatment on the tribological performance of epoxy-based nanocomposites was studied by Zhang and coauthors.[266b] Unlike micrometer silica, nanosilica could simultaneously provide epoxy with friction and wear-reducing functions at low filler content (~2 vol %). Figure 24 gives the coefficient of friction of epoxy and its composites determined at the pressures 3 and 5 MPa under a constant sliding velocity $v = 0.4$ m/s. It was seen that the frictional coefficient of epoxy was almost unchanged when the pressure increased from 3 to 5 MPa. The frictional coefficients of nanosilica-filled composites were lower than that of unfilled epoxy and decreased with increasing pressure. The lowest value of μ was recorded at a load of 5 MPa for SiO_2-*g*-PAAM/epoxy composites. These phenomena implied that nanosilica could improve the friction-reducing ability of the composites especially under higher load. The introduction of grafting PAAM further enhanced the role of the particles.

Table 11. Effects of Coupling Agent on the Thermal Properties of the PI/SiO_2 Hybrids[a]

run	SiO_2[b] (wt %)	GOTMS/TEOS	T_d[c] (°C)	CTE ($\times 10^{-5}$ K^{-1})	T_g[d] (°C)
1	0	0	561	5.41	289
2	10	0	581	4.86	294
3	20	0	588	3.45	301
4	30	0	600		310
5	10	1/10	572	2.53	298
6	20	1/10	576		309
7	30	1/10	592		316

[a] Adapted with permission from ref 227. Copyright 2002 American Chemical Society. [b] Calculated silica contents in hybrid films. [c] T_d determined by TGA in N_2, on-set. [d] T_g determined by DSC.

8.4. Thermal Properties

Thermal properties are the properties of materials that change with temperature. They are studied by thermal analysis techniques, which include DSC, TGA, DTA, TMA, DMA/DMTA, dielectric thermal analysis, etc. As is well-known, TGA/DTA and DSC are the two most widely used methods to determine the thermal properties of polymer nanocomposites. TGA can demonstrate the thermal stability, the onset of degradation, and the percent silica incorporated in the polymer matrix. DSC can be efficiently used to determine the thermal transition behavior of polymer/silica nanocomposites. Furthermore, the CTE, which is the criterion for the dimensional stability of materials, can be measured with TMA. In addition, thermal mechanical properties measured by DMA/DMTA are very important to understand the viscoelastic behavior of the nanocomposites. The storage modulus (G'), loss modulus (G''), and tan $\delta = G''/G'$ are three important parameters of dynamic mechanical properties that can be used to determine the occurrence of molecular mobility transitions, such as the T_g. Dielectric thermal analysis is also useful to understand the viscoelastic behavior of the nanocomposites

Generally, the incorporation of nanometer-sized inorganic particles into the polymer matrix can enhance thermal stability by acting as a superior insulator and mass transport barrier to the volatile products generated during decomposition.[452] Meanwhile, the incorporation of nanometer-sized inorganic particles such as silica is very effective in decreasing the CTE of the polymer matrix.

The thermal decomposition temperatures (T_d) determined by TGA, the CTEs determined by TMA, and the T_g determined by DSC of PI/SiO_2 hybrids prepared by the sol−gel process with identical GOTMS/TEOS molar ratios (1/10) but different SiO_2 contents are listed in Table 11.[227] From the table, it can be seen that the hybrids exhibit higher thermal stabilities and much lower CTEs than their counterparts. It can also be seen that the thermal decomposition temperature (T_d) of a hybrid increases with its silica content. The thermal stabilities of the hybrids with coupling agent were slightly lower than those of their counterparts without coupling agent because of the alkyl chains of GOTMS, but they were still higher than that of the corresponding PI. It can also be seen that the T_g of the hybrids increased with increasing silica content. The hybrid films with coupling agent exhibited higher T_g's. These phenomena could be explained as follows: First, the coupling agent strengthened

Table 12. Thermal Degradation Data of PMMA and the Nanocomposite Materials in Nitrogen[a]

	degradation temperatures (°C)				
sample[b]	head-to-head structure	unsaturated end	polymer backbone	char yield (wt %)	calcd silica content (wt %)
PMMA	165, 212	296	401	0	0
HM-40	177	296	388	39	43
HM-50	174	299	395	49	50
HM-60	177	297	388	60	63
HM-70	179	294	378	69	70
HM-80	180	299	378	75	76

[a] Adapted with permission from Liu, Y. L.; Hsu, C. Y.; Hsu, K. Y. Polymer 2005, 46, 1851. Copyright 2005 Elsevier Ltd. [b] The nanocomposite films containing silica 43, 50, 63, 70, and 76 wt % are abbreviated as HM-40, HM-50, HM-60, HM-70 and HM-80, respectively.

the interaction between the organic polymer matrix and the inorganic mineral particles, which caused an increased restricting strength of SiO_2 on the PI molecules. Second, the coupling agent reduced the size of the SiO_2 particles and thereby greatly increased the interfacial area at a given silica content. Furthermore, the reduced size of the SiO_2 particles, to some extent, resulted in an increase in the cross-linking density. All of these effects led to higher T_g and lower CTE values for the PI/SiO_2 hybrids with coupling agent than for their counterparts.

In some cases, the thermal stability of the nanocomposites is not enhanced by the addition of silica particles. TGA characterization of the thermal stability of silica/PMMA nanocomposites made by in situ radical polymerization showed that the addition of nanosilica particles slightly reduced the thermal stability of the nanocomposite sample at low temperatures and slightly delayed random initiation along the polymer backbone.[260]

Similar behavior was also observed with PMMA/silica nanocomposite films prepared by copolymerizing MMA with AGE-functionalized silica nanoparticles.[69b] Pure PMMA showed a four-stage degradation mechanism. It is known that the first two stages of weight loss for the pure PMMA might be from the degradation of head-to-head linkage. However, the first weight loss might also be from the residual solvent and/or MMA monomer in the polymer. The last two stages of weight loss corresponded to degradation initiating at the unsaturated ends (at about 296 °C) and at the polymer backbones (at about 400 °C). Similar degradation patterns were also observed with the PMMA nanocomposite films. The degradation temperatures of each stage are collected in Table 12. From the DTG data, it was concluded that incorporation of nanosilica particles into the PMMA polymer did not change the degradation mechanisms of the polymer. That is to say, the thermal stability of PMMA was not enhanced by the addition of silica particles.

Figure 25 shows the relationship between the silica content and the in-plane CTE of the PI and PI/silica hybrid films.[192] When the silica was introduced, the CTE was decreased. The CTE was decreased by 28.6% from 31.1 ppm for a pure PI to 22.2 ppm for a hybrid with 10 wt % silica. The CTE was further decreased to 19.2, 16.2, and 14.9 ppm for the hybrids with 20, 30, and 40 wt % silica, respectively. These data were close to the CTE of some inorganic substrates.

Studies on the effect of silica filler addition on polymer glass transition temperature show a wide variety of behavior. The effect of the nanofillers in polymer composites on the glass-transition behavior of the polymer matrix is controversial since T_g of polymer nanocomposites varies for a variety of reasons such as filler size, filler loading, and dispersion conditions.[268a] In some cases, the polymer nanocomposites showed an increase of the T_g.[67,227] In other cases, a depression in the T_g of the nanocomposites was observed.[225b,270a] An initial increase in T_g followed by a decrease in T_g with a higher filler loading,[268] an initial decrease in T_g followed by an increase in T_g with a higher filler loading,[273a] nanoparticles causing no significant change to the glass transition of the polymer,[67,129] and even the disappearance of T_g were also reported.[69b]

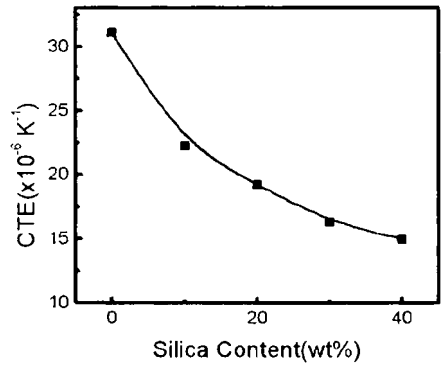

Figure 25. The CTE of copolyimide [PPA/MPA/PMDA (2:1:3)]/silica hybrids. Reprinted with permission from Huang, J. C.; Zhu, Z. K.; Yin, J.; Zhang, D. M.; Qian, X. F. J. Appl. Polym. Sci. 2001, 79, 794. Copyright 2001 John Wiley & Sons, Inc).

The T_g of the silica/epoxy composites with nanometer- and micrometer-sized fillers are shown in Figure 26a.[268a] The micrometer-sized filler did not have a significant effect on T_g of the composites, whereas the nanofiller had an appreciable impact. With an increase in the filler loading, the silica nanocomposites first showed a slight increase in T_g, and then T_g decreased significantly with higher filler loadings. In comparison with the control sample, the 40 wt % silica nanocomposite showed a drop in T_g of almost 30 °C. In order to determine the cause of this decrease, the thermomechanical and dielectric relaxation processes of the silica nanocomposites were investigated with DMA and dielectric analysis. Figure 26b shows the dynamic moduli of the three samples. There was a significant difference in the peak of the loss modulus around 150 °C, which is typically called the glass transition. There was another peak of the loss modulus around −50 °C, which is usually called the sub-T_g transition or relaxation. As shown in the figure, the position of the sub-T_g transition was not affected by the fillers. It was found that the T_g depression of the nanocomposite was closely related to the resin−filler interfacial properties. The increased resin−filler interface created extra free volume and, therefore, assisted the large-scale segmental motion of the polymer. As a result, T_g of the nanocomposites decreased with increasing filler loading. However, the sub-T_g transition involved local movement of the chain and required much less free volume. Therefore, the increased interface did not have a significant effect on the sub-T_g transition temperature.

The addition of nonpolar FS to nonpolar, stiff-chain poly(2,2-bis(trifluoromethyl)-4,5-difluoro-1,3-dioxole-*co*-tetrafluoroethylene) (AF2400) produced no measurable change in T_g.[129] From DSC scans, the T_g of AF2400 was 244 °C, which is within the typical range for this polymer. Subsequent scans of AF2400 films containing different loadings of FS (10, 25, and 40 wt %) showed no significant change

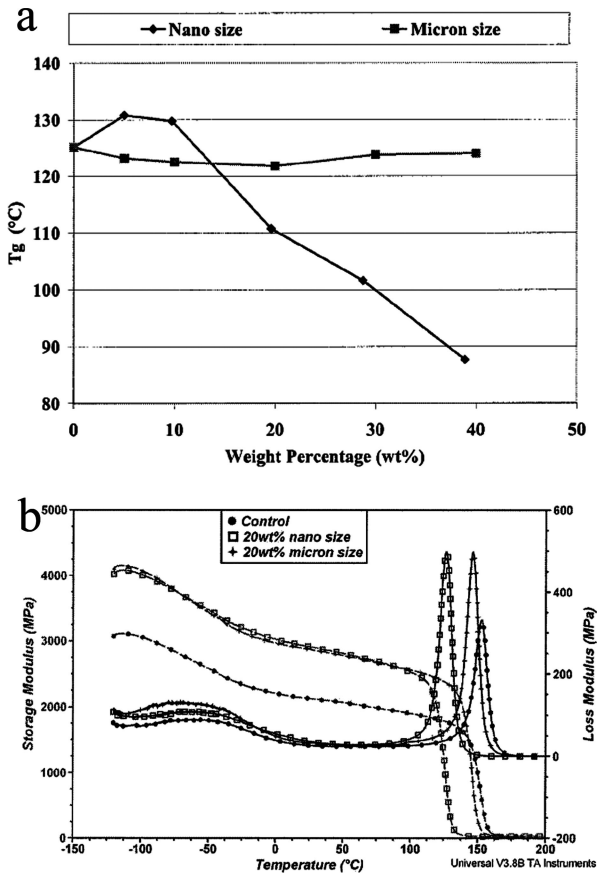

Figure 26. (a) T_g of the silica composites and (b) dynamic moduli of the silica composites and the blank resin. Reprinted with permission from Sun, Y. Y.; Zhang, Z. Q.; Moon, K. S.; Wong, C. P. J. Polym. Sci., Part B: Polym. Phys. 2004, 42, 3849. Copyright 2004 Wiley Periodicals, Inc.

in glass transition temperature (T_g ranged between 242 and 246 °C). This result indicated that the presence of FS particles did not measurably alter the long-range segmental dynamics important to the glass transition in AF2400. Given the nonpolar, hydrophobic nature of AF2400, it is reasonable that interactions between the two, which might affect T_g, were very weak and that the primary impact of FS addition was on chain packing and not on chain stiffness or mobility.

Figure 27 shows the DSC thermograms of PMMA and the nanocomposite materials.[69b] Only pure PMMA showed a T_g at about 115 °C. For all of the nanocomposite films, glass transition behavior was not observed with DSC. The glass transition behavior of the nanocomposite materials was also not observed by a thermal mechanical analyzer. The disappearance of T_g implied that the motion of the PMMA chains was seriously restricted by the silica particles. The restriction could be also coming from the cross-linking bonding between PMMA chains and silica particles,[265a] since a decrease in T_g was observed with the PMMA/silica nanocomposite materials[260] that did not have interphase bonding.

TSDC (thermally stimulated depolarization currents) is a dielectric technique that is used extensively to study relaxation mechanisms in polymeric materials. The PDMS/silica nanocomposites were investigated using TSDC in order to characterize the glass transition in more detail.[171b] The TSDC thermograms obtained for the pure PDMS and the PDMS/silica nanocomposites in the temperature range of the glass transition are shown in Figure 28. For the pure PDMS, a single relaxation was observed at −123 °C. This was the

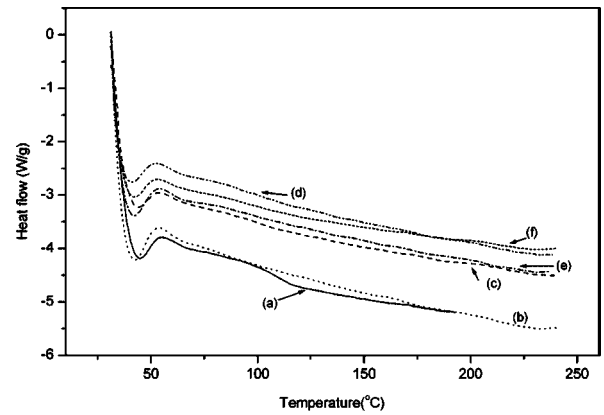

Figure 27. DSC thermograms of PMMA and its nanocomposite materials: (a) PMMA, (b) HM-40, (c) HM-50, (d) HM-60, (e) HM-70, and (f) HM-80 (the nanocomposite films containing silica 43, 50, 63, 70, and 76 wt % abbreviated as HM-40, HM-50, HM-60, HM-70 and HM-80, respectively). Reprinted with permission from Liu, Y. L.; Hsu, C. Y.; Hsu, K. Y. Polymer 2005, 46, 1851. Copyright 2005 Elsevier Ltd.

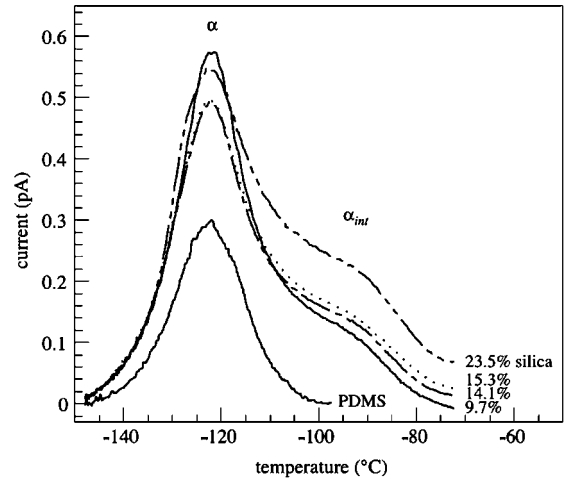

Figure 28. TSDC thermograms for PDMS and PDMS/silica nanocomposites in the region of the glass transition. Reprinted with permission from Fragiadakis, D.; Pissis, P.; Bokobza, L. Polymer 2005, 46, 6001. Copyright 2005 Elsevier Ltd).

primary α relaxation associated with the glass transition of the amorphous phase of PDMS. For the composites, the α relaxation was observed at the same temperature but with higher intensity due to the decrease in crystallinity. In addition, a shoulder appeared on the high-temperature side of the main peak extending up to approximately 30 °C higher, whose intensity increased with silica content. The shoulder in the TSDC thermograms of the composites was assigned to the a relaxation of PDMS chains in an interfacial layer close to the silica particles, where chain mobility was constrained due to interaction with the surface of the particles. The main relaxation at −123 °C in the composites was then attributed to the relaxation of the PDMS chains that were sufficiently far from the filler surface as to exhibit quasi-bulk behavior. The thickness of the interfacial layer was estimated from the TSDC data to be about 2.1−2.4 nm. DRS (dielectric relaxation spectroscopy) was also used to investigate the molecular dynamics in the bulk and interfacial layers by following the temperature dependence of the corresponding dielectric relaxations. The bulk and interfacial relaxations at higher temperatures observed by DRS were well-separated, their relaxation times differing by several decades.

Table 13. Heat Deflection Temperature Data[a]

sample	heat deflection temperature (°C)
PES	182
PES/fumed silica	187
PES/epoxy/fumed silica (80/20/10) cured at 200 °C for 3 h[b]	206.2
PES/epoxy/fumed silica (90/10/2) cured at 200 °C for 4 h[b]	206
PES/epoxy (80/20) cured at 200 °C for 4 h[b]	176.5

[a] Adapted with permission from Jana, S. C.; Jain, S. Polymer 2001, 42, 6897. Copyright 2001 Elsevier Science Ltd. [b] Compositions are in parts by weight.

The heat deflection temperature or heat distortion temperature (HDT) is the temperature at which a polymer sample deforms under a specified applied load. This property is relevant to many aspects of product with thermoplastic components. But, surprisingly, there are only a few examples concerning the heat deflection of polymer/silica nanocomposites. Table 13 presents the HDT data for virgin PES and its blends with fumed silica and epoxy, which were determined using ASTM D5945.[64] As expected, the presence of epoxy-aided nanodispersed fumed silica particles substantially improved the HDT of the blends, although epoxy separately caused reduction of HDT in PES/epoxy blends. The marginal improvement in HDT in melt-mixed PES/fumed silica system could be attributed to larger size particle aggregates.

8.5. Flame-Retardant Properties

A fire retardant is used to make materials harder to ignite by slowing decomposition and increasing the ignition temperature. It functions by a variety of methods such as absorbing energy away from the fire or preventing oxygen from reaching the fuel. Polymer nanocomposites for flame-retardant applications are attractive, and the nanoscale silica particle is a new type of nanoparticle for flame-retardant nanocomposites.[453]

The flammability behavior of polymer is defined on the basis of several processes or parameters, such as burning rates, spread rates, ignition characteristics, etc.[454] Meanwhile, the flame-retardant characteristics of the nanocomposites are generally studied by measuring their limiting oxygen index (LOI). The LOI is defined as the minimum fraction of O_2 in a mixture of O_2 and N_2 that will just support flaming combustion. Furthermore, the UL-94 test (Underwriter's Laboratory Test #94) is conducted to quantify and rank the flame retardance of the materials. The UL-94 covers two types of testing: vertical burn and horizontal burn. The vertical burning test uses a Bunsen burner as the ignition source, and specimens are classified according to their burning times as V0 (best), V1, V2, or nonclassifiable (fail). The horizontal burning test is less severe, and specimens are classified as HB or fail accordingly. The horizontal burning test is also used to evaluate the fire spread rate of materials by giving fire travel information on the horizontal surface including fire-spread rate, burning behavior, and ease of extinction if the material burns without dripping. In addition, the cone calorimeter is one of the most effective bench-scale methods for studying the fire-retardant properties of polymeric materials such as the heat release rate, heat peak release rate, etc.

Table 14. The UL-94 and LOI Test Results of Novolac-Type Phenolic/TEOS Hybrids[a]

TEOS content (wt %)	UL-94 standard	LOI
neat phenolic	94V-1	32
20	94V-0	35
40	94V-0	37
60	94V-0	40
80	94V-0	43

[a] Adapted with permission from Chiang, C. L.; Ma, C. C. M. Polym. Degrad. Stab. 2004, 83, 207. Copyright 2004 Elsevier Ltd.

Table 14 reveals a considerable increase in LOI (from 33 to 44) when TEOS was added to the phenolic resins.[212b] This change suggested that incorporating silicon significantly promoted the flame retardance of the resins. Neat phenolic resin may be placed in the UL-94 V1 class. The hybrids that contained 20 wt % TEOS could be classified as UL-94 V0 grade. Phenolic hybrids with good flame retardance (LOI 32−44, UL-94 V0 grade) and excellent thermal stability (T_g above 300 °C) were considered to suffice for applications as green flame-retardant materials.

An important characteristic of the fire retardant is the formation of char, which creates a protective layer that impedes oxygen penetration and creates an insulating layer between the heat and the fuel. Phosphorus compound is one of the best materials for forming char. The flame-retardant characterisics of epoxy resins have been demonstrated to improve with nanoscale phosphorus-containing epoxy/silica hybrids obtained via sol−gel process.[197] The epoxy/silica hybrid exhibited very high LOI values of 44.5. The high flame retardancy of this epoxy system came from the phosphorus and silica enhancing effect. Therefore, the synergistic effect on enhancing epoxy-resin flame retardancy could be achieved by the incorporation of phosphorus and nanometer-scale silica formed from the sol−gel process. However, it was suggested that using preformed silica particles in the formulations of epoxy resins did not exhibit significant synergistic effect with phosphorus on polymer's flame retardance improvement.[273a] In this work, this P−Si synergistic effect could still be considered being operative, although more weakly. The P−Si synergism effect of char formation was due to the migration of silica to the surface of the formed char to form a protecting layer in order to prevent further thermal degradation of the char. The preformed colloidal silica, dsepite having the size of 20 nm, was probably too large to migrate to the char surface under heating.

The heat release rates of the PMMA and the PMMA/nanosilica sample prepared by in situ polymerization of MMA with colloidal silica are shown in Figure 29.[260] The addition of nanosilica reduced the peak heat release rate of the PMMA sample to roughly 50% of the pure PMMA value, but it did not significantly change the thermal stability. The flame-retardant mechanism of the addition of the nanosilica particles to PMMA was inferred to be the coagulation of the particles and the accumulation of loose, granular particles near the sample surface to form a protective layer as a heat insulation and a barrier for evolved degradation products. Since the PMMA/nanosilica sample surface was covered by loose granular particles, part of the sample surface was still exposed to the external radiation through the granular particle layer. Therefore, the addition of nanosilica particles was not as effective in terms of flame retardance as that of silica gel

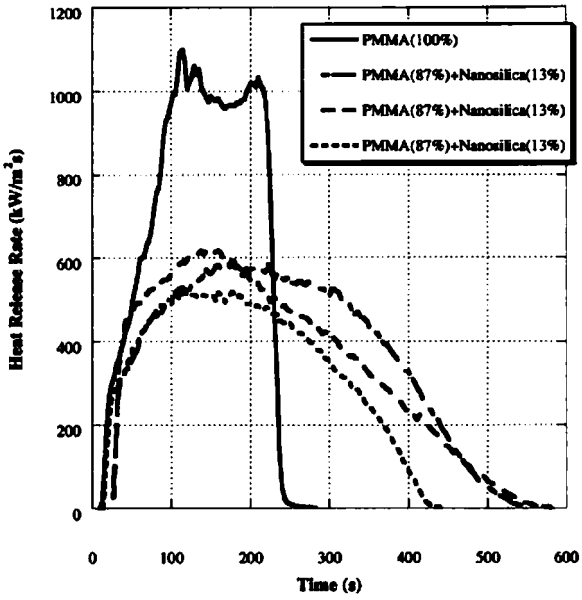

Figure 29. Effects of nanosilica addition on heat release rate of PMMA at 40 kW/m^2. The dashed lines are the results of three replicas of nanocomposites made at three different times. Reprinted with permission from Kashiwagi, T.; Morgan, A. B.; Antonucci, J. M.; VanLandingham, M. R.; Harris, R. H.; Awad, W. H.; Shields, J. R. J. Appl.Polym. Sci. 2003, 89, 2072. Copyright 2003 Wiley Periodicals, Inc.

in PMMA, which formed an in situ silica network to cover the entire sample surface.

Although polymer/silica nanocomposites exhibited good mechanical properties and thermal stabilities, they are not necessarily flame-retardant. Three polymer/silica nanocomposites: PMMA, PS, and PC/silica nanocomposites, prepared by a single-screw extrusion approach, were subjected to studies of flammability properties.[97] None of the materials studied were strictly flame-retardant when subjected to fire tests like oxygen index or horizontal burning test. However, the nanocomposites showed reduction in peak heat release rates and total heat release when evaluated by cone calorimetry. Moreover, the PC showed an improvement in flammability according to vertical burning tests. The strength of interfacial interaction between polymer and silica played a critical role in peak heat release rate reduction of nanocomposites. However, the mechanism of peak heat release rate reduction could be different for char-forming (PC) and non-char-forming (PMMA and PS) type nanocomposites. For char-forming nanocomposites, the presence of silica particles could enhance the char formation of the matrix material and form a protective surface barrier to prevent the immediate damage of substrate materials. In contrast, when the polymer simply melts during burning, silica could accumulate on the surface and reduce the area exposed to fire and therefore reduced the peak heat release rate: similar effect, similar result, but different mechanism.

PMMA/silica nanocomposites prepared by solution polymerization of MMA and silica modified with an appropriate surface modifier were also subjected to characterization of fire properties.[248] Although oxygen indices of the nanocomposites from solution polymerization showed very little improvement, it showed negative results for these materials as flame-retardant materials, because real flame retardancy will be achieved only when the oxygen index of the material reached 25−28. Below this number, materials are easily ignited, and not easily extinguished once ignited. The nanocomposites were not flame-retardant materials. They all exhibited substantially higher burning rates and lower average times of burning compared with PMMA. In other words, they burned faster. However, all the nanocomposites burned without dripping. This was very different from PMMA, which dripped badly during the test. The phenomenon could be explained by the "wick effect". For some organic/inorganic composites, fire will burn out the organic phase and leave the inorganic phase intact, which will lead to a faster burning rate of the composite.

8.6. Optical Properties

The most important optical properties of a material are its transparency and refractive index. Transparency is the physical property of allowing the transmission of light through a material. It is important for many practical applications of polymer nanocomposites. However, introduction of silica inorganic nanoparticles even at low contents into transparent polymers often leads to opaque nanocomposites due to light scattering caused by the nanoparticles. To remain transparent, SiO_2 should disperse in the composite at a very fine scale to allow light to transmit easily. For quantitative analysis, transmittance of the film is measured by UV−vis spectrometry. The refractive index is defined as the speed of light in vacuum divided by the speed of light in the medium. It is the most important property of optical systems that use refraction, and it can be measured by a refractometer.

It is difficult to maintain transparency when composites are prepared by conventional blending methods, in which the inorganic filler is simply mixed into the polymer matrix. It was surprising to find that hydrophilic SiO_2 nanoparticles could be homogeneously dispersed in a PP matrix.[82a] Spherulite growth rates of PP in PP/SiO_2 nanocomposites decreased significantly with increasing SiO_2 content and decreasing particle size. The spherulite growth rate was zero for PP/16 nm SiO_2 nanocomposites with SiO_2 content above 2.5 wt %, resulting in a highly transparent film. This result indicated a real possibility of developing high-transparency PP materials, which are eagerly sought for various applications.

The transparency of the PMMA/silica coat films derived from PHPS was almost 100%, indicating that the coat film prepared with PHPS was highly transparent on both the glass substrate and the PC substrate.[43i]

Since the silica prepared by the sol−gel method contains many lattice defects, the transparency of the nanocomposites prepared by the sol−gel process generally decreases with increasing SiO_2 content.[43] For example, based on a visual comparison, the TPU/silica hybrids with different SiO_2 contents using HCl as the catalyst containing 5% SiO_2 remained transparent with pristine TPU; the hybrid containing 10% SiO_2 was somewhat translucent; hybrids containing 15 and 20% SiO_2 were opaque.[175]

The appearances of the PI/SiO_2 hybrid films with different PI/SiO_2 contents and different amounts of coupling agent (GOTMS) are listed in Table 15.[227] It can be seen that the transparency of the PI/SiO_2 hybrid films was improved by the coupling agent. A hybrid film became translucent when the silica content was more than 10 wt % without GOTMS. However, this critical point moved to 20 wt % by the addition of GOTMS. This was because GOTMS hydrolyzed to form silanol groups that could polycondense with the hydrolysis product of TEOS. Moreover, the other end of GOTMS hydrolyzed to form hydroxyl groups that could form

Table 15. Transparency of the PI/SiO_2 Hybrids[a]

run	silica[b] (wt %)	GOTMS/TEOS (mole ratio)	remark[c]
1	0	0	T
2	5	0	T
3	10	0	T
4	20	0	O
5	30	0	O
6	40	0	O
7	10	1/10	T
8	20	1/10	T
9	30	1/10	O
10	20	1/4	T
11	20	1/7	T
12	20	1/10	T
13	20	1/15	O
14	20	0	O

[a] Adapted with permission from ref 227. Copyright 2002 American Chemical Society. [b] Silica contents were calculated theoretically. [c] T, transparent; O, opaque.

Table 16. Variation of Transmittance of PMMA/Silica Hybrid Copolymers[a]

sample code[b]	at 600 nm (% T)	at 700 nm (% T)
PMMA	90.6	91.2
PMMA−silica 10	86.8	88.1
PMMA−silica 20	89.2	90.1
PMMA−silica 30	89.5	90.4
PMMA−silica 40	90.1	91.1
PMMA−silica 50	89.5	91.0

[a] Adapted with permission from Sugimoto, H.; Daimatsu, K.; Nakanishi, E.; Ogasawara, Y.; Yasumura, T.; Inomata, K. Polymer 2006, 47, 3754. Copyright 2006 Elsevier Ltd. [b] PMMA−silica 10, 20, 30, 40, and 50 represent silica feed content (wt %) 10, 20, 30, 40, and 50, respectively.

hydrogen bonds with the carbonyl groups in PI, leading to increased compatibility with PI. These two factors led to a reduction of the average particle size and good dispersion of the SiO_2 particles in the PI matrix. The effect of the coupling agent reached a constant level when the content was sufficiently large.

As indicated in section 4.2, two series of the PI/silica hybrid optical thin films were synthesized using an in situ sol−gel reaction combined with spin coating and multistep curing.[214] Highly transparent hybrid thin films were obtained at a silica content as high as 54.9 wt %. Optical planar waveguides were prepared from the prepared hybrid thin films using a thermal oxide as the cladding layer. The refractive indices of the prepared hybrid thin films decreased linearly with increasing silica content, while the Abbe number of the hybrid thin films showed the opposite trend. The birefringence, defined as the difference between the in-plane and out-of-plane refractive indices, of the hybrid thin films was reduced by incorporating the silica moiety. The optical losses of these planar waveguides at 1310 nm were in the range of 0.5−1.9 dB/cm, which were due to the higher harmonics of the aromatic C−H vibration, the O−H vibration, and the extrinsic loss. The optical losses of the prepared PI/silica hybrid films were lower than their parent PIs and thus had potential applications in optical devices.

Table 16 summarizes the visible light transmittance data for the PMMA/silica hybrid obtained by reactive silica nanoparticles copolymerized with MMA and PMMA at 600 and 700 nm.[68] All the hybrid copolymers evaluated in the study kept high visible light transmittance, over 85% at each wavelength, compared with about 91% for PMMA. Therefore, this method was thought to be an effective method for preparing highly transparent nanohybrid materials.

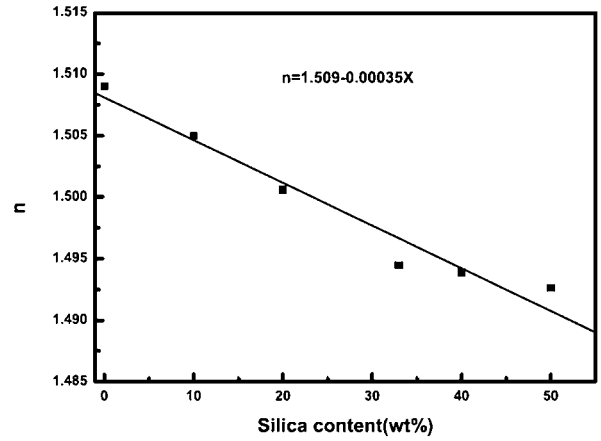

Figure 30. Variation of refractive index with the silica content in the hybrid films. Reprinted with permission from Yu, Y. Y.; Chen, C. Y.; Chen, W. C. Polymer 2003, 44, 593. Copyright 2003 Elsevier Science Ltd.

Poly(acrylic)/silica thin films prepared by in situ polymerization from acrylate monomer and monodispersed colloidal silica with a coupling agent showed tunable refractive index with the silica fraction in the films.[265a] As shown in Figure 30, the refractive index decreased linearly with increasing silica fraction. Excellent optical transparence was obtained in the prepared hybrid films. These results showed that such hybrid thin films have potential applications as passive films for optical devices.

8.7. Gas Transport Properties

Gas transport properties include solubility, diffusivity, permeability, and permselectivity; detailed definitions of them can be referred in literature.[123c,125b,129] Gas transport in nonporous polymer membranes typically proceeds by a solution−diffusion mechanism in which the permeability (P) is given by $S \times D$, where S and D denote the solubility and diffusivity of the permeating species, respectively. The solubility provides a measure of interaction between the polymer matrix and penetrant molecules, whereas the diffusivity describes molecule mobility, which is normally governed by the size of the penetrant molecule as it winds its way through the permanent and transient voids afforded by the free volume of the membrane.[447] Therefore, gas transport is to be strongly dependent on the amount of free volume in the polymer matrix.

Generally, incorporating inert, nonporous fillers into a polymer membrane results in a decrease in its gas permeability because filler particles typically lower both gas solubility and gas diffusivity within the polymer. For example, the permeability of thermally sprayed coatings measured using the permeability cup method (ASTM D1653-93) showed that the water vapor transmission rate through nanoreinforced coatings decreased by up to 50% compared with pure polymer coatings.[164c] The aqueous permeability of coatings produced from smaller particle size polymers (D-30) was lower than the permeability of coatings produced from larger particles because of the lower porosities and higher densities achieved in D-30 coatings.

Good permeability and selectivity of a membrane are commonly required in practical applications. Significant improvements in the polymer/inorganic nanocomposite mem-

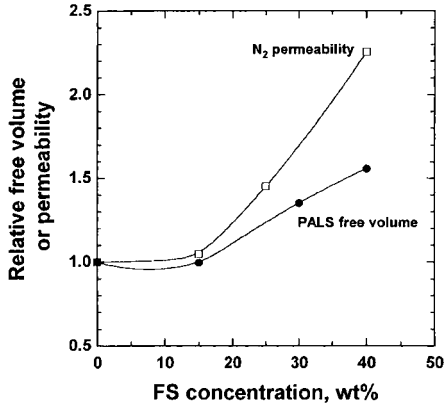

Figure 31. Relative PALS accessible free volume (●) and nitrogen permeability (□) in PMP as a function of FS content. Ordinate values are $\tau_3{}^3I_3 + \tau_4{}^3I_4$ (or N_2 permeability) for the nanocomposites normalized by the corresponding value for pure PMP. PALS data were acquired at room temperature, and nitrogen permeability was measured at 25 °C with a feed pressure of 4.4 atm and a permeate pressure of 1 atm. Reprinted with permission from ref 123c. Copyright 2003 American Chemical Society.

branes for gas separation have been made, as recently reviewed by Shen et al.[12] Many polymer/silica nanocomposite membranes with much higher gas permeabilities but similar or even improved gas selectivities compared with the corresponding pure polymer membranes have been reported. Since the permeability of a gas through a membrane is proportional to the solubility and diffusivity of the gas in the membrane, adding silica nanoparticles may affect the gas separation in two ways: the interaction between polymer-chain segments and nanofillers may disrupt the polymer-chain packing and increase the voids (free volumes) between the polymer chains, thus enhancing gas diffusion; the hydroxyl and other functional groups on the surface of the inorganic phase may interact with polar gases such as CO_2, improving the penetrants' solubility in the nanocomposite membranes.[12]

As mentioned in section 3.1, contrary to traditional filled polymer systems where addition of nonporous fillers reduces permeability, incorporation of FS into high-free-volume polyacetylene alters the polymer matrix to permit more rapid penetrant transport. This increase in penetrant flux upon FS addition was attributed to a FS-induced increase in system free volume. Figure 31 compares relative N_2 permeability and PALS accessible free volume in PMP as a function of FS content.[123c] There was an interestingly strong qualitative agreement between the manner in which both N_2 permeability and PALS free volume increase with increasing FS concentration in PMP, suggesting a close correspondence between increasing free volume, as probed by PALS, and enhanced transport properties.

Figure 32 presents methane permeability coefficients in AF2400 containing 0, 25, and 40 wt % FS at 25 °C as a function of the transmembrane pressure difference, Δp.[129] The permeability of this polymer is very high relative to that of conventional glassy polymers. Similar to the results for PMP and PTMSP, the permeability of AF2400 was increased by FS addition. For example at $\Delta p = 3.4$ atm, methane permeability in AF2400 containing 40 wt % FS was 340% higher than that in the unfilled polymer.

Membranes prepared from nanoreinforced nylon 6 via film casting also showed a significantly increased permeability for both CO_2 and N_2 over membranes made from pure nylon 6.[136d] The increase in permeability was also ascribed to the additional free volume obtained.

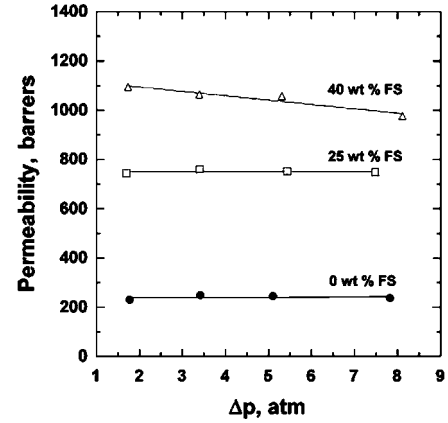

Figure 32. Methane permeability coefficients at 25 °C in AF2400 containing 0, 25, and 40 wt % FS as a function of the transmembrane pressure difference, Δp. Reprinted with permission from ref 129. Copyright 2003 American Chemical Society.

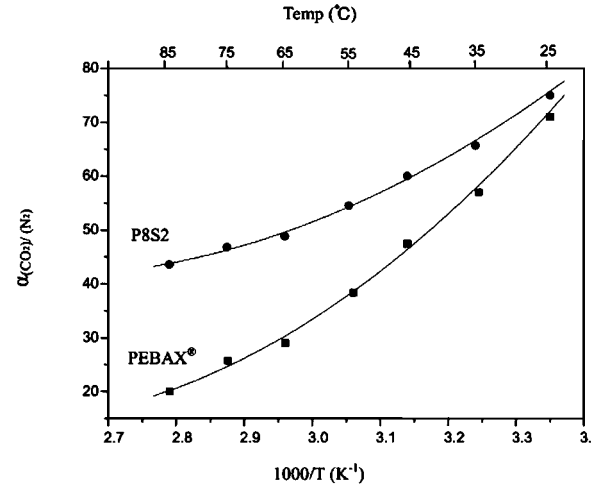

Figure 33. Temperature dependence of α_{CO_2}/N_2 (CO_2/N_2 permselectivity) at 3 atm for PEBAX and hybrid. Reprinted with permission from Kim, J. H.; Lee, Y. M. J. Membr. Sci. 2001, 193, 209. Copyright 2001 Elsevier Science B.V.

The gas transport properties of the organic/inorganic hybrids of poly(amide-6-*b*-ethylene oxide) (PEBAX) and silica prepared using the sol−gel process were studied.[185] The hybrid membranes exhibited higher gas permeability coefficients and permselectivities than those of PEBAX, particularly at an elevated temperature. The high permeability and permselectivity of the hybrid membranes were attributed to the strong interaction between CO_2 molecules and SiO_2 domains and additional sorption sites in PA block of PEBAX and the organic/inorganic interphase. Figure 33 shows the changes of $\alpha CO_2/N_2$ with various temperatures at 3 atm. It is known that PEO-containing films exhibited high P_{CO_2} and α_{CO_2}/N_2 for acidic gases because PEO segments can dissolve a large amount of acidic gases. At high temperatures, however, the performance of PEO based films dropped steeply because of a significant decrease in the solubility selectivity. Although the temperature dependence of α_{CO_2}/N_2 in hybrids showed similar behavior, the decrease was much smaller for the hybrids because the amount of sorption in hybrids was larger than that of PEBAX at high temperatures, resulting from the strong interaction between CO_2 molecules and SiO_2 domains and additional sorption sites in PA block.

Spontak et al.[447a,b] have desmontrated the efficacy of CO_2-selective nanocomposite membranes derived from cross-

linked PEGda oligomers and methacrylate-functionalized FS. These amorphous membranes exhibited surprisingly high CO_2/H_2 selectivity, coupled with high CO_2 permeability. In a further work,[447c] two PEGda oligomers differing in chain length and FS nanoparticles varying in surface functionality were exposed to CO_2 at low and high pressures to elucidate the roles of CO_2 pressure, network topology, and nanoparticle aggregation on molecular transport and solubility. Results confirmed that both penetrant diffusivity and solubility increased with increasing PEGda chain length and decreasing network density. Methacrylate-terminated FS nanoparticles were more effective in improving rheological properties and retaining high CO_2 selectivity than hydroxyl-terminated nanoparticles of comparable size. Analogous membranes prepared from PPGda also exhibited CO_2 selectivity.[447d] While the permeability of CO_2 in PPGda membranes was consistently and considerably higher than that measured in PEGda systems, the corresponding CO_2/H_2 and CO_2/N_2 selectivities, which constitute good indicators for H_2 and air purification, were significantly higher in the PEGda membranes.

Shen et al.[132b] measured the transport properties as a function of silica size and concentration for brominated poly(2,6-diphenyl-1,4-phenylene oxide) ($BPPO_{dp}$) exposed to pure CO_2, N_2, and CH_4. Silica-impregnated $BPPO_{dp}$ membranes exhibited enhanced CO_2 permeability relative to pure $BPPO_{dp}$ membranes due to higher gas solubility and, especially, higher gas diffusivity. Among the three silica sizes (2, 10, and 30 nm), the 10 nm silica was found to result in the highest gas permeability, about 5 times higher than that of the pure $BPPO_{dp}$ membranes. These permeability enhancements did not cause an appreciable loss of selectivity, which remained essentially unchanged. To explain why the addition of the nanoparticles enhanced gas permeability but did not affect the gas selectivity, a nanogap hypothesis was proposed. Due to the poor compatibility of the silica surface and the polymer, the polymer chains could not tightly contact the silica nanoparticles, thus forming a narrow gap surrounding the silica particles. The gas diffusion path was shortened and thus the apparent gas diffusivity and permeability were increased.

Takahashi and Paul[107] investigated the gas permeation in nanocomposite membranes based on surface-treated silica and a conventional polymer, PEI, with or without chemical coupling to matrix. The membrane was formed by both solution casting and melt processing techniques. In the case without chemical coupling to matrix,[107a] there was considerable evidence that these nanocomposites contained voids or defects, probably at the polymer−particle interface or within aggregates, regardless of the method of preparation, and this increased gas permeability and decreased selectivity. The relative permeabilities were much higher for solution-cast than melt-processed membranes. In the case with chemical coupling to matrix,[107b] nanocomposite membranes made by solution casting showed larger agglomerated filler particles and greater void volume fraction than melt-processed samples. In addition, reactive processed samples using sylilated SiO_2 had lower void volume. The chemical coupling strategy educed the void volume but did not entirely eliminate void formation. The relative gas permeability of the nanocomposite was decreased by the presence of SiO_2 particles. Diffusion coefficients also decreased with SiO_2 content. However, solubility coefficients increased with SiO_2 content contrary to simple composite theory.

8.8. Rheological Properties

Rheology is the study of the deformation and flow of matter under the influence of an applied stress. The measurement of rheological properties is helpful to predict the physical properties polymer nanocomposites during and after processing.

Oberdisse[153b] studied the rheological properties of a special nanocomposite material obtained by film formation of mixtures of colloidal silica and nanolatex solutions by means of uniaxial strain experiments. The reinforcement effect due to the introduction of hard silica beads was investigated as a function of silica volume fraction, Φ, pH in solution before film formation, and silica bead size and showed considerable sensitivity to these parameters. The stress−strain curves showed that the material could be stretched up to high elongations, λ, typically around four or more before rupture, indicating that the extensibility of the pure nanolatex film was conserved. It was found that the silica contributed differently at small and large deformations: In the small deformation regime ($\lambda \leq 1.2$), considerable reinforcement (a factor of 10 in Young's modulus with respect to the pure nanolatex) was obtained with silica volume fractions on the order of 10%. At higher elongations, the reinforcement factor decreased, and the rheology of the nanocomposite samples approached that of the pure nanolatex films.

The chemio-rheological behavior during the radical polymerization of the HEMA/grafted silica nanoparticles was found to be very dependent on the weight fraction of the silica particles.[263a] In the case of the neat HEMA reactive system, macrogelation occurred at the same time as the Trommosdorf effect. The reactive groups on the silica nanoparticles, which had a lower reactivity compared with that of the HEMA monomer, slowed down the mean radical polymerization rate of the filled reactive system. The reactions between the grafted groups of the neighboring silica particles led to the percolation, that is, macrogelation, of the reactive system at low conversion degree, even if the reactive system was kinetically at the stationary state. The reactive medium of the HEMA/grafted silica nanoparticles systems could be divided into two parts: the percolating nanoparticles part for which the polymerization rate was very slow and the bulk HEMA medium in which the radical polymerization rate was the same order of magnitude as for the neat HEMA.

8.9. Electrical Properties

Electrical properties of polymers include several electrical characteristics that are commonly associated with dielectric properties and conductivity properties. Electrical properties of nanofilled polymers are expected to be different when the fillers get to the nanoscale for several reasons. First, quantum effects begin to become important, because the electrical properties of nanoparticles can change compared with the bulk. Second, as the particle size decreases, the interparticle spacing decreases for the same volume fraction. Therefore, percolation can occur at lower volume fractions. In addition, the rate of resistivity decrease is lower than in micrometer-scale fillers. This is probably due to the large interfacial area and high interfacial resistance.[4a]

The incorporation of silica nanoparticles into PE by melt mixing increased the breakdown strength and voltage endurance significantly compared with the incorporation of micrometer scale fillers.[92] In addition, dielectric spectroscopy showed a decrease in dielectric permittivity for the nano-

composite over the base polymer. The most significant difference between micrometer scale and nanoscale fillers was the tremendous increase in interfacial area in nanocomposites. It suggested that the enhanced interfacial zone, in addition to particle−polymer bonding, played a very important role in determining the dielectric behavior of nanocomposites.

The electrical properties of UV-curable *co*-polyacrylate/silica nanocomposite resins prepared by the in situ sol−gel process were investigated.[299b] Experimental results revealed that the embedding of nanoscale silica particles in organic matrix effectively improved the electrical properties of resin samples. The intercalation of inorganic particles effectively inhibited the migration of charge carriers thus reducing the leakage current density of nanocomposite resin samples. Furthermore, friction was generated between the organic/inorganic functional groups such as $-O-CH_2CH_3$, −OH, and −Si−O−Si− groups capping silica nanoparticles and the *co*-polyacrylate chains. This restricted chain mobility and improved the dielectric properties of nanocomposite resin samples. It was found that, by an appropriate UV curing process and the formation of nanoscale silica particles finely dispersed in the resin matrix, the leakage current density of the nanocomposite resin films decreased from 235 to 1.3 $nA \cdot cm^{-2}$ at the applied electrical field of 10 $kV \cdot cm^{-1}$. Nanocomposite films with satisfactory dielectric properties (dielectric constant $\varepsilon = 3.93$ and tangent loss $\tan \delta = 0.0472$) could also be obtained.

It was shown by Wong et al.[268b] that the epoxy/silica nanocomposite had a higher dielectric loss at low frequency due to enhanced ionic conductivity caused by the contaminants from the sol−gel synthesized nanosized silica. The relaxation temperature of the nanocomposite was lower than those of the microcomposite and the blank resin due to the extra free volume at the filler−resin interface that assists the polymer mobility. The moisture had different dielectric loss effects on the pure epoxy and the epoxy composite, which could be explained by the combined effect of ionic conductivity and interfacial interaction in materials.

Dielectric measurements by Petrović et al.[277a] showed that although the nanosilica exhibited a stronger interaction with the matrix, there were no dramatic differences in the dielectric behavior between the two series of composites of PU/nanosilica and PU/microsilica.

It is reasonable that the conductivity of a conducting polymer/silica nanocomposite decreases with the increase of SiO_2 content. For example, the conductivity of poly-*N*-[5-(8-quinolinol)ylmethyl]aniline (PANQ)/nano-SiO_2 composite, which contained approximately 50% PANQ was 2.72×10^{-2} S cm^{-1} at 25 °C, which was reduced an order of magnitude in comparison with PANQ (0.122 S cm^{-1}).[432] The reasons were that the presence of nano-SiO_2 particles hindered the transport of carriers between different molecular chains of PANQ, and the interaction at the interface of PANQ macromolecules and nano-SiO_2 particles probably led to the reduction of the conjugation length of PANQ in PANQ/nano-SiO_2 composite. To increase the conductivity of the composites, silica should be coated completely with conductive polymer. The sunflower-like silica/PPy nanocomposites exhibited high conductivity of 8 S cm^{-1} at room temperature because of the special morphology of composites.[79]

Nanocomposites with improved conductivity were also reported. The dc conductivities of PNVC nanocomposite and the homopoly(*N*-vinylcarbazole) prepared in diethyl ether with $FeCl_3$ showed the following trend: PNVC nanocomposite (1.42×10^{-5} S/cm) > PNVC (10^{-10} S/cm).[434] The substantial increase in the bulk conductivity of the PNVC in the nanocomposite was noteworthy. Such enhancement in the conductivity was because the gluing of PNVC grains together with silica grains occurred, resulting in improved linkage between the PNVC particles, which was responsible for the manifestation of a higher conductivity for the nanocomposite, compared with that for unmodified PNVC. The electrical conductivity of the poly(2-chloroaniline) (P2ClAn) and P2ClAn/SiO_2 were described as 4.6×10^{-7} and 1.3×10^{-5} S cm^{-1}.[429] The conductivity of the P2ClAn/SiO_2 composite was higher than that of P2ClAn. The increase in conductivity would be due to the increase of efficiency of charge transfer between SiO_2 and polymer chains. SiO_2 might be increase protonation effect of polymer.

8.10. Other Characterization Techniques

The particle size distributions of the colloidal nanocomposites can be assessed using two techniques: dynamic light scattering (DLS) and disk centrifuge photosedimentometry (DCP). The former technique reports an intensity-average diameter (based on the Stokes−Einstein equation), and the latter reports a weight-average diameter. Given the different biases of these two techniques, it is expected that the DLS diameters would always exceed the DCP diameters.[403] The size of the nanocomposite particles can also be estimated from the microscopy diagrams.

X-ray photoelectron spectroscopy (XPS, also called electron spectroscopy for chemical analysis, ESCA) is a surface analytical technique for assessing surface compositions. The sample is placed under high vacuum and is bombarded with X-rays, which penetrate into the top layer of the sample (approximately nanometers) and excite electrons (referred to as photoelectrons). Some of these electrons from the upper layer are emitted from the sample and can be detected. The electron binding energy is dependent on the chemical environment of the atom, making XPS useful to identify the elemental composition of the surface region.[8b] XPS is especially suitable to assess the surface compositions of colloidal particles since its typical sampling depth is only 2−5 nm. The XPS data combined with TEM studies of the ultramicrotomed particles can shed further light on the particle morphology. Armes et al.[354] reported a detailed XPS study of the surface compositions of selected vinyl polymer/silica nanocomposites. Typical spectra are shown in Figure 34. Each nanocomposite was synthesized by (co)polymerizing 4VP in the presence of an ultrafine silica sol. Thus, N and Si were utilized as unique elemental markers for the (co)polymer and silica components, respectively, and the Si/N atomic ratios determined by XPS were used to assess the surface compositions of the particles. For all the homopoly(4VP)/silica nanocomposites examined, the XPS surface compositions were comparable to the bulk compositions determined by TGA and elemental microanalyses. This was consistent with the "currant-bun" particle morphologies observed by TEM and indicated that the silica particles were uniformly distributed throughout the nanocomposite particles. In contrast, the particle surface of a P(St-*co*-4VP)/silica nanocomposite was distinctly silica-rich, as judged by XPS; this suggested a core−shell morphology, with the silica component forming the shell and the hydrophobic copolymer forming the core. Both the "currant-bun" and core−shell particle morphologies were supported by TEM studies of nanocomposite particles sectioned using cryo-ultramicro-

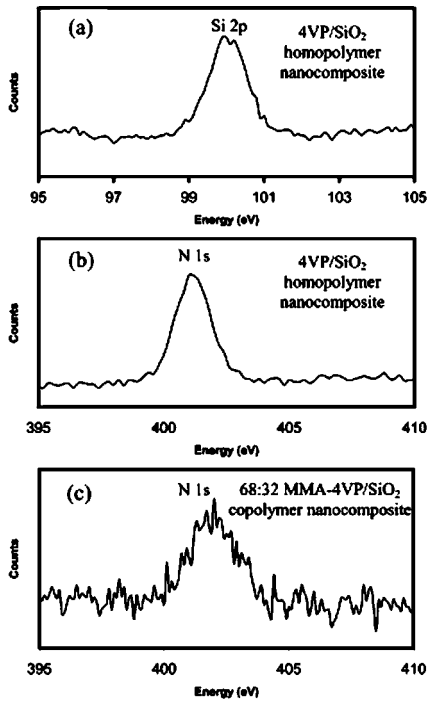

Figure 34. Typical XPS silicon and nitrogen core line spectra obtained for vinyl (co)polymer/silica nanocomposites: (a) Si 2p core line spectrum for a 4VP/SiO_2 homopolymer nanocomposite; (b) N 1s core line spectrum for a 4VP/SiO_2 homopolymer nanocomposite; (c) N 1s core line spectrum for a 68:32 MMA−4VP/SiO_2 copolymer nanocomposite. Reprinted with permission from Percy, M. J.; Amalvy, J. I.; Barthet, C.; Armes, S. P.; Greaves, S. J.; Watts, J. F.; Wiese, H. J. Mater. Chem. 2002, 12, 697. Copyright 2002 The Royal Society of Chemistry.

tomy. A P(MMA-*co*-4VP)/silica nanocomposite showed an XPS surface composition that was intermediate between those found for the "currant-bun" particles and the core−shell particles. In view of its relatively high silica content, a "raspberry" particle morphology was suggested. Finally, it was shown that, in the case of the P(MMA-*co*-4VP)/silica nanocomposite, it was possible to use the carbonyl carbon signal of the MMA residues as an unambiguous marker for the copolymer component; the surface composition obtained from this alternative analysis was consistent with that calculated using the nitrogen XPS signal. This approach may be particularly useful for assessing the surface compositions of nanocomposites containing a relatively low (or zero) proportion of 4VP comonomer.

Electrophoresis is the motion of dispersed particles relative to a fluid in a uniform electric field. Aqueous electrophoresis is also an ideal method to analyze the surface compositions of colloidal particles. The aqueous electrophoresis for a 4VP/SiO_2 nanocomposite, two MMA−4VP/SiO_2 nanocomposites, and also the original ultrafine silica sol were recorded, as shown in Figure 35.[385b] The ultrafine silica sol exhibited a negative ζ potential across the whole pH range, as expected. In contrast, the ζ potential curve for the 4VP/SiO_2 nanocomposite had a classic "S" shape, with an isoelectric point at approximately pH 6. This indicated that the basic 4VP residues were located at the surface of the nanocomposite particles and strongly influenced the electrophoretic response at low pH, where they were protonated and hence cationic. This hypothesis was also consistent with the electrophoretic data obtained for the two MMA−4VP/SiO_2 nanocomposites. The isoelectric points of them were both shifted to much lower pH, which reflected the reduced surface concentrations of the basic 4VP residues.

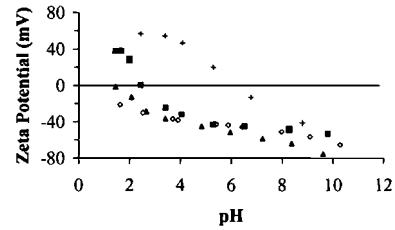

Figure 35. SiO_2 nanocomposite particles synthesized with increasing 4VP content. Data for the 20 nm silica sols are included as a comparison. Key: (◇) 20 nm Nyacol 2040 silica sol; (▲) 10 mol % 4VP; (■) 20 mol % 4VP; (+) 100 mol % 4VP. Reprinted with permission from ref 385b. Copyright 2000 American Chemical Society.

9. Applications

Since the polymer/silica nanocomposites not only can improve the physical properties such as the mechanical properties and thermal properties of the materials, but can also exhibit some unique properties, they have attracted strong interest in many industries. Besides common plastics and rubber reinforcement, many other potential and practical applications of this type of nanocomposite have been reported: coatings,[287–291,297,298,364,397] flame-retardant materials,[194,197,212,260] optical devices,[214,265] electronics and optical packaging materials,[268,448] photoresist materials,[294,402] photoluminescent conducting film,[430] pervaporation membrane,[69c,133] ultrapermeable reverse-selective membranes,[123] proton exchange membranes,[41,69e,134,135,188,226] grouting materials,[281] sensors,[304,426] materials for metal uptake,[415] etc. As for the colloidal polymer/silica nanocomposites with various morphologies, they usually exhibit enhanced, even novel, properties compared with the traditional nanocomposites and have many potential applications in various areas such as coatings, catalysis, and biotechnologies. Here, only a few applications will be presented, which are based on specific properties of the nanocomposites.

9.1. Coatings

In the past decade, scientists have paid attention to a new type of coating: hybrid organic/inorganic coatings. These coatings combine the flexibility and easy processing of polymers with the hardness of inorganic materials and have been successfully applied on various substrates. In general, these hybrid coatings are transparent, show a good adhesion, and enhance the scratch and abrasion resistance of a polymeric substrate.[290]

As described in secion 5.2, the reinforcement of acrylates by surface-modified nanosilica led to acrylate nanocomposite coatings with improved scratch and abrasion resistance. These coatings can be used on substrates such as polymer films, paper, metal, wood, and engineered wood.[287] In addition, compared with nanocomposite materials, a much better abrasion resistance was obtained for coatings containing both silica nanoparticles and corundum microparticles. These nano/microhybrid composites are recommended as clear coats for parquet and flooring applications.[288]

It was shown that polymer/silica nanocomposites can be obtained in a variety of structures and compositions by using miniemulsion polymerization.[397] The resulting hybrid structures are possibly interesting for the generation of waterborne

hybrid coatings, which show the ability of the polymer for spontaneous film formation in combination with a high mechanical scratch resistance provided by the inorganic nanoparticles.

9.2. Proton Exchange Membranes

The proton exchange membrane (PEM) is one of the major components in solid-type fuel cells, such as in the proton exchange membrane fuel cell (PEMFC) and the direct methanol fuel cells (DMFC). Up to now, a large number of research groups have reported the fabrication of polymer/silica nanocomposites as PEM.

Sulfonated poly(phthalazinone ether ketone) (sPPEK) with a degree of sulfonation of 1.23 was mixed with silica nanoparticles to form hybrid materials for use as PEMs.[134] The hybrid membranes exhibited improved swelling behavior, thermal stability, and mechanical properties. The methanol crossover behavior of the membrane was also depressed such that these membranes were suitable for a high methanol concentration in the feed in a cell test. The membrane with 5 phr silica nanoparticles showed an open cell potential of 0.6 V and an optimum power density of 52.9 mW cm^{-2} at a current density of 264.6 mA cm^{-2}, which was better than the performance of the pristine sPPEK membrane and Nafion 117.

Sulfonated P(St-*co*-MA)−PEG/silica nanocomposite polyelectrolyte membranes were prepared with varied silica content using PEG of different molecular weights to have a fine control over spacing between silica domains, up to a few nanometers by chemically bound interior polymer chain.[188] These membranes were extensively characterized for DMFC applications. Although these nanocomposite polyelectrolyte membranes offered no significant advantages over Nafion 117 membrane as far as ion-exchange capacity and proton conductivity were concerned, the comparable activation energy needed for proton transport, current−voltage polarization characteristics, and relatively lower methanol permeability of these membranes in comparison to Nafion 117 membrane made them applicable to DMFC. Moreover, this system showed clear improvement over the Nafion membrane as seen by selectivity parameter values, due to low methanol permeability at temperatures of 30 and 70 °C, while Nafion showed almost the same selectivity parameter values at both temperatures. Relatively high selectivity parameter values at 70 °C of these membranes indicated a great advantage for the composite over Nafion 117 membranes for targeting higher temperature applications.

9.3. Pervaporation Membranes

In the pervaporation separation process, a liquid mixture is brought in direct contact with the feed side of the membrane, and the permeate is removed as vapor from the other side of the membrane. The mass flux is driven by maintaining the downstream partial pressure below the saturation pressure of the liquid feed solution. The transport of liquids through the membranes differs from other membrane processes such as gas separation, because the permeants in pervaporation usually show high solubility in polymeric membranes. The effects of silica and silane-modified silica fillers on the pervaporation properties of PPO dense membranes have been studied.[133] Pervaporation separation of methanol/methyl *tert*-butyl ether (MTBE) mixtures over the entire range of concentration was carried out using both filled and unfilled membranes. Compared with the unfilled PPO membrane, the filled PPO membranes exhibited higher methanol selectivity and lower permeability. For methanol concentration in liquid feed mixture lower than 50 wt %, methanol selectivity of the filled PPO membranes with silane-modified silica was better than that of the silica-filled and unfilled PPO membranes. The modified silica nanoparticles had stronger affinity and enhanced compatibility with PPO polymer than the unmodified silica nanoparticles. This generated more tortuous pathways in PPO dense membrane matrix, reduced the diffusion of both methanol and MTBE, and consequently the pervaporation permeation flux decreased.

9.4. Encapsulation of Organic Light-Emitting Devices

Direct encapsulation of organic light-emitting devices (OLEDs) is realized by using highly transparent, photocurable *co*-polyacrylate/silica nanocomposite resin. The feasibility of such a resin for OLED encapsulation was evaluated by physical/electrical property analysis of resins and driving voltage/luminance/lifetime measurement of OLEDs.[299c] Electrical property analysis revealed a higher electrical insulation of photocured nanocomposite resin film at 3.20×10^{12} Ω in comparison with that of oligomer film at 1.18×10^{12} Ω at 6.15 V to drive the bare OLED. This resulted in a lower leakage current, and the device driving voltage was efficiently reduced so that the nanocomposite-encapsulated OLED could be driven at a lower driving voltage of 6.09 V rather than 6.77 V for the oligomer-encapsulated OLED at the current density of 20 mA/cm^2. Luminance measurements revealed a less than 1.0% luminance difference of OLEDs encapsulated by various types of resins, which indicated that the photopolymerization took very little effect on the light-emitting property of OLEDs. Lifetime measurement of OLEDs found that t_{80}, the time span for the normalized luminance of device drops to 80%, for nanocomposite-encapsulated OLED was 350.17 h in contrast to 16.83 h for bare OLED and 178.17 h for the oligomer-encapsulated OLED. This demonstrated that nanocomposite resin with optimum properties was feasible for OLED packaging and a compact device structure could be achieved via the method of direct encapsulation.

9.5. Chemosensors

An approach for preparing polydiacetylene/silica nanocomposite for use as a chemosensor was reported.[304] The disordered 10,12-pentacosadiynoic acid (PCDA) aggregates could absorb on the surfaces of silica nanoparticles in aqueous solution. The disordered PCDA molecules in aggregates were turned into an ordered arrangement with the help of a silica nanoparticle template. After irradiation with UV light, polydiacetylene/silica nanocomposites took on a blue color. A variety of environmental perturbations, such as temperature, pH, and amphiphilic molecules, could result in a colorimetric change of the polydiacetylene/silica nanocomposites from the blue to the red phase. The material may find some interesting potential applications as a new chemosensor.

9.6. Metal Uptake

The nanocomposites of electroactive polymers PANI or PPy with ultrafine SiO_2 particles have potential commercial applications for metal uptake based on the fact that they possess a surface area substantially higher than that estimated from the particle size and hence can aid the process of metal uptake. The use of electroactive polymer/SiO_2 nanocomposites for the uptake of gold and palladium from $AuCl_3$ and $PdCl_2$ in acid solutions, respectively, was investigated.[415] In the case of gold uptake, the reaction rate increased with temperature from 0 to 60 °C. The accumulation of elemental gold on the nanocomposites increased the diameter and decreased the surface area. The surface Au/N ratio as determined using XPS was highly dependent on the rate of reactions even for the same amount of gold uptake. The uptake of palladium from $PdCl_2$ was much more difficult to accomplish. High rates of uptake could only be achieved with the electroactive polymers reduced to their lowest oxidation state, and unlike the case of gold uptake, the palladium on the microparticles did not exist in the elemental form but as a Pd(II) compound.

10. Summary and Outlook

Currently, an increasing amount of work is being published on polymer/silica nanocomposites. The recent developments on the preparation, characterization, properties, and application of this type of nanocomposite have been reviewed. Principally, three methods for the preparation of polymer/silica nanocomposites can be used, blending, the sol−gel process, and in situ polymerization. All the three methods have been investigated extensively. Moreover, colloidal polymer/silica nanocomposites, which represent a new category of polymer/silica nanocomposites, have attracted growing interest in recent years.

Apart from the properties of individual components in a nanocomposite, the degree of dispersion of nanoparticles in the polymer and the interfacial interaction play important roles in enhancing or limiting the overall properties of the system. Some trends are observed but no universal patterns for the behavior of polymer nanocomposites can be deduced in general.[10] The properties of polymer/silica nanocomposites, however, are generally superior to the pure polymer matrix and polymer microcomposites. In particular, they commonly exhibit improved mechanical properties and thermal stability regardless of the preparative method.

"It's all interface" refers to the large volume fraction of interfacial polymer compared with the volume fraction of filler. By taking advantage of this large interfacial area and interfacial volume, unique combinations of properties of polymer nanocomposites can be achieved.[4c] Although much work has already been done on various aspects of polymer/silica nanocomposites, more research is required in order to further understand the complex structure−property relationships. Tailoring the interfacial interaction of filler/matrix is conducive to a better understanding of the relationships.

11. Abbreviations

AFM	atomic force microscopy
AGE	allylglycidylether
AIBA	2,2′-azobis(2-amidinopropane)dihydrochloride
AIBN	2,2′-azobis(isobutyronitrile)
AN	acrylonitrile
APS	ammonium peroxodisulfate
BA	butyl acrylate
BMA	butyl methacrylate
CTAB	cetyl trimethylammonium bromide
CTE	coefficient of thermal expansion
DGEBA	diglycidyl ether of bisphenol A
DM(T)A	dynamic mechanical (thermal) analysis
DMAc	*N*,*N*-dimethylacetamide
DMF	*N*,*N*-dimethylformamide
DSC	differential scanning calorimetry
DTA	differential thermal analysis
EA	ethyl acrylate
EDX	energy-dispersive X-ray spectroscopy
ESI	electron spectroscopy imaging
FS	fumed silica
FTIR	Fourier transform infrared
GMA	glycidylmethacrylate
HEMA	2-hydroxyethylmethacrylate
HPMA	2-hydroxypropyl methacrylate
IPN	interpenetrating networks
KPS	potassium peroxodisulfate
LCP	liquid crystalline polymer
LOI	limiting oxygen index
MA	maleic anhydride
MEK	methylethyl ketone
MIBK	methylisobutyl ketone
MMA	methyl methacrylate
NMP	*N*-methyl-2-pyrrolidinone
NMR	nuclear magnetic resonance
P ∼	poly ∼
PA	polyamide
PAA	poly(amic acid)
PAAm	polyacrylamide
PALS	positron annihilation lifetime spectroscopy
PAI	poly(amide imide)
PANI	polyaniline
PC	polycarbonate
PCL	poly(ε-caprolactone)
PDMS	poly(dimethylsiloxane)
PE	polyethylene
PEDOT	poly(3,4-ethylenedioxythiophene)
PEEK	polyetheretherketone
PEG	poly(ethylene glycol)
PEN	poly(ethylene 2,6-naphthalate)
PEO	poly(ethylene oxide)
PES	poly(ether sulfone)
PET	poly(ethylene terephthalate)
PHPS	perhydropolysilazan
PI	polyimide
PMMA	poly(methyl methacrylate)
PNVC	poly(*N*-vinylcarbazole)
PP	polypropylene
PPO	poly(phenylene oxide)
PPy	polypyrrole
PS	polystyrene
PSF	polysulfone
PT	polythiophene
PVA	poly(vinyl alcohol)
PVP	poly(vinyl pyrrolidone)
PU	polyurethane
SANS	small-angle neutron scattering
SAXS	small-angle X-ray scattering
SEM	scanning electron microscope
St	styrene
TEM	transmission electron microscope
TEOS	tetraethyloxysilane
TGA	thermogravimetric analysis
THF	tetrahydrofuran
TMA	thermomechanical analysis
TMOS	tetramethoxysilane
TPO	thermoplastic olefin
2VP	2-vinylpyridine

4VP	4-vinylpyridine
WAXD	wide-angle X-ray diffraction
WAXS	wide-angle X-ray scattering
XPS	X-ray photoelectron spectroscopy
XRD	X-ray diffraction

12. Acknowledgments

The authors are grateful to a number of friends and coworkers, in particular Juan Zhou (University of Bristol), Shushan Deng (Nanjing University), Qianping Ran (Jiangsu Institute of Building Science) Hanqing Ge (Nanjing University of Technology), Xin Li (Jiaying University), Juqing Cui (Nanjing Forestry University), and Kaihe Du (Nanjing Normal University) for their great help in the preparation of this review. We also thank Samantha Lord, Rodrigo Sanchez, Nisha Doshi, and Kevin Mutch (all from University of Bristol) for the critical reading of the manuscript. Finally, we are indebted to the anonymous manuscript reviewers for their valuable comments in the revision of the manuscript.

13. References

(1) Balazs, A. C.; Emrick, T.; Russell, T. P. *Science* **2006**, *314*, 1107.
(2) (a) Winey, K. I.; Vaia, R. A. *MRS Bull.* **2007**, *32*, 314. (b) Krishnamoorti, R.; Vaia, R. A. *J. Polym. Sci., Part B: Polym. Phys.* **2007**, *45*, 3252.
(3) (a) Caseri, W. In *Encyclopedia of Nanoscience and Nanotechnology*; Nalwa, H. S., Ed.; American Scientific Publishers: Stevenson Ranch, CA, 2004; Vol *6*, pp 235−247. (b) Caseri, W. R. *Mater. Sci. Technol.* **2006**, *22*, 807. (c) Caseri, W. In *Hybrid Materials. Synthesis, Characterization, and Applications*; Kickelbick, G., Ed.; Wiley-VCH: Weinheim, Germany, 2007; Chapter 2.
(4) (a) Schadler, L. S. *Nanocomposite Science and Technology*; Wiley-VCH: Weinheim, Germany, 2003; Chapter 2. (b) Schadler, L. S.; Kumar, S. K.; Benicewicz, B. C.; Lewis, S. L.; Harton, S. E. *MRS Bull.* **2007**, *32*, 335. (c) Schadler, L. S.; Brinson, L. C.; Sawyer, W. G. *JOM* **2007**, *59*, 53.
(5) Schaefer, D. W.; Justice, R. S. *Macromolecules* **2007**, *40*, 8501.
(6) Hajji, P.; David, L.; Gerard, J. F.; Pascault, J. P.; Vigier, G. *J. Polym. Sci., Part B: Polym. Phys.* **1999**, *37*, 3172.
(7) Althues, H.; Henle, J.; Kaskel, S. *Chem. Soc. Rev.* **2007**, *36*, 1454.
(8) (a) Kickelbick, G. *Prog. Polym. Sci.* **2003**, *28*, 83. (b) Kickelbick, G. In *Hybrid Materials. Synthesis, Characterization, and Applications*; Kickelbick, G., Ed.; Wiley-VCH: Weinheim, Germany, 2007; Chapter 1.
(9) Schmidt, G.; Malwitz, M. M. *Curr. Opin. Colloid Interface Sci.* **2003**, *8*, 103.
(10) Jordan, J.; Jacob, K. I.; Tannenbaum, R.; Sharaf, M. A.; Jasiuk, I. *Mater. Sci. Eng., A* **2005**, *393*, 1.
(11) Tjong, S. C. *Mater. Sci Eng., R* **2006**, *53*, 73.
(12) Cong, H. L.; Radosz, M.; Towler, B. F.; Shen, Y. Q. *Sep. Purif. Technol.* **2007**, *55*, 281.
(13) (a) Zhang, M. Q.; Rong, M. Z.; Friedrich, K. In *Handbook of Organic-Inorganic Hybrid Materials and Nanocomposites*; Nalwa, H. S., Ed.; Ameican Scientific Publishers: Stevenson Ranch, CA, 2003; Vol *2*, pp 113−150. (b) Rong, M. Z.; Zhang, M. Q.; Ruan, W. H. *Mater. Sci. Technol.* **2006**, *22*, 787.
(14) Novak, B. M. *Adv. Mater.* **1993**, *5*, 422.
(15) (a) Sanchez, C.; Ribot, R. *New. J. Chem.* **1994**, *18*, 1007. (b) Sanchez, C.; Julián, B.; Belleville, P.; Popall, M. *J. Mater. Chem.* **2005**, *15*, 3559. (c) Mammeri, F.; Le Bourhis, E.; Rozes, L.; Sanchez, C. *J. Mater. Chem.* **2005**, *15*, 3787.
(16) Schubert, U.; Hüsing, N.; Lorenz, A. *Chem. Mater.* **1995**, *7*, 2010.
(17) Judeinstein, P.; Sanchez, C. *J. Mater. Chem.* **1996**, *6*, 511.
(18) Wen, J. Y.; Wilkes, G. L. *Chem. Mater.* **1996**, *8*, 1667.
(19) Pomogailo, A. D. *Russ. Chem. Rev.* **2000**, *69*, 53.
(20) Schottner, G. *Chem. Mater.* **2001**, *13*, 3422.
(21) *Polymer Brushes*; Advincula, R. C., Brittain, W. J., Caster, K. C., Rühe, J., Eds; Wiley-VCH: Weinheim, Germany, 2004.
(22) (a) Pyun, J.; Matyjaszewski, K. *Chem. Mater.* **2001**, *13*, 3436. (b) Pyun, J.; Kowalewski, T.; Matyjaszewski, K. *Macromol. Rapid Commun.* **2003**, *24*, 1043.
(23) (a) Advincula, R. C. *J. Dispersion Sci. Technol.* **2003**, *24*, 343. (b) Advincula, R. C. In *Encyclopedia of Polymer Science and Technology*; Kroschwitz, J. I., Ed.; John Wiley & Sons: Hoboken, NJ, 2004; Vol *11*, pp 114−134. (c) Advincula, R. *Adv. Polym. Sci.* **2006**, *197*, 107.
(24) Edmondson, S.; Osborne, V. L.; Huck, W. T. S. *Chem. Soc. Rev.* **2004**, *33*, 14.
(25) Radhakrishnan, B.; Ranjan, R.; Brittain, W. J. *Soft Matter* **2006**, *2*, 386.
(26) Ghannam, L.; Parvole, J.; Laruelle, G.; Francois, J.; Billon, L. *Polym. Int.* **2006**, *55*, 1199.
(27) Tsujii, Y.; Ohno, K.; Yamamoto, S.; Goto, A.; Fukuda, T. *Adv. Polym. Sci.* **2006**, *197*, 1.
(28) Buchmeiser, M. R. *Adv. Polym. Sci.* **2006**, *197*, 137.
(29) Caruso, F. *Adv. Mater.* **2001**, *13*, 11.
(30) (a) Xia, Y. N.; Gates, B.; Yin, Y. D.; Lu, Y. *Adv. Mater.* **2000**, *12*, 693. (b) Jeong, U.; Wang, Y. L.; Ibisate, M.; Xia, Y. N. *Adv. Funct. Mater.* **2005**, *15*, 1907.
(31) Castelvetro, V.; De Vita, C. *Adv. Colloid Interface Sci.* **2004**, *108*−*109*, 167.
(32) (a) Bourgeat-Lami, E. *J. Nanosci. Nanotechnol.* **2002**, *2*, 1. (b) Bourgeat-Lami, E. In *Encyclopedia of Nanoscience and Nanotechnology*; Nalwa, H. S., Ed.; American Scientific Publishers: Stevenson Ranch, CA, 2004; Vol *8*, pp 305−332. (c) Bourgeat-Lami, E.; Duguet, E. In *Functional Coatings*; Ghosh, S. K., Ed.; Wiley-VCH: Weinheim, Germany, 2006; Chapter 4. (d) Bourgeat-Lami, E., In *Hybrid Materials. Synthesis, Characterization, and Applications*; Kickelbick, G., Ed.; Wiley-VCH: Weinheim, Germany, 2007; Chapter 3.
(33) Kickelbick, G.; Liz-Marźan, L. M. In *Encyclopedia of Nanoscience and Nanotechnology*; Nalwa, H. S., Ed.; American Scientific Publishers: Stevenson Ranch, CA, 2004; Vol *2*, pp 199−220.
(34) Caruso, R. A.; Antonietti, M. *Chem. Mater.* **2001**, *13*, 3272.
(35) (a) Gangopadhyay, R.; De, A. *Chem. Mater.* **2000**, *12*, 608. (b) Gangopadhyay, R.; De, A. In *Handbook of Organic-Inorganic Hybrid Materials and Nanocomposites*; Nalwa, H. S., Ed.; American Scientific Publishers: Stevenson Ranch, CA, 2003; Vol *2*, pp 217−267.
(36) Jang, J. *Adv. Polym. Sci.* **2006**, *199*, 189.
(37) McCaughey, B.; Hampsey, J. E.; Wang, D. H.; Lu, Y. F. In *Encyclopedia of Nanoscience and Nanotechnology*; Nalwa, H. S., Ed.; American Scientific Publishers: Stevenson Ranch, CA, 2004; Vol *9*, pp 529−559.
(38) Hsiue, G. H.; Kuo, W. J.; Huang, Y. P.; Jeng, R. J. *Polymer* **2000**, *41*, 2813.
(39) Liu, Y. L.; Wu, C. S.; Chiu, Y. S.; Ho, W. H. *J. Polym. Sci., Part A: Polym. Chem.* **2003**, *41*, 2354.
(40) (a) Honma, I.; Hirakawa, S.; Yamada, K.; Bae, J. M. *Solid State Ionics* **1999**, *118*, 29. (b) Honma, I.; Takeda, Y.; Bae, J. M. *Solid State Ionics* **1999**, *120*, 225. (c) Honma, I.; Nomura, S.; Nakajima, H. *J. Membr. Sci.* **2001**, *185*, 83.
(41) (a) Chang, H. Y.; Lin, C. W. *J. Membr. Sci.* **2003**, *218*, 295. (b) Chang, H. Y.; Thangamuthu, R.; Lin, C. W. *J. Membr. Sci.* **2004**, *228*, 217.
(42) (a) Wu, C. M.; Xu, T. W.; Yang, W. H. *Eur. Polym. J.* **2005**, *41*, 1901. (b) Zhang, S. L.; Xu, T. W.; Wu, C. M. *J. Membr. Sci.* **2006**, *269*, 142.
(43) (a) Saito, R.; Kuwano, K.; Tobe, T. *J. Macromol. Sci., Pure Appl. Chem* **2002**, *A39*, 171. (b) Saito, R.; Mori, Y. *J. Macromol. Sci., Pure Appl. Chem.* **2002**, *A39*, 915. (c) Mori, Y.; Saito, R. *J. Macromol. Sci., Pure Appl. Chem.* **2003**, *A40*, 671. (d) Mori, Y.; Saito, R. *Polymer* **2004**, *45*, 95. (e) Saito, R.; Tobe, T. *J. Appl. Polym. Sci.* **2004**, *93*, 749. (f) Saito, R.; Tobe, T. *Polym. Adv. Technol.* **2005**, *16*, 232. (g) Saito, R.; Kobayashi, S. I.; Hosoya, T. *J. Appl. Polym. Sci.* **2005**, *97*, 1835. (h) Saito, R. *J. Polym. Sci., Part A: Polym. Chem.* **2006**, *44*, 5174. (i) Saito, R.; Kobayashi, S. I.; Hayashi, H.; Shimo, T. *J. Appl. Polym. Sci.* **2007**, *104*, 3338.
(44) (a) Wang, H. T.; Zhong, W.; Du, Q. G.; Yang, Y. L.; Okamoto, H.; Inoue, S. *Polym. Bull.* **2003**, *51*, 63. (b) Wang, H. T.; Zhong, W.; Xu, P.; Du, Q. G. *Macromol. Mater. Eng.* **2004**, *289*, 793. (c) Shen, L.; Zhong, W.; Wang, H. T.; Du, Q. G.; Yang, Y. L. J. *Appl. Polym. Sci.* **2004**, *93*, 2289. (d) Shen, L.; Du, Q. G.; Wang, H. T.; Zhong, W.; Yang, Y. L. *Polym. Int.* **2004**, *53*, 1153.
(45) Cornelissen, J. J. L. M.; Connor, E. F.; Kim, H. C.; Lee, V. Y.; Magibitang, T.; Rice, P. M.; Volksen, W.; Sundberg, L. K.; Miller, R. D. *Chem. Commun.* **2003**, 1010.
(46) Ding, X. F.; Jiang, Y. Q.; Yu, K. F.; Hari-Bala; Tao, N. N.; Zhao, J. Z.; Wang, Z. C. *Mater. Lett.* **2004**, *58*, 1722.
(47) Laugel, N.; Hemmerlé, J.; Porcel, C.; Voegel, J. C.; Schaaf, P.; Ball, V. *Langmuir* **2007**, *23*, 3706.
(48) Senkevich, J. J.; Desu, S. B. *Chem. Mater.* **1999**, *11*, 1814.
(49) Suffner, J.; Schechner, G.; Sieger, H.; Hahn, H. *Chem. Vap. Deposition* **2007**, *13*, 459.
(50) Grund, S.; Kempe, P.; Baumann, G.; Seifert, A.; Spange, S. *Angew. Chem., Int. Ed.* **2007**, *46*, 628.
(51) Darbandi, M.; Thomann, R.; Nann, T. *Chem. Mater.* **2007**, *19*, 1700.
(52) Stöber, W.; Fink, A.; Bohn, E. *J. Colloid Interface Sci.* **1968**, *26*, 62.

(53) Kolbe, G. Ph.D. Thesis, Friedrich-Schiller-Universität Jena, Germany, 1956.
(54) van Helden, A. K.; Jansen, J. W.; Vrij, A. *J. Colloid Interface Sci.* **1981**, *81*, 354.
(55) (a) Philipse, A. P. *Colloid Polym. Sci.* **1988**, *266*, 1174. (b) Philipse, A. P.; Vrij, A. *J. Colloid Interface Sci.* **1988**, *128*, 121.
(56) (a) Bogush, G. H.; Tracy, M. A.; Zukoski, C. F., IV *J. Non-Cryst. Solids* **1988**, *104*, 95. (b) Bogush, G. H.; Zukoski, C. F., IV *J. Colloid Interface Sci.* **1991**, *142*, 1. (c) Bogush, G. H.; Zukoski, C. F., IV *J. Colloid Interface Sci.* **1991**, *142*, 19.
(57) (a) van Blaaderen, A.; van Geest, J.; Vrij, A. *J. Colloid Interface Sci.* **1992**, *154*, 481. (b) van Blaaderen, A.; Vrij, A. *Langmuir* **1992**, *8*, 2921. (c) van Blaaderen, A.; Vrij, A. J. *Colloid Interface Sci.* **1993**, *156*, 1.
(58) Iler, R. K. *The Chemistry of Silica*; Wiley: New York, 1979.
(59) Kim, H. C.; Dubois, G. *Dekker Encyclopedia of Nanoscience and Nanotechnology*; Taylor & Francis: New York, 2005; pp 1−10.
(60) Osseo-Asare, K.; Arriagada, F. J. *Colloids Surf.* **1990**, *50*, 321.
(61) Vassiliou, A. A.; Papageorgiou, G. Z.; Achilias, D. S.; Bikiaris, D. N. *Macromol. Chem. Phys.* **2007**, *208*, 364.
(62) Kim, S. H.; Ahn, S. H.; Hirai, T. *Polymer* **2003**, *44*, 5625.
(63) Wu, C. L.; Zhang, M. Q.; Rong, M. Z.; Friedrich, K. *Compos. Sci. Technol.* **2005**, *65*, 635.
(64) Jana, S. C.; Jain, S. *Polymer* **2001**, *42*, 6897.
(65) Blum, F. D. In *Encyclopedia of Polymer Science and Technology*; Kroschwitz, J. I., Ed.; John Wiley & Sons: Hoboken, NJ, 2004; Vol *8*, pp 38−50.
(66) (a) Yoshinaga, K.; Shimada, J.; Nishida, H.; Komatsu, M. *J. Colloid Interface Sci.* **1999**, *214*, 180. (b) Yoshinaga, K.; Tani, Y.; Tanaka, Y. *Colloid Polym. Sci.* **2002**, *280*, 85.
(67) Kang, S.; Hong, S. I.; Choe, C. R.; Park, M.; Rim, S.; Kim, J. *Polymer* **2001**, *42*, 879.
(68) Sugimoto, H.; Daimatsu, K.; Nakanishi, E.; Ogasawara, Y.; Yasumura, T.; Inomata, K. *Polymer* **2006**, *47*, 3754.
(69) (a) Liu, Y. L.; Hsu, C. Y.; Wang, M. L.; Chen, H. S. *Nanotechnology* **2003**, *14*, 813. (b) Liu, Y. L.; Hsu, C. Y.; Hsu, K. Y. *Polymer* **2005**, *46*, 1851. (c) Liu, Y.L.; Hsu, C. Y.; Su, Y. H.; Lai, J. Y. *Biomacromolecules* **2005**, *6*, 368. (d) Su, Y. H.; Wei, T. Y.; Hsu, C. H.; Liu, Y. L.; Sun, Y. M.; Lai, J. Y. *Desalination* **2006**, *200*, 656. (e) Su, Y. H.; Liu, Y. L.; Sun, Y. M.; Lai, J. Y.; Wang, D. M.; Gao, Y.; Liu, B. J.; Guiver, M. D. *J. Membr. Sci.* **2007**, *296*, 21.
(70) Moncada, E.; Quijada, R.; Retuert, J. *Nanotechnology* **2007**, *18*, 335606.
(71) (a) Rong, M. Z.; Zhang, M. Q.; Zheng, Y. X.; Zeng, H. M.; Walter, R.; Friedrich, K. *J. Mater. Sci. Lett.* **2000**, *19*, 1159. (b) Rong, M. Z.; Zhang, M. Q.; Zheng, Y. X.; Zeng, H. M.; Walter, R.; Friedrich, K. *Polymer* **2001**, *42*, 167. (c) Zhang, M. Q.; Rong, M. Z.; Zeng, H. M.; Schmitt, S.; Wetzel, B.; Friedrich, K. *J. Appl. Polym. Sci.* **2001**, *80*, 2218. (d) Rong, M. Z.; Zhang, M. Q.; Zheng, Y. X.; Zeng, H. M.; Friedrich, K. *Polymer* **2001**, *42*, 3301. (e) Wu, C. L.; Zhang, M. Q.; Rong, M. Z.; Lehmann, B.; Friedrich, K. *Polym. Polym. Compos.* **2003**, *11*, 559. (f) Ruan, W. H.; Zhang, M. Q.; Rong, M. Z.; Friedrich, K. *J. Mater. Sci.* **2004**, *39*, 3475. (g) Rong, M. Z.; Zhang, M. Q.; Pan, S. L.; Lehmann, B.; Friedrich, K. *Polym. Int.* **2004**, *53*, 176. (h) Rong, M. Z.; Zhang, M. Q.; Pan, S. L.; Friedrich, K. *J. Appl. Polym. Sci.* **2004**, *92*, 1771. (i) Ruan, W. H.; Huang, X. B.; Wang, X. H.; Rong, M. Z.; Zhang, M. Q. *Macromol. Rapid Commun.* **2005**, *27*, 581. (j) Ruan, W. H.; Mai, Y. L.; Wang, X. H.; Rong, M. Z.; Zhang, M. Q. *Compos. Sci. Technol.* **2007**, *67*, 2747. (k) Wu, C. L.; Zhang, M. Q.; Rong, M. Z.; Friedrich, K. *Compos. Sci. Technol.* **2002**, *62*, 1327. (l) Cai, L. F.; Huang, X. B.; Rong, M. Z.; Ruan, W. H.; Zhang, M. Q. *Polymer* **2006**, *47*, 7043. (m) Cai, L. F.; Huang, X. B.; Rong, M. Z.; Ruan, W. H.; Zhang, M. Q. *Macromol. Chem. Phys.* **2006**, *207*, 2093. (n) Zhang, M. Q.; Rong, M. Z.; Zhang, H. B.; Friedrich, K. *Polym. Eng. Sci.* **2003**, *43*, 490.
(72) Wu, T. M.; Chu, M. S. *J. Appl. Polym. Sci.* **2005**, *98*, 2058.
(73) Ahn, S. H.; Kim, S. H.; Lee, S. G. *J. Appl. Polym. Sci.* **2004**, *94*, 812.
(74) Lai, Y. H.; Kuo, M. C.; Huang, J. C.; Chen, M. *Mater. Sci. Eng., A* **2007**, *458*, 158.
(75) (a) Ding, X. F.; Zhao, J. Z.; Liu, Y. H.; Zhang, H. B.; Wang, Z. C. *Mater. Lett.* **2004**, *58*, 3126. (b) Ding, X. F.; Wang, Z. C.; Han, D. X.; Zhang, Y. J.; Shen, Y. F.; Wang, Z. J.; Niu, L. *Nanotechnology* **2006**, *17*, 4796.
(76) Mahdavian, A. R.; Ashjari, M.; Makoo, A. B. *Eur. Polym. J.* **2007**, *43*, 336.
(77) (a) Tang, J. C.; Lin, G. L.; Yang, H. C.; Jiang, G. J.; Chen-Yang, Y. W. *J. Appl. Polym. Sci.* **2007**, *104*, 4096. (b) Tang, J. C.; Yang, H. C.; Chen, S. Y.; Chen-Yang, Y. W. *Polym. Compos.* **2007**, *28*, 575.
(78) (a) Reculusa, S.; Poncet-Legrand, C.; Ravaine, S.; Mingotaud, C.; Duguet, E.; Bourgeat-Lami, E. *Chem. Mater.* **2002**, *14*, 2354. (b) Reculusa, S.; Poncet-Legrand, C.; Perro, A.; Duguet, E.; Bourgeat-Lami, E.; Mingotaud, S.; Ravaine, S. *Chem. Mater.* **2005**, *17*, 3338. (c) Perro, A.; Reculusa, S.; Bourgeat-Lami, E.; Duguet, E.; Ravaine, S. *Colloids Surf., A* **2006**, *284*, 78.
(79) Yang, X. M.; Dai, T. Y.; Lu, Y. *Polymer* **2006**, *47*, 441.
(80) (a) Bikiaris, D. N.; Papageorgiou, G. Z.; Pavlidou, E.; Vouroutzis, N.; Palatzoglou, P.; Karayannidis, G. P. *J. Appl. Polym. Sci.* **2006**, *100*, 2684. (b) Papageorgiou, G. Z.; Achilias, D. S.; Bikiaris, D. N.; Karayannidis, G. P. *Thermochim. Acta* **2005**, *427*, 117. (c) Bikiaris, D. N.; Vassiliou, A.; Pavlidou, E.; Karayannidis, G. P. *Eur. Polym. J.* **2005**, *41*, 1965. (d) Vladimirov, V.; Betchev, C.; Vassiliou, A.; Papageorgiou, G.; Bikiaris, D. *Compos. Sci. Technol.* **2006**, *66*, 2935. (e) Vassiliou, A.; Bikiaris, D.; Pavlidou, E. *Macromol. React. Eng.* **2007**, *1*, 488.
(81) García, M.; van Vliet, G.; Jain, S.; Schrauwen, B. A. G.; Sarkissov, A.; van Zyl, W. E.; Boukamp, B. *Rev. Adv. Mater. Sci.* **2004**, *6*, 169.
(82) (a) Asuka, K.; Liu, B. P.; Terano, M.; Nitta, K. H. *Macromol. Rapid Commun.* **2006**, *27*, 910. (b) Nitta, K.; Asuka, K.; Liu, B. P.; Terano, M. *Polymer* **2006**, *47*, 6457.
(83) Qian, J. S.; He, P. S.; Nie, K. M. *J. Appl. Polym. Sci.* **2004**, *91*, 1013.
(84) Huang, L.; Zhan, R. B.; Lu, Y. F. *J. Reinf. Plast. Compos.* **2006**, *25*, 1001.
(85) Zhou, T. H.; Ruan, W. H.; Yang, J. L.; Rong, M. Z.; Zhang, M. Q.; Zhang, Z. *Compos. Sci. Technol.* **2007**, *67*, 2297.
(86) Rottstegge, J.; Zhang, X.; Zhou, Y.; Xu, D.; Han, C. C.; Wang, D. *J. Appl. Polym. Sci.* **2007**, *103*, 218.
(87) Reddy, C. S.; Das, C. K. *J. Appl. Polym. Sci.* **2006**, *102*, 2117.
(88) Reddy, C. S.; Das, C. K.; Narkis, M. *Polym. Compos.* **2005**, *26*, 806.
(89) Reddy, C. S.; Das, C. K. *Compos. Interfaces* **2005**, *11*, 687.
(90) Huang, Y. Q.; Jiang, S. L.; Wu, L. B.; Hua, Y. Q. *Polym. Test.* **2004**, *23*, 9.
(91) Kontou, E.; Niaounakis, M. *Polymer* **2006**, *47*, 1267.
(92) Roy, M.; Nelson, J. K.; MacCrone, R. K.; Schadler, L. S.; Reed, C. W.; Keefe, R.; Zenger, W. *IEEE Trans. Dielectr. Electr. Insul.* **2005**, *12*, 629.
(93) Gao, X. W.; Hu, G. J.; Qian, Z. Z.; Ding, Y. F.; Zhang, S. M.; Wang, D. J.; Yang, M. S. *Polymer* **2007**, *48*, 7309.
(94) Lee, J. A.; Kontopoulou, M.; Parent, J. S. *Polymer* **2005**, *46*, 5040.
(95) Tanahashi, M.; Hirose, M.; Lee, J. C.; Takeda, K. *Polym. Adv. Technol.* **2006**, *17*, 981.
(96) Kontou, E.; Anthoulis, G. *J. Appl. Polym. Sci.* **2007**, *105*, 1723.
(97) Yang, F.; Nelson, G. L. *Polym. Adv. Technol.* **2006**, *17*, 320.
(98) Katsikis, N.; Zahradnik, F.; Helmschrott, A.; Münstedt, H.; Vital, A. *Polym. Degrad. Stab.* **2007**, *92*, 1966.
(99) Nodera, A.; Kanai, T. *J. Appl. Polym. Sci.* **2006**, *101*, 3862.
(100) Tanahashi, M.; Hirose, M.; Watanabe, Y.; Lee, J. C.; Takeda, K. *J. Nanosci. Nanotechnol.* **2007**, *7*, 2433.
(101) Chung, S. C.; Hahm, W. G.; Im, S. S.; Oh, S. G. *Macromol. Res.* **2002**, *10*, 221.
(102) Bikiaris, D.; Karavelidis, V.; Karayannidis, G. *Macromol. Rapid Commun.* **2006**, *27*, 1199.
(103) Todorov, L. V.; Viana, J. C. *J. Appl. Polym. Sci.* **2007**, *106*, 1659.
(104) García, M.; van Vliet, G.; ten Cate, M. G. J.; Chávez, F.; Norder, B.; Kooi, B.; van Zyl, W. E.; Verweij, H.; Blank, D. H. A. *Polym. Adv. Technol.* **2004**, *15*, 164.
(105) (a) Hasan, M. M.; Zhou, Y. X.; Mahfuz, H.; Jeelani, S. *Mater. Sci. Eng., A* **2006**, *429*, 181. (b) Mahfuz, H.; Hasan, M. M.; Rangari, V. K.; Jeelani, S. *Macromol. Mater. Eng.* **2007**, *292*, 437.
(106) Zhang, H.; Zhang, Z.; Yang, J. L.; Friedrich, K. *Polymer* **2006**, *47*, 679.
(107) (a) Takahashi, S.; Paul, D. R. *Polymer* **2006**, *47*, 7519. (b) Takahashi, S.; Paul, D. R. *Polymer* **2006**, *47*, 7535.
(108) Winberg, P.; Eldrup, M.; Maurer, F. H. J. *Polymer* **2004**, *45*, 8253.
(109) Bogoslovov, R. B.; Roland, C. M.; Ellis, A. R.; Randall, A. M.; Robertson, C. G. *Macromolecules* **2008**, *41*, 1289.
(110) Aso, O.; Eguiazábal, J. I.; Nazábal, J. *Compos. Sci. Technol.* **2007**, *67*, 2854.
(111) Arrighi, V.; McEwen, I. J.; Qian, H.; Prieto, M. B. S. *Polymer* **2003**, *44*, 6259.
(112) Gauthier, C.; Reynaud, E.; Vassoille, R.; Ladauce-Stelandre, L. *Polymer* **2004**, *45*, 2761.
(113) (a) Cassagnau, P. *Polymer* **2003**, *44*, 2455. (b) Cassagnau, P.; Mélis, F. *Polymer* **2003**, *44*, 6607.
(114) Liu, Y. Q.; Kontopoulou, M. *Polymer* **2006**, *47*, 7731.
(115) (a) Zhang, Q.; Yang, H.; Fu, Q. *Polymer* **2004**, *45*, 1913. (b) Yang, H.; Zhang, Q.; Guo, M.; Wang, C.; Du, R. N.; Fu, Q. *Polymer* **2006**, *47*, 2106. (c) Yang, H.; Zhang, X. Q.; Qu, C.; Li, B.; Zhang, L. J.; Zhang, Q.; Fu, Q. *Polymer* **2007**, *48*, 860. (d) Qu, C.; Yang, H.; Liang, D.; Cao, W.; Fu, Q. *J. Appl. Polym. Sci.* **2007**, *104*, 2288.
(116) Elias, L.; Fenouillot, F.; Majeste, J. C.; Cassagnau, P. *Polymer* **2007**, *48*, 6029.

(117) (a) Lee, M. W.; Hu, X.; Yue, C. Y.; Li, L.; Tam, K. C.; Nakayama, K. *J. Appl. Polym. Sci.* **2002**, *86*, 2070. (b) Zhang, L.; Tam, K. C.; Gan, L. H.; Yue, C. Y.; Lam, Y. C.; Hu, X. *J. Appl. Polym. Sci.* **2003**, *87*, 1484. (c) Lee, M. W.; Hu, X.; Li, L.; Yue, C. Y.; Tam, K. C. *Polym. Int.* **2003**, *52*, 276. (d) Lee, M. W.; Hu, X.; Yue, C. Y.; Li, L.; Tam, K. C. *Compos. Sci. Technol.* **2003**, *63*, 339. (e) Lee, M. W.; Hu, X.; Li, L.; Yue, C. Y.; Tam, K. C.; Cheong, L. Y. *Compos. Sci. Technol.* **2003**, *63*, 1921.

(118) (a) Wu, L. C.; Chen, P.; Zhang, J.; He, J. S. *Polymer* **2006**, *47*, 448. (b) Wu, L. C.; Chen, P.; Chen, J.; Zhang, J.; He, J. S. *Polym. Eng. Sci.* **2007**, *47*, 757. (c) Chen, J.; Chen, P.; Wu, L. C.; Zhang, J.; He, J. S. *Polymer* **2007**, *48*, 4242.

(119) (a) Wu, T. B.; Ke, Y. C. *Thin Solid Films* **2007**, *515*, 5220. (b) Ke, Y. C.; Wu, T. B.; Xia, Y. F. *Polymer* **2007**, *48*, 3324.

(120) (a) Avella, M.; Bondioli, F.; Cannillo, V.; Errico, M. E.; Ferrari, A. M.; Focher, B.; Malinconico, M.; Manfredini, T.; Montorsi, M. *Mater. Sci. Technol.* **2004**, *20*, 1340. (b) Avella, M.; Bondioli, F.; Cannello, V.; Cosco, S.; Errico, M. E.; Ferrari, A. M.; Focher, B.; Malinconico, M. *Macromol. Symp.* **2004**, *218*, 201. (c) Avella, M.; Bondioli, F.; Cannillo, V.; Di Pace, E.; Errico, M. E.; Ferrari, A. M.; Focher, B.; Malinconico, M. *Compos. Sci. Technol.* **2006**, *66*, 886. (d) Cannillo, V.; Bondioli, F.; Lusvarghi, L.; Montorsi, M.; Avella, M.; Errico, M. E.; Mahnconco, M. *Compos. Sci. Technol.* **2006**, *66*, 1030.

(121) Lim, J. S.; Noda, I.; Im, S. S. *Polymer* **2007**, *48*, 2745.

(122) Yan, S. F.; Yin, J. B.; Yang, Y.; Dai, Z. Z.; Ma, J.; Chen, X. S. *Polymer* **2007**, *48*, 1688.

(123) (a) Pinnau, I.; He, Z. U.S. Patent 6,316,684, 2001. (b) Merkel, T. C.; Freeman, B. D.; Spontak, R. J.; He, Z.; Pinnau, I.; Meakin, P.; Hill, A. J. *Science* **2002**, *296*, 519. (c) Merkel, T. C.; Freeman, B. D.; Spontak, R. J.; He, Z.; Pinnau, I.; Meakin, P.; Hill, A. J. *Chem. Mater.* **2003**, *15*, 109.

(124) He, Z. J.; Pinnau, I.; Morisato, A. *Desalination* **2002**, *146*, 11.

(125) (a) Merkel, T. C.; Toy, L. G.; Andrady, A. L.; Gracz, H.; Stejskal, E. O. *Macromolecules* **2003**, *36*, 353. (b) Merkel, T. C.; He, Z. J.; Pinnau, I.; Freeman, B. D.; Meakin, P.; Hill, A. J. *Macromolecules* **2003**, *36*, 6844. (c) Andrady, A. L.; Merkel, T. C.; Toy, L. G. *Macromolecules* **2004**, *37*, 4329.

(126) (a) Winberg, P.; De Sitter, K.; Dotremont, C.; Mullens, S.; Vankelecom, I. F. J.; Maurer, F. H. J. *Macromolecules* **2005**, *38*, 3776. (b) De Sitter, K.; Winberg, P.; D'Haen, J.; Dotremont, C.; Leysen, R.; Martens, J. A.; Mullens, S.; Maurer, F. H. J.; Vankelecom, I. F. J. *J. Membr. Sci.* **2006**, *278*, 83. (c) De Sitter, K.; Leysen, R.; Mullens, S.; Vankelecom, I.; Maurer, F. *Desalination* **2006**, *199*, 293.

(127) Kelman, S. D.; Matteucci, S.; Bielawski, C. W.; Freeman, B. D. *Polymer* **2007**, *48*, 6881.

(128) Kono, T.; Hu, Y. M.; Masuda, T.; Tanaka, K.; Priestley, R. D.; Freeman, B. D. *Polym. Bull.* **2007**, *58*, 995.

(129) Merkel, T. C.; He, Z.; Pinnau, I.; Freeman, B. D.; Meakin, P.; Hill, A. J. *Macromolecules* **2003**, *36*, 8406.

(130) (a) Zhong, J. Y.; Wen, W. Y.; Jones, A. A. *Macromolecules* **2003**, *36*, 6430. (b) Zhong, J. Y.; Lin, G. X.; Wen, W. Y.; Jones, A. A.; Kelman, S.; Freeman, B. D. *Macromolecules* **2005**, *38*, 3754.

(131) (a) Hill, R. J. *Phys. Rev. Lett.* **2006**, *96*, 216001. (b) Hill, R. J. *Ind. Eng. Chem. Res.* **2006**, *45*, 6890.

(132) (a) Hu, X. D.; Cong, H. L.; Shen, Y. Q.; Radosz, M. *Ind. Eng. Chem. Res.* **2007**, *46*, 1547. (b) Cong, H. L.; Hu, X. D.; Radosz, M.; Shen, Y. Q. *Ind. Eng. Chem. Res.* **2007**, *46*, 2567.

(133) Khayet, M.; Villaluenga, J. P. G.; Valentin, J. L.; López-Manchado, M. A.; Mengual, J. I.; Seoane, B. *Polymer* **2005**, *46*, 9881.

(134) Su, Y. H.; Liu, Y. L.; Sun, Y. M.; Lai, J. Y.; Guiver, M. D.; Gao, Y. *J. Power Sources* **2006**, *155*, 111.

(135) (a) Kim, J. Y.; Mulmi, S.; Lee, C. H.; Park, H. B.; Chung, Y. S.; Lee, Y. M. *J. Membr. Sci.* **2006**, *283*, 172. (b) Lee, C. H.; Hwang, S. Y.; Sohn, J. Y.; Park, H. B.; Kim, J. Y.; Lee, Y. M. *J. Power Sources* **2006**, *163*, 339. (c) Lee, C. H.; Min, K. A.; Park, H. B.; Hong, Y. T.; Jung, B. O.; Lee, Y. M. *J. Membr. Sci.* **2007**, *303*, 258.

(136) (a) van Zyl, W. E.; García, M.; Schrauwen, B. A. G.; Kooi, B. J.; De Hosson, J. M.; Verweij, H. *Macromol. Mater. Eng.* **2002**, *287*, 106. (b) García, M.; de Rooij, M.; Winnubst, L.; van Zyl, W. E.; Verweij, H. *J. Appl. Polym. Sci.* **2004**, *92*, 1855. (c) García, M.; García-Turiel, J.; Norder, B.; Chavez, F.; Kooi, B. J.; van Zyl, W. E.; Verweij, H.; Blank, D. H. A. *Adv. Eng. Mater.* **2004**, *6*, 724. (d) García, M.; Barsema, J.; Galindo, R. E.; Cangialosi, D.; García-Turiel, J.; van Zyl, W. E.; Verweij, H.; Blank, D. H. A. *Polym. Eng. Sci.* **2004**, *44*, 1240.

(137) Hernández-Padrón, G.; Rojas, F.; Castaño, V. M. *Nanotechnology* **2004**, *15*, 98.

(138) Kuo, M. C.; Tsai, C. M.; Huang, J. C.; Chen, M. *Mater. Chem. Phys.* **2005**, *90*, 185.

(139) Yu, T. S.; Lin, J. P.; Xu, J. F.; Ding, W. W. *J. Polym. Sci., Part B: Polym. Phys.* **2005**, *43*, 3127.

(140) García, N.; Corrales, T.; Guzmán, J.; Tiemblo, P. *Polym. Degrad. Stab.* **2007**, *92*, 635.

(141) Huang, S. L.; Chin, W. K.; Yang, W. P. *Polymer* **2005**, *46*, 1865.

(142) Yu, Y. Y.; Chen, W. C. *Polym. Int.* **2005**, *54*, 500.

(143) Lach, R.; Kim, G. M.; Michler, G. H.; Grellmann, W.; Albrecht, K. *Macromol. Mater. Eng.* **2006**, *291*, 263.

(144) Im, J. S.; Lee, J. H.; An, S. K.; Song, K. W.; Jo, N. J.; Lee, J. O.; Yoshinaga, K. *J. Appl. Polym. Sci.* **2006**, *100*, 2053.

(145) (a) Ho, P. K. H.; Thomas, D. S.; Friend, R. H.; Tessler, N. *Science* **1999**, *285*, 233. (b) Ho, P. K. H.; Kim, J. S.; Tessler, N.; Friend, R. H. *J. Chem. Phys.* **2001**, *115*, 2709. (c) Ho, P. K. H.; Friend, R. H. *J. Chem. Phys.* **2002**, *116*, 6782.

(146) (a) Yang, S. H.; Nguyen, T. P.; Le Rendu, P.; Hsu, C. S. *Thin Solid Films* **2005**, *471*, 230. (b) Yang, S. H.; Le Rendu, P.; Nguyen, T. P.; Hsu, C. S. *Rev. Adv. Mater. Sci.* **2007**, *15*, 144.

(147) (a) Yoon, K. H.; Park, S. B.; Yang, B. D. *Mater. Chem. Phys.* **2004**, *87*, 39. (b) Yang, B. D.; Yoon, K. H.; Chung, K. W. *Synth. Met.* **2004**, *143*, 25.

(148) (a) Sternstein, S. S.; Zhu, A. J. *Macromolecules* **2002**, *35*, 7262. (b) Narayanan, R. A.; Thiyagarajan, P.; Zhu, A. J.; Ash, B. J.; Shofner, M. L.; Schadler, L. S.; Kumar, S. K.; Sternstein, S. S. *Polymer* **2007**, *48*, 5734.

(149) Lin, Q. H.; Cohen, S. A.; Gignac, L.; Herbst, B.; Klaus, D.; Simonyi, E.; Hedrick, J.; Warlaumont, J.; Lee, H. J.; Wu, W. L. *J. Polym. Sci., Part B: Polym. Phys.* **2007**, *45*, 1482.

(150) García, N.; Corrales, T.; Guzmán, J.; Tiemblo, P. *Polym. Degrad. Stab.* **2007**, *92*, 635.

(151) Wu, Z. J.; Han, H.; Han, W. J.; Kim, B.; Ahn, K. H.; Lee, K. *Langmuir* **2007**, *23*, 7799.

(152) Nguyen, V. K.; Lee, J. W.; Yoo, Y. *Sensor. Actuat. B* **2007**, *120*, 529.

(153) (a) Oberdisse, J.; Demé, B. *Macromolecules* **2002**, *35*, 4397. (b) Oberdisse, J. *Macromolecules* **2002**, *35*, 9441. (c) Oberdisse, J.; El Harrak, A.; Carrot, G.; Jestin, J.; Boué, F. *Polymer* **2005**, *46*, 6695. (d) Oberdisse, J. *Soft Matter* **2006**, *2*, 29. (e) Oberdisse, J.; Hine, P.; Pyckhout-Hintzen, W. *Soft Matter* **2007**, *3*, 476.

(154) Naderi, N.; Sharifi-Sanjani, N.; Khayyat-Naderi, B.; Faridi-Majidi, R. *J. Appl. Polym. Sci.* **2006**, *99*, 2943.

(155) (a) Zhang, Q.; Archer, L. A. *Langmuir* **2002**, *18*, 10435. (b) Zhang, Q.; Archer, L. A. *Macromolecules* **2004**, *37*, 1928.

(156) (a) Boisvert, J. P.; Persello, J.; Guyard, A. *J. Polym. Sci., Part B: Polym. Phys.* **2003**, *41*, 3127. (b) Persello, J.; Boisvert, J. P.; Guyard, A.; Cabane, B. *J. Phys. Chem. B* **2004**, *108*, 9678. (c) Guyard, A.; Persello, J.; Boisvert, J. P.; Cabane, B. *J. Polym. Sci., Part B: Polym. Phys.* **2006**, *44*, 1134.

(157) Bansal, A.; Yang, H.; Li, C. Z.; Benicewicz, B. C.; Kumar, S. K.; Schadler, L. S. *J. Polym. Sci., Part B: Polym. Phys.* **2006**, *44*, 2944.

(158) Peng, C. C.; Göpfert, A.; Drechsler, M.; Abetz, V. *Polym. Adv. Technol.* **2005**, *16*, 770.

(159) Inoubli, R.; Dagréou, S.; Lapp, A.; Billon, L.; Peyrelasse, J. *Langmuir* **2006**, *22*, 6683.

(160) Grillet, A. C.; Brunel, S.; Chevalier, Y.; Usoni, S.; Ansanay-Alex, V.; Allemand, J. *Polym. Int.* **2004**, *53*, 569.

(161) Hong, R. Y.; Fu, H. P.; Zhang, Y. J.; Liu, L.; Wang, J.; Li, H. Z.; Zheng, Y. *J. Appl. Polym. Sci.* **2007**, *105*, 2176.

(162) (a) Zhu, Y. G.; Li, Z. Q.; Zhang, D.; Tanimoto, T. *J. Polym. Sci., Part B: Polym. Phys.* **2006**, *44*, 1161. (b) Zhu, Y. G.; Li, Z. Q.; Zhang, D.; Tanimoto, T. *J. Polym. Sci., Part B: Polym. Phys.* **2006**, *44*, 1351.

(163) Castrillo, P. D.; Olmos, D.; Amador, D. R.; González-Benito, J. *J. Colloid Interface Sci.* **2007**, *308*, 318.

(164) (a) Schadler, L. S.; Laul, K. O.; Smith, R. W.; Petrovicova, E. *J. Therm. Spray Technol.* **1997**, *6*, 475. (b) Petrovicova, E.; Knight, R.; Schadler, L. S.; Twardowski, T. E. *J. Appl. Polym. Sci.* **2000**, *77*, 1684. (c) Petrovicova, E.; Knight, R.; Schadler, L. S.; Twardowski, T. E. J. *Appl. Polym. Sci.* **2000**, *78*, 2272.

(165) Huang, H. H.; Orler, B.; Wilkes, G. L. *Polym. Bull.* **1985**, *14*, 557.

(166) Schmidt, H. *J. Non-Cryst. Solids* **1985**, *73*, 681.

(167) Chen, Y.; Iroh, J. O. *Chem. Mater.* **1999**, *11*, 1218.

(168) Patel, S.; Bandyopadhyay, A.; Vijayabaskar, V.; Bhowmick, A. K. *Polymer* **2005**, *46*, 8079.

(169) Nakane, K.; Yamashita, T.; Iwakura, K.; Suzuki, F. *J. Appl. Polym. Sci.* **1999**, *74*, 133.

(170) Bandyopadhyay, A.; De Sarkar, M.; Bhowmick, A. K. *J. Mater. Sci.* **2005**, *40*, 5233.

(171) (a) Dewimille, L.; Bresson, B.; Bokobza, L. *Polymer* **2005**, *46*, 4135. (b) Fragiadakis, D.; Pissis, P.; Bokobza, L. *Polymer* **2005**, *46*, 6001. (c) Fragiadakis, D.; Pissis, P.; Bokobza, L. *J. Non-Cryst. Solids* **2006**, *352*, 4969. (d) Fragiadakis, D.; Pissis, P. *J. Non-Cryst. Solids* **2007**, *353*, 4344.

(172) Li, Z. L.; Han, W.; Kozodaev, D.; Brokken-Zijp, J. C. M.; de With, G.; Thüne, P. C. *Polymer* **2006**, *47*, 1150.

(173) (a) Sengupta, R.; Bandyopadhyay, A.; Sabharwal, S.; Chaki, T. K.; Bhowmick, A. K. *Polymer* **2005**, *46*, 3343. (b) Sengupta, R.; Sabharwal, S.; Bhowmick, A.; Bhowmick, A. K. *Polym. Degrad. Stab.* **2006**, *91*, 1311.
(174) Jang, J.; Park, H. *J. Appl. Polym. Sci.* **2002**, *83*, 1817.
(175) Lai, S. M.; Wang, C. K.; Shen, H. F. *J. Appl. Polym. Sci.* **2005**, *97*, 1316.
(176) Hsiao, C. N.; Huang, K. S. *J. Appl. Polym. Sci.* **2005**, *96*, 1936.
(177) Wang, Y. J.; Wang, X. H.; Li, J.; Mo, Z. S.; Zhao, X. J.; Jing, X. B.; Wang, F. S. *Adv. Mater.* **2001**, *13*, 1582.
(178) Shchipunov, Y. A.; Karpenko, T. Y. *Langmuir* **2004**, *20*, 3882.
(179) (a) Tian, D.; Dubois, P.; Jérôme, R. *J. Polym. Sci., Part A: Polym. Chem.* **1997**, *35*, 2295. (b) Tian, D.; Blacher, S.; Dubois, P.; Jérôme, R. *Polymer* **1998**, *39*, 855. (c) Tian, D.; Blacher, S.; Pirard, J. P.; Jérôme, R. *Langmuir* **1998**, *14*, 1905. (d) Tian, D.; Blacher, S.; Jérôme, R. *Polymer* **1999**, *40*, 951.
(180) Nie, K. M.; Zheng, S. X.; Lu, F.; Zhu, Q. R. *J. Polym. Sci., Part B: Polym. Phys.* **2005**, *43*, 2594.
(181) Hsu, Y. G.; Chiang, I. L.; Lo, J. F. *J. Appl. Polym. Sci.* **2000**, *78*, 1179.
(182) Huang, Y.; Gu, Y. *J. Appl. Polym. Sci.* **2003**, *88*, 2210.
(183) Yen, C. T.; Chen, W. C.; Liaw, D. J.; Lu, H. Y. *Polymer* **2003**, *44*, 7079.
(184) Lee, T. M.; Ma, C. C. M. *J. Polym. Sci., Part A: Polym. Chem.* **2006**, *44*, 757.
(185) Kim, J. H.; Lee, Y. M. *J. Membr. Sci.* **2001**, *193*, 209.
(186) Kim, D. S.; Liu, B. J.; Guiver, M. D. *Polymer* **2006**, *47*, 7871.
(187) Martínez, Y.; Retuert, J.; Yazdani-Pedram, M.; Cölfen, H. *Polymer* **2004**, *45*, 3257.
(188) Saxena, A.; Tripathi, B. P.; Shahi, V. K. *J. Phys. Chem. B* **2007**, *111*, 12454.
(189) (a) Gao, Y.; Choudhury, N. R.; Dutta, N.; Matisons, J.; Reading, M.; Delmotte, L. *Chem. Mater.* **2001**, *13*, 3644. (b) Gao, Y.; Choudhury, N. R.; Dutta, N.; Delmotte, L. *Polymer* **2005**, *46*, 4013.
(190) (a) Joly, C.; Goizet, S.; Schrotter, J. C.; Sanchez, J.; Escoubes, M. *J. Membr. Sci.* **1997**, *130*, 63. (b) Joly, C.; Smaihi, M.; Porcar, L.; Noble, R. D. *Chem. Mater.* **1999**, *11*, 2331.
(191) Hsiue, G. H.; Chen, J. K.; Liu, Y. L. *J. Appl. Polym. Sci.* **2000**, *76*, 1609.
(192) Huang, J. C.; Zhu, Z. K.; Yin, J.; Zhang, D. M.; Qian, X. F. *J. Appl. Polym. Sci.* **2001**, *79*, 794.
(193) Jiang, L. Z.; Wang, W. C.; Wei, X. W.; Wu, D. Z.; Jin, R. G. *J. Appl. Polym. Sci.* **2007**, *104*, 1579.
(194) (a) Liu, J.; Gao, Y.; Wang, F. D.; Wu, M. *J. Appl. Polym. Sci.* **2000**, *75*, 384. (b) Liu, J.; Gao, Y.; Wang, F. D.; Li, D. C.; Xu, J. *J. Mater. Sci.* **2002**, *37*, 3085.
(195) Sarwar, M. I.; Zulfiqar, S.; Ahmad, Z. *Polym. Int.* **2008**, *57*, 292.
(196) (a) Bandyopadhyay, A.; Bhowmick, A. K.; De Sarkar, M. *J. Appl. Polym. Sci.* **2004**, *93*, 2579. (b) Bandyopadhyay, A.; De Sarkar, M.; Bhowmick, A. K. *J. Appl. Polym. Sci.* **2005**, *95*, 1418. (c) Bandyopadhyay, A.; De Sarkar, M.; Bhowmick, A. K. *J. Mater. Sci.* **2005**, *40*, 53. (d) Bandyopadhyay, A.; De Sarkar, M.; Bhowmick, A. K. *J. Polym. Sci., Part B: Polym. Phys.* **2005**, *43*, 2399.
(197) Hsiue, G. H.; Liu, Y. L.; Liao, H. H. *J. Polym. Sci., Part A: Polym. Chem.* **2001**, *39*, 986.
(198) Huang, C. J.; Fu, S. Y.; Zhang, Y. H.; Lauke, B.; Li, L. F.; Ye, L. *Cryogenics* **2005**, *45*, 450.
(199) Yao, X. F.; Zhao, H. P.; Yeh, H. Y. *J. Reinf. Plast. Compos.* **2006**, *25*, 189.
(200) Sun, D. H.; Zhang, R.; Liu, Z. M.; Huang, Y.; Wang, Y.; He, J.; Han, B. X.; Yang, G. Y. *Macromolecules* **2005**, *38*, 5617.
(201) Lu, G. T.; Huang, Y. *J. Mater. Sci.* **2002**, *37*, 2305.
(202) Chang, T. C.; Wang, Y. T.; Hong, Y. S.; Chiu, Y. S. *J. Polym. Sci., Part A: Polym. Chem.* **2000**, *38*, 1972.
(203) Jang, J.; Bae, J.; Kang, D. *J. Appl. Polym. Sci.* **2001**, *82*, 2310.
(204) (a) Al-Kandary, S.; Ali, A. A. M.; Ahmad, Z. *J. Appl. Polym. Sci.* **2005**, *98*, 2521. (b) Al-Kandary, S.; Ali, A. A. M.; Ahmad., Z. *J. Mater. Sci.* **2006**, *41*, 2907. (c) Khalil, M.; Saeed, S.; Ahmad, Z. *J. Appl. Polym. Sci.* **2008**, *107*, 1257.
(205) Smaihi, M.; Schrotter, J. C.; Lesimple, C.; Prevost, I.; Guizard, C. *J. Membr. Sci.* **1999**, *161*, 157.
(206) (a) Suzuki, T.; Yamada, Y. *Polym. Bull.* **2005**, *53*, 139. (b) Suzuki, T.; Yamada, Y. J. *Polym. Sci., Part B: Polym. Phys.* **2006**, *44*, 291.
(207) Tsai, M. H.; Huang, S. L.; Chiang, P. C.; Chen, C. J. *J. Appl. Polym. Sci.* **2007**, *106*, 3185.
(208) Park, H. B.; Kim, J. H.; Kim, J. K.; Lee, Y. M. *Macromol. Rapid Commun.* **2002**, *23*, 544.
(209) Tamai, T.; Matsuura, Y.; Watanabe, M.; Matsukawa, K. *J. Polym. Sci., Part A: Polym. Chem.* **2006**, *44*, 2107.
(210) (a) Mammeri, F.; Bourhis, E. L.; Rozes, L.; Sanchez, C. *J. Eur. Ceram. Soc.* **2006**, *26*, 259. (b) Mammeri, F.; Rozes, L.; Bourhis, E. L.; Sanchez, C. *J. Eur. Ceram. Soc.* **2006**, *26*, 267.
(211) (a) Tan, C. S.; Juan, C. C.; Kuo, T. W. *Polymer* **2004**, *45*, 1805. (b) Tan, C. S.; Kuo, T. W. *J. Appl. Polym. Sci.* **2005**, *98*, 750.
(212) (a) Chiang, C. L.; Ma, C. C. M.; Wu, D. L.; Kuan, H. C. *J. Polym. Sci., Part A: Polym. Chem.* **2003**, *41*, 905. (b) Chiang, C. L.; Ma, C. C. M. *Polym. Degrad. Stab.* **2004**, *83*, 207.
(213) Zhou, W.; Dong, J. H.; Qiu, K. Y.; Wei, Y. *J. Polym. Sci., Part A: Polym. Chem.* **1998**, *36*, 1607.
(214) Chang, C. C.; Chen, W. C. *Chem. Mater.* **2002**, *14*, 4242.
(215) Qiu, F. X.; Zhou, Y. M.; Liu, J. Z. *Eur. Polym. J.* **2004**, *40*, 713.
(216) (a) Cornelius, C.; Hibshman, C.; Marand, E. *Sep. Purif. Technol.* **2001**, *25*, 181. (b) Cornelius, C. J.; Marand, E. *Polymer* **2002**, *43*, 2385. (c) Cornelius, C. J.; Marand, E. *J. Membr. Sci.* **2002**, *202*, 97. (d) Hibshman, C.; Cornelius, C. J.; Marand, E. *J. Membr. Sci.* **2003**, *211*, 25. (e) Hibshman, C.; Mager, M.; Marand, E. *J. Membr. Sci.* **2004**, *229*, 73.
(217) Chen, B. K.; Chiu, T. M.; Tsay, S. Y. *J. Appl. Polym. Sci.* **2004**, *94*, 382.
(218) (a) Chen, B. K.; Su, C. T.; Tseng, M. C.; Tsay, S. Y. *Polym. Bull.* **2006**, *57*, 671. (b) Chen, B. K.; Du, J. U.; Hou, C. W. *IEEE Trans. Dielectr. Electr. Insul.* **2008**, *15*, 127.
(219) Liaw, W. C.; Chen, K. P. *J. Appl. Polym. Sci.* **2007**, *105*, 809.
(220) Park, H. B.; Kim, J. K.; Nam, S. Y.; Lee, Y. M. *J. Membr. Sci.* **2003**, *220*, 59.
(221) (a) Sarwar, M. I.; Zulfiqar, S.; Ahmad, Z. *Colloid Polym. Sci.* **2007**, *285*, 1733. (b) Sarwar, M. I.; Zulfiqar, S.; Ahmad, Z. *J. Sol-Gel. Sci. Technol.* **2008**, *45*, 89.
(222) Park, Y. W.; Lee, D. S. *J. Appl. Polym. Sci.* **2004**, *94*, 1780.
(223) Messori, M.; Toselli, M.; Pilati, F.; Fabbri, E.; Fabbri, P.; Busoli, S.; Pasquali, L.; Nannarone, S. *Polymer* **2003**, *44*, 4463.
(224) Saccani, A.; Toselli, M.; Messori, M.; Fabbri, P.; Pilati, F. *J. Appl. Polym. Sci.* **2006**, *102*, 4870.
(225) (a) Jain, S.; Goossens, H.; Picchioni, F.; Magusin, P.; Mezari, B.; van Duin, M. *Polymer* **2005**, *46*, 6666. (b) Jain, S.; Goossens, H.; van Duin, M.; Lemstra, P. *Polymer* **2005**, *46*, 8805. (c) Jain, S.; Goossens, J. G. P.; van Duin, M. *Macromol. Symp.* **2006**, *233*, 225.
(226) Chuang, S. W.; Hsu, S. L. C.; Liu, Y. H. *J. Membr. Sci.* **2007**, *305*, 353.
(227) Shang, X. Y.; Zhu, Z. K.; Yin, J.; Ma, X. D. *Chem. Mater.* **2002**, *14*, 71.
(228) (a) Musto, P.; Ragosta, G.; Scarinzi, G.; Mascia, L. *Polymer* **2004**, *45*, 1697. (b) Abbate, M.; Musto, P.; Ragosta, G.; Scarinzi, G.; Mascia, L. *Macromol. Symp.* **2004**, *218*, 211. (c) Musto, P.; Mascia, L.; Mensitieri, G.; Ragosta, G. *Polymer* **2005**, *46*, 4492.
(229) Karataş, S.; Kayaman-Apohan, N.; Demirer, H.; Güngör, A. *Polym. Adv. Technol.* **2007**, *18*, 490.
(230) Nunes, S. P.; Peinemann, K. V.; Ohlrogge, K.; Alpers, A.; Keller, M.; Pires, A. T. N. *J. Membr. Sci.* **1999**, *157*, 219.
(231) Wang, L. H.; Tian, Y.; Ding, H. Y.; Li, J. D. *Eur. Polym. J.* **2006**, *42*, 2921.
(232) Li, S. J.; Tian, J. X.; Gan, W. J.; Zhao, L.; Li, L.; Wang, J. C. *Polym. Adv. Technol.* **2005**, *16*, 133.
(233) Gomes, D.; Nunes, S. P.; Peinemann, K. V. *J. Membr. Sci.* **2005**, *246*, 13.
(234) Yan, S. F.; Yin, J. B.; Yang, J. Y.; Chen, X. S. *Mater. Lett.* **2007**, *61*, 2683.
(235) Guo, R. L.; Hu, C. L.; Pan, F. S.; Wu, H.; Jiang, Z. Y. *J. Membr. Sci.* **2006**, *281*, 454.
(236) Ahmad, Z.; Mark, J. E. *Chem. Mater.* **2001**, *13*, 3320.
(237) Tamaki, R.; Chujo, Y. *Chem. Mater.* **1999**, *11*, 1719.
(238) Ogoshi, T.; Chujo, Y. *Macromolecules* **2005**, *38*, 9110.
(239) (a) Matějka, L.; Dušk, K.; Pleštil, J.; Kříž, J.; Lednický, F. *Polymer* **1999**, *40*, 171. (b) Matějka, L.; Pleštil, J.; Dušk, K. *J. Non-Cryst. Solids* **1998**, *226*, 114. (c) Matějka, L.; Dukh, O.; Kolařík, J. *Polymer* **2000**, *41*, 1449. (d) Matějka, L.; Dukh, O. *Macromol. Symp.* **2001**, *171*, 181.
(240) Fujiwara, M.; Kojima, K.; Tanaka, Y.; Nomura, R. *J. Mater. Chem.* **2004**, *14*, 1195.
(241) Ogoshi, T.; Itoh, H.; Kim, K. M.; Chujo, Y. *Macromolecules* **2002**, *35*, 334.
(242) Kumar, A. A.; Adachi, K.; Chujo, Y. *J. Polym. Sci., Part A: Polym. Chem.* **2004**, *42*, 785.
(243) Patel, S.; Bandyopadhyay, A.; Vijayabaskar, V.; Bhowmick, A. K. *J. Mater. Sci.* **2006**, *41*, 927.
(244) Ma, J. Z.; Hu, J.; Zhang, Z. J. *Eur. Polym. J.* **2007**, *43*, 4169.
(245) Li, S. X.; Shah, A.; Hsieh, A. J.; Haghighat, R.; Praveen, S. S.; Mukherjee, I.; Wei, E.; Zhang, Z. T.; Wei, Y. *Polymer* **2007**, *48*, 3982.
(246) Hernández, J. C. R.; Sánchez, M. S.; Ribelles, J. L. G.; Pradas, M. M. *Eur. Polym. J.* **2007**, *43*, 2775.
(247) Charpentier, P. A.; Xu, W. Z.; Li, X. S. *Green Chem.* **2007**, *9*, 768.
(248) Yang, F.; Nelson, G. L. *J. Appl. Polym. Sci.* **2004**, *91*, 3844.

(249) (a) Yang, F.; Ou, Y. C.; Yu, Z. Z. *J. Appl. Polym. Sci.* **1998**, *69*, 355. (b) Ou, Y. C.; Yang, F.; Yu, Z. Z. *J. Polym. Sci., Part B: Polym. Phys.* **1998**, *36*, 789.
(250) Reynaud, E.; Jouen, T.; Gauthier, C.; Vigier, G.; Varlet, J. *Polymer* **2001**, *42*, 8759.
(251) (a) Li, Y.; Yu, J.; Guo, Z. X. *J. Appl. Polym. Sci.* **2002**, *84*, 827. (b) Li, Y.; Yu, J.; Guo, Z. X. *Polym. Int.* **2003**, *52*, 981.
(252) Liu, W. T.; Tian, X. Y.; Cui, P.; Li, Y.; Zheng, K.; Yang, Y. *J. Appl. Polym. Sci.* **2004**, *91*, 1229.
(253) Yang, Y. Z.; Xu, H.; Gu, H. C. *J. Appl. Polym.Sci.* **2006**, *102*, 655.
(254) Zheng, J.; Cui, P.; Tian, X. Y.; Zheng, K. *J. Appl. Polym. Sci.* **2007**, *104*, 9.
(255) Zheng, H.; Wu, J. L. *J. Appl. Polym. Sci.* **2007**, *103*, 2564.
(256) Mo, T. C.; Wang, H. W.; Chen, S. Y.; Dong, R. X.; Kuo, C. H.; Yeh, Y. C. *J. Appl. Polym. Sci.* **2007**, *104*, 882.
(257) Takai, C.; Fuji, M.; Takahashi, M. *Colloids Surf., A* **2007**, *292*, 79.
(258) Huang, J. W.; Wen, Y. L.; Kang, C. C.; Yeh, M. Y. *Polym. J.* **2007**, *39*, 654.
(259) Su, H. L.; Hsu, J. M.; Pan, J. P.; Chern, C. S. *J. Appl. Polym. Sci.* **2007**, *103*, 3600.
(260) Kashiwagi, T.; Morgan, A. B.; Antonucci, J. M.; VanLandingham, M. R.; Harris, R. H.; Awad, W. H.; Shields, J. R. *J. Appl. Polym. Sci.* **2003**, *89*, 2072.
(261) Hu, Y. H.; Chen, C. Y.; Wang, C. C. *Polym. Degrad. Stab.* **2004**, *84*, 545.
(262) Becker, C.; Kutsch, B.; Krug, H.; Kaddami, H. *J. Sol-Gel. Sci. Technol.* **1998**, *13*, 499.
(263) (a) Kaddami, H.; Gerard, J. F.; Hajji, P.; Pascault, J. P. *J. Appl. Polym. Sci.* **1999**, *73*, 2701. (b) Kaddami, H.; Pascault, J. P.; Gerard, J. F. *Polym. Eng. Sci.* **2004**, *44*, 1231.
(264) Jia, X.; Li, Y. F.; Cheng, Q.; Zhang, S. J.; Zhang, B. *Eur. Polym. J.* **2007**, *43*, 1123.
(265) (a) Yu, Y. Y.; Chen, C. Y.; Chen, W. C. *Polymer* **2003**, *44*, 593. (b) Yu, Y. Y.; Chen, W. C. *Mater. Chem. Phys.* **2003**, *82*, 388.
(266) (a) Zhang, M. Q.; Rong, M. Z.; Yu, S. L.; Wetzel, B.; Friedrich, K. *Macromol. Mater. Eng.* **2002**, *287*, 111. (b) Zhang, M. Q.; Rong, M. Z.; Yu, S. L.; Wetzel, B.; Friedrich, K. *Wear* **2002**, *253*, 1086.
(267) Zheng, Y. P.; Zheng, Y.; Ning, R. C. *Mater. Lett.* **2003**, *57*, 2940.
(268) (a) Sun, Y. Y.; Zhang, Z. Q.; Moon, K. S.; Wong, C. P. *J. Polym. Sci., Part B: Polym. Phys.* **2004**, *42*, 3849. (b) Sun, Y. Y.; Zhang, Z. Q.; Wong, C. P. *Polymer* **2005**, *46*, 2297.
(269) Bondioli, F.; Cannillo, V.; Fabbri, E.; Messori, M. *J. Appl. Polym. Sci.* **2005**, *97*, 2382.
(270) (a) Rosso, P.; Ye, L.; Friedrich, K.; Sprenger, S. *J. Appl. Polym. Sci.* **2006**, *100*, 1849. (b) Rosso, P.; Ye, L. *Macromol. Rapid Commun.* **2007**, *28*, 121.
(271) Johnsen, B. B.; Kinloch, A. J.; Mohammed, R. D.; Taylor, A. C.; Sprenger, S. *Polymer* **2007**, *48*, 530.
(272) Ghaemy, M.; Nasab, S. M. A.; Barghamadi, M. *J. Appl. Polym. Sci.* **2007**, *104*, 3855.
(273) (a) Liu, Y. L.; Hsu, S. H.; Wei, W. L.; Jeng, R. J. *Polymer* **2003**, *44*, 5159. (b) Liu, Y. L.; Wei, W. L.; Hsu, K. Y.; Ho, W. H. *Thermochim. Acta* **2004**, *412*, 139. (c) Liu, Y. L.; Li, S. H. *J. Appl. Polym. Sci.* **2005**, *95*, 1237.
(274) Ragosta, G.; Abbate, M.; Musto, P.; Scarinzi, G.; Mascia, L. *Polymer* **2005**, *46*, 10506.
(275) (a) Preghenella, M.; Pegoretti, A.; Migliaresi, C. *Polymer* **2005**, *46*, 12065. (b) Preghenella, M.; Pegoretti, A.; Migliaresi, C. *Polym. Test.* **2006**, *25*, 443.
(276) Hartwig, A.; Sebald, M.; Pütz, D.; Aberle, L. *Macromol. Symp.* **2005**, *221*, 127.
(277) (a) Petrović, Z. S.; Javni, I.; Waddon, A.; Bánhegyi, G. *J. Appl. Polym. Sci.* **2000**, *76*, 133. (b) Petrović, Z. S.; Cho, Y. J.; Javni, I.; Magonov, S.; Yerina, N.; Schaefer, D. W.; Ilavský, J.; Waddon, A. *Polymer* **2004**, *45*, 4285.
(278) (a) Zhou, S. X.; Wu, L. M.; Sun, J.; Shen, W. D. *Prog. Org. Coat.* **2002**, *45*, 33. (b) Chen, G. D.; Zhou, S. X.; Gu, G. X.; Yang, H. H.; Wu, L. M. *J. Colloid Interface Sci.* **2004**, *281*, 339. (c) Zhou, S. X.; Wu, L. M.; Sun, J.; Shen, W. D. *J. Appl. Polym. Sci.* **2003**, *88*, 189. (d) Chen, Y. C.; Zhou, S. X.; Chen, G. D.; Wu, L. M. *Prog. Org. Coat.* **2005**, *54*, 120. (e) Chen, Y. C.; Zhou, S. X.; Yang, H. H.; Gu, G. X.; Wu, L. M. *J. Colloid Interface Sci.* **2004**, *279*, 370. (f) Chen, Y. C.; Zhou, S. X.; Yang, H. H.; Wu, L. M. *J. Appl. Polym. Sci.* **2005**, *95*, 1032.
(279) Lee, S. I.; Hahn, Y. B.; Nahm, K. S.; Lee, Y. S. *Polym. Adv. Technol.* **2005**, *16*, 328.
(280) Seo, J. W.; Kim, B. K. *Polym. Bull.* **2005**, *54*, 123.
(281) Xiang, X. J.; Qian, J. W.; Yang, W. Y.; Fang, M. H.; Qian, X. Q. *J. Appl. Polym. Sci.* **2006**, *100*, 4333.
(282) Chrissafis, K.; Antoniadis, G.; Paraskevopoulos, K. M.; Vassiliou, A.; Bikiaris, D. N. *Compos. Sci. Technol.* **2007**, *67*, 2165.
(283) Lim, J. S.; Hong, S. M.; Kim, D. K.; Im, S. S. *J. Appl. Polym. Sci.* **2008**, *107*, 3598.
(284) (a) Berriot, J.; Lequeux, F.; Monnerie, L.; Montes, H.; Long, D.; Sotta, P. *J. Non-Cryst. Solids* **2002**, *307*, 719. (b) Berriot, J.; Lequeux, F.; Montes, H.; Pernot, H. *Polymer* **2002**, *43*, 6131. (c) Berriot, J.; Martin, F.; Montes, H.; Monnerie, L.; Sotta, P. *Polymer* **2003**, *44*, 1437. (d) Berriot, J.; Montes, H.; Martin, F.; Mauger, M.; Pyckhout-Hintzen, W.; Meier, G.; Frielinghaus, H. *Polymer* **2003**, *44*, 4909. (e) Berriot, J.; Montes, H.; Lequeux, F.; Long, D.; Sotta, P. *Macromolecules* **2002**, *35*, 9756. (f) Montes, H.; Lequeux, F.; Berriot, J. *Macromolecules* **2003**, *36*, 8107.
(285) (a) Sunkara, H. B.; Jethmalani, J. M.; Ford, W. T. *Chem. Mater.* **1994**, *6*, 362. (b) Jethmalani, J. M.; Ford, W. T. *Chem. Mater.* **1996**, *8*, 2138. (c) Jethmalani, J. M.; Ford, W. T. *Langmuir* **1997**, *13*, 3338. (d) Jethmalani, J. M.; Sunkara, H. B.; Ford, W. T. *Langmuir* **1997**, *13*, 2633.
(286) Pu, Z. C.; Mark, J. E.; Jethmalani, J. M.; Ford, W. T. *Chem. Mater.* **1997**, *9*, 2442.
(287) (a) Bauer, F.; Ernst, H.; Decker, U.; Findeisen, M.; Gläsel, H. J.; Langguth, H.; Hartmann, E.; Mehnert, R.; Peuker, C. *Macromol. Chem. Phys.* **2000**, *201*, 2654. (b) Gläsel, H. J.; Bauer, F.; Ernst, H.; Findeisen, M.; Hartmann, E.; Langguth, H.; Mehnert, R.; Schubert, R. *Macromol. Chem. Phys.* **2000**, *201*, 2765. (c) Bauer, F.; Sauerland, V.; Gläsel, H. J.; Ernst, H.; Findeisen, M.; Hartmann, E.; Langguth, H.; Marquardt, B.; Mehnert, R. *Macromol. Mater. Eng.* **2002**, *287*, 546. (d) Bauer, F.; Sauerland, V.; Ernst, H.; Gläsel, H. J.; Naumov, S.; Mehnert, R. *Macromol. Chem. Phys.* **2003**, *204*, 375. (e) Bauer, F.; Ernst, H.; Hirsch, D.; Naumov, S.; Pelzing, M.; Sauerland, V.; Mehnert, R. *Macromol. Chem. Phys.* **2004**, *205*, 1587. (f) Bauer, F.; Mehnert, R. *J. Polym. Res.* **2005**, *12*, 483.
(288) (a) Bauer, F.; Gläsel, H. J.; Decker, U.; Ernst, H.; Freyer, A.; Hartmann, E.; Sauerland, V.; Mehnert, R. *Prog. Org. Coat.* **2003**, *47*, 147. (b) Bauer, F.; Flyunt, R.; Czihal, K.; Buchmeiser, M. R.; Langguth, H.; Mehnert, R. *Macromol. Mater. Eng.* **2006**, *291*, 493. (c) Bauer, F.; Flyunt, R.; Czihal, K.; Langguth, H.; Mehnert, R.; Schubert, R.; Buchmeiser, M. R. *Prog. Org. Coat.* **2007**, *60*, 121.
(289) (a) Bauer, F.; Ernst, H. ; Flyunt, R.; Gläsel, H.-J.; Hartmann, E.; Sauerland, V.; Buchmeiser, M. R.; Mehnert, R. In *Produktgestaltung in der Partikeltechnologie*; Teipel, U., Ed.; Fraunhofer IRB Verlag: Stuttgart, Germany, 2006; Vol *3.* (b) Bauer, F.; Flyunt, R.; Czihal, K.; Schubert, R.; Buchmeiser, M. R.; Langguth, H.; Mehnert, R. *Pitture Vernici, Eur. Coat.* **2007**, *83*, 13.
(290) Soloukhin, V. A.; Posthumus, W.; Brokken-Zijp, J. C. M.; Loos, J.; de With, G. *Polymer* **2002**, *43*, 6169.
(291) Shu, C. H.; Chiang, H. C.; Tsiang, R. C. C.; Liu, T. J.; Wu, J. J. *J. Appl. Polym. Sci.* **2007**, *103*, 3985.
(292) Kim, S.; Kim, E.; Kim, S.; Kim, W. *J. Colloid Interface Sci.* **2005**, *292*, 93.
(293) Saric, M.; Dietsch, H.; Schurtenberger, P. *Colloids Surf., A* **2006**, *291*, 110.
(294) Cho, J. D.; Ju, H. T.; Park, Y. S.; Hong, J. W. *Macromol. Mater. Eng.* **2006**, *291*, 1155.
(295) Zhang, L.; Zeng, Z. H.; Yang, J. W.; Chen, Y. L. *J. Appl. Polym. Sci.* **2003**, *87*, 1654.
(296) (a) Xu, G. C.; Li, A. Y.; Zhang, L. D.; Wu, G. S.; Yuan, X. Y.; Xie, T. *J. Appl. Polym. Sci.* **2003**, *90*, 837. (b) Xu, G. C.; Li, A. Y.; Zhang, L. D.; Yu, X. Y.; Xie, T.; Wu, G. S. *J. Reinf. Plast. Compos.* **2004**, *23*, 1365.
(297) (a) Li, F. S.; Zhou, S. X.; Wu, L. M. *J. Appl. Polym. Sci.* **2005**, *98*, 2274. (b) Li, F. S.; Zhou, S. X.; Gu, G. X.; You, B.; Wu, L. M. *J. Appl. Polym. Sci.* **2005**, *96*, 912. (c) Li, F. S.; Zhou, S. X.; Wu, L. M. *J. Appl. Polym. Sci.* **2005**, *98*, 1119. (d) Li, F. S.; Zhou, S. X.; You, B.; Wu, L. M. *J. Appl. Polym. Sci.* **2005**, *99*, 1429.
(298) Sangermano, M.; Malucelli, G.; Amerio, E.; Priola, A.; Billi, E.; Rizza, G. *Prog. Org. Coat.* **2005**, *54*, 134.
(299) (a) Chou, Y. C.; Wang, Y. Y.; Hsieh, T. E. *J. Appl. Polym. Sci.* **2007**, *105*, 2073. (b) Wang, Y. Y.; Hsieh, T. E.; Chen, I. C.; Chen, C. H. *IEEE Trans. Adv. Packag.* **2007**, *30*, 421. (c) Wang, Y. Y.; Hsieh, T. E. *Macromol. Chem. Phys.* **2007**, *208*, 2396.
(300) Cho, J. D.; Ju, H. T.; Hong, J. W. *J. Polym. Sci., Part A: Polym. Chem.* **2005**, *43*, 658.
(301) Lee, T. Y.; Bowman, C. N. *Polymer* **2006**, *47*, 6057.
(302) Müh, E.; Stieger, M.; Klee, J. E.; Frey, H.; Mülhaupt, R. *J. Polym. Sci., Part A: Polym. Chem.* **2001**, *39*, 4274.
(303) (a) Malucelli, G.; Priola, A.; Sangermano, M.; Amerio, E.; Zini, E.; Fabbri, E. *Polymer* **2005**, *46*, 2872. (b) Ceccorulli, G.; Zini, E.; Scandola, M. *Macromol. Chem. Phys.* **2006**, *207*, 864. (c) Malucelli, G.; Priola, A.; Amerio, E.; Pollicino, A.; di Pasquale, G.; Pizzi, D.; de Angelis, M. G.; Doghieri, F. J. *Appl. Polym. Sci.* **2007**, *103*, 4107. (d) Mazzocchetti, L.; Scandola, M.; Amerio, E.; Malucelli, G.; Marano, C. *Macromol. Chem. Phys.* **2006**, *207*, 2103. (e) Amerio, E.; Sangermano, M.; Malucelli, G.; Priola, A.; Voit, B. *Polymer* **2005**, *46*, 11241. (f) Amerio, E.; Sangermano, M.; Malucelli, G.; Priola, A.; Rizza, G. *Macromol. Mater. Eng.* **2006**, *291*, 1287. (g) Sanger-

mano, M.; Amerio, E.; Epicoco, P.; Priola, A.; Rizza, G.; Malucelli, G. *Macromol. Mater. Eng.* **2007**, *292*, 634.
(304) Su, Y. L. *React. Funct. Polym.* **2006**, *66*, 967.
(305) Chen, C. G.; Anderson, D. P. J. *Appl. Polym. Sci.* **2007**, *106*, 2132.
(306) (a) Shirai, Y.; Tsubokawa, N. *React. Funct. Polym.* **1997**, *32*, 153. (b) Hayashi, S.; Takeuchi, Y.; Eguchi, M.; Iida, T.; Tsubokawa, N. *J. Appl. Polym. Sci.* **1999**, *71*, 1491. (c) Yokoyama, R.; Suzuki, S.; Shirai, K.; Yamauchi, T.; Tsubokawa, N.; Tsuchimochi, M. *Eur. Polym. J.* **2006**, *42*, 3221. (d) Ueda, J.; Yamaguchi, H.; Yamauchi, T.; Tsubokawa, N. J. *Polym. Sci., Part A: Polym. Chem.* **2007**, *45*, 1143. (e) Shirai, Y.; Shirai, K.; Tsubokawa, N. *J. Polym. Sci., Part A: Polym. Chem.* **2001**, *39*, 2157. (f) Satoh, M.; Shirai, K.; Saitoh, H.; Yamauchi, T.; Tsubokawa, N. *J. Polym. Sci., Part A: Polym. Chem.* **2005**, *43*, 600. (g) Tsubokawa, N.; Ichioka, H.; Satoh, T.; Hayashi, S.; Fujiki, K. *React. Funct. Polym.* **1998**, *37*, 75. (h) Okazaki, M.; Murota, M.; Kawaguchi, Y.; Tsubokawa, N. *J. Appl. Polym. Sci.* **2001**, *80*, 573. (i) Murota, M.; Sato, S.; Tsubokawa, N. *Polym. Adv. Technol.* **2002**, *13*, 144. (j) Tsubokawa, N.; Kotama, K.; Saitoh, H.; Nishikubo, T. *Compos. Interfaces* **2003**, *10*, 609. (k) Kaneko, Y.; Imai, Y.; Shirai, K.; Yamauchi, T.; Tsubokawa, N. *Colloids Surf., A* **2006**, *289*, 212. (l) Hayashi, S.; Fujiki, K.; Tsubokawa, N. *React. Funct. Polym.* **2000**, *46*, 193. (m) Tsubokawa, N. *Polym. J.* **2007**, *39*, 983. (n) Taniguchi, Y.; Shirai, K.; Saitoh, H.; Yamauchi, T.; Tsubokawa, N. *Polymer* **2005**, *46*, 2541. (o) Tsubokawa, N.; Hayashi, S.; Nishimura, J. *Prog. Org. Coat.* **2002**, *44*, 69. (p) Ueda, J.; Sato, S.; Tsunokawa, A.; Yamauchi, T.; Tsubokawa, N. *Eur. Polym. J.* **2005**, *41*, 193. (q) Nishizawa, N.; Nishimura, J.; Saitoh, H.; Fujiki, K.; Tsubokawa, N. *Prog. Org. Coat.* **2005**, *53*, 306. (r) Yoshikawa, S.; Satoh, T.; Tsubokawa, N. *Colloids Surf., A* **1999**, *153*, 395.
(307) Sulitzky, C.; Rückert, B.; Hall, A. J.; Lanza, F.; Unger, K.; Sellergren, B. *Macromolecules* **2002**, *35*, 79.
(308) (a) von Werne, T.; Patten, T. E. *J. Am. Chem. Soc.* **1999**, *121*, 7409. (b) von Werne, T.; Patten, T. E. *J. Am. Chem. Soc.* **2001**, *123*, 7497.
(309) (a) Perruchot, C.; Khan, M. A.; Kamitsi, A.; Armes, S. P.; von Werne, T.; Patten, T. E. *Langmuir* **2001**, *17*, 4479. (b) Perruchot, C.; Khan, M. A.; Kamitsi, A.; Armes, S. P.; Watts, J. F.; von Werne, T.; Patten, T. E. *Eur. Polym. J.* **2004**, *40*, 2129. (c) Chen, X. Y.; Randall, D. P.; Perruchot, C.; Watts, J. F.; Patten, T. E.; von Werne, T.; Armes, S. P. *J. Colloid Interface Sci.* **2003**, *257*, 56.
(310) (a) Chen, X. Y.; Armes, S. P. *Adv. Mater.* **2003**, *15*, 1558. (b) Chen, X. Y.; Armes, S. P.; Greaves, S. J.; Watts, J. F. *Langmuir* **2004**, *20*, 587. (c) Vo, C. D.; Schmid, A.; Armes, S. P.; Sakai, K.; Biggs, S. *Langmuir* **2007**, *23*, 408.
(311) Carrot, G.; Diamanti, S.; Manuszak, M.; Charleux, B.; Vairon, J. P. *J. Polym. Sci., Part A: Polym. Chem.* **2001**, *39*, 4294.
(312) (a) El Harrak, A.; Carrot, G.; Oberdisse, J.; Eychenne-Baron, C.; Boué, F. *Macromolecules* **2004**, *37*, 6376. (b) El Harrak, A.; Carrot, G.; Oberdisse, J.; Jestin, J.; Boué, F. *Polymer* **2005**, *46*, 1095. (c) El Harrak, A.; Carrot, G.; Oberdisse, J.; Jestin, J.; Boué, F. *Macromol. Symp.* **2005**, *226*, 263. (d) Carrot, G.; El Harrak, A.; Oberdisse, J.; Jestin, J.; Boué, F. *Soft Matter* **2006**, *2*, 1043.
(313) Böttcher, H.; Hallensleben, M. L.; Nuss, S.; Wurm, H. *Polym. Bull.* **2000**, *44*, 223.
(314) Mori, H.; Seng, D. C.; Zhang, M. F.; Müller, A. H. E. *Langmuir* **2002**, *18*, 3682.
(315) Bai, J.; Pang, J. B.; Qiu, K. Y.; Wei, Y. *Chin. J. Polym. Sci.* **2002**, *20*, 261.
(316) Liu, P.; Tian, J.; Liu, W. M.; Xue, Q. J. *Polym. Int.* **2004**, *53*, 127.
(317) Savin, D. A.; Pyun, J.; Patterson, G. D.; Kowalewski, T.; Matyjaszewski, K. *J. Polym. Sci., Part B: Polym. Phys.* **2002**, *40*, 2667.
(318) Pyun, J.; Jia, S. J.; Kowalewski, T.; Patterson, G. D.; Matyjaszewski, K. *Macromolecules* **2003**, *36*, 5094.
(319) Goel, V.; Chatterjee, T.; Bombalski, L.; Yurekli, K.; Matyjaszewski, K.; Krishnamoorti, R. *J. Polym. Sci., Part B: Polym. Phys.* **2006**, *44*, 2014.
(320) Bombalski, L.; Min, K.; Dong, H. C.; Tang, C. B.; Matyjaszewski, K. *Macromolecules* **2007**, *40*, 7429.
(321) (a) Ohno, K.; Morinaga, T.; Koh, K.; Tsujii, Y.; Fukuda, T. *Macromolecules* **2005**, *38*, 2137. (b) Morinaga, T.; Ohkura, M.; Ohno, K.; Tsujii, Y.; Fukuda, T. *Macromolecules* **2007**, *40*, 1159. (c) Ohno, K.; Morinaga, T.; Takeno, S.; Tsujii, Y.; Fukuda, T. *Macromolecules* **2007**, *40*, 9143.
(322) (a) Li, D. J.; Sheng, X.; Zhao, B. *J. Am. Chem. Soc.* **2005**, *127*, 6248. (b) Zhao, B.; Zhu, L. *J. Am. Chem. Soc.* **2006**, *128*, 4574.
(323) (a) Li, D. J.; Jones, G. L.; Dunlap, J. R.; Hua, F. J.; Zhao, B. *Langmuir* **2006**, *22*, 3344. (b) Li, D. J.; Zhao, B. *Langmuir* **2007**, *23*, 2208.
(324) Lei, Z. L.; Bi, S. X. *Mater. Lett.* **2007**, *61*, 3531.
(325) Mu, B.; Wang, T. M.; Liu, P. *Ind. Eng. Chem. Res.* **2007**, *46*, 3069.
(326) Zhang, K.; Ma, J.; Zhang, B.; Zhao, S.; Li, Y. P.; Xu, Y. X.; Yu, W. Z.; Wang, J. Y. *Mater. Lett.* **2007**, *61*, 949.
(327) Wu, T.; Zhang, Y. F.; Wang, X. F.; Liu, S. Y. *Chem. Mater.* **2008**, *20*, 101.
(328) Zhou, L. L.; Yuan, W. Z.; Yuan, J. Y.; Hong, X. Y. *Mater. Lett.* **2008**, *62*, 1372.
(329) (a) Parvole, J.; Billon, L.; Montfort, J. P. *Polym. Int.* **2002**, *51*, 1111. (b) Parvole, J.; Laruelle, G.; Guimon, C.; Francois, J.; Billon, L. *Macromol. Rapid Commun.* **2003**, *24*, 1074. (c) Parvole, J.; Montfort, J. P.; Billon, L. *Macromol. Chem. Phys.* **2004**, *205*, 1369. (d) Laruelle, G.; Parvole, J.; Francois, J.; Billon, L. *Polymer* **2004**, *45*, 5013. (e) Parvole, J.; Laruelle, G.; Khoukh, A.; Billon, L. *Macromol. Chem. Phys.* **2005**, *206*, 372. (f) Inoubli, R.; Dagréou, S.; Khoukh, A.; Roby, F.; Peyrelasse, J.; Billon, L. *Polymer* **2005**, *46*, 2486. (g) Inoubli, R.; Dagréou, S.; Delville, M-H.; Lapp, A.; Peyrelasse, J.; Billon, L. *Soft Matter* **2007**, *3*, 1014. (h) Sonnenberg, L.; Parvole, J.; Borisov, O.; Billon, L.; Gaub, H. E.; Seitz, M. *Macromolecules* **2006**, *39*, 281.
(330) Blomberg, S.; Ostberg, S.; Harth, E.; Bosman, A. W.; Horn, B. V.; Hawker, C. J. J. *Polym. Sci., Part A: Polym. Chem.* **2002**, *40*, 1309.
(331) Kasseh, A.; Ait-Kadi, A.; Riedl, B.; Pierson, J. F. *Polymer* **2003**, *44*, 1367.
(332) (a) Bartholome, C.; Beyou, E.; Bourgeat-Lami, E.; Chaumont, P.; Zydowicz, N. *Macromolecules* **2003**, *36*, 7946. (b) Bartholomea, C.; Beyou, E.; Bourgeat-Lami, E.; Cassagnau, P.; Chaumont, P.; David, L.; Zydowicz, N. *Polymer* **2005**, *46*, 9965. (c) Bartholome, C.; Beyou, E.; Bourgeat-Lami, E.; Chaumont, P.; Lefebvre, F.; Zydowicz, N. *Macromolecules* **2005**, *38*, 1099. (d) Bartholome, C.; Beyou, E.; Bourgeat-Lami, E.; Chaumont, P.; Zydowicz, N. *Polymer* **2005**, *46*, 8502.
(333) Tsujii, Y.; Ejaz, M.; Sato, K.; Goto, A.; Fukuda, T. *Macromolecules* **2001**, *34*, 8872.
(334) (a) Li, C. Z.; Benicewicz, B. C. *Macromolecules* **2005**, *38*, 5929. (b) Li, C. Z.; Han, J.; Ryu, C. Y.; Benicewicz, B. C. *Macromolecules* **2006**, *39*, 3175.
(335) Liu, C. H.; Pan, C. Y. *Polymer* **2007**, *48*, 3679.
(336) (a) Ranjan, R.; Brittain, W. J. *Macromolecules* **2007**, *40*, 6217. (b) Ranjan, R.; Brittain, W. J. *Macromol. Rapid Commun.* **2007**, *28*, 2084.
(337) Zhao, Y. L.; Perrier, S. *Macromolecules* **2007**, *40*, 9116.
(338) Zhou, Q. Y.; Wang, S. X.; Fan, X. W.; Advincula, R.; Mays, J. *Langmuir* **2002**, *18*, 3324.
(339) (a) Spange, S. *Prog. Polym. Sci.* **2000**, *25*, 781. (b) Eismann, U.; Spange, S. *Macromolecules* **1997**, *30*, 3439. (c) Spange, S.; Höhne, S.; Francke, V.; Günther, H. *Macromol. Chem. Phys.* **1999**, *200*, 1054. (d) Höhne, S.; Spange, S. *Macromol. Chem. Phys.* **2003**, *204*, 841.
(340) Zirbs, R.; Binder, W.; Gahleitner, M.; Machl, D. *Macromol. Symp.* **2007**, *254*, 93.
(341) Carrot, G.; Rutot-Houzé, D.; Pottier, A.; Degée, P.; Hilborn, J.; Dubois, P. *Macromolecules* **2002**, *35*, 8400.
(342) Yoon, K. R.; Lee, Y. W.; Lee, J. K.; Choi, I. S. *Macromol. Rapid Commun.* **2004**, *25*, 1510.
(343) (a) Joubert, M.; Delaite, C.; Bourgeat-Lami, E.; Dumas, P. *J. Polym. Sci., Part A: Polym. Chem.* **2004**, *42*, 1976. (b) Joubert, M.; Delaite, C.; Bourgeat-Lami, E.; Dumas, P. *New J. Chem.* **2005**, *29*, 1601. (c) Joubert, M.; Delaite, C.; Bourgeat-Lami, E.; Dumas, P. *Macromol. Rapid Commun.* **2005**, *26*, 602.
(344) Mingotaud, A. F.; Reculusa, S.; Mingotaud, C.; Keller, P.; Sykes, C.; Duguet, E.; Ravaine, S. *J. Mater. Chem.* **2003**, *13*, 1920.
(345) Jordi, M. A.; Seery, T. A. P. *J. Am. Chem. Soc.* **2005**, *127*, 4416.
(346) (a) Wang, Y. P.; Pei, X. W.; Yuan, K. *Mater. Lett.* **2005**, *59*, 520. (b) Wang, Y. P.; Pei, X. W.; He, X. Y.; Yuan, K. *Eur. Polym. J.* **2005**, *41*, 1326.
(347) Wu, L. B.; Cao, D.; Huang, Y.; Li, B. G. *Polymer* **2008**, *49*, 742.
(348) Chen, S.; Sui, J. J.; Chen, L.; Pojman, J. A. *J. Polym. Sci., Part A: Polym. Chem.* **2005**, *43*, 1670.
(349) García, M.; van Zyl, W. E.; ten Cate, M. G. J.; Stouwdam, J. W.; Verweij, H.; Pimplapure, M. S.; Weickert, G. *Ind. Eng. Chem. Res.* **2003**, *42*, 3750.
(350) Hoogenboom, R.; Schubert, U. S. *Macromol. Rapid Commun.* **2007**, *28*, 368.
(351) Liu, P.; Su, Z. X. *Mater. Chem. Phys.* **2005**, *94*, 412.
(352) Rusu, G.; Rusu, E. *High Perform. Polym.* **2006**, *18*, 355.
(353) Sun, L. H.; Yang, Z. G.; Li, X. H. *J. Appl. Polym. Sci.* **2008**, *107*, 1842.
(354) Percy, M. J.; Amalvy, J. I.; Barthet, C.; Armes, S. P.; Greaves, S. J.; Watts, J. F.; Wiese, H. *J. Mater. Chem.* **2002**, *12*, 697.
(355) (a) Tissot, I.; Novat, C.; Lefebvre, F.; Bourgeat-Lami, E. *Macromolecules* **2001**, *34*, 5737. (b) Tissot, I.; Reymond, J. P.; Lefebvre, F.; Bourgeat-Lami, E. *Chem. Mater.* **2002**, *14*, 1325.
(356) Ding, X. F.; Yu, K. F.; Jiang, Y. Q.; Hari-Bala; Zhang, H. B.; Wang, Z. C. *Mater. Lett.* **2004**, *58*, 3618.
(357) Lu, Y.; McLellan, J.; Xia, Y. N. *Langmuir* **2004**, *20*, 3464.
(358) Zhang, S. W.; Zhou, S. X.; Weng, Y. M.; Wu, L. M. *Langmuir* **2006**, *22*, 4679.
(359) Chen, M.; Zhou, S. X.; Wu, L. M.; Xie, S. H.; Chen, Y. *Macromol. Chem. Phys.* **2005**, *206*, 1896.

(360) Graf, C.; Vossen, D. L. J.; Imhof, A.; van Blaaderen, A. *Langmuir* **2003**, *19*, 6693.
(361) Chen, Y. W.; Kang, E. T.; Neoh, K. G.; Greiner, A. *Adv. Funct. Mater.* **2005**, *15*, 113.
(362) Sertchookm, H.; Avnir, D. *Chem. Mater.* **2003**, *15*, 1690.
(363) (a) Tong, X.; Tang, T.; Zhu, N.; Feng, Z. L.; Huang, B. T. *Chem. J. Chin. Univ.* **2002**, *23*, 306. (b) Tong, X.; Tang, T.; Zhang, Q. L.; Feng, Z. L.; Huang, B. T. *J. Appl. Polym. Sci.* **2002**, *83*, 446. (c) Tong, X.; Tang, T.; Feng, Z. L.; Huang, B. T. *J. Appl. Polym. Sci.* **2002**, *86*, 3532.
(364) (a) Tamai, T.; Watanabe, M. *J. Polym. Sci., Part A: Polym. Chem.* **2006**, *44*, 273. (b) Watanabe, M.; Tamai, T. *J. Polym. Sci., Part A: Polym. Chem.* **2006**, *44*, 4736. (c) Watanabe, M.; Tamai, T. *Langmuir* **2007**, *23*, 3062.
(365) Yang, J. X.; Hu, D. D.; Fang, Y.; Bai, C. L.; Wang, H. Y. *Chem. Mater.* **2006**, *18*, 4902.
(366) Yuan, J. J.; Mykhaylyk, O. O.; Ryan, A. J.; Armes, S. P. *J. Am. Chem. Soc.* **2007**, *129*, 1717.
(367) Sertchook, H.; Elimelech, H.; Makarov, C.; Khalfin, R.; Cohen, Y.; Shuster, M.; Babonneau, F.; Avnir, D. *J. Am. Chem. Soc.* **2007**, *129*, 98.
(368) Palkovits, R.; Althues, H.; Rumplecker, A.; Tesche, B.; Dreier, A.; Holle, U.; Fink, G.; Cheng, C. H.; Shantz, D. F.; Kaskel, S. *Langmuir* **2005**, *21*, 6048.
(369) Jia, G. W.; Xu, Y. S.; Qian, J.; Xu, J. X. *Macromol. Mater. Eng.* **2008**, *293*, 149.
(370) Ogoshi, T.; Chujo, Y. *Polymer* **2006**, *47*, 4036.
(371) (a) Bourgeat-Lami, E.; Espiard, P.; Guyot, A. *Polymer* **1995**, *36*, 4385. (b) Espiard, P.; Guyot, A. *Polymer* **1995**, *36*, 4391. (c) Espiard, P.; Guyot, A.; Perez, J.; Vigier, G.; David, L. *Polymer* **1995**, *36*, 4397.
(372) (a) Luna-Xavier, J. L.; Bourgeat-Lami, E.; Guyot, A. In *Organic/Inorganic Hybrid Materials--2000*; Laine, R. M., Sanchez, C., Brinker, C., Gianellis, E., Eds.; Materials Research Society Symposia Proceedings, Vol. 628; Materials Research Society: Warrendale, PA, 2001; CC3.5. (b) Bourgeat-Lami, E.; Insulaire, M.; Reculusa, S.; Perro, A.; Ravaine, S.; Duguet, E. *J. Nanosci. Nanotechnol.* **2006**, *6*, 432.
(373) Reculusa, S.; Mingotaud, C.; Bourgeat-Lami, E.; Duguet, E.; Ravaine, S. *Nano Lett.* **2004**, *4*, 1677.
(374) (a) Zhang, K.; Chen, H. T.; Chen, X.; Chen, Z. M.; Cui, Z. C.; Yang, B. *Macromol. Mater. Eng.* **2003**, *288*, 380. (b) Zhang, K.; Zheng, L. L.; Zhang, X. H.; Chen, X.; Yang, B. *Colloids Surf., A* **2006**, *277*, 145.
(375) (a) Zeng, Z.; Yu, J.; Guo, Z. X. *J. Polym. Sci., Part A: Polym. Chem.* **2004**, *42*, 2253. (b) Zeng, Z.; Yu, J.; Guo, Z. X. *Macromol. Chem. Phys.* **2004**, *205*, 2197.
(376) Li, H.; You, B.; Gu, G. X.; Wu, L. M.; Chen, G. D. *Polym. Int.* **2005**, *54*, 191.
(377) Wang, Y. Q.; Li, Y. P.; Zhang, R. Y.; Huang, L.; He, W. W. *Polym. Compos.* **2006**, *27*, 282.
(378) Liu, X. Y.; Zhao, H. P.; Li, L.; Yan, J.; Zha, L. S. *J. Macromol. Sci., Pure Appl. Chem.* **2006**, *43*, 1757.
(379) Xiong, M. N.; Wu, L. M.; Zhou, S. X.; You, B. *Polym. Int.* **2002**, *51*, 693.
(380) Liu, W. F.; Guo, Z. X.; Yu, J. *J. Appl. Polym. Sci.* **2005**, *97*, 1538.
(381) Qu, A. L.; Wen, X. F.; Pi, P. H.; Cheng, J.; Yang, Z. R. *J. Colloid Interface Sci.* **2008**, *317*, 62.
(382) (a) Mizutani, T.; Arai, K.; Miyamoto, M.; Kimura, Y. *J. Appl. Polym. Sci.* **2006**, *99*, 659. (b) Mizutani, T.; Arai, K.; Miyamoto, M.; Kimura, Y. *Prog. Org. Coat.* **2006**, *55*, 276.
(383) (a) Luna-Xavier, J. L.; Bourgeat-Lami, E.; Guyot, A. *Colloid Polym. Sci.* **2001**, *279*, 947. (b) Luna-Xavier, J. L.; Guyot, A.; Bourgeat-Lami, E. *J. Colloid Interface Sci.* **2002**, *250*, 82. (c) Luna-Xavier, J. L.; Guyot, A.; Bourgeat-Lami, E. *Polym. Int.* **2004**, *53*, 609.
(384) (a) Qi, D. M.; Bao, Y. Z.; Huang, Z. M.; Weng, Z. X. *J. Appl. Polym. Sci.* **2006**, *99*, 3425. (b) Qi, D. M.; Bao, Y. Z.; Huang, Z. M.; Weng, Z. X. *Colloid Polym. Sci.* **2008**, *286*, 233.
(385) (a) Barthet, C.; Hickey, A. J.; Cairns, D. B.; Armes, S. P. *Adv. Mater.* **1999**, *11*, 408. (b) Percy, M. J.; Barthet, C.; Lobb, J. C.; Khan, M. A.; Lascelles, S. F.; Vamvakaki, M.; Armes, S. P.; Wiese, H. *Langmuir* **2000**, *16*, 6913. (c) Amalvy, J. I.; Percy, M. J.; Armes, S. P. *Langmuir* **2001**, *17*, 4770. (d) Agarwal, G. K.; Titman, J. J.; Percy, M. J.; Armes, S. P. *J. Phys. Chem. B* **2003**, *107*, 12497. (e) Amalvy, J. I.; Percy, M. J.; Armes, S. P.; Leite, C. A. P.; Galembeck, F. *Langmuir* **2005**, *21*, 1175.
(386) (a) Chen, M.; Wu, L. M.; Zhou, S. X.; You, B. *Macromolecules* **2004**, *37*, 9613. (b) Chen, M.; Zhou, S. X.; You, B.; Wu, L. M. *Macromolecules* **2005**, *38*, 6411.
(387) (a) Percy, M. J.; Armes, S. P. *Langmuir* **2002**, *18*, 4562. (b) Percy, M. J.; Amalvy, J. I.; Randall, D. P.; Armes, S. P.; Greaves, S. J.; Watts, J. F. *Langmuir* **2004**, *20*, 2184.
(388) Dupin, D.; Schmid, A.; Balmer, J. A.; Armes, S. P. *Langmuir* **2007**, *23*, 11812.
(389) Caregnato, P.; Le Roux, G. C.; Mártire, D. O.; Gonzalez, M. C. *Langmuir* **2005**, *21*, 8001.
(390) Zeng, Z.; Yu, J.; Guo, Z. X. *J. Polym. Sci., Part A: Polym. Chem.* **2005**, *43*, 2826.
(391) Lee, J.; Hong, C. K.; Choe, S.; Shim, S. E. *J. Colloid Interface Sci.* **2007**, *310*, 112.
(392) Zhang, H.; Su, Z. X.; Liu, P.; Zhang, F. Z. *J. Appl. Polym. Sci.* **2007**, *104*, 415.
(393) Zhang, F. A.; Yu, C. L. *Eur. Polym. J.* **2007**, *43*, 1105.
(394) (a) Landfester, K. *Macromol. Rapid Commun.* **2001**, *22*, 896. (b) Antonietti, M.; Landfester, K. *Prog. Polym. Sci.* **2002**, *27*, 689. (c) Landfester, K. *Top. Curr. Chem.* **2003**, *227*, 75. (d) Landfester, K. *Annu. Rev. Mater. Res.* **2006**, *36*, 231.
(395) Schork, F. J.; Luo, Y. W.; Smulders, W.; Russum, J. P.; Butte, A.; Fontenot, K. *Adv. Polym. Sci.* **2005**, *175*, 129.
(396) Qi, D. M.; Bao, Y. Z.; Weng, Z. X.; Huang, Z. M. *Polymer* **2006**, *47*, 4622.
(397) Tiarks, F.; Landfester, K.; Antonietti, M. *Langmuir* **2001**, *17*, 5775.
(398) (a) Zhang, S. W.; Zhou, S. X.; Weng, Y. M.; Wu, L. M. *Langmuir* **2005**, *21*, 2124. (b) Zhou, J.; Zhang, S. W.; Qiao, X. G.; Li, X. Q.; Wu, L. M. *J. Polym. Sci., Part A: Polym. Chem.* **2006**, *44*, 3202. (c) Qiao, X. G.; Chen, M.; Zhou, J.; Wu, L. M. *J. Polym. Sci., Part A: Polym. Chem.* **2007**, *45*, 1028.
(399) Boutti, S.; Bourgeat-Lami, E.; Zydowicz, N. *Macromol. Rapid Commun.* **2005**, *26*, 1860.
(400) Qiang, W. L.; Wang, Y. L.; He, P.; Xu, H.; Gu, H. C.; Shi, D. L. *Langmuir* **2008**, *24*, 606.
(401) (a) Bourgeat-Lami, E.; Lang, J. *J. Colloid Interface Sci.* **1998**, *197*, 293. (b) Bourgeat-Lami, E.; Lang, J. *J. Colloid Interface Sci.* **1999**, *210*, 281. (c) Corcos, F.; Bourgeat-Lami, E.; Novat, C.; Lang, J. *Colloid Polym. Sci.* **1999**, *277*, 1142. (d) Bourgeat-Lami, E.; Lang, J. *Macromol. Symp.* **2000**, *151*, 377. (e) Chalaye, S.; Bourgeat-Lami, E.; Putaux, J. L.; Lang, J. *Macromol. Symp.* **2001**, *169*, 89.
(402) Sondi, I.; Fedynyshyn, T. H.; Sinta, R.; Matijević, E. *Langmuir* **2000**, *16*, 9031.
(403) Percy, M. J.; Michailidou, V.; Armes, S. P.; Perruchot, C.; Watts, J. F.; Greaves, S. J. *Langmuir* **2003**, *19*, 2072.
(404) (a) Schmid, A.; Fujii, S.; Armes, S. P. *Langmuir* **2005**, *21*, 8103. (b) Schmid, A.; Fujii, S.; Armes, S. P. *Langmuir* **2006**, *22*, 4923. (c) Schmid, A.; Fujii, S.; Armes, S. P.; Leite, C. A. P.; Galembeck, F.; Minami, H.; Saito, N.; Okubo, M. *Chem. Mater.* **2007**, *19*, 2435.
(405) Liu, Q. P.; Gao, L. X.; Gao, Z. W.; Yang, L. *Mater. Lett.* **2007**, *61*, 4456.
(406) (a) Wang, Q.; Xia, H. S.; Zhang, C. H. *J. Appl. Polym. Sci.* **2001**, *80*, 1478. (b) Xia, H. S.; Zhang, C. H.; Wang, Q. *J. Appl. Polym. Sci.* **2001**, *80*, 1130.
(407) (a) Mecking, S. *Colloid Polym. Sci.* **2007**, *285*, 605. (b) Monteil, V.; Stumbaum, J.; Thomann, R.; Mecking, S. *Macromolecules* **2006**, *39*, 2056.
(408) Cheng, W. X.; Wang, Z.; Ren, C. Y.; Chen, H.; Tang, T. *Mater. Lett.* **2007**, *61*, 3193.
(409) Yang, Z. Z.; Qiu, D.; Li, J. *Macromol. Rapid Commun.* **2002**, *23*, 479.
(410) Yu, J.; Yu, J.; Gao, Y. F.; Guo, Z. X. *Chin. J. Polym. Sci.* **2001**, *20*, 71.
(411) Chow, P. Y.; Gan, L. M. *J. Nanosci. Nanotechnol.* **2004**, *4*, 197.
(412) Xu, P.; Wang, H. T.; Tong, R.; Du, Q. G.; Zhong, W. *Colloid Polym. Sci.* **2006**, *284*, 755.
(413) Jang, J.; Lim, B. *Angew. Chem., Int. Ed.* **2003**, *42*, 5600.
(414) (a) Maeda, S.; Armes, S. P. *J. Colloid Interface Sci.* **1993**, *159*, 257. (b) Maeda, S.; Armes, S. P. *J. Mater. Chem.* **1994**, *4*, 935. (c) Flitton, R.; Johal, J.; Maeda, S.; Armes, S. P. *J. Colloid Interface Sci.* **1995**, *173*, 135. (d) Maeda, S.; Corradi, R.; Armes, S. P. *Macromolecules* **1995**, *28*, 2905. (e) McCarthy, G. P.; Armes, S. P.; Greaves, S. J.; Watts, J. F. *Langmuir* **1997**, *13*, 3686. (f) Saoudi, B.; Jammul, N.; Chehimi, M. M.; McCarthy, G. P.; Armes, S. P. *J. Colloid Interface Sci.* **1997**, *192*, 269. (g) Perruchot, C.; Chehimi, M. M.; Delamar, M.; Lascelles, S. F.; Armes, S. P. *J. Colloid Interface Sci.* **1997**, *193*, 190. (h) Azioune, A.; Pech, K.; Saoudi, B.; Chehimi, M. M.; McCarthy, G. P.; Armes, S. P. *Synth. Met.* **1999**, *102*, 1419. (i) Gill, M.; Mykytiuk, J.; Armes, S. P.; Edwards, J. L.; Yeates, T.; Moreland, P. J.; Mollett, C. *J. Chem. Soc., Chem. Commun.* **1992**, 108. (j) Terrill, N. J.; Crowley, T.; Gill, M.; Armes, S. P. *Langmuir* **1993**, *9*, 2093. (k) Stejskal, J.; Kratochvíl, P.; Armes, S. P.; Lascelles, S. F.; Riede, A.; Helmstedt, M.; Prokeš, J.; Křivka, I. *Macromolecules* **1996**, *29*, 6814. (l) Maeda, S.; Gill, M.; Armes, S. P.; Fletcher, I. W. *Langmuir* **1995**, *11*, 1899. (m) Butterworth, M. D.; Corradi, R.; Johal, J.; Maeda, S.; Lascelles, S. F.; Armes, S. P. *J. Colloid Interface Sci.* **1995**, *174*, 510.
(415) Neoh, K. G.; Tan, K. K.; Goh, P. L.; Huang, S. W.; Kang, E. T.; Tan, K. L. *Polymer* **1999**, *40*, 887.

(416) Goller, M. I.; Barthet, C.; McCarthy, G. P.; Corradi, R.; Newby, B. P.; Wilson, S. A.; Armes, S. P.; Luk, S. Y. *Colloid Polym. Sci.* **1998**, *276*, 1010.
(417) Azioune, A.; Slimane, A. B.; Hamou, L. A.; Pleuvy, A.; Chehimi, M. M.; Perruchot, C.; Armes, S. P. *Langmuir* **2004**, *20*, 3350.
(418) Lascelles, S. F.; McCarthy, G. P.; Butterworth, M. D.; Armes, S. P. *Colloid Polym. Sci.* **1998**, *276*, 893.
(419) Han, M. G.; Armes, S. P. *J. Colloid Interface Sci.* **2003**, *262*, 418.
(420) Hao, L. Y.; Zhu, C. L.; Chen, C. N.; Kang, P.; Hu, Y.; Fan, W. C.; Chen, Z. Y. *Synth. Met.* **2003**, *139*, 391.
(421) Dutta, K.; De, S. K. *Solid State Commun.* **2006**, *140*, 167.
(422) Xia, H. S.; Wang, Q. *J. Appl. Polym. Sci.* **2003**, *87*, 1811.
(423) Liu, P.; Liu, W. M.; Xue, Q. J. *Mater. Chem. Phys.* **2004**, *87*, 109.
(424) Lei, X. P.; Su, Z. X. *Polym. Adv. Technol.* **2007**, *18*, 472.
(425) (a) Li, X. W.; Wang, G. C.; Li, X. X. *Surf. Coat. Technol.* **2005**, *197*, 56. (b) Li, X. W.; Dai, N.; Wang, G. C.; Song, X. M. *J. Appl. Polym. Sci.* **2008**, *107*, 403.
(426) Jang, J.; Ha, J.; Lim, B. *Chem. Commun.* **2006**, 1622.
(427) (a) Dutta, K.; De, S. K. *J. Nanosci. Nanotechnol.* **2006**, *6*, 499. (b) Dutta, K. *Phys. Lett. A* **2007**, *361*, 141.
(428) Lee, C. F.; Tsai, H. H.; Wang, L. Y.; Chen, C. F.; Chiu, W. Y. *J. Polym. Sci., Part A: Polym. Chem.* **2005**, *43*, 342.
(429) Gök, A.; Şen, S. *J. Appl. Polym. Sci.* **2006**, *102*, 935.
(430) Li, X. W.; Li, X.; Wang, G. C. *Mater. Lett.* **2006**, *60*, 3342.
(431) (a) Lee, K. P.; Gopalan, A. I.; Lee, S. H.; Showkat, A. M.; Nho, Y. C. *J. Appl. Polym. Sci.* **2006**, *102*, 3912. (b) Zhang, Y. P.; Lee, S. H.; Reddy, K. R.; Gopalan, A. I.; Lee, K. P. *J. Appl. Polym. Sci.* **2007**, *104*, 2743.
(432) Han, M. G.; Armes, S. P. *Langmuir* **2003**, *19*, 4523.
(433) Han, M. G.; Foulger, S. H. *Chem. Commun.* **2004**, 2154.
(434) Ray, S. S.; Biswas, M. *Mater. Res. Bull.* **1998**, *33*, 533.
(435) Gök, A.; Koçak, E. D.; Aydoğdu, S. *J. Appl. Polym. Sci.* **2005**, *96*, 746.
(436) (a) Maity, A.; Biswas, M. *Polym. J.* **2003**, *35*, 993. (b) Maity, A.; Biswas, M. *Polym. Int.* **2005**, *54*, 710.
(437) (a) Decher, G.; Hong, H.-G. *Makromol. Chem. Macromol. Symp.* **1991**, *46*, 321. (b) Decher, G. *Science* **1997**, *277*, 1232.
(438) (a) Caruso, F.; Lichtenfeld, H.; Giersig, M.; Möhwald, H. *J. Am. Chem. Soc.* **1998**, *120*, 8523. (b) Caruso, F.; Caruso, R. A.; Möhwald, H. *Science* **1999**, *282*, 1111. (c) Caruso, F.; Möhwald, H. *Langmuir* **1999**, *15*, 8276. (d) Caruso, F.; Caruso, R. A.; Möhwald, H. *Chem. Mater.* **1999**, *11*, 3309. (e) Caruso, R. A.; Susha, A.; Caruso, F. *Chem. Mater.* **2001**, *13*, 400.
(439) (a) Peng, Z.; Kong, L. X.; Li, S. D. *Polymer* **2005**, *46*, 1949. (b) Peng, Z.; Kong, L. X.; Li, S. D. *J. Appl. Polym. Sci.* **2005**, *96*, 1436. (c) Kong, L. X.; Peng, Z. *Key Eng. Mater.* **2005**, *295*−*296*, 39. (d) Peng, Z.; Kong, L. X.; Li, S. D. *Synth. Met.* **2005**, *152*, 25. (e) Peng, Z.; Kong, L. X.; Li, S. D. *Synth. Met.* **2005**, *152*, 321. (f) Peng, Z.; Kong, L. X.; Li, S. D.; Spiridonov, P. *J. Nanosci. Nanotechnol.* **2006**, *6*, 3934. (g) Peng, Z.; Kong, L. X. *Polym. Degrad. Stab.* **2007**, *92*, 1061. (h) Peng, Z.; Kong, L. X. *Polym. Bull.* **2007**, *59*, 207. (i) Li, S. D.; Peng, Z.; Kong, L. X.; Zhong, J. P. *J. Nanosci. Nanotechnol.* **2006**, *6*, 541. (j) Peng, Z.; Kong, L. X.; Li, S. D.; Chen, Y.; Huang, M. F. *Compos. Sci. Technol.* **2007**, *67*, 3130.
(440) Fleming, M. S.; Mandal, T. K.; Walt, D. R. *Chem. Mater.* **2001**, *13*, 2210.
(441) (a) Mori, H.; Müller, A. H. E.; Klee, J. E. *J. Am. Chem. Soc.* **2003**, *125*, 3712. (b) Mori, H.; Lanzendörfer, M. G.; Müller, A. H. E. *Langmuir* **2004**, *20*, 1934.
(442) Bringley, J. F.; Wunder, A.; Howe, A. M.; Wesley, R. D.; Qiao, T. C. A.; Liebert, N. B.; Kelley, B.; Minter, J.; Antalek, B.; Hewitt, J. M. *Langmuir* **2006**, *22*, 4198.
(443) Guo, Z. X.; Yu, J. *J. Mater. Chem.* **2002**, *12*, 468.
(444) Liu, Y. L.; Li, S. H. *Macromol. Rapid Commun.* **2004**, *25*, 1392.
(445) Xu, N.; Zhou, W.; Shi, W. F. *Polym. Adv. Technol.* **2004**, *15*, 654.
(446) Gomes, D.; Buder, I.; Nunes, S. P. *J. Polym. Sci., Part B: Polym. Phys.* **2006**, *44*, 2278.
(447) (a) Patel, N. P.; Miller, A. C.; Spontak, R. J. *Adv. Mater.* **2003**, *15*, 729. (b) Patel, N. P.; Miller, A. C.; Spontak, R. J. *Adv. Funct. Mater.* **2004**, *14*, 699. (c) Patel, N. P.; Aberg, C. M.; Sanchez, A. M.; Capracotta, M. D.; Martin, J. D.; Spontak, R. J. *Polymer* **2004**, *45*, 5941. (d) Patel, N. P.; Zielinski, J. M.; Samseth, J.; Spontak, R. J. *Macromol. Chem. Phys.* **2004**, *205*, 2409.
(448) Sun, Y. Y.; Jiang, H. J.; Zhu, L. B.; Wong, C. P. *IEEE Trans. Compos. Packag. Technol.* **2008**, *31*, 135.
(449) Gao, Y.; Choudhury, N. R. In *Handbook of Organic-Inorganic Hybrid Materials and Nanocomposites*; Nalwa, H. S., Ed.; American Scientific Publishers: Stevenson Ranch, CA, 2003; Vol *1*, pp 271−293.
(450) Crosby, A. J.; Lee, J. Y. *Polym. Rev.* **2007**, *47*, 217.
(451) Zhang, S.; Sun, D.; Fu, Y. Q.; Du, H. J. *Surf. Coat. Technol.* **2003**, *167*, 113.
(452) Ray, S. S.; Okamoto, M. *Prog. Polym. Sci.* **2003**, *28*, 1539.
(453) *Flame Retardant Polymer Nanocomposites*; Morgan, A. B., Wilkie, C. A., Eds; John Wiley & Sons: Hoboken, NJ, 2007.
(454) Bourbigot, S.; Duquesne, S. *J. Mater. Chem.* **2007**, *17*, 2283.

CR068035Q